Coefficient Identification Problems in Heat Transfer

Mohammed Sabah Hussein

Submitted in accordance with the requirements for the degree of
Doctor of Philosophy

The University of Leeds
Department of Applied Mathematics

March, 2016

The candidate confirms that the work submitted is his/her own, except where work which has formed part of jointly authored publications has been included. The contribution of the candidate and the other authors to this work has been explicitly indicated below. The candidate confirms that appropriate credit has been given within the thesis where reference has been made to the work of others.

Joint publications

Some of the work presented in this thesis has been published, accepted or submitted for publication, as follows:

▶ Some of the material of Chapter 2 is included in:

1. M.S. Hussein, D. Lesnic, and M.I. Ismailov. An inverse problem of finding the time-dependent diffusion coefficient from an integral condition. *Mathematical Methods in the Applied Sciences*, 39, 963-980, 2016.

▶ Some of the material of Chapter 3 is included in:

1. M.S. Hussein and D. Lesnic. Determination of the time-dependent thermal conductivity in the heat equation with spacewise-dependent heat capacity. In I. Dimov, I. Farag, and L. Vulkov, editors, *Finite Difference Methods, Theory and Applications*, volume 9045 of *Lecture Notes in Computer Science*, pages 217-224. Springer International Publishing, 2015.

2. M.S. Hussein and D. Lesnic. Identification of the time-dependent conductivity of an inhomogeneous diffusive material. *Applied Mathematics and Computation*, 269, 35–58, 2015.

▶ Some of the material of Chapter 4 is included in:

1. M.S. Hussein, D. Lesnic, and M.I. Ivanchov. Simultaneous determination of time-dependent coefficients in the heat equation. *Computers and Mathematics with Applications*, 67, 1065-1091, 2014.

▶ Some of the material of Chapter 5 is included in:

1. M.S. Hussein and D. Lesnic. Simultaneous determination of time-dependent coefficients and heat source. *International Journal for Computational Methods in Engineering Science and Mechanics*, submitted, 2015.

▶ Some of the material of Chapter 6 is included in:

1. M.S. Hussein and D. Lesnic. Simultaneous determination of time and space-dependent coefficients in a parabolic equation. *Communications in Nonlinear Science and Numerical Simulation*, 33, 194-217, 2016.

▶ Some of the material of Chapter 7 is included in:

1. M.S. Hussein, D. Lesnic, and M.I. Ivanchov. Free boundary determination in nonlinear diffusion. *East Asian Journal on Applied Mathematics*, 3(4), 295-310, 2013.

▶ Some of the material of Chapter 8 is included in:

1. M.S. Hussein and D. Lesnic. Determination of a time-dependent thermal diffusivity and free boundary in heat conduction. *International Communications in Heat and Mass Transfer*, 53, 154-163, 2014.

▶ Some of the material of Chapter 9 is included in:

1. M.S. Hussein, D. Lesnic, M.I. Ivanchov and H.A. Snitko. Multiple time-dependent coefficient identification thermal problems with a free boundary. *Applied Numerical Mathematics*, 99, 24–50, 2016.

▶ Some of the material of Chapter 10 is included in:

1. M.S. Hussein, D. Lesnic and M.I. Ivanchov. Identification of a heterogeneous orthotropic conductivity in a rectangular domain, Accepted by *International Journal of Novel Ideas: Mathematics*, 2016.

In all these papers I have performed all the numerical implementation and the computational work, as well as many other aspects of the papers. Some of the theoretical proofs jointly performed with co-authors have not been included in this thesis.

Acknowledgments

First and foremost I would like to thank my supervisor Professor D. Lesnic for his patience, support and guidance throughout my PhD study. He has made himself available and offered assistance even at the busiest of times. His help has been greatly appreciated. I would also like to thank Professor Grant D. Lythe and Dr Rob J. Sturman for their constructive comments and advices during my annual reviews.

I would like to give my thanks to all the staff at the School of Mathematics for their help with all the little things that keep everything running smoothly. I would also like to give special mention to Jeanne Shuttleworth for her patience dealing with my many enquiries. I am thankful also to my postgraduate colleagues for their company and friendship during my time in Leeds.

My gratitude extend to Professor M.I. Ivanchov for his valuable advice on my research during his visiting to the University of Leeds on March 2013.

My special thanks are due to my parents, my dear wife, Asawer, and my children, Hamsa and Abdulrahman, for their continuous love, tolerance, support, and praying that always kept me going.

Finally, I would like to thank the people that made this whole thing possible, the Higher committee for Education Development in Iraq (HCEDiraq).

Mohammed Sabah Hussein

Abstract

The aim of this thesis is to find the numerical solution for various coefficient identification problems in heat transfer and extend the possibility of simultaneous determination of several physical properties. In particular, the problems of coefficient identification in a fixed or moving domain for one and multiple unknowns are investigated. These inverse problems are solved subject to various types of overdetermination conditions such as non-local, heat flux, Cauchy data, mass/energy specification, general integral type overdetermination, time-average condition, time-average of heat flux, Stefan condition and heat momentum of the first and second order. The difficulty associated with these problems is that they are ill-posed, as their solutions are unstable to inclusion of random noise in input data, therefore traditional techniques fail to provide accurate and stable solutions.

Throughout this thesis, the Crank-Nicolson finite-difference method (FDM) is mainly used as a direct solver except in Chapter 7 where a three-level scheme is employed in order to deal with the nonlinear heat equation. An explicit FDM scheme is also employed in Chapter 10 for the two-dimensional case.

The inverse problems investigated are discretised using the FDM and recast as nonlinear least-squares minimization problems with simple bounds on the unknown coefficients. The resulting problem is efficiently solved using the *fmincon* or *lsqnonlin* routines from MATLAB optimization toolbox. The Tikhonov regularization method is included where necessary. The choice of the regularization parameter(s) is thoroughly discussed. The stability of the numerical solution is investigated by introducing Gaussian random noise into the input data. The numerical solutions are compared with their known analytical solution, where available, and with the corresponding direct problem numerical solution where no analytical solution is available.

Nomenclature

The following is a list of notation. Some of these symbols are used more than once to represent different quantities from chapter to chapter due to the enormous amount of notation present in this thesis. In some cases the use of a symbol not listed below is local to a short portion of the text and in such circumstances it is defined where it is introduced.

Latin symbols

a	time-dependent function (eq.(9.31) in Chapter 9), time-dependent thermal diffusivity in (Chapters 4 and 8), time-dependent thermal conductivity in (Chapters 3 and 6), and space, time-dependent function in eq. (9.1) in Chapter 9, and Chapter 10)
$\tilde{a}$	the maximum value of $a(y,t)$ (Chapter 10)
A_j, $A_{i,j}$	vector components of difference equation (in all chapters)
b	the coefficient function of space (Chapters 3 and 6), function of time (Chapters 4 and 9) and space, time-dependent function (Chapter 10)
$\tilde{b}$	the maximum value of $b(x,t)$ (Chapter 10)
$\tilde{\mathbf{b}}$	vector for Neumann problem (Chapter 5)
B_j, $B_{i,j}$	vector components of difference equation (in all chapters)
c	the space-dependent heat capacity function (Chapter 3), time-dependent absorbtion (Chapter 6) and time-dependent reaction function (Chapter 9)
C	the time-dependent coefficient function (Chapter 4)
C	constant in expressions (3.7) and (3.10) (Chapter 3)
C_j, $C_{i,j}$	the vector components of difference equation (in all chapters)
$C[a,b]$	the space of continuous functions in $[a,b]$
$C^3[a,b]$	the space of functions three times continuously differentiable in $[a,b]$
$C^{2,1}(\Omega)$	the space of functions twice continuously differentiable in first variable and once continuously differentiable in the second variable in Ω

$C^{2+\gamma,1}$	the space of twice continuous functions with the second-order derivative being Hölder continuous with exponent $\gamma \in (0,1)$ for the first variable and once continuously differentiable in the second variable
d	reaction rate (Chapter 4)
D	matrix given by expression (2.15) (Chapter 2)
D	the solution domain $(0,h) \times (0,\ell)$ (Chapter 10)
$\overline{D}$	the closure of D (Chapter 10)
$\mathcal{D}(\mathcal{F})$	the domain of $\mathcal{F}$ (Chapter 1)
$\tilde{D}$, $\tilde{E}$	matrices for Neumann problem (Chapter 5)
D_+, D_-, D_0	the forward, backward and central difference operators, respectively (Chapter 7)
E	matrix given by expression (2.15) (Chapter 2)
E^ϵ	the perturbed function of E given by expression (2.23) (Chapter 2)
f, F	heat sources (Chapters 5 and 4)
F	nonlinear objective least-squares function (Chapters 2 and 7–10)
F_1, F_2, F_3	nonlinear objective least-squares functions (Chapter 4, 6 and 9)
$\tilde{F}$, $\tilde{F}_1$	nonlinear objective least-squares functions (Chapter 9)
F_I,F_{II}	nonlinear objective least-squares functions (Chapters 5 and 6)
$\mathcal{F}$	operator (Chapter 1)
$fmincon$	MATLAB optimization routine
G	the right hand side of equations (2.8) and (4.10)
h	length for y-axis (Chapter 10) and the time-dependent free boundary (Chapters 7–9)
$H^{2+\gamma}$	the space of twice continuously differentiable functions with the second-order derivative being Hölder continuous with exponent γ
$H^{1+\gamma/2}$	the space of once continuously differentiable functions with the first derivative being Hölder continuous with exponent $\gamma/2$
i, j, k	indices

k	time-dependent coefficient function (Chapter 2)
K	time-dependent coefficient function (Chapter 4)
L	matrix (Chapters 4 and 7) and length of the conductor (Chapter 4)
$L^2[a,b]$	the space of square integrable functions in $[a,b]$
lsqnonlin	MATLAB optimization routine
M	number of finite differences in x coordinate (all chapters except Chapter 10)
M_x	number of finite differences in x coordinate (Chapter 10)
M_y	number of finite differences in y coordinate (Chapter 10)
N	number of finite differences in t coordinate
normrnd	MATLAB function generating Gaussian random numbers
p	percentage of noise (Chapters 3–10)
Q	coefficient function of time (Chapter 4)
Q	fixed domain $(0,1)\times(0,T)$ (Chapters 7 and 8)
Q_T	fixed domain $[-\ell,\ell]\times[0,T]$ (Chapter 5) and $(0,L)\times(0,T)$ (Chapter 6)
R_{II}	residual least-squares function without penalty term (Chapter 5)
t	time variable
t_j	time node
T	final time
u	solution / temperature / concentration
u_q	solution of the state equation (Chapter 1)
$u_{i,j}$	values of u at the node (i,j)
$u^k_{i,j}$	values of u at the node (i,j,k) (Chapter 10)
v	coefficient function of time for velocity of fluid (Chapter 4)
v	the transformed solution (Chapters 7–9)
$v_{i,j}$	components of transformed solution v (Chapters 7–9)
$\hat{v}_{i,j}$	average of transformed solution $v_{i,j}$ (Chapter 7)
x	space variable
x_i	space nodes
$\mathcal{X},\mathcal{Y}$	Hilbert spaces (Chapter 1)
y	space variable (Chapter 10)
y^ϵ	perturbed data (Chapter 1)

Greek symbols

α	segregation parameter (Chapter 2)
β	segregation parameter (Chapter 2) and regularization parameter (Chapters 4 and 8)
β_i	regularization parameter
γ	segregation parameter (Chapter 2)
γ	number in $(0, 1)$
Δt, Δx, Δy	sizes of time and space steps
ϵ	total amount of noise
ϵk	Gaussian random variables
Λ_{ad}	set of admissible functions (Chapter 7)
ρ	percentage of noise (Chapter 2)
σ_k	standard deviation
φ	initial condition function (Chapter 2)
	integral overdetermination condition (Chapter 5)
ψ	integral overdetermination condition (Chapter 5)
	the time-average condition (Chapter 6)
ω	weight function (Chapter 5)
Ω	fixed solution domain (Chapter 4)
	moving solution domain (Chapters 7–9)

Abbreviations

BEM	boundary element method
BFGS	Broyden, Fletcher, Goldfarb and Shannon
FDM	finite difference method
FEM	finite element method
FVM	finite volume method
ICIP	inverse coefficient identification problem
IP	inverse problem
LB	lower bound
O	order of
PDEs	partial differential equations

PCG	preconditioning conjugate gradients
rmse	root mean square error
rrmse	relative root mean square error
TTF	trace type functional
TTR	trust-region-reflective
UB	upper bound

Contents

List of Figures

List of Tables

Chapter 1

General introduction

1.1 Introduction

Many physical situations can be modeled by partial differential equations (PDE's) and if all the necessary input data for a certain problem are known, then the solution can be evaluated and used to predict how the system will be behave under various conditions, [29]. The necessary inputs include such information as initial or boundary conditions, forcing terms, coefficients and even the shape of the domain. On the other hand, if any of this information is missing or unknown, then it is not possible to use the model for studying the physical system. However, it may be possible to measure certain outputs experimentally from the system and use this information together with the inputs that are known in order to retrieve the missing input data. The last situation is known as an *inverse problem*.

Most inverse problems are ill-posed (unstable) problems. This usually means that in such problems a slight change in the input data may cause an huge change in the output solution. It was long believed that these problems have no practical value and, hence, their study cannot lead to significant mathematical results. This opinion was so strong that it outlasted 1943, the year of issue of the pioneering paper by Tikhonov [117], where the practical importance of ill-posed problems was emphasized and a method for stable solution was pointed out.

The scope of inverse problems has existed in various branches of physics, engineering and mathematics for a long time. The theory of inverse problems has been extensively developed within the past decade due partly to its importance in applications; on the other hand, the numerical solutions to such problems need huge computations and also reliable numerical methods. For instance, deconvolution in seismic exploration, image reconstruction and parameter identification all require high performance computers and reliable solution methods to carry out the computation [123].

The coefficient entries a PDE model are generally related to the physical properties of the system that is modeled. In simple cases, these physical properties can be identified directly from some kind of experiment and the results used to reduce the model to a specific physical system. In complicated situations it may be hard or impossible to measure the physical properties associated with a coefficient in a model equation. In such cases it may be necessary to proceed indirectly due to lack of information, i.e. to formulate and solve the inverse problem for the missing data.

Parameter identification problems consist in using the input of actual observation or indirect measurement contaminated with noise, to infer the values of the parameters characterizing the system under investigation. Often, these inverse problems are ill-posed according to the Hadamard postulate [43], which is: if the solution does not exist or, is not unique or, if it violates the continuous dependence upon input data. Most identification problems satisfy the first two conditions and violate the third one which is the stability.

Inverse coefficient identification problems have been the point of interest to many significant researchers in recent years. In the past few decades a great deal of interest has been directed towards the determination of unknown coefficients in PDE's. The main motivation behind this research is to determine the unknown properties of a region by measuring only data on its boundary, and particular attention has been paid on coefficients that represent physical quantities, for example, the conductivity of a medium. The techniques used depend mainly on the type of equation (linear, semilinear and nonlinear) and the variables on which the unknown coefficient is assumed a priori to depend. An important, but hard case, is when the unknown conductivity, for instance, depends on the dependent variable, [19]. However, if the material or medium is uniform, we do not expect the unknown coefficient(s) to depend on the spatial variable. If, in addition, the characteristic properties do not change with time when the dependent variables are held fixed, then we may expect also that the coefficients do not depend on time, [103].

Determination of leading coefficient or, the coefficient of the high-order derivative in the parabolic heat equation has been investigated widely and in many practical applications. For example, in [47] the problem of space-dependent diffusivity identification has been studied, while the time-dependent case has been investigated in [90]. Also, for the temperature-dependent case we refer to [13, 122].

1.2 Inverse problems

From the mathematical point of view, problems are inverse when the corresponding mathematical models contain some unknown parameters and therefore the process of solving them reduces to restoring these parameters proceeding from some additional information about the process (the so-called *overdetermination conditions*).

From the physical point of view, the direct problem is more fundamental and is related to a cause-effect sequence based on well-established physical laws, such as heat conduction. The inverse problem is to find the unknown causes from the known consequences (effects).

The application of inverse problems is of special importance in the case when the immediate measurement of suitable parameters is impossible, for instance, because of inaccessibility of either material or environment and also the rapidity of the process, [70].

Inverse problems can be classified, as follows:

- **coefficient identification problems**, i.e. problems in which the coefficient(s) of equation is(are) unknown(s), see Chapters 2–10.
- **retrospective**, i.e. problems with reverse direction of time, like backward heat conduction problem.
- **boundary**, i.e. problems related to the determination of unknown parameters in the boundary conditions.
- **geometrical**, i.e. problems concerning the determination of unknown domain or boundary, see Chapters 7–9.

All the above categories of inverse problems are ill-posed in the Hadamard concept. Therefore, they are unstable and hence a sort of regularization must be employed in order to retrieve the loss of stability.

1.3 Stefan problems

In 1890, the physicist J. Stefan modelled the melting of arctic ice in the summer by a simple one-dimensional model, [84]. Consider a homogeneous block of ice filling the region $x \geq \ell = h(0)$ at the time $t = 0$. The ice starts to melt by heating the block at the left end. Thus, at $t \geq 0$ the region between $x = 0$ and $x = h(t) > 0$ is filled with water and the region $x \geq h(t)$ is filled with ice. If

$u(x,t)$ represents the temperature over $0 < x < h(t)$ at time t, then the system of equations that model this problem is

$$\begin{aligned} u_t(x,t) &= u_{xx}(x,t), \quad (x,t) \in (0,h(t)) \times [0,\infty), && (1.1)\\ u(x,0) &= u_0(x), \quad x \in (0,h(0)), && (1.2)\\ u_x(0,t) &= f(t), \quad t \in [0,T], && (1.3)\\ u(h(t),t) &= 0, \quad t \in [0,T]. && (1.4) \end{aligned}$$

Moreover, the speed at which the interface between water and ice moves is proportional to the heat flux. This is described by the following Stefan interface condition:

$$h'(t) = -u_x(h(t),t), \quad t \in [0,T]. \tag{1.5}$$

Stefan problems model many real world and engineering situations in which there is freezing or melting causing a boundary to vary in time. Stefan problems (direct statement) are boundary value problems for parabolic equations in regions with unknown and moving boundaries, which require determining the temperature $u(x,t)$ and the moving boundary $h(t)$. Conversely, inverse Stefan problems require determining the initial and/or boundary conditions, and/or thermal properties from additional inputs which may involve the temperature, heat moment (first, second) order, and/or measurement of the free boundary position, [41].

We mention that in Chapters 7–9 we focus on the one-phase coefficient inverse Stefan problem which is the task of finding the unknown boundary function in addition to the unknown coefficient(s).

1.4 Stability analysis

Coefficient identification problems and inverse geometric problems are nonlinear problems in nature. These nonlinear problems can be cast into an abstract framework as a nonlinear operator equation

$$\mathcal{F}(x) = y, \tag{1.6}$$

where $\mathcal{F}$ acts between two Hilbert spaces $\mathcal{X}$ and $\mathcal{Y}$. For example, in parameter identification problems, the parameter-to-output map $\mathcal{F}$ maps the parameter q (for example) onto the solution u_q of the state equation or the heat flux $q\frac{\partial u_q}{\partial n}$.

1.4.1 Tikhonov regularization method

In practice, the right-hand side data in (1.6) is perturbed as y^ϵ with $||y - y^\epsilon|| \approx \epsilon$ (ϵ is called noise level). Then instead of (1.6) one has to solve $\mathcal{F}(x) = y^\epsilon$. But of course this equation may have no solution if $y^\epsilon \notin \mathcal{R}(\mathcal{F})$, where $\mathcal{R}(\mathcal{F}) \subset \mathcal{Y}$ denotes the range of the operator $\mathcal{F}$. In this situation one has to define a quasi-solution given by the minimization of the least-squares gap $\|\mathcal{F}(x) - y^\epsilon\|$. Moreover, since the inverse problems under investigation are ill-posed we employ the Tikhonov regularization method based on minimizing

$$\|\mathcal{F}(x) - y^\epsilon\|^2 + \beta\|x\|^2 \to \min, \quad x \in \mathcal{D}(\mathcal{F}), \tag{1.7}$$

where $\mathcal{D}(\mathcal{F})$ represents the domain of $\mathcal{F}$. For a positive regularization parameter β, a minimizer to (1.7) always exists under certain conditions but may not be unique, [31].

1.4.2 The choice of regularization parameter

With any regularization method, the choice of regularization parameter $\beta > 0$ plays a crucial rule. Its choice always represents a compromise between accuracy and stability: if β is too small, (i.e. $\beta \searrow 0$) the solution exhibits oscillatory behavior and becomes unstable. On the other hand, with large values of β, the solution is damped and deviates from the exact result, [116].

Throughout the years a variety of regularization parameter choice strategies have been proposed. These methods can roughly be divided into two classes depending on their assumption about $\|\mathcal{F}(x) - y^\epsilon\|$, the norm of perturbation of the right-hand side of (1.6). The two classes can be characterized as follows:

Class A. Methods based on knowledge or good estimate of $\|\mathcal{F}(x) - y^\epsilon\|$,

Class B. Methods that do not require knowledge of $\|\mathcal{F}(x) - y^\epsilon\|$, but seek to extract this information from the data and nature of the problem.

A method belonging to Class A is the discrepancy principle of Morozov [96], which amounts to choosing the regularization parameter such that the residual norm of regularized solution becomes approximately equal to the amount of noise ϵ.

A method belonging to Class B is the L-curve method which is a log-log plot for many positive regularization parameters of the norm of the regularized solution versus the corresponding residual norm. In this way, the L-curve displays the compromise between minimising theses two quantities, [44].

1.5 Optimization technique

Throughout the thesis we employ the nonlinear Tikhonov regularization method which minimizes the residual functional by adding the penalty term to stabilise the solution, see (1.7). Therefore, we recast the nonlinear inverse problems into nonlinear constrained minimization problems subject to simple bounds on the variables. In this thesis, we mainly employ two optimization toolbox routines, namely, *fmincon* and *lsqnonlin*, [95].

1.5.1 *fmincon* routine

fmincon is a MATLAB routine used to find the minimum of a problem specified by

$$\min_{\underline{x}} f(\underline{x}) \qquad \text{such that} \quad \begin{cases} \underline{C}(\underline{x}) \leq \underline{0}, \\ \underline{Ceq}(\underline{x}) = \underline{0}, \\ A\underline{x} \leq \underline{b}, \\ Aeq\underline{x} = \underline{beq}, \\ \underline{LB} \leq \underline{x} \leq \underline{UB}. \end{cases} \tag{1.8}$$

where $\underline{b}$, $\underline{beq}$, $\underline{LB}$ and $\underline{UB}$ are vectors, A and Aeq are matrices, $\underline{C}(\underline{x})$ and $\underline{Ceq}(\underline{x})$ are vectorial functions, and $f(\underline{x})$ is scaler function. The inequalities between vectors are understood component-wise.
MATLAB syntax: the syntax used in our computational work is

```
>> x=fmincon(fun,x0,A,b,Aeq,beq,LB,UB,nonlcon,options)
```

where `x0` is the initial guess for $\underline{x}$. The quantities `A`, `b`, `Aeq`, `beq`, `nonlcon` can be passed as empty by setting them as `A=[ ]`, `b=[ ]`, `Aeq=[ ]`, `beq=[ ]` and `nonlcon=[ ]`. The `options` are passed to routine as follows:

```
% Start with the default options
options = optimset;
% Modify options setting
options = optimset(options,'Display', 'iter');
options = optimset(options,'MaxFunEvals', MaxFunEvals_Data);
options = optimset(options,'MaxIter', MaxIter_Data);
options = optimset(options,'TolFun', TolFun_Data);
options = optimset(options,'Algorithm', 'interior-point');
```

Input arguments:

`fun:` the function to be minimized which accepts a vector `x` and returns a scalar value f.

`x0:` initial guess to start the minimization process.

`A, b, Aeq, beq:` linear constraint matrices `A`, `Aeq` and their corresponding vectors `b` and `beq`.

`nonlcon:` the functions that compute the nonlinear inequality $\underline{C}(\underline{x}) \leq \underline{0}$ and the nonlinear equality $\underline{Ceq}(\underline{x}) = \underline{0}$.

fmincon allows us to choose among several algorithms which are 'interior-point' (the default choice), 'trust-region-reflective', 'sqp' (sequential quadratic programming) and 'active-set'. In our computational work in Chapters 4 and 6 we choose the 'interior-point' algorithm, for more details about the mathematical setting we refer to [9, 10, 121].

1.5.2 *lsqnonlin* routine

lsqnonlin solves nonlinear least-squares problems including nonlinear data-fitting problems of the form

$$\min_{\underline{x}} \|\underline{F}(\underline{x})\|_2^2 = \min_{\underline{x}} \left(\sum_{i=1}^{n} F_i^2(\underline{x}) \right),$$

with optional lower and upper bounds on the components of x. Rather than computing the norm $\|\underline{F}(\underline{x})\|_2^2$ (the sum of squares), *lsqnonlin* requires user-defined functions to compute the vector-valued function in the form of

$$\underline{F}(\underline{x}) = \begin{bmatrix} F_1(\underline{x}) \\ F_2(\underline{x}) \\ \vdots \\ F_n(\underline{x}) \end{bmatrix}.$$

MATLAB syntax: we call *lsqnonlin* in command window of MATLAB as follows:

```
>> x=lsqnonlin(fun,x0,LB,UB,options)
```

This routine allows us to choose the 'trust-region-reflective' algorithm (default choice) which is a subspace trust-region method based on the interior-reflective Newton method described in [21, 22]. In each iteration it involves the solution of a large linear system of equations using the method of preconditioned conjugate

gradients (PCG) or 'Levenberg-Marquardt', where the `options` quantity is the same as before but the last line is replaced with

```
options = optimset(options,'Algorithm', 'trust-region-reflective');
```

1.5.3 Limitations of *fmincon* and *lsqnonlin*

- *fmincon* is a gradient-based method that is designed to work on problems where the objective and constraints functions are both continuous and have continuous first derivatives.
- does not allow for equal $\underline{LB}$ and $\underline{UB}$ bounds for $\underline{x}$.
- the 'trust-region-reflective' algorithm for *lsqnonlin* cannot accept underdetermined nonlinear systems of equations, i.e. the number of elements of $\underline{F}$ must be at least as the length of $\underline{x}$.
- Levenberg-Marquardt algorithm does not handle bound constraints.

1.6 Numerical methods

There are various numerical methods to solve PDEs, for example, finite difference, finite element, finite volume, boundary element, spectral and meshless methods, [93].

Finite Difference Method (FDM) seems to be the easiest technique to solve a differential equation. The main idea is to replace the differentials in the PDE by finite differences. Because of its clarity and simplicity, the FDM is usually the first choice for those who are aim to solve PDEs, [51]. One drawback of this method is that it becomes quite complicated when solving PDEs in irregular domains and the other is that it is difficult to carry out the mathematical analysis such as stability and convergence for nonlinear PDEs.

Finite Element Method (FEM) is a popular method for solving various PDEs, [105]. It works by rewriting the governing equation into an equivalent variational form. Meshing the domain into small finite elements and looking for appropriate solutions at the mesh nodes using appropriate basis functions over each elements.

Finite Volume Method (FVM) is popular in computational fluid dynamics (CFD). The main idea of FVM is to integrate the differential equation over a finite size control volume surrounding each node point on a mesh, and then changing the volume integrals to surface integrals, for more details we refer to [91, 120].

Boundary Elements Method (BEM) is used to solve those PDEs which possess a fundamental solution available explicitly. Then the use of Green's formula recasts the PDE as a boundary integral equation. The BEM attempts to utilize the given boundary conditions to fit the boundary values into the integral equation. Therefore, BEM reduces the dimensionality of the problem by one. The BEM typically produces a fully populated matrix (different from FDM which is tridiagonal).

Spectral Methods can be applied efficiently if the physical domain is simple and the solution is smooth. The main idea is to write the solution of the differential equation as a sum of certain basis function and then to choose the coefficients in the sum in order to satisfy the differential equation. Interested readers can consult [42].

Meshless Methods. Mesh-based methods such as FEM, BEM and FVM share the disadvantage of tedious meshing and re-meshing in crack propagation problem, melting of a solid or freezing process, etc. The aim of a meshless method is to overcome these drawbacks by getting rid of meshing or re-meshing the entire domain and only adding or deleting nodes, instead. The early idea goes back to the smooth particle hydrodynamic method developed in [39]. There are various meshless methods, for example, element free Galerkin method; reproducing kernel particle method; radial basis function method, method of fundamental solutions, etc.

1.7 Procedures for solving inverse problems

In this section, we present numerical procedures for solving inverse and ill-posed problems. One of them is the so-called adjoint problem approach, based on integral relationships between the input and output data. An alternative to this is the output least-squares method which seeks to minimize an objective functional comparing the computed output to the measured value in an appropriate norm. In this thesis, we adopt the second approach which mainly recasts the nonlinear inverse problem as a constrained nonlinear optimization problem. Our procedure can be expressed by the flowchart which explains the main logical steps, see Figure 1.1. From this figure, one can notice that our procedure starts with initializing the model, say $\underline{x}_0$. Then this information is passed to the direct solver in order to obtain the first value for the objective function, say f_0. After that, we invoke the MATLAB optimization routine $fmincon$ or $lsqnonlin$ and the process of minimization starts to search for a better value for $\underline{x}$, but with a lower objective function value f. This process is repeated until the tolerance allowance is satisfied

or the prescribed number of iterations is reached.

1.8 Purpose and structure of the thesis

Nevertheless, coefficient identification problems have been investigated theoretically and numerically by many authors. Several studies concern determining a single coefficient in the parabolic heat equation assuming that is constant [12], time-dependent [75, 76], space-dependent [2], or temperature-dependent [85, 100, 101]. In these papers, the authors investigated the existence and uniqueness of solution of inverse problems, but no numerical method/solution was presented. However, some numerical technique was proposed in [108], based on space decomposition in a reproducing kernel space. Also, in [36], the author considered retrieving lower-order time-dependent coefficients using the Trace-Type Functional approach, [15].

The problem of retrieving two time-dependent coefficients simultaneously has been investigated theoretically in the monographs [70, 104]. While, the case of multiple time-dependent coefficients identification has been investigated in [111, 112, 113, 114], but no numerical solution/method has been attempted to solve such inverse problems.

Based on the above literature research, this thesis aims to fill in the gaps on the numerical solution for multiple (mainly time-dependent) coefficient identification problems in one and two-dimensions. Our technique is based on the minimization of the objective functional which naturally represents the gap between the measured and computed data. This optimization problem has been solved effectively using MATLAB optimization toolbox routines. This gives accurate and stable solutions if combined with Tkhonov's regularization method for noisy input data.

The main purpose of this thesis is to find the numerical solution for various coefficient identification problems and extend the possibility of simultaneous determination of physical properties of interest. Most of the problems investigated in this thesis model real phenomena such as heat conduction, melting and freezing food or water, solidification, etc. Initially, we investigate numerically the identification of one parameter (thermal diffusivity) in Chapter 2 and develop the numerical procedure to handle the case of multi-parameters i.e. two parameter or more, in the subsequent chapters.

This thesis is structured upon the type of domain (fixed or moving) and then with this classification we arrange the chapters according to the number of unknown coefficients. Chapters 2–6 are fixed domain problems with one and two coefficients to be determined, whilst Chapters 7–9 are moving domains with one, two, three, and four coefficients to be determined. Finally, Chapter 10 presents

an extension to two-dimensions.

Throughout this thesis, FDM with Crank-Nicolson scheme is used as direct solver except in Chapter 7 where the scheme of [88] is employed in order to deal with the nonlinearity. An explicit FDM scheme is also used in Chapter 10 for the two-dimensional case. The optimization routine *lsqnonlin* or *fmincon* are used in order to find the numerical solution of inverse problems.

In Chapter 2, we investigate the numerical reconstruction of the time-dependent diffusion coefficient from a nonlinear integral condition. Three test examples are considered according to the nature of unknown coefficient such as linear or nonlinear and even in the case where the analytical solution is not available.

The problem of identifying the time-dependent thermal conductivity when the space-dependent heat capacity is known is considered in Chapter 3. Cauchy data are used in both Dirichlet and Neumann inverse problem formulations and their existence, uniqueness and continuous dependence upon the data are carefully investigated.

Chapters 4 and 5 extend the purpose of the thesis to the simultaneous determination of several time-dependent coefficients from Cauchy boundary data or average temperature measurements.

In Chapter 6, we consider the numerical solution of a couple of inverse time and space-dependent coefficient identification problems in the heat equation from time-averaging temperature measurements and overspecified Cauchy boundary data. The next three Chapters 7–9 present extensions to inverse free boundary problems.

In Chapter 7, we consider a novel inverse problem where a free boundary is determined from the mass/energy specification in a one-dimensional nonlinear diffusion problem. Moreover, in Chapter 8, the problem of simultaneous determination of the free boundary and time-dependent thermal diffusivity is considered. Unlike the problem in Chapter 7 this problem is ill-posed and needs to be stabilised through the Tikhonov regularization method. Chapter 9 can be viewed as the natural extension of Chapter 8 to the problem of multiple time-dependent coefficient identification.

The problem of identification of a heterogeneous orthotropic conductivity in a fixed rectangular domain is investigated in Chapter 10. An explicit FDM scheme is used to discretise the governing equation and the unknown coefficients are computed via the solution to a nonlinear least-squares minimization problem.

Finally, in Chapter 11, general conclusions and suggestions for possible future work are highlighted.

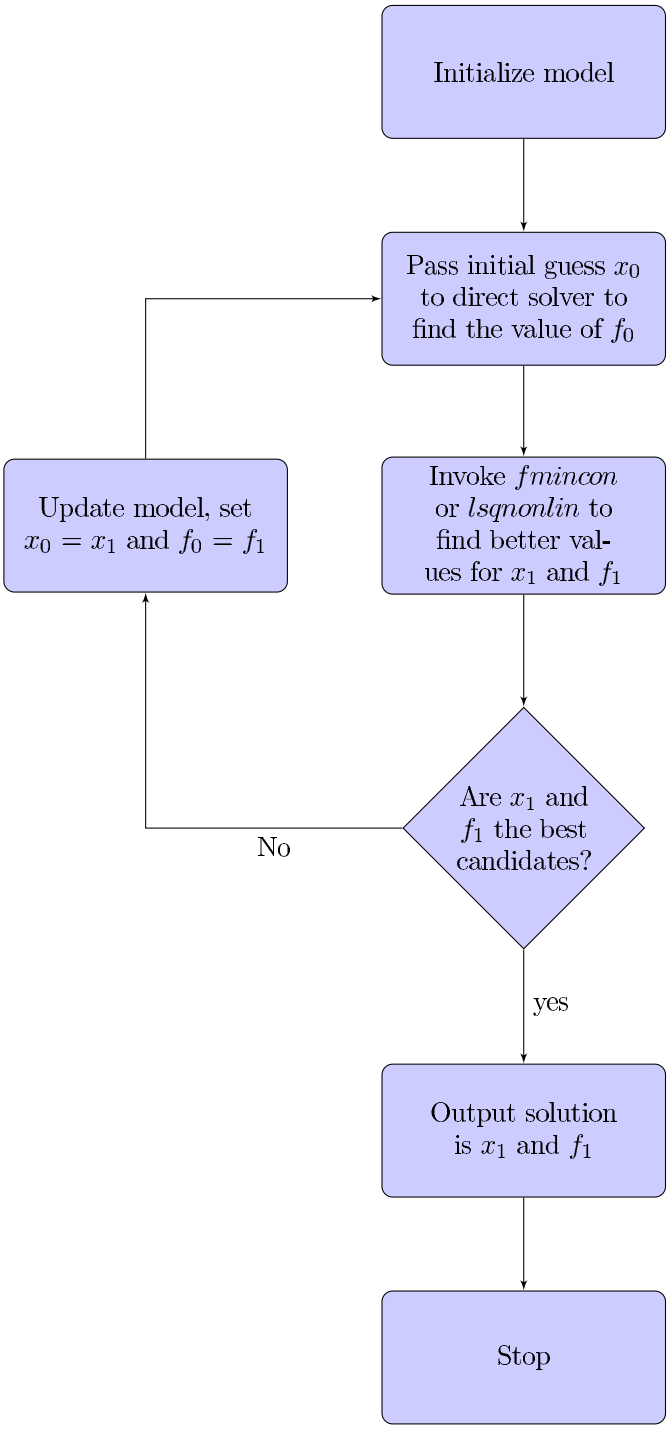

Figure 1.1: Flowchart of the procedure for solving an inverse problem.

Chapter 2

Determining the time-dependent diffusion coefficient from an integral condition

2.1 Introduction

Parameter identification from over-specified data plays an important role in applied mathematics, physics and engineering. The problem of identifying the diffusivity was investigated by many researchers under various boundary and overdetermination conditions, [62, 64, 90, 125].

In this chapter, a nonlocal over-specified data is used together with periodic boundary conditions for the determination of the time-dependent diffusivity. The mathematical formulation of the inverse problem is given in Section 2.2. In Section 2.3, the unique solvability of a classical solution to the inverse problem is recalled. The numerical methods for solving the direct and inverse problems are described in Sections 2.4 and 2.5, respectively. Numerical results are presented in Section 2.6. Finally, conclusions are highlighted in Section 2.7.

2.2 Mathematical formulation

In the rectangle $Q_T = \{(x,t) | \, 0 < x < 1, \, 0 < t \leq T\} = (0,1) \times (0,T]$, we consider the inverse problem given by the heat equation

$$u_t(x,t) = k(t) u_{xx}(x,t), \qquad (x,t) \in Q_T, \tag{2.1}$$

with unknown concentration/temperature $u(x,t)$ and unknown time-dependent diffusivity $k(t) > 0$, subject to the initial condition

$$u(x,0) = \varphi(x), \qquad 0 \leq x \leq 1, \tag{2.2}$$

where φ is a given function, the periodic and homogeneous heat flux boundary conditions

$$u(0,t) = u(1,t), \qquad t \in (0,T], \tag{2.3}$$

$$u_x(1,t) = 0, \qquad t \in (0,T], \tag{2.4}$$

and the over-determination condition, [98, 99],

$$p(t)u(0,t) + \int_0^1 u(x,t)dx = E(t), \qquad t \in [0,T], \tag{2.5}$$

where E is a given function and $p(t) = \alpha + \beta k^{-\gamma}(t)$, where α, β, $\gamma > 0$ are segregation coefficients. This problem arises in the mathematical modelling of the technological process of external guttering applied, for example, in cleaning admixtures from silicon chips, [98]. In this case, $\varphi(x)$ is the distribution of admixture in the chip for $x \in (0,1)$ at the initial time $t = 0$, while $u(x,t)$ is its distribution at time t. Condition (2.3) means that the admixtures in the left and right boundaries of the chip are the same. The adiabatic condition (2.4) means that the right boundary $x = 1$ of the chip is perfectly insulated. Condition (2.5) means that part of the substance is concentrated (segregated) on the left side $x = 0$ of the chip, [98, 99].

When $\alpha = \beta = 0$ then, the resulting inverse problem has been previously investigated in [62], and it is the purpose of this chapter to investigate the non-trivial case when α and β are non-zero.

2.3 Mathematical analysis

The pair $(k(t), u(x,t))$ from the class $C[0,T] \times \left(C^{2,1}(Q_T) \cap C^{1,0}\left(\overline{Q}_T\right)\right)$ for which conditions (2.2)-(2.5) are satisfied and $k(t) > 0$ on the interval $[0,T]$, is called the classical solution of the inverse problem (2.1)-(2.5). Its unique solvability has been established in [56], as given by the following theorem.

Theorem 2.1. *Let the functions* $\varphi(x) \in C^3[0,1]$, $E(t) \in C[0,T]$ *satisfy the*

conditions

$$\varphi(0) = \varphi(1),\ \varphi'(1) = 0,\ \varphi''(0) = \varphi''(1), \tag{2.6a}$$

$$\varphi_{2k} \geq 0,\ \varphi_{2k-1} \leq 0,\ k = 1, 2, ...,\ \varphi_0 + 2\varphi_1 < 0,\ E(t) < 2\varphi_0, \forall t \in [0, T], \tag{2.6b}$$

where $\varphi_n = \int_0^1 \varphi(x) Y_n(x) dx$ *for* $n = 0, 1, 2, \cdots,$

$$Y_0(x) = x, \quad Y_{2n-1}(x) = x\cos(2\pi n x), \quad Y_{2n}(x) = \sin(2\pi n x),\ n = 1, 2, ... \tag{2.7}$$

Then, there exist positive numbers α_0 *and* γ_0 *such that the inverse problem (2.1)-(2.5) with the parameters* $\alpha < \alpha_0$, $\gamma > \gamma_0$ *has a unique solution.*

2.4 Numerical solution of direct problem

In this section, we consider the direct initial boundary value problem given by equations (2.1)–(2.4) when $k(t)$ is given and the dependent variable $u(x, t)$ is the solution to be determined. We use the finite-difference method (FDM) with a Crank-Nicolson scheme, [110], which is unconditionally stable and second-order accurate in space and time.

The discrete form of the direct problem is as follows. Take two positive integer M and N and let $\Delta x = 1/M$ and $\Delta t = T/N$ be step lengths in space and time directions, respectively. We subdivided the domain $Q_T = (0, 1) \times (0, T)$ into $M \times N$ subintervals of equally step length. At the node (i, j) we denote $u_{i,j} = u(x_i, t_j)$, $k(t_j) = k_j$, where $x_i = i\Delta x$, $t_j = j\Delta t$, for $i = \overline{0, M}$, $j = \overline{0, N}$. Considering the general partial differential equation

$$u_t = G(x, t, u_{xx}), \tag{2.8}$$

equation (2.8) subject to (2.2)–(2.4) can approximated as:

$$\frac{u_{i,j+1} - u_{i,j}}{\Delta t} = \frac{1}{2}\left(G_{i,j} + G_{i,j+1}\right), \quad i = \overline{1, M},\ j = \overline{0, (N-1)}, \tag{2.9}$$

$$u_{i,0} = \varphi(x_i), \quad i = \overline{0, M}, \tag{2.10}$$

$$u_{0,j} = u_{M,j}, \quad j = \overline{0, N}, \tag{2.11}$$

$$u_{M+1,j} = u_{M-1,j}, \quad j = \overline{0, N}, \tag{2.12}$$

where

$$G_{i,j} = G\left(x_i, t_j, \frac{u_{i+1,j} - 2u_{i,j} + u_{i-1,j}}{(\Delta x)^2}\right), \quad i = \overline{1, M},\ j = \overline{0, (N-1)}. \tag{2.13}$$

In (2.12) and (2.13), $u_{M+1,j} = u(x_{M+1}, t_j)$ for $j = \overline{0, N}$, where $x_{M+1} = (M+1)\Delta x$ is a fictitious point located outside the boundary $x = 1$.

For our problem, equation (2.1) can be discretised in the form of (2.9) as

$$-A_{j+1}u_{i-1,j+1} + (1 + B_{j+1})u_{i,j+1} - A_{j+1}u_{i+1,j+1} = A_j u_{i-1,j} + (1 - B_j)u_{i,j} + A_j u_{i+1,j}, \quad (2.14)$$

for $i = \overline{1, M}$, $j = \overline{0, (N-1)}$, where

$$A_j = \frac{(\Delta t)k_j}{2(\Delta x)^2}, \qquad B_j = \frac{(\Delta t)k_j}{(\Delta x)^2}.$$

At each time step t_{j+1}, for $j = \overline{0, (N-1)}$, using the periodic boundary conditions (2.11), the above difference equation can be reformulated as a $M \times M$ system of linear equations of the form,

$$D\mathbf{u}_{j+1} = \mathrm{E}\mathbf{u}_j, \quad (2.15)$$

where

$$\mathbf{u}_{j+1} = (u_{1,j+1}, u_{2,j+1}, ..., u_{M,j+1})^{\mathrm{T}},$$

$$D = \begin{pmatrix} 1+B_{j+1} & -A_{j+1} & 0 & \cdots & 0 & 0 & -A_{j+1} \\ -A_{j+1} & 1+B_{j+1} & -A_{j+1} & \cdots & 0 & 0 & 0 \\ \vdots & \vdots & \vdots & \ddots & \vdots & \vdots & \vdots \\ 0 & 0 & 0 & \cdots & -A_{j+1} & 1+B_{j+1} & -A_{j+1} \\ 0 & 0 & 0 & \cdots & 0 & -2A_{j+1} & 1+B_{j+1} \end{pmatrix}_{M\times M},$$

and

$$E = \begin{pmatrix} 1-B_j & A_j & 0 & \cdots & 0 & 0 & A_j \\ A_j & 1-B_j & A_j & \cdots & 0 & 0 & 0 \\ \vdots & \vdots & \vdots & \ddots & \vdots & \vdots & \vdots \\ 0 & 0 & 0 & \cdots & A_j & 1-B_j & A_j \\ 0 & 0 & 0 & \cdots & 0 & 2A_j & 1-B_j \end{pmatrix}_{M\times M}.$$

2.4.1 Example

As an example, consider the direct problem (2.1)–(2.4) with $T = 1$ and

$$k(t) = \frac{1+t}{2\pi^2}, \quad u(x,0) = \varphi(x) = -\cos(2\pi x). \quad (2.16)$$

The exact solution is given by

$$u(x,t) = -\cos(2\pi x)e^{-t^2-2t}. \tag{2.17}$$

The required output (2.5) is

$$E(t) = p(t)u(0,t) + \int_0^1 u(x,t)dx = -\left(\alpha + \beta\left(\frac{1+t}{2\pi^2}\right)^{-\gamma}\right)e^{-t^2-2t}. \tag{2.18}$$

The numerical and exact solutions for $u(x,t)$ at interior points are shown in Figure 2.1 and also the absolute error between them is included. One can notice that an excellent agreement is obtained. Figure 2.2 shows the numerical solution in comparison with the exact one for $E(t)$ for $\alpha = \beta = \gamma = 1$. The numerical values for E have been calculated using equation (2.11) and the trapezoidal rule approximation to the integral in (2.18) to result in the formula

$$E(t_j) = p(t_j)u_{0,j} + \frac{1}{M}\sum_{i=0}^{M-1} u_{i,j}, \quad j = \overline{0,N}. \tag{2.19}$$

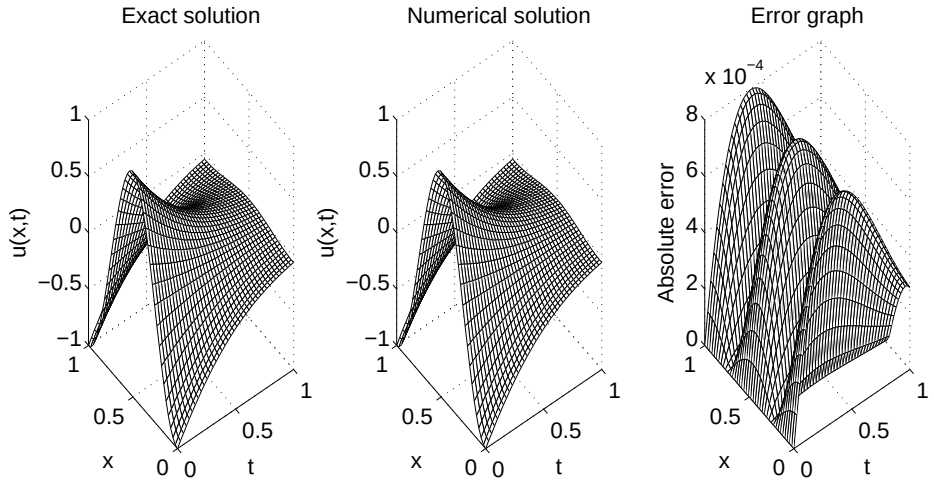

Figure 2.1: Exact and numerical solutions for $u(x,t)$ and the absolute error for the direct problem obtained with $M = N = 40$.

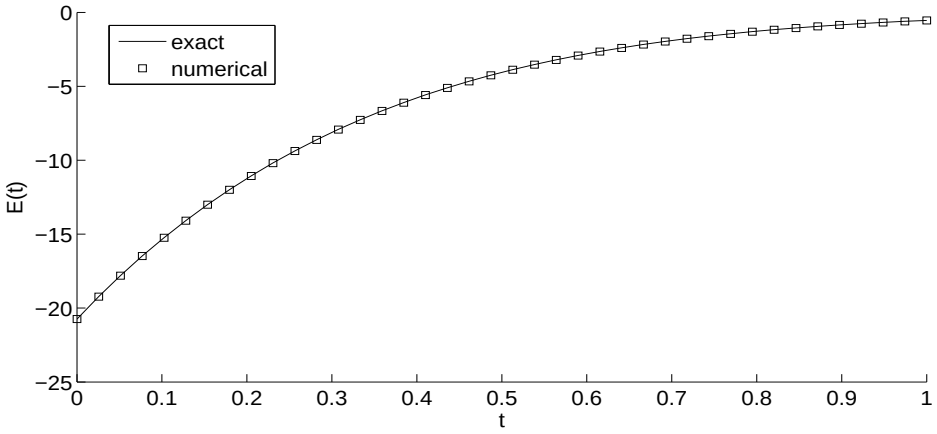

Figure 2.2: Exact and numerical solutions for $E(t)$ with $\alpha = \beta = \gamma = 1$ for the direct problem obtained with $M = N = 40$.

2.5 Numerical solution of inverse problem

We wish to obtain stable and accurate reconstructions of the time-dependent thermal conductivity $k(t)$ and the temperature $u(x,t)$ satisfying the equations (2.1)–(2.5). We reduce the inverse problem to a nonlinear minimization of the least-squares objective function

$$F(k) := \left\| u(0,t)(\alpha + \beta k^{-\gamma}(t)) + \int_0^1 u(x,t)dx - E(t) \right\|^2_{L^2[0,T]}. \tag{2.20}$$

The discretised form of (2.20) is

$$F(\underline{k}) = \sum_{j=1}^{N} \left[u(0,t_j)(\alpha + \beta k_j^{-\gamma}) + \frac{1}{M} \sum_{i=0}^{M-1} u_{i,j} - E(t_j) \right]^2, \tag{2.21}$$

where $\underline{k} = (k_j)_{j=\overline{1,N}}$, the values $u_{i,j}$ are computed from (2.15) and, for simplicity, we have dropped the time-step multiplier T/N. It is worth mentioning that if the compatibility condition $u(0,0) = \varphi(0)$ is satisfied then (2.5) applied at $t = 0$, yields

$$k(0) = \left(\frac{\beta\varphi(0)}{E(0) - \int_0^1 \varphi(x)dx - \alpha\varphi(0)} \right)^{1/\gamma}. \tag{2.22}$$

The minimization of the objective functional (2.21), subjected to the physical simple bound constraints $\underline{k} > \underline{0}$ is accomplished using the MATLAB optimization toolbox routine *lsqnonlin*, which does not require supplying (by the user) the gradient of the objective function, [95]. Furthermore, within *lsqnonlin* we use the Trust-Region-Reflective (TRR) algorithm which is based on the interior-reflective

Newton method, [25]. Each iteration involves a large linear system of equations whose solution, based on a preconditioned conjugate gradient method, allows a regular and sufficiently smooth decrease of the objective functional (2.21), [3].

In the numerical computation, we take the parameters of the routine *lsqnonlin* as follows:

- Number of variables $M = N = 40$.
- Maximum number of iterations = $10^2 \times$ (number of variables).
- Maximum number of objective function evaluations = $10^3 \times$(number of variables).
- Solution and object function tolerances = 10^{-10}.

The inverse problem (2.1)–(2.5) is solved subject to both exact and noisy measurements (2.5). The noisy data is numerically simulated as

$$E^{\epsilon}(t_j) = E(t_j) + \epsilon_j, \quad j = \overline{1, N}, \tag{2.23}$$

where ϵ_j are random variables generated from a Gaussian normal distribution with mean zero and standard deviation σ given by

$$\sigma = \rho \times \max_{t \in [0,T]} |E(t)|, \tag{2.24}$$

where ρ represents the percentage of noise. We use the MATLAB function *normrnd* to generate the random variables $\underline{\epsilon} = (\epsilon_j)_{j=\overline{1,N}}$ as follows:

$$\underline{\epsilon} = normrnd(0, \sigma, N). \tag{2.25}$$

The total amount of noise ϵ is given by

$$\epsilon = \left|\underline{\epsilon}\right| = \sqrt{\sum_{j=1}^{N} (E^{\epsilon}(t_j) - E(t_j))^2}. \tag{2.26}$$

In the case of noisy data (2.23), we replace $E(t_j)$ by $E^{\epsilon}(t_j)$ in (2.21).

2.6 Numerical results and discussion

In this section, we present and discuss a few test examples in order to illustrate the accuracy, stability and robustness of the numerical scheme based on the

FDM combined with the minimization of the least-squares functional (2.21), as described in Section 2.5.

2.6.1 Example 1

In this example, we consider the inverse problem (2.1)-(2.5) with $T = 1$ and the input data

$$u(x,0) = \varphi(x) = -\frac{\cos(2\pi x)}{e},\ E(t) = -\left(1 + 8\pi^2\sqrt{1+t}\right)\exp(-\sqrt{1+t}), \quad (2.27)$$

and $\alpha = \beta = \gamma = 1$. One can easily check that $E(t) \in C[0,1]$ and that $C^3[0,1] \ni \varphi(x)$ satisfies the conditions in (2.6a). Moreover, using (2.7) we have

$$\begin{aligned}
\varphi_0 &= \int_0^1 \varphi(x)Y_0(x)dx = -\frac{1}{e}\int_0^1 x\cos(2\pi x)dx = 0,\\
\varphi_1 &= \int_0^1 \varphi(x)Y_1(x)dx = -\frac{1}{e}\int_0^1 x\cos^2(2\pi x)dx = -\frac{1}{4e},\\
\varphi_{2k} &= \int_0^1 \varphi(x)Y_{2k}(x)dx = -\frac{1}{e}\int_0^1 \cos(2\pi x)\sin(2\pi kx)dx = 0, \quad k \geq 1\\
\varphi_{2k-1} &= \int_0^1 \varphi(x)Y_{2k-1}(x)dx = -\frac{1}{e}\int_0^1 x\cos(2\pi x)\cos(2\pi kx)dx = 0, \quad k \geq 2
\end{aligned}$$

and hence, one can easily check that the conditions in (2.6b) are also satisfied. According the Theorem 2.1 the solution of the inverse problem exits and is unique. In fact, it can easily be checked by direct substitution that the analytical solution is given by

$$k(t) = \frac{1}{8\pi^2\sqrt{1+t}}, \quad u(x,t) = -\cos(2\pi x)\exp(-\sqrt{1+t}). \quad (2.28)$$

We take the initial guess for the unknown thermal diffusivity $k(t)$ equal to the constant $k(0) = 1/(8\pi^2)$ which is known from expression (2.22).

First, we attempt to retrieve the unknown diffusivity $k(t)$ and the concentration/ temperature $u(x,t)$ for exact input data, i.e. $\rho = 0$, as well as for $\rho \in \{2\%, 20\%\}$ noisy data. The objective function (2.21) is plotted, as a function of the number of iterations, in Figure 2.3. From this figure, it can be seen that a very fast convergence is achieved in 4 to 8 iterations to reach a very low value of $O(10^{-25})$. The associated numerically obtained results for $k(t)$ and $u(x,t)$ are presented in Figures 2.4 and 2.5, respectively. From these figures it can be seen clearly that the agreement between the numerical results and the analytical solutions is excellent for exact data, i.e. $\rho = 0$, and is consistent with the

errors in the input data for $\rho > 0$. The numerical solutions for $k(t)$ and $u(x,t)$ converge to their corresponding exact solutions in (2.28), as the percentage of noise ρ decreases from 20% to 2% and then to zero. The nonlinear least-squares minimization (2.21) produces good and consistent reconstructions of the solution even for a large amount of noise such as 20%, when the total amount of noise computed by (2.26) is $\epsilon = 33.7$.

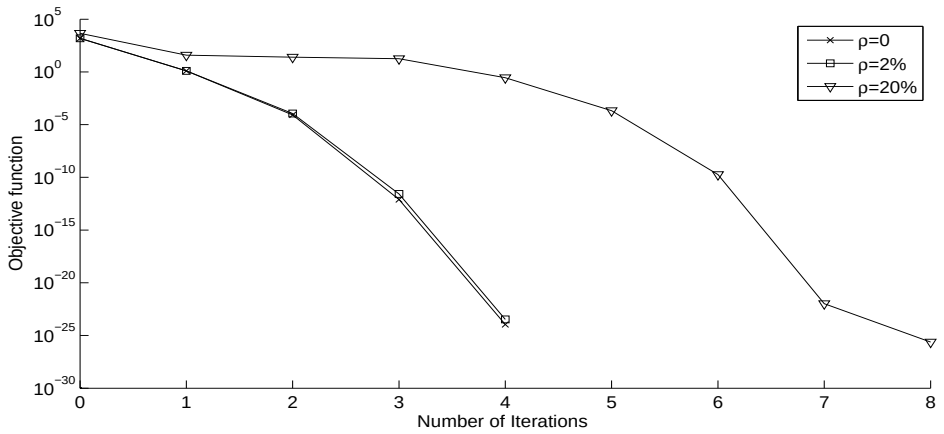

Figure 2.3: Objective function (2.21), for Example 1 with $\rho \in \{0, 2\%, 20\%\}$ noise.

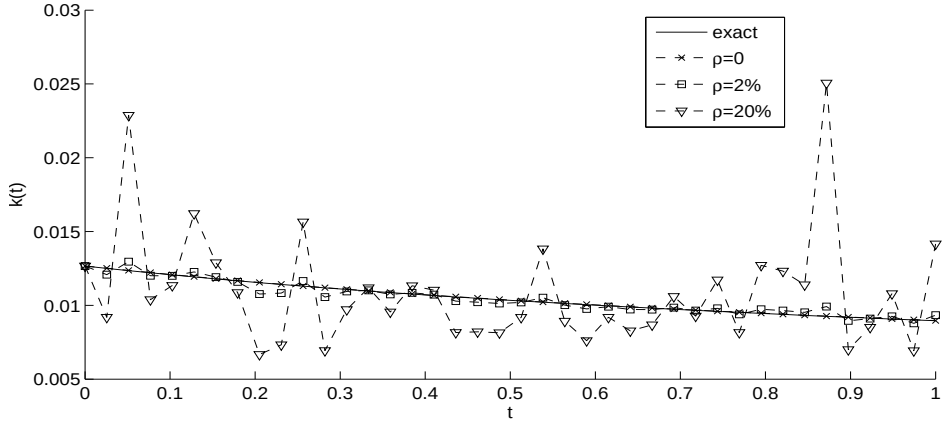

Figure 2.4: Exact and numerical solutions for $k(t)$, for Example 1 with $\rho \in \{0, 2\%, 20\%\}$ noise.

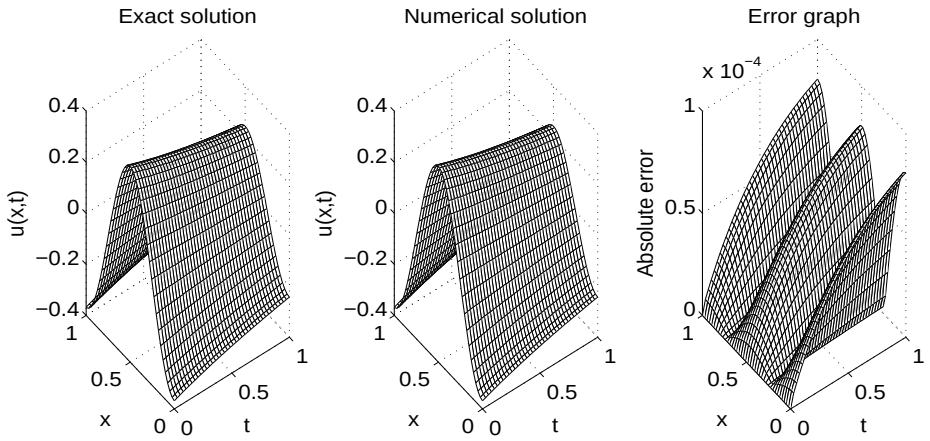

(a)

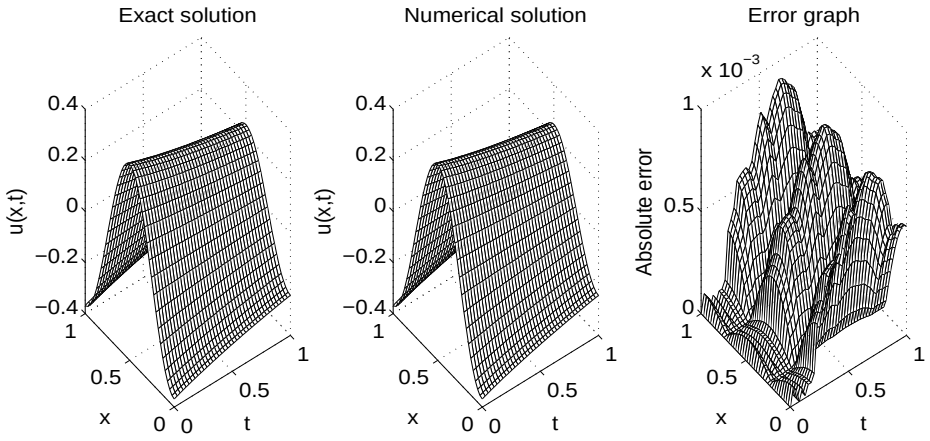

(b)

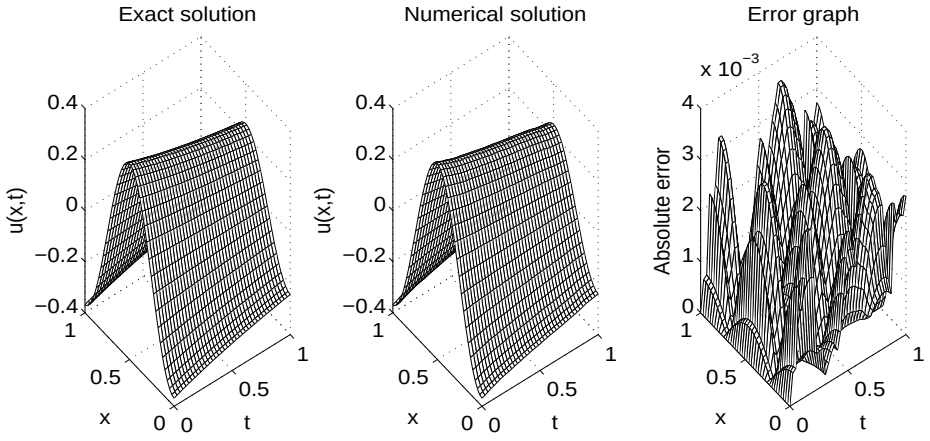

(c)

Figure 2.5: Exact and numerical solutions for $u(x,t)$, for Example 1 with (a) no noise, (b) $\rho = 2\%$ noise, and (c) $\rho = 20\%$ noise. The absolute error between them is also included.

2.6.2 Example 2

Consider the inverse problem (2.1)-(2.5) with $T = 1$ and the input data

$$u(x,0) = \varphi(x) = -\cos(2\pi x), \quad E(t) = -\left(1 + \left(\frac{1+t}{2\pi^2}\right)^{-1}\right) e^{-t^2-2t}, \tag{2.29}$$

and $\alpha = \beta = \gamma = 1$. As in Example 1, it is easy to check conditions (2.6a) and (2.6b) of Theorem 2.1 are satisfied, but the condition $1 < \alpha < \alpha_0 = 0.516$ is not satisfied, [56]. Hence, cannot conclude the uniqueness but, the solution at least exists and is given by

$$k(t) = \frac{1+t}{2\pi^2}, \quad u(x,t) = -\cos(2\pi x)\exp(-t^2 - 2t). \tag{2.30}$$

which can easily be verified by direct substitution.

The FDM numerical solution of the direct problem associated to this example has already been presented and discussed in Subsection 2.4.1. The uniqueness of solution (2.30) is not guaranteed from theory, but numerically we can at least investigate the obtained results from various initial guesses for the unknown diffusivity vector $\underline{k}$ which initiate the minimization of the objective function (2.21). This will also test the robustness of the iterative method with respect to the independence on the initial guess. This investigation is illustrated in Figures 2.6, 2.7 and Table 2.1 for exact data with various initial guesses

$$k^0(t) \in \{1/(2\pi^2), 1, 2\}, \quad t \in [0,1]. \tag{2.31}$$

Note that from (2.30) the initial guess $k^0(t) = 1/(2\pi^2)$ corresponds to the value of $k(0)$, which can be assumed to be known from (2.22). In Table 2.1, the root mean square error $rmse$ value of k is calculated as

$$rmse(k) = \sqrt{\frac{1}{N}\sum_{j=1}^{N}(k_j - k_{exact}(t_j))^2}. \tag{2.32}$$

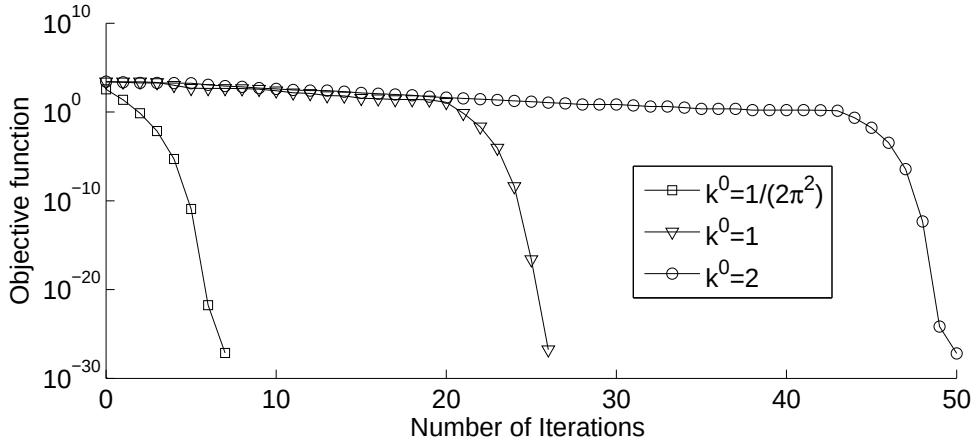

Figure 2.6: Objective function (2.21) for Example 2 with no noise and various initial guesses (2.31).

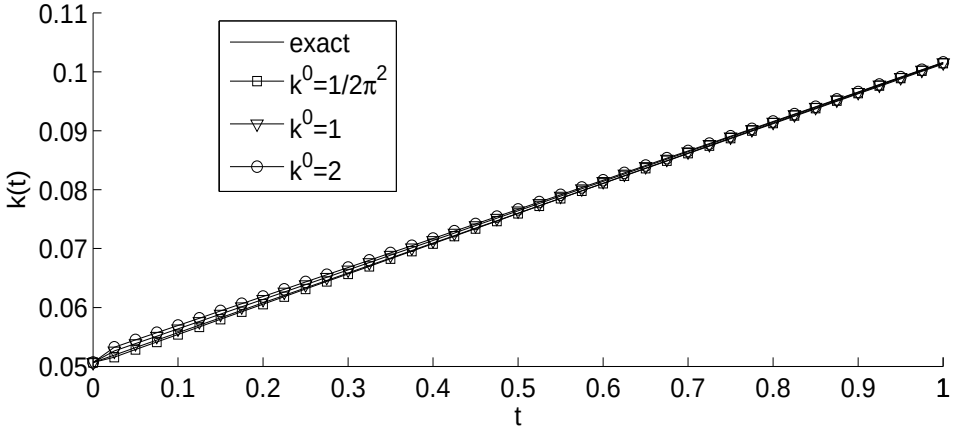

Figure 2.7: Exact and numerical solutions for $k(t)$, for Example 2 with no noise and various initial guesses (2.31).

Table 2.1: Number of iterations, number of function evaluations, value of the objective function (2.21) at final iteration, $rmse$ value (2.32) and the computational time, for Example 2 with no noise and various initial guesses (2.31).

$\rho = 0$	$k^0 = \frac{1}{2\pi^2}$	$k^0 = 1$	$k^0 = 2$
No. of iterations	7	26	50
No. function evaluations	336	1134	2142
Value of objective function (2.21) at final iteration	7.3E-28	1.7E-27	6.2E-28
$rmse(k)$	1.6E-4	4.4E-4	7.6E-4
Computational time	31 sec	105 sec	198 sec

From Figure 2.6 and Table 2.1 it can be seen that, as expected, the farther the initial guess is the more iterations and larger computational time are required to achieve convergence. However, for all initial guesses (2.31) the objective function (2.21) converges to the same minimum low value of $O(10^{-28})$. This shows robustness with respect to the independence on the initial guess. Furthermore, from Figure 2.7 and Table 2.1 it can be seen that the agreement between the exact and the numerically obtained solutions with various initial guesses is very good being of $O(10^{-4})$. There is also a slightly better accuracy for the closer initial guess $k^0 = 1/(2\pi^2)$ to the exact solution for $k(t)$ from (2.30).

In what follows, we take the initial guess for the unknown diffusivity $k(t)$ equal to the constant $k(0) = 1/(2\pi^2)$ which is known from expression (2.22).

Figure 2.8 shows the objective function (2.21) for $\rho \in \{0, 1\%\}$ as a function of the number of iterations. From this figure, it can be seen that the objective functional (2.21) decreases rapidly to a very low level of $O(10^{-28})$ in about 7 to 8 iterations. The corresponding exact and numerical solutions for $k(t)$ and $u(x,t)$ are presented in Figures 2.9 and 2.10, respectively. First, from Figures 2.5 and 2.10 it can be observed that accurate and stable solutions for $u(x,t)$ are obtained for both Examples 1 and 2. Secondly, for exact data, i.e. $\rho = 0$, the same conclusion regarding the excellent accuracy of the numerical solution for $k(t)$, as it was obtained for Example 1, can be drawn from Figure 2.4. However, for $\rho = 1\%$ noisy data some instability starts to manifest in Figure 2.9, as it also happened for Example 1 in Figure 2.4 for a much larger $\rho = 20\%$ amount of noise.

We also mention that for higher amounts of noise, such as $\rho = 2\%$, the *lsqnonlin* minimization routine did not make significant progress after a large number of over 1000 iterations probably becoming trapped in a local minimum. One possible reason could be that the expressions for $k(t)$ given by equations (2.28) and (2.30) yield a stronger nonlinearity in $k^{-\gamma}(t)$ in (2.20) for Example 2 than for Example 1.

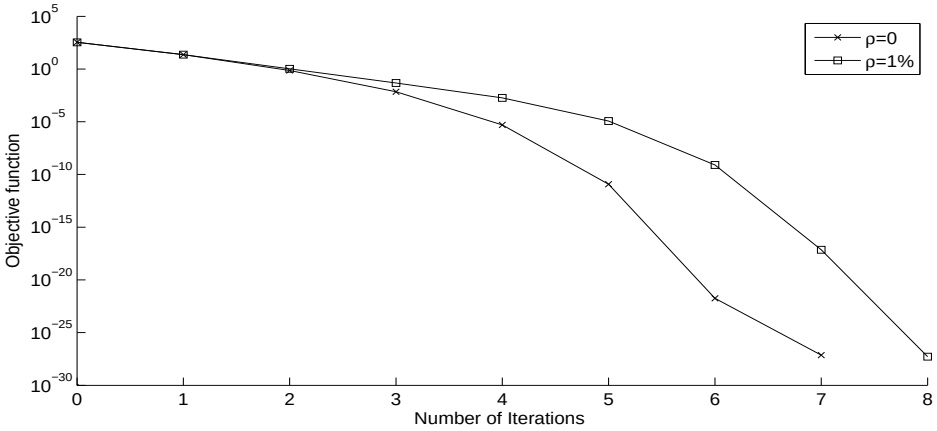

Figure 2.8: Objective function (2.21), for Example 2 with $\rho \in \{0, 1\%\}$ noise.

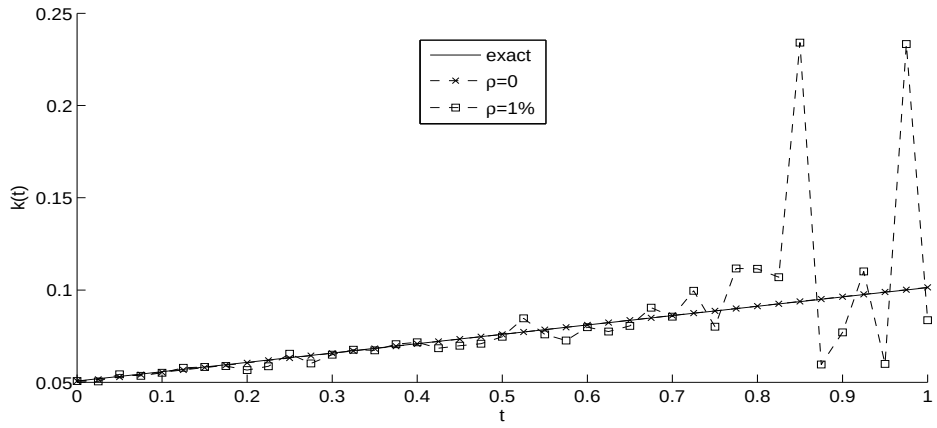

Figure 2.9: Exact and numerical solutions for $k(t)$, for Example 2 with $\rho \in \{0, 1\%\}$ noise.

2.6.3 Example 3

The previous examples possessed analytical solutions available for the pair $(k(t), u(x,t))$, as given by equations (2.28) and (2.30). In this subsection, we investigate an example for which an explicit analytical solution for $u(x,t)$ is not available. We take the initial condition (2.2) given by

$$u(x,0) = \varphi(x) = \begin{cases} 0, & 0 \leq x < 1/4, \\ \frac{1}{4} - x, & 1/4 < x \leq 1/2, \\ x - \frac{3}{4}, & 1/2 < x < 3/4, \\ 0, & 3/4 < x \leq 1. \end{cases} \tag{2.33}$$

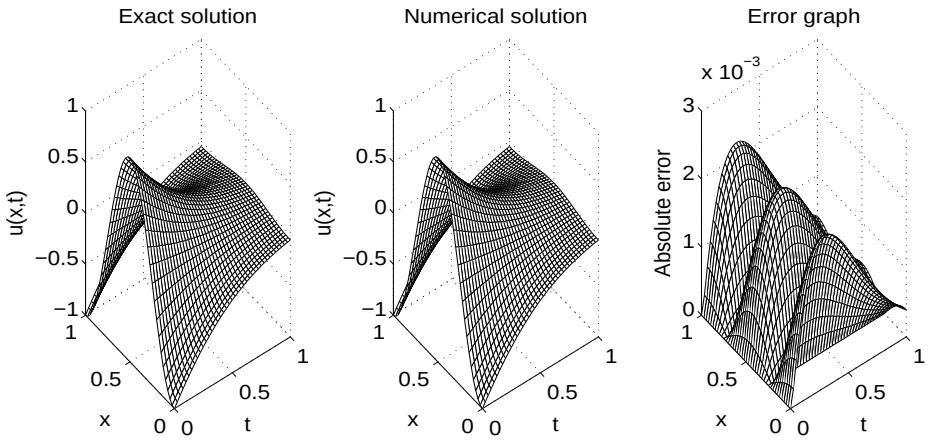

(a)

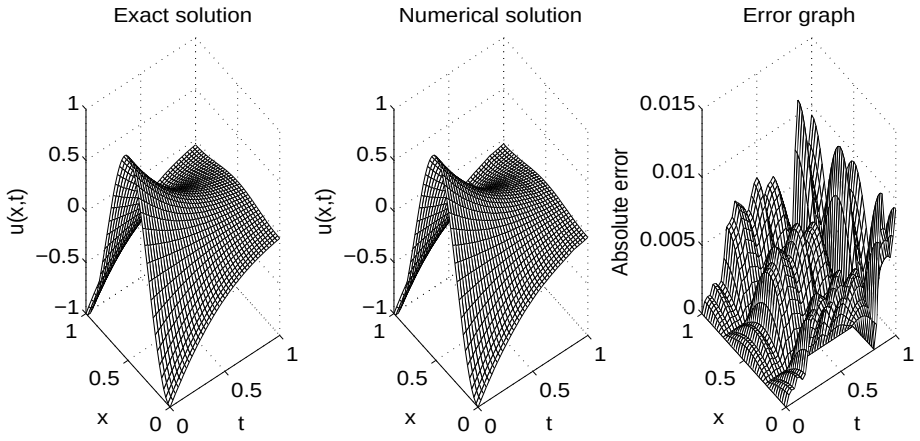

(b)

Figure 2.10: Exact and numerical solutions for $u(x,t)$, for Example 2 with (a) no noise, and (b) $\rho = 1\%$ noise. The absolute error between them is also included.

This is severe test example because the initial data (2.33) is non-smooth function. Clearly, the initial data (2.33) violates some of the conditions of Theorem 2.1 which is not applicable for this example. However, we can make the inverse problem at least solvable by solving first the direct well-posed problem (2.1)–(2.4) with $\varphi(x)$ given by (2.33) and the diffusivity $k(t)$ given by

$$k(t) = \frac{1}{1+t}, \quad t \in [0,1], \tag{2.34}$$

in order to provide the data (2.5). This is performed numerically using FDM described in Section 2.4.

The numerical results for $E(t)$ (with $\alpha = \beta = \gamma = 1$) are shown in Figure 2.11, for various mesh sizes $M = N \in \{20, 40, 80\}$. From this figure it can be seen that that numerical solution is convergent as the FDM mesh sizes decreases. Also, there is only a small difference between the numerical results obtained

with various mesh sizes showing that the independence on the mesh has been achieved. Consequently, we take the results for $E(t)$ simulated from solving the direct problem with $M = N = 80$ as our exact input data (2.5) in the inverse problem (2.1)–(2.5). In order to avoid committing an inverse crime, in the inverse problem the number of space intervals is taken as $M = 70$ (different than 80), whilst the number of time steps N is kept the same 80.

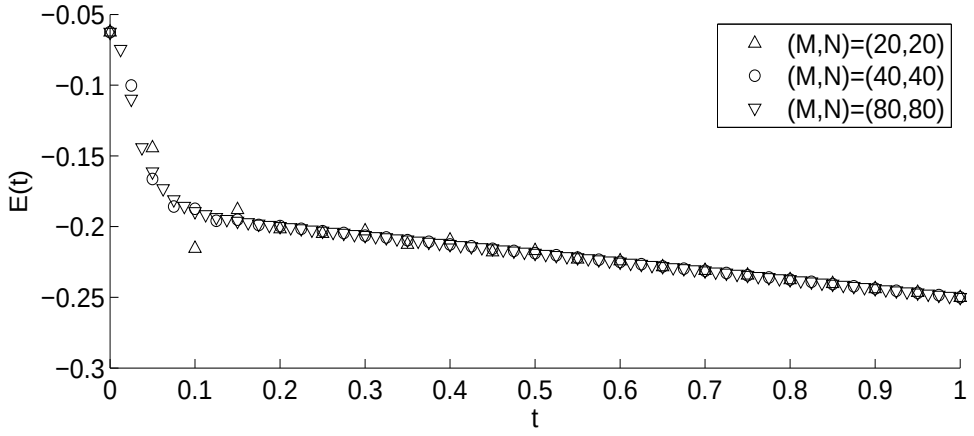

Figure 2.11: Numerical solution for $E(t)$, for the direct problem of Example 3 with various mesh sizes.

We take the initial guess $k^0 = 1$, noting at the same time that since $\varphi(0) = 0$ and $E(0) = -1/16$ equation (2.22) cannot be directly applied as it yields the non-determination $0/0$ division.

Figure 2.12 shows the objective function evolution (2.21), as a function of the number of iterations for no noise in the input data (2.5). From this figure it can be seen that a fast convergence is achieved in 20 iterations to reach a very low value of $O(10^{-12})$. The associated numerically obtained results for $k(t)$ are presented in Figure 2.13. From this figure it can be seen that the agreement between the numerical and the exact solutions is excellent, except for some slight unexpected discrepancy near $t = 0$.

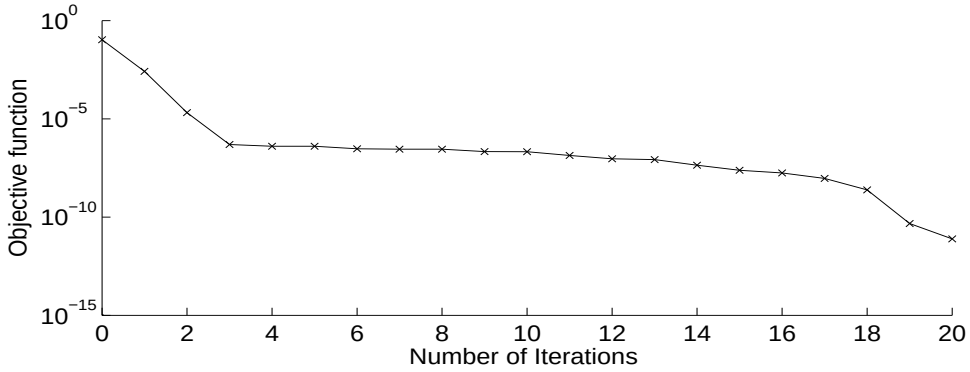

Figure 2.12: Objective function (2.21), for Example 3 with no noise.

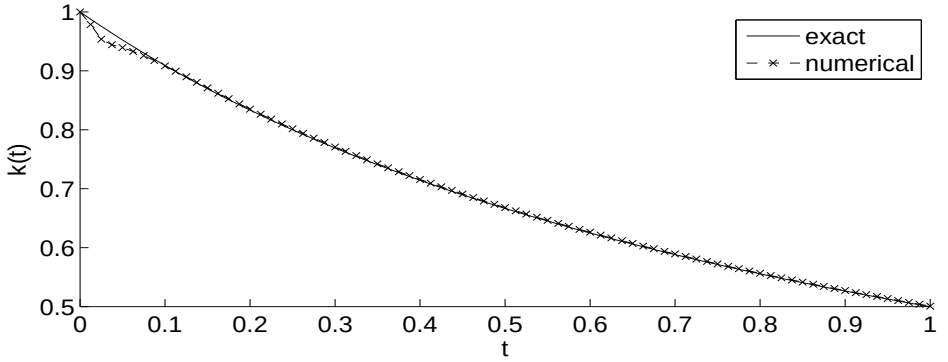

Figure 2.13: Exact and numerical solutions for $k(t)$, for Example 3 with no noise.

Next we add $\rho = 1\%$ noise in the input data (2.5) numerically simulated as in (2.23). Figure 2.14(a) presents the objective function (2.21), as a function of the number of iterations together with the horizontal noise threshold ϵ^2=7.05E-4 computed by (2.26). This threshold is useful when applying the discrepancy principle in order to stop the iteration process before the instability of solutions sets in. According to Figure 2.14(a) this criterion yields the iteration number $\text{iter}_{discr.} = 2$. Figure 2.14(a) also shows that the objective function (2.21) has converged after $\text{iter}_{conv.} = 38$ iterations. The $rmse(k)$ values (2.32) for unknown $k(t)$ are plotted, versus the number of iterations in Figure 2.14(b). Form this figure it can be remarked that the best retrieval occurs at $\text{iter}_{opt.} = 6$. For more clarity, the results of Figure 2.14 are summarised in Table 2.2 where the computational time is also included.

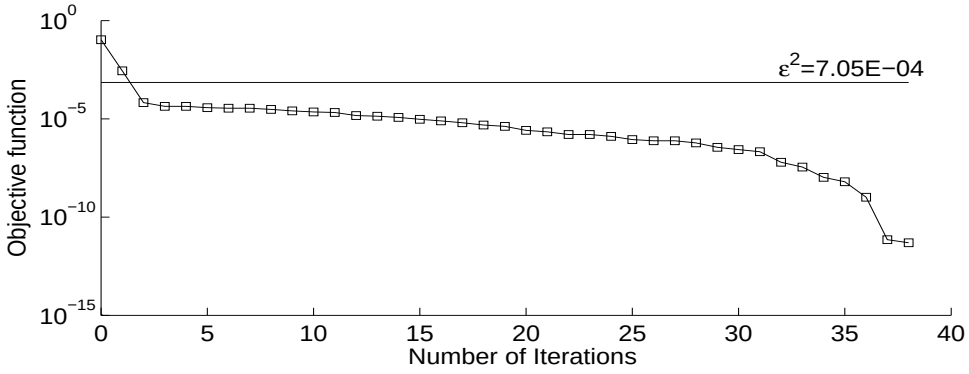

(a)

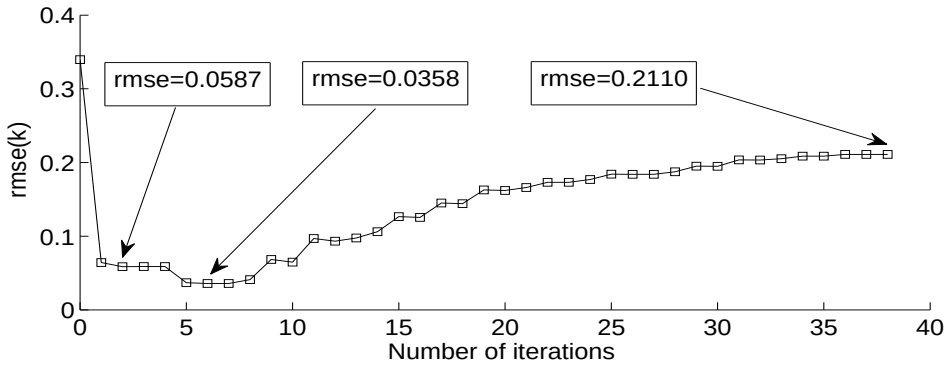

(b)

Figure 2.14: (a) Objective function (2.21) with horizontal noise threshold ϵ^2=7.05E-4, and (b) the $rmse(k)$ values (2.32), for Example 3 with $\rho = 1\%$ noise.

Finally, Figure 2.15 shows the exact solution (2.34) for $k(t)$ in comparison with the numerical solutions obtained at the iterations given by stopping criteria of Table 2.2. From this figure it can be seen that if the iterative process is not stopped, after $\text{iter}_{conv.} = 38$ iterations we obtain a numerical approximation with $rmse(k) = 0.2110$ which moreover is not so accurate in the region $t \in [0, 0.2]$. However, if we stop the iterative process after $\text{iter}_{discr.} = 2$ iterations given by the discrepancy principle, which is graphically illustrated in Figure 2.14(a), then an accurate and stable numerical solution is achieved. Moreover, it yields an $rmse(k) = 0.0587$ which is close to the optimal one of $rmse(k) = 0.0358$.

Table 2.2: The number of iterations, the $rmse(k)$ values (2.32) and the computational time based on several stopping criteria, for Example 3 with $p = 1\%$ noise.

Criterion	No. of iterations	$rmse(k)$	Computational time
to achieve convergence	$\text{iter}_{conv.} = 38$	0.2110	41 min
to achieve minimum $rmse(k)$	$\text{iter}_{opt.} = 6$	0.0358	8 min
discrepancy principle	$\text{iter}_{discr.} = 2$	0.0587	3 min

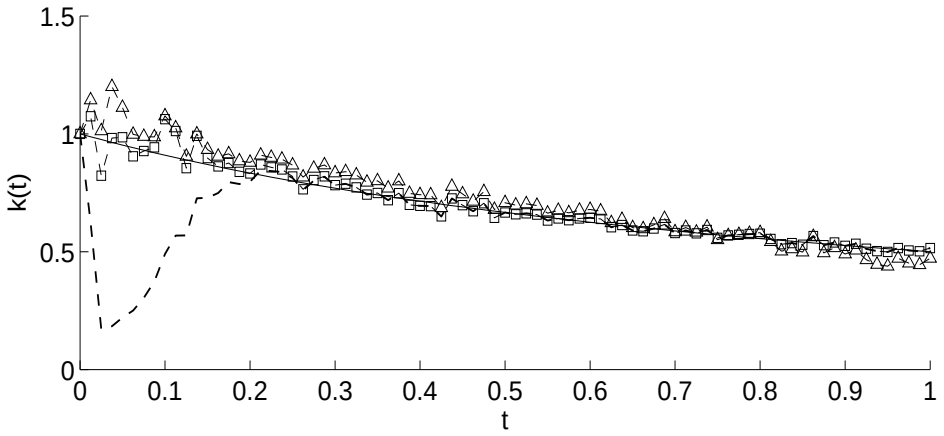

Figure 2.15: Exact (—) and the numerical solutions for $k(t)$ obtained after $\text{iter}_{conv.}$=38 (- - -), $\text{iter}_{opt.}$=6 (-□-), and $\text{iter}_{discr.}$=2 (-△-), for Example 3 with $\rho = 1\%$ noise.

2.7 Conclusions

An inverse nonlinear problem which requires identifying the time-dependent diffusivity with periodic boundary condition and non-local boundary measurement has been investigated. Numerically, the resulting inverse problem has been reformulated as a nonlinear least-squares optimization problem which has been solved using the MATLAB toolbox routine *lsqnonlin*. Numerical results show that accurate, robust and reasonably stable solutions have been obtained. This problem seems rather stable and hence, in general, no regularization was found necessary to be employed. However, for more severe examples which violate the sufficient conditions under which the well-posedness of the inverse problem hold, as expected, some regularization needs to be applied. For example, in Subsection 2.6.3 for the minimization of the *lsqnonlin* routine used, the discrepancy principle has been applied in order to terminate the iterative process before instability sets in and this, in turn, has produced a stable and accurate numerical solution.

Chapter 3

Identification of the time-dependent conductivity of an inhomogeneous diffusive material

3.1 Introduction

In this chapter, we consider the reconstruction of the time-dependent multiplier of the highest-order derivative in the parabolic heat equation. Physically, in heat transfer this unknown thermal property coefficient corresponds to the thermal conductivity of an inhomogeneous heat conductor which has a space-varying known heat capacity. It is this later physically realistic feature that makes some of the methods of previous studies [19, 62, 63, 125] of time-dependent thermal diffusivity identification inapplicable. The same problem can be formulated in porous media by replacing the thermal properties with the corresponding hydraulic ones.

With respect to what boundary conditions are specified and what additional measurements are performed, the mathematical formulations of two inverse problems are given in Section 3.2. In that section, we also recall the previous well-posedness results of [70, Section 4.3] and [54]. A numerical method based on the Crank-Nicholson finite-difference scheme is employed as direct solver in a nonlinear least-squares minimization, as described in Sections 3.3 and 3.4, respectively. This combination yields accurate and stable numerical solutions, as it will be discussed in Section 3.5. Finally, the conclusions of this chapter are highlighted in Section 3.6.

3.2 Mathematical formulation

Let $L > 0$ and $T > 0$ be fixed numbers and consider the inverse problem of finding the time-dependent thermal conductivity $C[0,T] \ni a(t) > 0$ for $t \in [0,T]$, and the temperature $u(x,t) \in C^{2,1}(Q_T) \cap C^{1,0}(\overline{Q}_T)$, which satisfy the heat equation

$$c(x)u_t(x,t) = a(t)u_{xx}(x,t) + F(x,t), \quad (x,t) \in Q_T := (0,L) \times (0,T), \tag{3.1}$$

where $c(x) > 0$ is the heat capacity and F is a heat source, the initial condition

$$u(x,0) = \phi(x), \qquad x \in [0,L], \tag{3.2}$$

the Dirichlet boundary conditions

$$u(0,t) = \mu_1(t), \qquad u(L,t) = \mu_2(t), \qquad t \in [0,T], \tag{3.3}$$

and the heat flux additional measurement

$$-a(t)u_x(0,t) = \mu_3(t), \qquad t \in [0,T]. \tag{3.4}$$

Dividing equation (3.1) by $c(x)$ and denoting

$$b(x) = \frac{1}{c(x)}, \quad f(x,t) = \frac{F(x,t)}{c(x)} \tag{3.5}$$

we obtain

$$u_t(x,t) = a(t)b(x)u_{xx}(x,t) + f(x,t), \qquad (x,t) \in Q_T. \tag{3.6}$$

3.2.1 Inverse Problem I

The above inverse problem (termed Inverse Problem I) was previously investigated theoretically in Section 4.3 of [70] where its unique solvability has been established, as follows.

Theorem 3.1. (Existence of solution of Inverse Problem I)
Suppose that the following conditions hold:

1. *(regularity conditions)* $b \in C^1[0,L]$, $\phi \in C^1[0,L]$, $\mu_i \in C^1[0,T]$ *for* $i = 1,2$, $\mu_3 \in C[0,T]$, $f \in C^{1,0}(\overline{Q}_T)$;

2. *(compatibility conditions)* $\phi(0) = \mu_1(0)$, $\phi(L) = \mu_2(0)$.

3. *(non-vanishing and monotonicity conditions)* $\phi'(x) > 0$, $b(x) > 0$, $b'(x) \leq 0$ *for* $x \in [0, L]$, $\mu_3(t) < 0$, $\mu_1'(t) - f(0,t) \leq 0$, $\mu_2'(t) - f(L,t) \geq 0$ *for* $t \in [0, T]$, $f_x(x,t) \geq 0$ *for* $(x,t) \in \overline{Q}_T$;

Then there exists a solution to the inverse problem (3.2)–(3.4) and (3.6).

Theorem 3.2. (Uniqueness of solution of Inverse Problem I)
If $b \in C^1[0, L]$, $b(x) > 0$ *for* $x \in [0, L]$, $\mu_3(t) \neq 0$ *for* $t \in [0, T]$, *then the solution of the inverse problem (3.2)–(3.4) and (3.6) is unique.*

Next, we address the stability of solution, as given by the following theorem proved in [54].

Theorem 3.3. (Local stability of solution of Inverse Problem I)
Suppose that the conditions of Theorem 3.1 are satisfied. Let μ_3 *and* $\tilde{\mu}_3$ *be two data in (3.4) and let* $(a(t), u(x,t))$ *and* $(\tilde{a}(t), \tilde{u}(x,t))$ *be the corresponding solutions of the inverse problem (3.2)–(3.4) and (3.6). Then, for sufficiently small* T, *the following local stability estimate holds:*

$$\|a - \tilde{a}\|_{C[0,T]} \leq C \|\mu_3 - \tilde{\mu}_3\|_{C[0,T]}, \tag{3.7}$$

for some positive constant C.

Later on, in the numerical results of Section 3.5, the well-posedness of the Inverse Problem I established in Theorems 3.1–3.3 will be highlighted through the fact that no regularization is needed for obtaining a stable and accurate numerical solution.

3.2.2 Inverse Problem II

For completeness, we also investigate another related inverse problem (termed Inverse Problem II) which requires the determination of the thermal conductivity $C[0, T] \ni a(t) > 0$ for $t \in [0, T]$ and the temperature $u(x,t) \in C^{2,1}(\overline{Q}_T)$, which satisfy the heat equation (3.6), the initial condition (3.2), the Neumann boundary conditions

$$-u_x(0,t) = \nu_1(t), \qquad u_x(L,t) = \nu_2(t), \qquad t \in [0, T], \tag{3.8}$$

and the boundary temperature additional measurement

$$u(0,t) = \mu_1(t), \qquad t \in [0, T]. \tag{3.9}$$

This inverse problem was also previously investigated in Section 4.3 of [70], where its unique solvability has been established, as follows.

Theorem 3.4. (Existence of solution of Inverse Problem II)
Suppose that the following conditions hold:

1. $b \in C^2[0,L]$, $\phi \in C^2[0,L]$, $\nu_i \in C^1[0,T]$, $i = 1,2$, $\mu_1 \in C^1[0,T]$, $f \in C^{1,0}(\overline{Q}_T)$;

2. $b(x) > 0$, $\phi'(x) \geq 0$, $(\phi'(x)\sqrt{b(x)})' > 0$, $b'(x) \leq 0$, $b''(x) \leq 0$ *for* $x \in [0,L]$; $\nu_1(t) \leq 0$, $\nu_2(t) \geq 0$, $\mu_1'(t) - f(0,t) > 0$, $f_x(0,t) + \mu_1'(t) \geq 0$, $\nu_2'(t) - f_x(L,t) \geq 0$ *for* $t \in [0,T]$; $f_x(x,t) \geq 0$, $(f_x(x,t)\sqrt{b(x)})_x \geq 0$ *for* $(x,t) \in \overline{Q}_T$;

3. $\phi'(0) = -\nu_1(0)$, $\phi'(L) = \nu_2(0)$, $\phi(0) = \mu_1(0)$.

Then there exists a solution to the inverse problem (3.2), (3.6), (3.8) and (3.9).

Theorem 3.5. (Uniqueness of solution of Inverse Problem II)
If $b \in C^1[0,L]$, $b(x) > 0$ *for* $x \in [0,L]$, $\mu_1'(t) - f(0,t) \neq 0$ *for* $t \in [0,T]$, *then the solution of the inverse problem (3.2), (3.6), (3.8) and (3.9) is unique.*

The next stability theorem was proved in [54].

Theorem 3.6. (Local stability of solution of Inverse Problem II)
Suppose that the conditions of Theorem 3.4 are satisfied. Let μ_1 *and* $\tilde{\mu}_1$ *be two data in (3.9) and let* $(a(t), u(x,t))$ *and* $(\tilde{a}(t), \tilde{u}(x,t))$ *be the corresponding solutions of the inverse problem (3.2), (3.6), (3.8) and (3.9). Then for sufficiently small* T, *the following local stability estimate holds:*

$$\|a - \tilde{a}\|_{C[0,T]} \leq C\|\mu_1 - \tilde{\mu}_1\|_{C^1[0,T]}, \tag{3.10}$$

for some positive constant C.

Note that unlike Inverse Problem I, in the Inverse Problem II, the estimate (3.10) involves the derivatives of the noisy functions μ_1 and $\tilde{\mu}_1$ which in itself is an unstable procedure which needs to be regularized.

We finally mention that another related inverse formulation given by equations (3.2), (3.3), (3.6) and the additional measurement

$$-u_x(0,t) = \nu_1(t), \quad t \in [0,T] \tag{3.11}$$

has been investigated in [65]. The choice of additional measurements (3.4), or (3.9), or (3.11), is important for the inverse problem formulation, as it contains the richness of the information supplied in order to retrieve more effectively the unknown time-dependent conductivity.

3.3 Solution of direct problems

3.3.1 The Dirichlet direct problem

In this section, we consider the direct (the inverse of the Inverse Problem I) initial Dirichlet boundary value problem given by equations (3.2), (3.3) and (3.6), where $a(t)$, $b(x)$, $f(x,t)$, $\phi(x)$ and $\mu_i(t)$, $i = 1, 2$, are known and the temperature $u(x,t)$ is the solution to be determined. We use the FDM described in Section 2.4.

The discrete form of the direct problem (3.2), (3.3) and (3.6) is as follows. We subdivide the domain $Q_T = (0, L) \times (0, T)$ into $M \times N$ subintervals of equal step length $\Delta x = L/M$ and $\Delta t = T/N$. At the node (i, j) we denote $u_{i,j} = u(x_i, t_j)$, $a(t_j) = a_j$, $b(x_i) = b_i$ and $f(x_i, t_j) = f_{i,j}$, where $x_i = i\Delta x$, $t_j = j\Delta t$ for $i = \overline{0, M}$, $j = \overline{0, N}$.

The Crank-Nicolson FDM for the general partial differential equation (2.8) is

$$\frac{u_{i,j+1} - u_{i,j}}{\Delta t} = \frac{1}{2}\left(G_{i,j} + G_{i,j+1}\right), \quad i = \overline{1, (M-1)},\ j = \overline{0, (N-1)}, \tag{3.12}$$

where

$$G_{i,j} = G\left(x_i, t_j, \frac{u_{i+1,j} - 2u_{i,j} + u_{i-1,j}}{(\Delta x)^2}\right),\ i = \overline{1, (M-1)},\ j = \overline{0, (N-1)}. \tag{3.13}$$

Equation (3.12) has to be solved subject to the discretised form of equations (3.2) and (3.3), namely,

$$u_{i,0} = \phi(x_i), \qquad i = \overline{0, M}, \tag{3.14}$$

$$u_{0,j} = \mu_1(t_j), \qquad u_{M,j} = \mu_2(t_j), \qquad j = \overline{0, N}. \tag{3.15}$$

For our problem, equation (3.6) can be discretised in the form of (3.12) as

$$\begin{aligned} &- C_{i,j+1}u_{i-1,j+1} + (1 + B_{i,j+1})u_{i,j+1} - C_{i,j+1}u_{i+1,j+1} \\ &\qquad = C_{i,j}u_{i-1,j} + (1 - B_{i,j})u_{i,j} + C_{i,j}u_{i+1,j} + \frac{\Delta t}{2}\left(f_{i,j} + f_{i,j+1}\right) \end{aligned} \tag{3.16}$$

for $i = \overline{1, (M-1)}$, $j = \overline{0, (N-1)}$, where

$$C_{i,j} = \frac{(\Delta t)a_j b_i}{2(\Delta x)^2}, \qquad B_{i,j} = \frac{(\Delta t)a_j b_i}{(\Delta x)^2}.$$

At each time step t_{j+1} for $j = \overline{0, (N-1)}$, using the Dirichlet boundary conditions (3.15), the difference equation (3.16) can be reformulated as a $(M-1) \times (M-1)$

system of linear equations of the form,

$$D\mathbf{u}_{j+1} = E\mathbf{u}_j + \mathbf{b}, \tag{3.17}$$

where

$$\mathbf{u}_{j+1} = (u_{1,j+1}, u_{2,j+1}, ..., u_{M-1,j+1})^{\mathrm{T}},$$

$$D = \begin{pmatrix} 1+B_{1,j+1} & -C_{1,j+1} & 0 & \cdots & 0 & 0 & 0 \\ -C_{2,j+1} & 1+B_{2,j+1} & -C_{2,j+1} & \cdots & 0 & 0 & 0 \\ \vdots & \vdots & \vdots & \ddots & \vdots & \vdots & \vdots \\ 0 & 0 & 0 & \cdots & -C_{M-2,j+1} & 1+B_{M-2,j+1} & -C_{M-2,j+1} \\ 0 & 0 & 0 & \cdots & 0 & -C_{M-1,j+1} & 1+B_{M-1,j+1} \end{pmatrix},$$

$$E = \begin{pmatrix} 1-B_{1,j} & C_{1,j} & 0 & \cdots & 0 & 0 & 0 \\ C_{2,j} & 1-B_{2,j} & C_{2,j} & \cdots & 0 & 0 & 0 \\ \vdots & \vdots & \vdots & \ddots & \vdots & \vdots & \vdots \\ 0 & 0 & 0 & \cdots & C_{M-2,j} & 1-B_{M-2,j} & C_{M-2,j} \\ 0 & 0 & 0 & \cdots & 0 & C_{M-1,j} & 1-B_{M-1,j} \end{pmatrix},$$

and

$$\mathbf{b} = \begin{pmatrix} \frac{\Delta t}{2}(f_{1,j} + f_{1,j+1}) + C_{1,j+1}\mu_1(t_j) \\ \frac{\Delta t}{2}(f_{2,j} + f_{2,j+1}) \\ \vdots \\ \frac{\Delta t}{2}(f_{M-2,j} + f_{M-2,j+1}) \\ \frac{\Delta t}{2}(f_{M-1,j} + f_{M-1,j+1}) + C_{M-1,j+1}\mu_2(t_j) \end{pmatrix}.$$

3.3.1.1 Example

As an example, consider the direct problem (3.2), (3.3) and (3.6) with $T = L = 1$ and

$$\begin{aligned} a(t) = 1 + t, \quad b(x) = 2 - x^2, \quad \phi(x) = u(x,0) = x + \sin(x), \\ \mu_1(t) = u(0,t) = 8t, \quad \mu_2(t) = u(1,t) = 1 + \sin(1) + 8t, \\ f(x,t) = 8 + (1+t)(2-x^2)\sin(x). \end{aligned}$$

The exact solution is given by

$$u(x,t) = x + \sin(x) + 8t \tag{3.18}$$

and the desired heat flux output (3.4) is

$$\mu_3(t) = -a(t)u_x(0,t) = -2 - 2t. \tag{3.19}$$

The numerical and exact solutions for the temperature $u(x,t)$ at interior points are shown in Figure 3.1 and one can observe that an excellent agreement is obtained. Figure 3.2 shows the numerical solution in comparison with the exact one for $\mu_3(t)$ and the curves look indistinguishable. The x-partial derivative of $u(x,t)$ at $x = 0$ has been evaluated using the following $O(h^2)$ finite-difference approximation formula:

$$u_x(0,t_j) = \frac{4u_{1,j} - u_{2,j} - 3u_{0,j}}{2(\Delta x)}, \qquad j = \overline{0,N}. \tag{3.20}$$

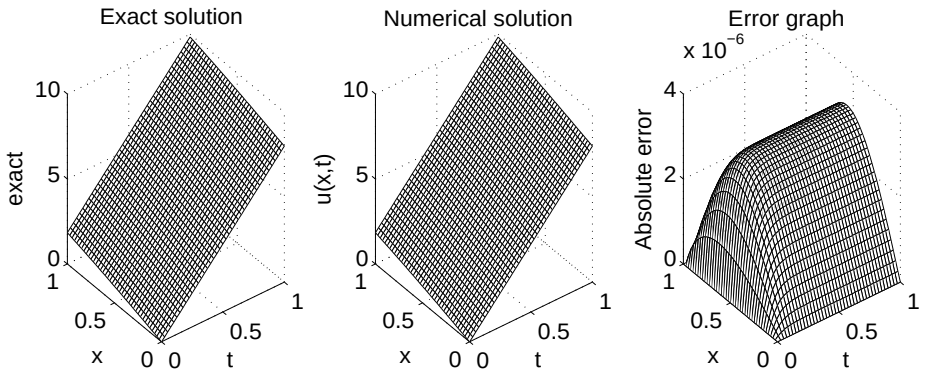

Figure 3.1: Exact and numerical solutions for the temperature $u(x,t)$ and the absolute error for the Dirichlet direct problem obtained with $M = N = 40$.

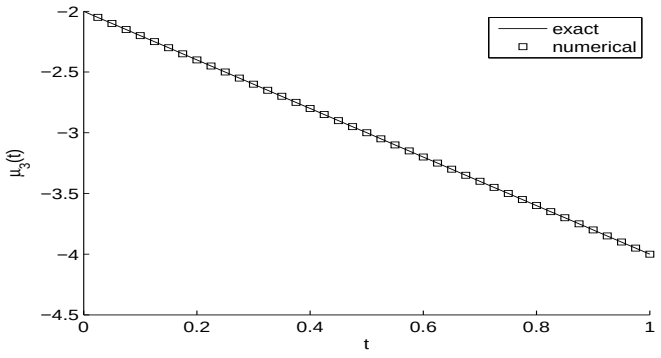

Figure 3.2: Exact and numerical solutions for the heat flux $\mu_3(t)$ of the Dirichlet direct problem obtained with $M = N = 40$.

3.3.2 The Neumann direct problem

The FDM analysis for the direct (the inverse of the Inverse Problem II) initial Neumann boundary value problem given by equations (3.2), (3.6) and (3.8) is similar to that of direct Dirichlet problem of previous subsection. In this case, we discretise equations (2.8), (3.2) and (3.8) as:

$$\frac{u_{i,j+1}-u_{i,j}}{\Delta t}=\frac{1}{2}\left(G_{i,j}+G_{i,j+1}\right), \qquad i=\overline{0,M},\ j=\overline{0,(N-1)}, \tag{3.21}$$

$$u_{i,0}=\phi(x_i), \qquad i=\overline{0,M}, \tag{3.22}$$

$$u_{-1,j}-u_{1,j}=-2(\Delta x)\nu_1(t_j),\ u_{M+1,j}-u_{M-1,j}=2(\Delta x)\nu_2(t_j),\ j=\overline{1,N}, \tag{3.23}$$

where $G_{i,j}$ is given by (3.13), and $u_{-1,j}$ and $u_{M+1,j}$ for $j=\overline{1,N}$ are fictitious values at points located outside the computational domain. Equations (3.21) can be rewritten in the form of the system (3.16) for $i=\overline{0,M}$, $j=\overline{0,(N-1)}$. At each time step t_{j+1} for $j=\overline{0,(N-1)}$, using the Neumann boundary conditions (3.23), we obtain a $M\times M$ system of linear equations of the form,

$$\tilde{D}\tilde{\mathbf{u}}_{j+1}=\tilde{E}\tilde{\mathbf{u}}_j+\tilde{\mathbf{b}}, \tag{3.24}$$

where

$$\tilde{\mathbf{u}}_{j+1}=(u_{0,j+1},u_{1,j+1},...,u_{M,j+1})^{\mathrm{T}},$$

$$\tilde{D}=\begin{pmatrix} 1+B_{0,j+1} & -2C_{0,j+1} & 0 & \cdots & 0 \\ -C_{1,j+1} & & & & 0 \\ 0 & & D & & \vdots \\ \vdots & & & & -C_{M-1,j+1} \\ 0 & \cdots & 0 & -2C_{M,j+1} & 1+B_{M,j+1} \end{pmatrix},$$

$$\tilde{E}=\begin{pmatrix} 1-B_{0,j} & 2C_{0,j} & 0 & \cdots & 0 \\ C_{1,j} & & & & 0 \\ 0 & & E & & \vdots \\ \vdots & & & & C_{M-1,j} \\ 0 & \cdots & 0 & 2C_{M,j} & 1-B_{M,j} \end{pmatrix},$$

and

$$\tilde{\mathbf{b}} = \begin{pmatrix} \frac{\Delta t}{2}(f_{0,j} + f_{0,j+1}) - 2(\Delta x)(C_{0,j}\nu_1(t_j) + C_{0,j+1}\nu_1(t_{j+1})) \\ \frac{\Delta t}{2}(f_{1,j} + f_{1,j+1}) \\ \vdots \\ \frac{\Delta t}{2}(f_{M-1,j} + f_{M-1,j+1}) \\ \frac{\Delta t}{2}(f_{M,j} + f_{M,j+1}) + 2(\Delta x)(C_{M,j}\nu_2(t_j) + C_{M,j+1}\nu_2(t_{j+1})) \end{pmatrix}.$$

In the above expressions the matrices $\tilde{D}$ and $\tilde{E}$ contain the matrices D and E of the Dirichlet direct problem defined in subsection 3.3.1.

3.3.2.1 Example

As an example, consider the direct problem (3.2), (3.6) and (3.8) with $T = L = 1$ and

$$\begin{aligned} a(t) = 1 + t, \quad b(x) = 2 - x^2, \quad \phi(x) = u(x,0) = x + \sin(x), \\ \nu_1(t) = -u_x(0,t) = -2, \quad \nu_2(t) = u_x(1,t) = 1 + \cos(1), \\ f(x,t) = 8 + (1+t)(2-x^2)\sin(x). \end{aligned}$$

The exact solution is given by (3.18) and the desired boundary temperature output (3.9) is

$$\mu_1(t) = u(0,t) = 8t. \tag{3.25}$$

The numerical and exact solutions for the temperature $u(x,t)$ at interior points are shown in Figure 3.3 and one can observe that an excellent agreement is obtained. Figure 3.4 shows excellent agreement between the numerical solution and the exact one for $\mu_1(t)$.

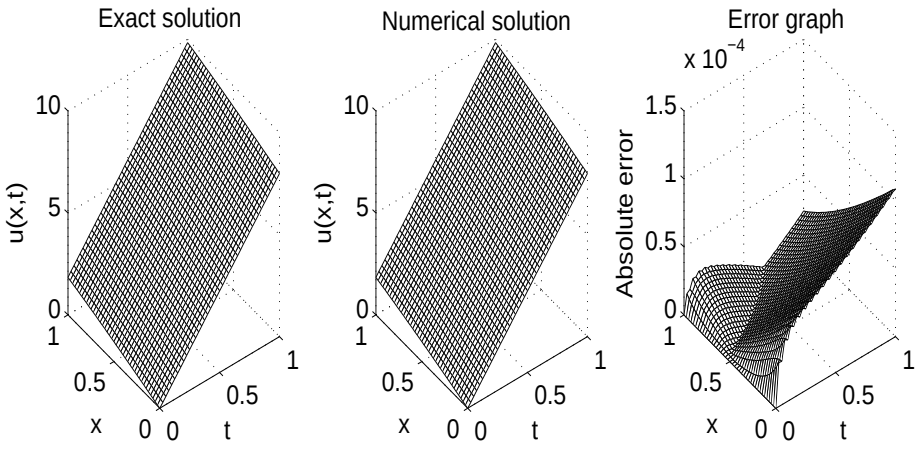

Figure 3.3: Exact and numerical solutions for the temperature $u(x,t)$ and the absolute error for the Neumann direct problem obtained with $M = N = 40$.

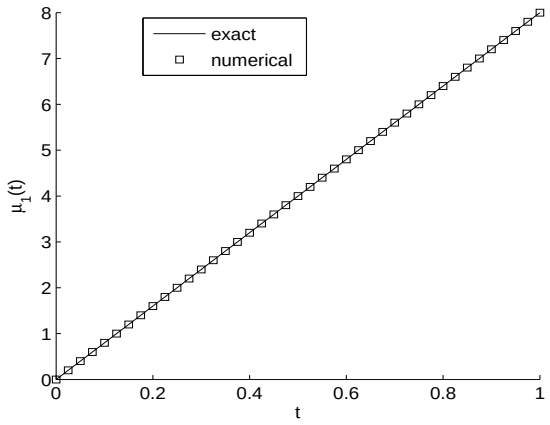

Figure 3.4: Exact and numerical solutions for $\mu_1(t)$ of the direct Neumann problem obtained with $M = N = 40$.

3.4 Solution of inverse problems

We wish to obtain stable and accurate reconstructions of the time-dependent thermal conductivity $a(t)$ and the temperature $u(x,t)$ satisfying the equations (3.2)–(3.4) and (3.6) for Inverse Problem I, and equations (3.2), (3.6), (3.8) and (3.9) for Inverse Problem II.

The most common approach based on imposing the measurement (3.4) or (3.9) in a least-squares sense, is minimizing

$$F_I(a) := \big\|a(t)u_x(0,t) + \mu_3(t)\big\|^2 + \beta\big\|a(t)\big\|^2, \tag{3.26}$$

for Inverse Problem I, and

$$F_{II}(a) := \left\|u(0,t) - \mu_1(t)\right\|^2 + \beta\left\|a(t)\right\|^2, \tag{3.27}$$

for Inverse Problem II, where $\beta \geq 0$ is a regularization parameter to be prescribed and the norm is usually the $L^2[0,T]$-norm. In (3.26) or (3.27) we have added the penalty term $\beta\left\|a(t)\right\|^2$ in order to alleviate any instability that may arise from the inverse coefficient problem being ill-posed.

The discretization of (3.26) and (3.27) yields

$$F_I(\underline{a}) = \sum_{j=0}^{N}\Big[a_j u_x(0,t_j) + \mu_3(t_j)\Big]^2 + \beta\sum_{j=0}^{N} a_j^2, \tag{3.28}$$

$$F_{II}(\underline{a}) = \sum_{j=1}^{N}\Big[u(0,t_j) - \mu_1(t_j)\Big]^2 + \beta\sum_{j=0}^{N} a_j^2, \tag{3.29}$$

where $\underline{a} = (a_j)_{j=\overline{0,N}}$. It is worth mentioning that in (3.28) at the first time step, i.e. $j = 0$, the derivative $u_x(0,0)$ is obtained from the initial condition (3.2), via (3.20), as

$$u_x(0,0) = \frac{4\phi_1 - \phi_2 - 3\phi_0}{2(\Delta x)}, \tag{3.30}$$

where $\phi_i = \phi(x_i)$ for $i = \overline{0,M}$. Also, in (3.29), the value of $a(0)$ can be obtained by differentiating condition (3.9) with respect to t and using equation (3.1) at $x = 0$, namely,

$$a(0) = \frac{\mu_1'(0) - f(0,0)}{b(0)\phi''(0)}. \tag{3.31}$$

The minimization of the objective function (3.28), or (3.29), subjected to the physical simple lower bound constraints $\underline{a} > \underline{0}$ is accomplished using the MATLAB toolbox routine *lsqnonlin*, as described in Section 2.5. The positive components of the vector $\underline{a}$ are sought in the interval $[10^{-10},10^3]$.

In the numerical implementation, we take the parameters of the routine *lsqnonlin* as follows:

- Number of variables $M = N = 40$.
- Maximum number of iterations = $10^2 \times$ (number of variables).
- Maximum number of objective function evaluations = $10^3 \times$(number of variables).

- Solution and object function Tolerances = $10^{-20} \div 10^{-15}$.

The inverse problems under investigation are solved subjected to both exact and noisy heat flux measurement, (3.4) or (3.9) for Inverse Problems I and II, respectively. The noisy data is numerically simulated as

$$\mu_k^{\epsilon}(t_j) = \mu_k(t_j) + \epsilon_j^{(k)}, \quad j = \overline{0, N},\ k \in \{1, 3\}, \tag{3.32}$$

where ϵ_j are random variables generated from a Gaussian normal distribution with mean zero and standard deviation σ_k given by

$$\sigma_k = p \times \max_{t \in [0,T]} |\mu_k(t)|, \quad k \in \{1, 3\}, \tag{3.33}$$

where p represents the percentage of noise. We use the MATLAB function *normrnd* to generate the random variables $\underline{\epsilon}_k = \left(\epsilon_j^{(k)}\right)_{j=\overline{0,N}}$ as follows:

$$\underline{\epsilon}_k = normrnd(0, \sigma_k, N + 1). \tag{3.34}$$

The total amount of noise ϵ_k is given by

$$\epsilon_k = \left|\underline{\epsilon}_k\right| = \sqrt{\sum_{j=0}^{N} (\mu_k^{\epsilon}(t_j) - \mu_k(t_j))^2}, \quad k \in \{1, 3\}. \tag{3.35}$$

In the case of noisy data (3.32), we replace $\mu_3(t_j)$ by $\mu_3^{\epsilon}(t_j)$ for $j = \overline{0, N}$ in (3.28), and $\mu_1(t_j)$ by $\mu_1^{\epsilon}(t_j)$ for $j = \overline{1, N}$ in (3.29).

3.5 Numerical results and discussion

In this section, we present a few test examples to illustrate the accuracy and stability of the numerical scheme based on the FDM combined with the minimization of the least-squares functional (3.28), or (3.29), as described in Section 3.4. In order to explain the accuracy of the numerical results we introduce the root mean square error ($rmse$), defined as

$$rmse(a) = \sqrt{\frac{1}{N+1} \sum_{j=0}^{N} \left(a_{numerical}(t_j) - a_{exact}(t_j)\right)^2}. \tag{3.36}$$

We take $L = T = 1$ and present the numerical results obtained with $M = N = 40$. Unless otherwise specified, we take the initial guess as $\underline{a}^{(0)} = \underline{1}$.

3.5.1 Numerical results for Inverse Problem I

We consider a couple of examples for the Inverse Problem I. Before we present the numerical results, we mention that regularization has not been found necessary and hence we consider $\beta = 0$ in the functional (3.28). This was to expected since, according to Theorem 3.3, the Inverse Problem I is stable in the $C[0,T]$ maximum norm with respect to small errors in the input data μ_3^ϵ.

3.5.1.1 Example 1

In this example, we consider the inverse problem (3.2)-(3.4) and (3.6) with the input data

$$\begin{aligned}
&\phi(x) = u(x,0) = x + \sin(x), \quad b(x) = 2 - x^2,\\
&\mu_1(t) = u(0,t) = 8t, \quad \mu_2(t) = u(1,t) = 1 + \sin(1) + 8t,\\
&f(x,t) = 8 + (1+t)(2-x^2)\sin(x), \quad \mu_3(t) = -a(t)u_x(0,t) = -2 - 2t.
\end{aligned}$$

One can observe that the conditions of Theorems 3.1 and 3.2 are satisfied hence the problem is uniquely solvable. The analytical solution is given by

$$a(t) = 1 + t, \quad u(x,t) = x + \sin(x) + 8t. \tag{3.37}$$

We start with the case of exact input data, i.e. there is no noise included in (3.4). Figure 3.5 represents the objective functional (3.28), as a function of the number of iterations. From this figure it can be seen that the decreasing convergence is very fast and is achieved in 10 iterations to reach a stationary value of $O(10^{-24})$. In fact, the objective function reaches this plateau immediately after only four iterations. The numerical results for the time-dependent thermal conductivity $a(t)$ are depicted in Figure 3.6. From this figure it can be seen that the agreement between the numerical (final iteration 10) and exact solutions for $a(t)$ is excellent. Also, the $rmse$ values versus the number of iterations are shown in Figure 3.7. From this figure it can be easily remarked that the $rmse(a)$ quickly decreases in the first two iterations after which it becomes stationary at a very low value of 0.0002.

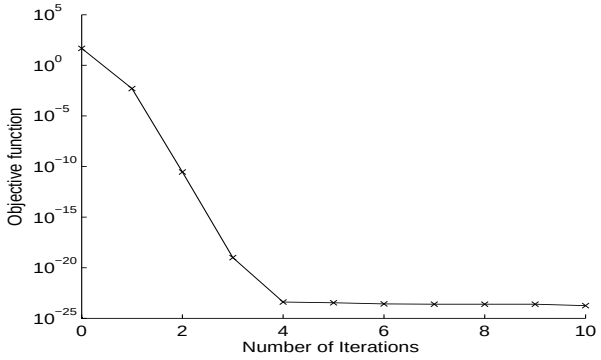

Figure 3.5: The objective function (3.28), for Example 1 with no noise.

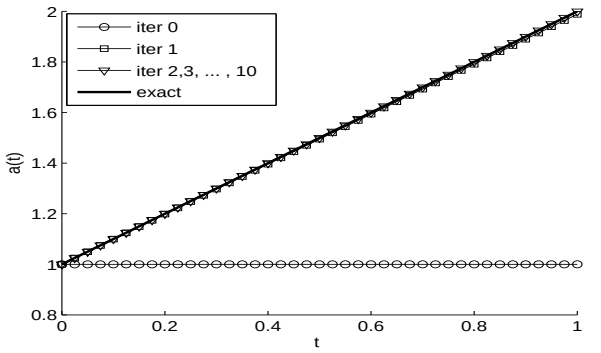

Figure 3.6: The thermal conductivity $a(t)$, for Example 1 with no noise.

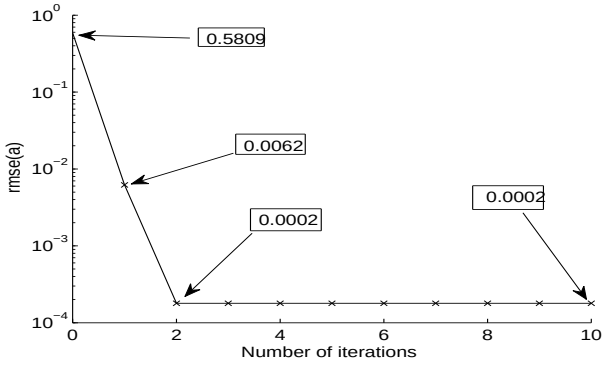

Figure 3.7: The *rmse* values of $a(t)$, versus the number of iterations, for Example 1 with no noise.

Next, we investigate the stability of the numerical solution with respect to noise in the data (3.4), defined by equation (3.32). We include $p \in \{2\%, 20\%\}$ noise and then, the total amount of noise that is applied is $\epsilon_3 \in \{0.3540, 3.5392\}$, respectively, as defined by equation (3.35). Figure 3.8 represents the exact $\mu_3(t)$ and a typical noisy measurement input data $\mu_3^\epsilon(t)$.

Figure 3.9 represents the objective functional (3.28), as a function of number of iterations, when $p \in \{2\%, 20\%\}$. From this figure it can be seen that a very fast decreasing convergence is achieved for $p \in \{2\%, 20\%\}$ in 8 iterations each, to reach a stationary value of $O(10^{-24})$.

Figures 3.10–3.12 show the numerical solutions for the thermal conductivity $a(t)$, the heat flux $a(t)u_x(1,t)$ at $x = 1$, and the $rmse(a)$ values, respectively, for $p \in \{2\%, 20\%\}$ noise. From these figures, as well as Figure 3.6, it can be seen that the numerical solution for the thermal conductivity $a(t)$ approximates better to the exact solution $a(t) = 1 + t$, as the percentage of noise p decreases from 20% to 2% and then to 0. The nonlinear least-squares minimization produces good and consistent retrievals of the solution even for a large amount of noise such as 20%. In Figure 3.12, for $p = 20\%$ a slight 'semi-convergence' phenomenon seems to appear after a couple of iterations, but this is more likely to be attributed to a non-monotonic decreasing convergence rather than to the former phenomenon which is commonly encountered when solving ill-posed problems iteratively, [30]. That is to say, our inverse problem is rather stable and in fact, as mentioned before at the beginning of Section 3.5.1, no regularization was needed to be included in the least-squares functional (3.28).

Finally, Figure 3.13 shows the exact solution, the numerical solution for the temperature $u(x,t)$ and the relative error between them. From this figure it can be seen that the numerical solution is stable and furthermore, its accuracy is consistent with the amount of noise shown in Figure 3.8, which was included into the input data (3.4).

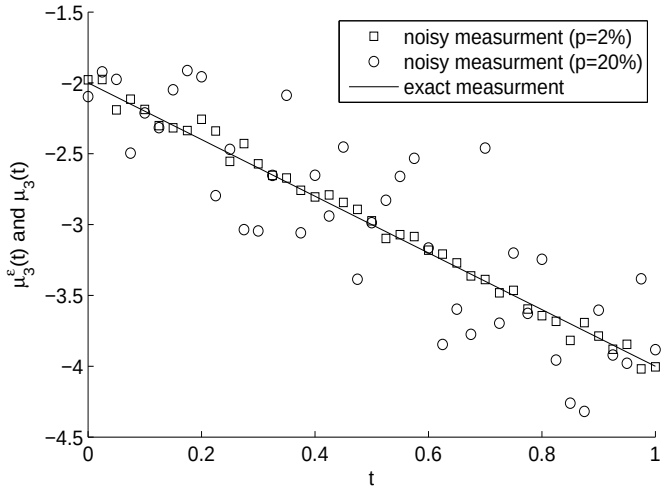

Figure 3.8: The noisy $\mu_3^\epsilon(t)$ and exact $\mu_3(t)$, for Example 1 with $p \in \{2\%, 20\%\}$ noise.

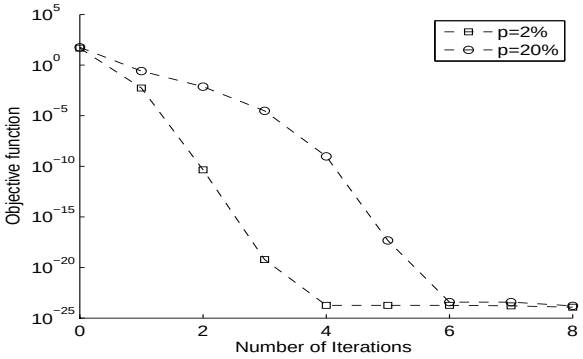

Figure 3.9: The objective function (3.28), for Example 1 with $p \in \{2\%, 20\%\}$ noise.

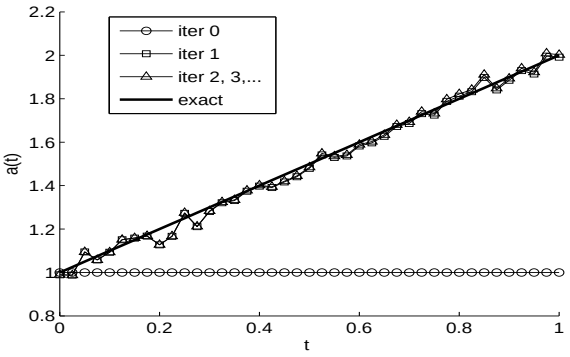

(a)

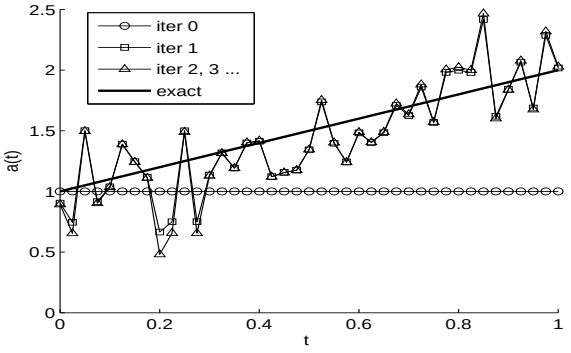

(b)

Figure 3.10: The thermal conductivity $a(t)$, for Example 1 with (a) $p = 2\%$ and (b) $p = 20\%$ noise.

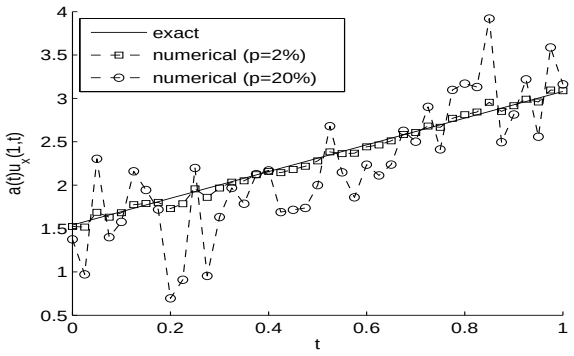

Figure 3.11: The exact and numerical heat flux $a(t)u_x(1,t)$, for Example 1 with $p \in \{2\%, 20\%\}$ noise.

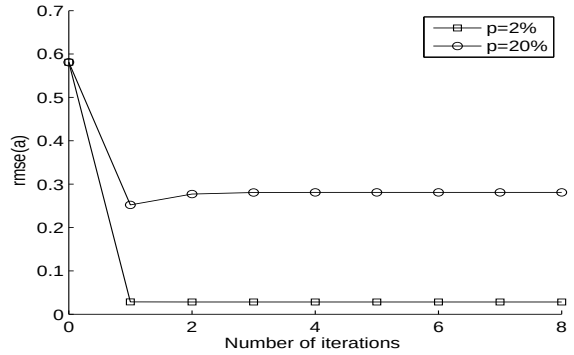

Figure 3.12: The *rmse* values of $a(t)$, versus the number of iterations, for Example 1 with $p \in \{2\%, 20\%\}$ noise.

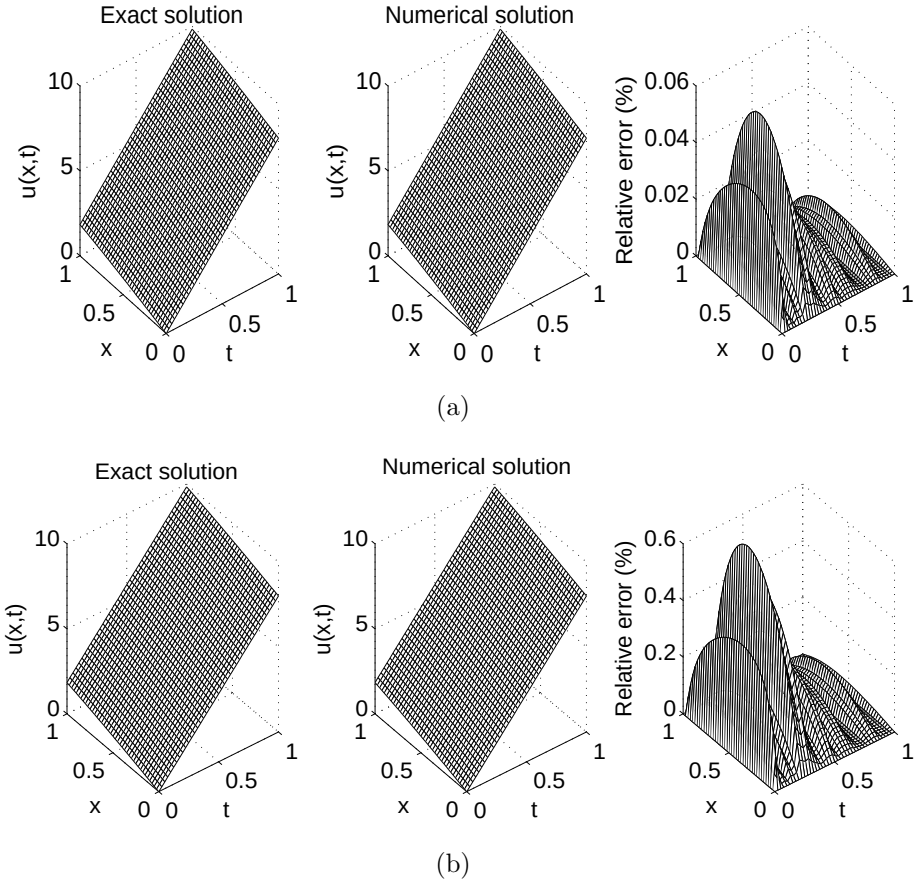

Figure 3.13: The exact and numerical temperature $u(x,t)$, for Example 1 with (a) $p = 2\%$ and (b) $p = 20\%$ noise. The relative error between them is also included.

3.5.1.2 Example 2

In the previous example we have inverted the unknown thermal conductivity $a(t) = 1+t$ which is a smooth function. In this example, we consider a non-smooth test function, see equation (3.38). We consider the inverse problem (3.2)–(3.4) and (3.6) with the following input data

$$\begin{aligned}\phi(x) =& u(x,0) = xe^x, \quad b(x) = 2 - x^2, \quad \mu_1(t) = u(0,t) = t^2,\\ &\mu_2(t) = u(1,t) = e + t^2, \quad \mu_3(t) = -a(t)u_x(0,t) = -1 - \left|t - \frac{1}{2}\right|,\\ f(x,t) =& 2t - \left(1 + \left|t - \frac{1}{2}\right|\right)(2 - x^2)(xe^x + 2e^x).\end{aligned}$$

One can notice that the conditions of Theorem 3.2 are satisfied hence the uniqueness of the solution holds. With this data, the analytical solution of the Inverse Problem I is given by

$$a(t) = 1 + \left|t - \frac{1}{2}\right|, \quad u(x,t) = xe^x + t^2. \tag{3.38}$$

We study the case of exact and noisy input data (3.4). The objective function (3.28), as a function of the number of iterations, is presented in Figure 3.14. Form this figure it can be seen that the same fast decreasing convergence is achieved as in Example 1.

The numerical results for the corresponding time-dependent thermal conductivity $a(t)$, the heat flux $a(t)u_x(1,t)$, the $rmse(a)$ values and the interior temperature $u(x,t)$ are presented in Figures 3.15–3.18, respectively. The same conclusions as those obtained for Example 1 can be drawn by observing these figures.

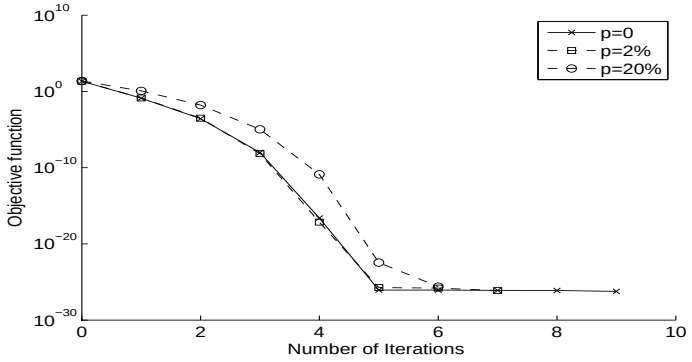

Figure 3.14: The objective function (3.28), for Example 2 with $p \in \{0, 2\%, 20\%\}$ noise.

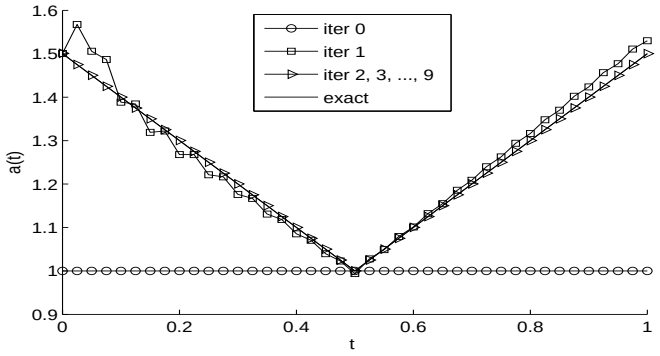

(a)

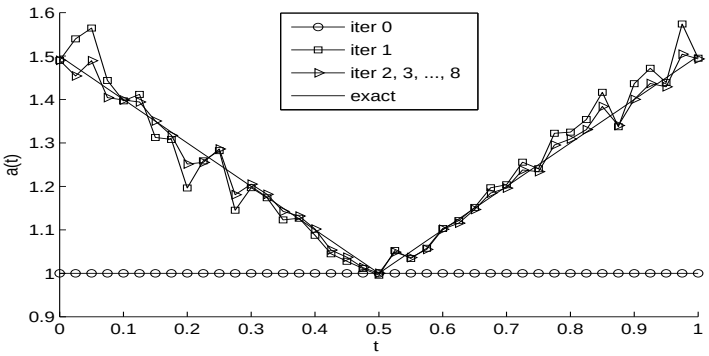

(b)

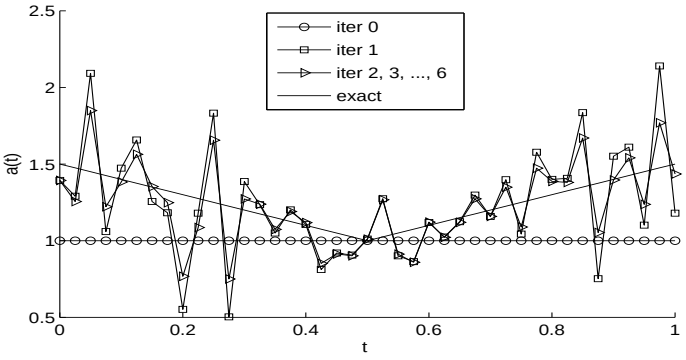

(c)

Figure 3.15: The thermal conductivity $a(t)$, for Example 2 with (a) $p = 0$, (b) $p = 2\%$ and (c) $p = 20\%$.

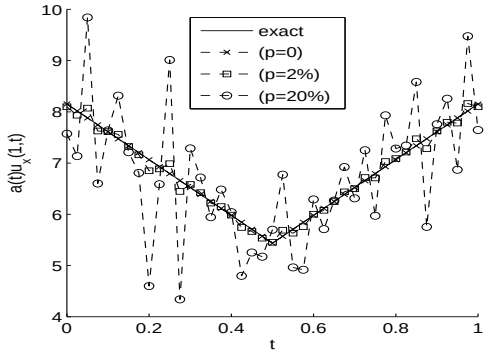

Figure 3.16: The exact and numerical heat flux $a(t)u_x(1,t)$, for Example 2 with $p \in \{0, 2\%, 20\%\}$ noise.

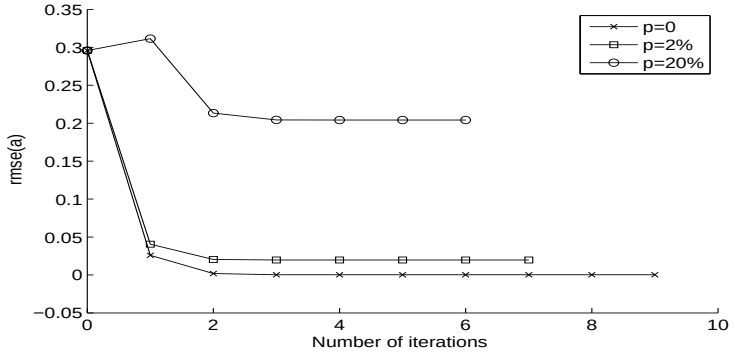

Figure 3.17: The $rmse$ values of $a(t)$, versus the number of iterations, for Example 2 with $p \in \{0, 2\%, 20\%\}$ noise.

Numerical outputs such as the number of iterations and function evaluations, as well as the final value of the convergent objective function are provided in Table 3.1 for both Examples 1 and 2.

Table 3.1: Number of iterations, number of function evaluations, value of objective function (3.28) at final iteration, for Examples 1 and 2 with $p \in \{0, 2\%, 20\%\}$ noise.

Example	Numerical outputs	$p = 0$	$p = 2\%$	$p = 20\%$
1	No. of iterations	10	8	8
	No. of function evaluations	451	328	328
	Function value	$1.7E-24$	$1.1E-24$	$1.6E-24$
	$rmse(a)$	$1.7E-4$	0.0282	0.2809
2	No. of iterations	9	7	6
	No. of function evaluations	369	287	246
	Function value	$5.8E-27$	$7.4E-27$	$2.8E-26$
	$rmse(a)$	$2.6E-4$	0.0197	0.2041

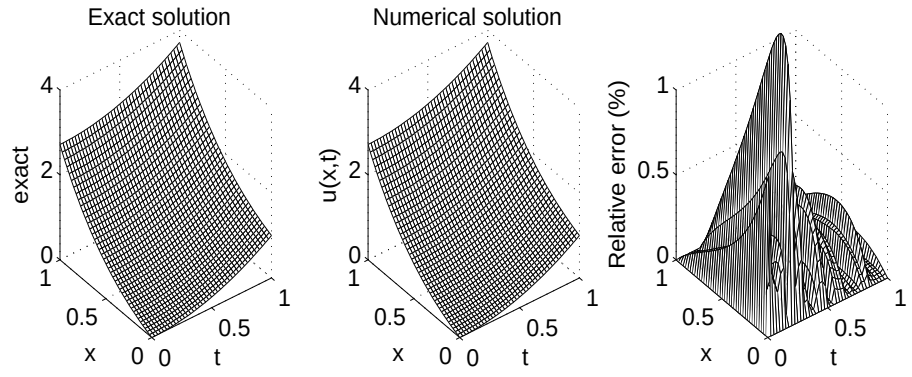

(a)

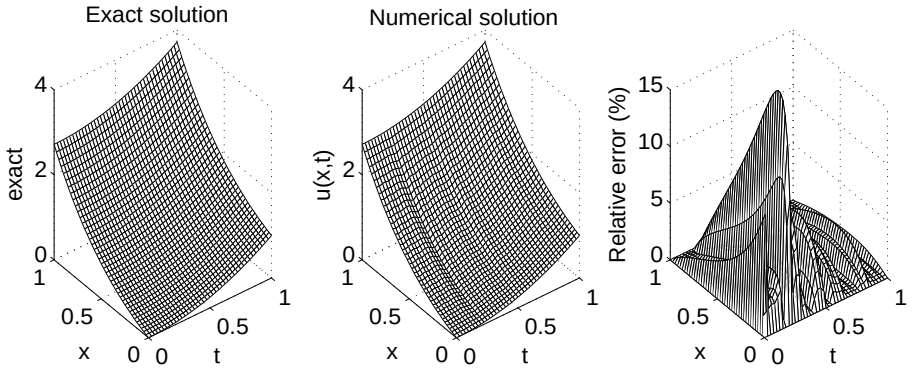

(b)

Figure 3.18: The exact and numerical temperature $u(x,t)$, for Example 2 with (a) $p = 2\%$ and (b) $p = 20\%$ noise. The relative error between them is also included.

3.5.2 Numerical results for Inverse Problem II

We now consider a couple of examples for the Inverse Problem II. Unlike for the Inverse Problem I which has been found stable with respect to noise in the input data (3.4), for the Inverse Problem II regularization was found necessary to be included in the functional (3.29) in order to obtain stable numerical solutions. This is to be expected since in the stability estimate (3.10) of Theorem 3.6, the right-hand side term contains the noisy data $(\mu_1^\epsilon - \mu_1)$ in the $C^1[0,T]$-norm which where differentiated produces an unstable numerical solution.

3.5.2.1 Example 3

In this example, we consider the inverse problem (3.2), (3.6), (3.8) and (3.9) with the input data

$$\begin{aligned} \phi(x) = u(x,0) = 1 + xe^x, \quad b(x) = 2 - x^2, \\ \nu_1(t) = -u_x(0,t) = -1, \quad \nu_2(t) = u_x(1,t) = -2e, \\ f(x,t) = e^t - (1+t)(2-x^2)(xe^x + 2e^x), \quad \mu_1(t) = u(0,t) = e^t. \end{aligned}$$

One can observe that the conditions of Theorem 3.5 are satisfied hence, a solution is unique. The analytical solution is given by

$$a(t) = 1 + t, \quad u(x,t) = xe^x + e^t. \tag{3.39}$$

We start the investigation with exact input data (3.9), i.e. there is no noise included. Figure 3.19 represents the evolution of objective functional (3.29), as a function of the number of iterations, with no regularization, i.e. $\beta = 0$. From this figure it can be seen that a fast decreasing convergence is achieved in 7 iterations to reach a very low value of order $O(10^{-26})$. The corresponding numerical results of the time-dependent thermal conductivity $a(t)$ are displayed in Figure 3.20. From this figure it can be seen that there is an excellent agreement between the exact and numerical solutions with an $rmse(a)$= 0.0086.

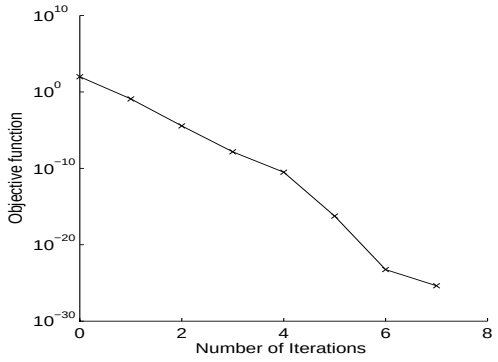

Figure 3.19: The objective function (3.29), for Example 3 with no noise and no regularization.

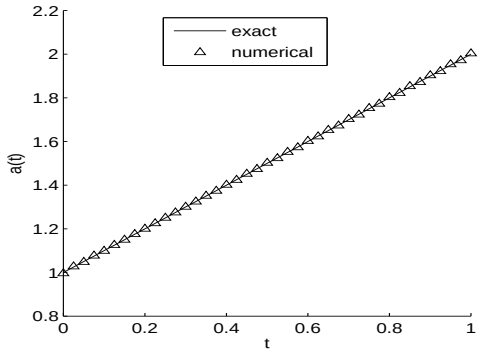

Figure 3.20: The thermal conductivity $a(t)$, for Example 3 with no noise and no regularization.

In order to test the stability of the problem, we add $p = 2\%$ random Gaussian additive noise as in (3.32) which, according to (3.35), yields the total amount of noise $\epsilon_1 = 0.2314$. Let us denote by

$$R_{II}(\underline{a}) = \sum_{j=1}^{N} [u(0, t_j) - \mu_1^{\epsilon}(t_j)]^2, \tag{3.40}$$

the least-squares residual associated to the regularized Tikhonov functional (3.29).

Figure 3.21 shows the residual functional (3.40), as a function of the number of iterations, for various regularization parameters $\beta \in \{0, 10^{-3}, 10^{-2}, 10^{-1}\}$. From this figure one can observe that convergence is rapidly achieved for each value of β. The resulting thermal conductivity is plotted in Figure 3.22 for various regularization parameters. As expected, when no regularization is employed, i.e. $\beta = 0$, the estimated $a(t)$ is highly unstable and inaccurate. This shows that the Inverse Problem II is ill-posed. Consequently, a small perturbation in input data (3.9) causes a drastic error in the output solution $a(t)$. In order to overcome this instability, we employ the Tikhonov regularization method with $\beta > 0$. From Figure 3.22 and Table 3.2, it can be observed that the stability is indeed restored and the value of $\beta = O(10^{-2})$ produces the most accurate numerical results.

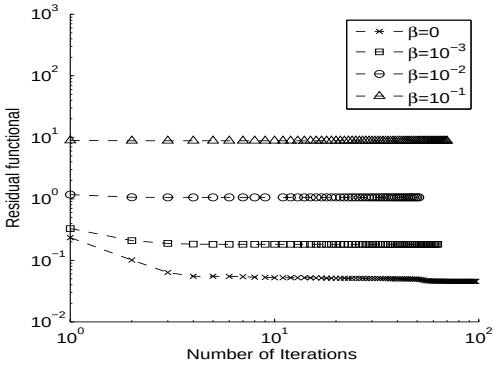

Figure 3.21: The residual function (3.40), for Example 3 with $p = 2\%$ noise, and various regularization parameters.

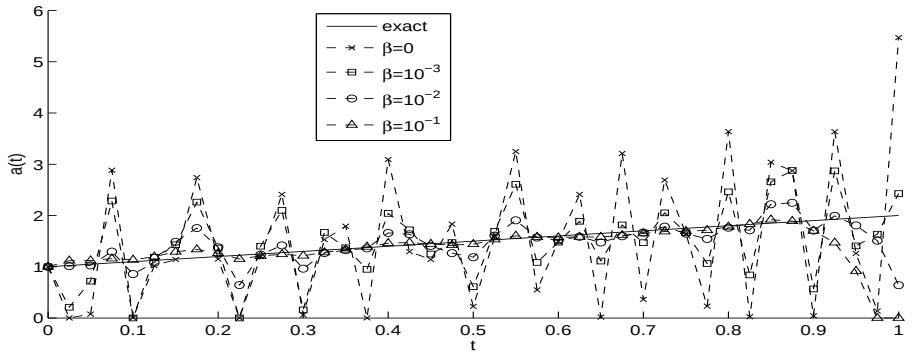

Figure 3.22: The thermal conductivity $a(t)$, for Example 3 with $p = 2\%$ noise and various regularization parameters.

Finally, Figure 3.23 shows the exact solution, the numerical solution for the temperature $u(x,t)$ and the relative error between them. From this figure it can be seen that the numerical solution for $u(x,t)$ is stable for all values of β with only very small instabilities manifesting for $\beta = 0$ or 10^{-3}.

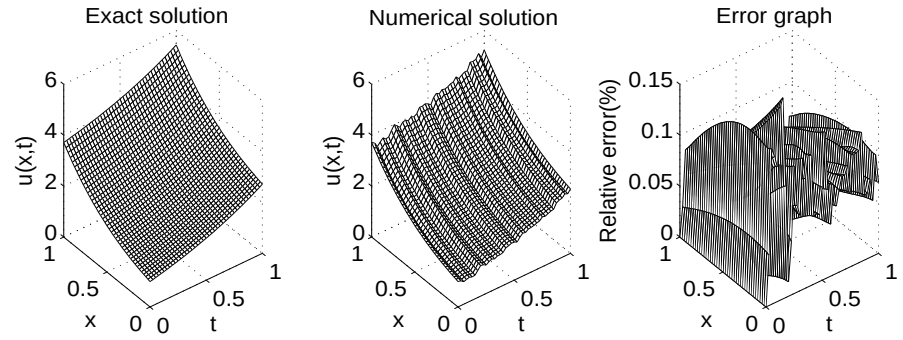

(a)

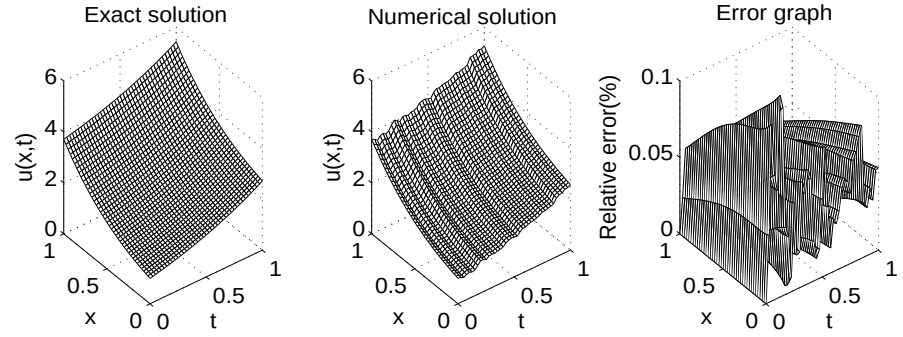

(b)

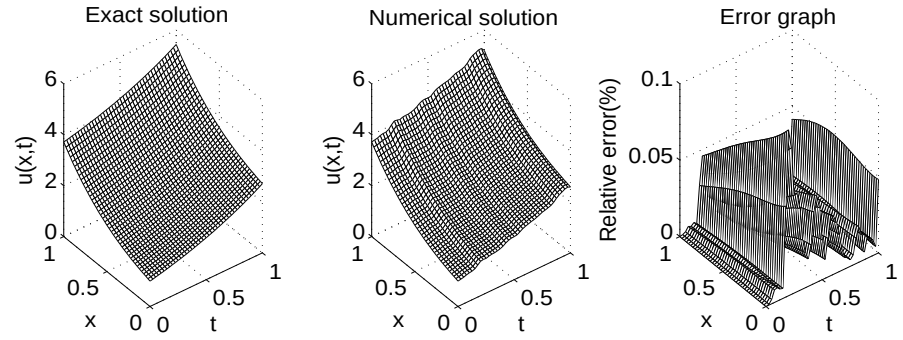

(c)

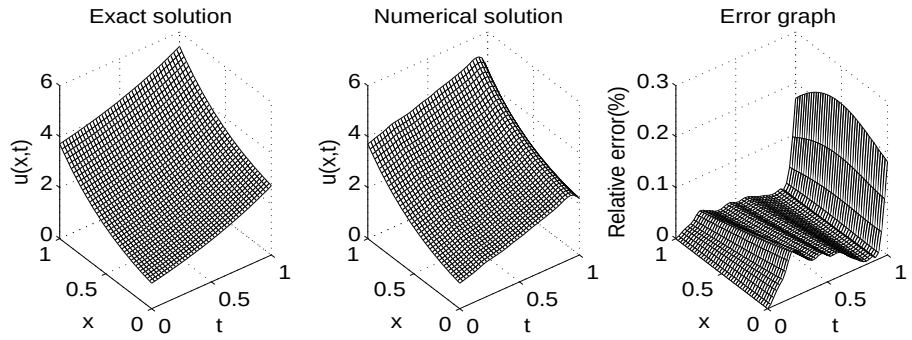

(d)

Figure 3.23: The exact and numerical temperature $u(x,t)$, for Example 3 with $p = 2\%$ noise and (a) $\beta = 0$, (b) $\beta = 10^{-3}$, (c) $\beta = 10^{-2}$, and (d) $\beta = 10^{-1}$. The relative error between them is also included.

3.5.2.2 Example 4

Consider the inverse problem (3.2), (3.6), (3.8) and (3.9) with the input data

$$\begin{aligned}
\phi(x) &= u(x,0) = e^x, \quad b(x) = 2 - x^2, \\
\nu_1(t) &= -u_x(0,t) = -e^t, \quad \nu_2(t) = u_x(1,t) = e^{1+t}, \\
f(x,t) &= e^{x+t} - (1 + 2\pi\cos^2(2\pi t))(2 - x^2)e^{x+t}, \quad \mu_1(t) = u(0,t) = e^t.
\end{aligned}$$

The analytical solution is given by

$$a(t) = 1 + 2\pi\cos^2(2\pi t), \quad u(x,t) = e^{x+t}. \tag{3.41}$$

For this thermal conductivity the initial guess was $\underline{a}_0 = \underline{1 + 2\pi}$. The objective function (3.29), as a function of the number of iterations, is depicted in Figure 3.24 for no noise and no regularization. From this figure it can be seen that the objective function (3.29) with $\beta = 0$, i.e the residual functional (3.40), is decreasing over several orders of magnitude, as the number of iterations increases, reaching a very low value of $O(10^{-15})$ after 400 iterations. The computational time taken by the *lsqnonlin* to produce this convergence was about 10.6 minutes. The resulting thermal conductivity is shown in Figure 3.25 and very good agreement between the exact and numerical solutions can be observed.

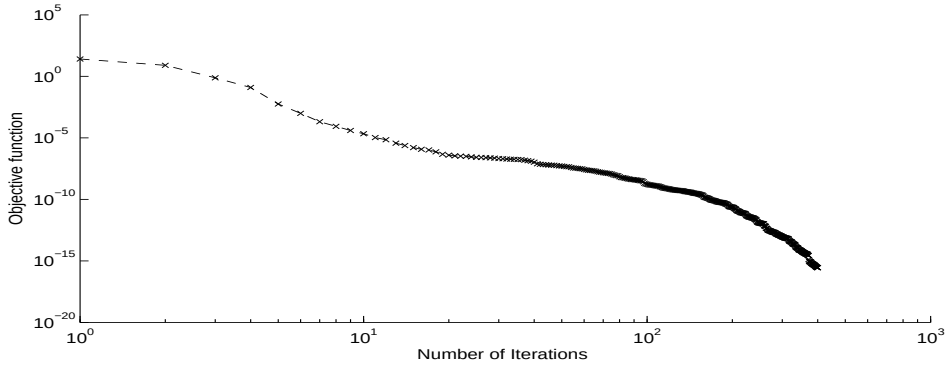

Figure 3.24: The objective function (3.29), for Example 4 with no noise and no regularization.

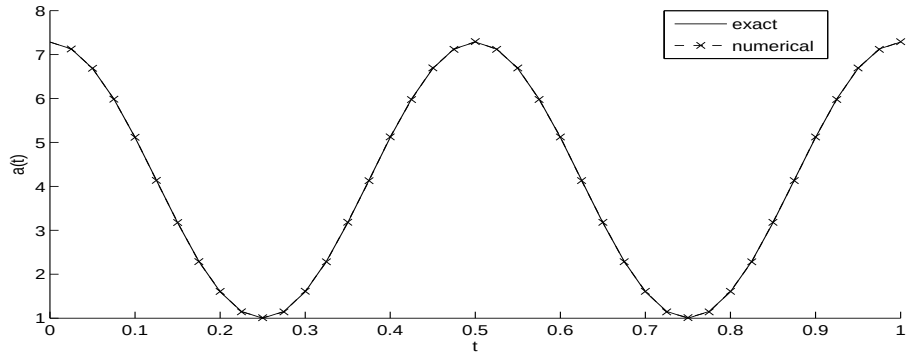

Figure 3.25: The thermal conductivity $a(t)$, for Example 4 with no noise and no regularization.

Next, the input data (3.9) was perturbed by $p = 2\%$ noise. The residual function (3.40), as a function of the number of iterations, and the numerical results for $a(t)$ are plotted in Figures 3.26 and 3.27, respectively, for various regularization parameters $\beta \in \{0, 10^{-3}, 10^{-2}, 10^{-1}\}$. As in Example 3, one can see that the numerically obtained results for $\beta = 0$ in Figure 3.27 are unstable being highly oscillatory and unbounded. However, the inclusion of some regularization with $\beta > 0$ in the objective functional (3.29) restores the stability of the numerical solution, as shown further in Figure 3.27. One can observe that the choice $\beta = 10^{-1}$ is too large and it oversmooths the solution, whilst the choice $\beta = 10^{-3}$ is too small and it undersmooths the solution. It seems that a regularization parameter β of $O(10^{-2})$ realizes the desired compromise of balancing the under- and over-smooth regions. Finally, Figure 3.27, as well as Figure 3.22 for Example 3, give some insight about how one may choose the regularization parameters $\beta > 0$. Based on practical experience, on can start with a rather large values for β, and then decrease it until oscillations in the numerical solution start to appear [28].

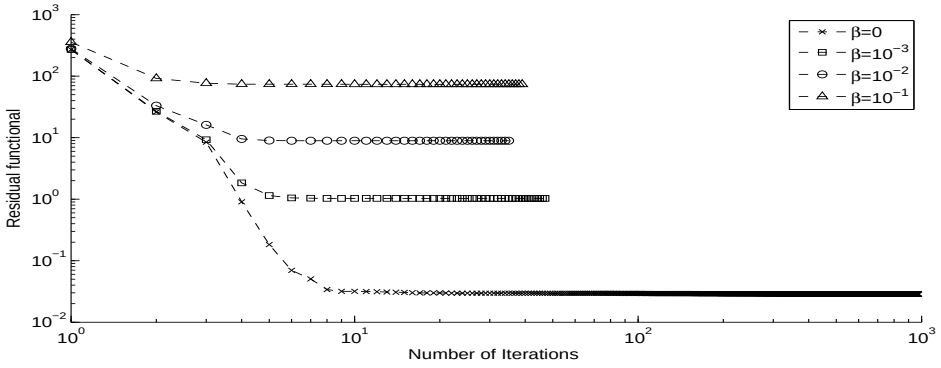

Figure 3.26: The residual function (3.40), for Example 4 with $p = 2\%$ noise and various regularization parameters.

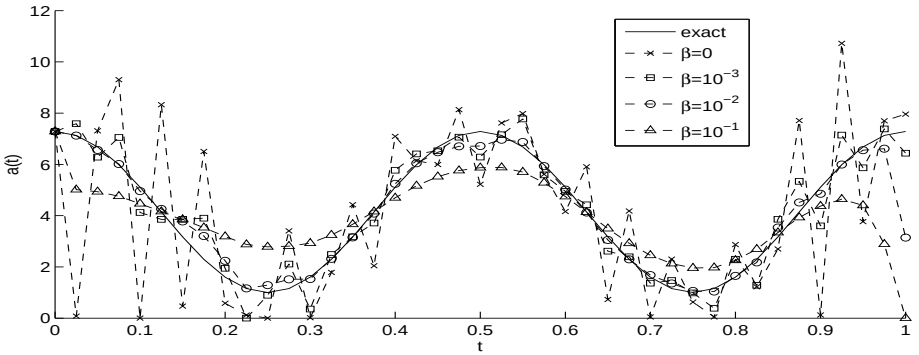

Figure 3.27: The thermal conductivity $a(t)$, for Example 4, with $p = 2\%$ noise and various regularization parameters.

For completeness, numerical outputs such as the number of iterations and function evaluations, the final value of the convergent objective function, as well as the $rmse(a)$ are provided in Table 3.2 for Examples 3 and 4.

The numerical results for the temperature $u(x,t)$ were found, as in Figure 3.23 for Example 3.5.2.1, accurate and stable and therefore they are not presented. Finally, although not illustrated, it is reported that an accurate and stable retrieval also was obtained for a non-smooth thermal conductivity.

Table 3.2: Number of iterations, number of function evaluations, value of regularized objective function (3.29) at final iteration, and the $rmse(a)$ for Examples 3 and 4 with $\beta \in \{0, 10^{-3}, 10^{-2}, 10^{-1}\}$ and $p = 2\%$ noise.

Example	Numerical outputs	$\beta = 0$	$\beta = 10^{-3}$	$\beta = 10^{-2}$	$\beta = 10^{-1}$
3	No. of iterations	97	63	51	70
	No. of function evaluations	4116	2688	2184	2982
	Objective function (3.28) value at final iteration	0.0455	0.1818	1.0574	8.7697
	$rmse(a)$	1.2697	0.6829	0.3158	0.4836
4	No. of iterations	976	49	41	42
	No. of function evaluations	40016	2016	1764	1806
	Objective function (3.29) value at final iteration	0.0286	1.029	8.917	73.817
	$rmse(a)$	2.4973	0.7479	0.7135	1.7179

3.6 Conclusions

A couple of inverse problems which require determining a time-dependent thermal conductivity when the spacewise dependent heat capacity is given for the heat parabolic equation under overspecified Cauchy boundary data have been investigated. The Inverse Problem I given by equations (3.2)–(3.4) and (3.6) was found to be well-posed, whilst the Inverse Problem II given by equations (3.2), (3.6), (3.8) and (3.9) was found to be ill-posed and regularization was needed in order to obtain a stable solution. A direct solver based on a Crank-Nicolson finite difference scheme has been developed. For the inverse problems, the resulting nonlinear least-squares minimizations have been solved numerically using the MATLAB toolbox routine *lsqnonlin*. Numerical results illustrated for several benchmarks test examples showed that an accurate and stable solution has been obtained.

Chapter 4

Simultaneous determination of time-dependent coefficients

4.1 Introduction

Simultaneous determination of several unknown coefficients in parabolic partial differential equations has been investigated in some studies in the past, see e.g. the monographs of Prilepko et al. [104] and Ivanchov [70]. In heat conduction for example, attention was paid to the unique solvability of one-dimensional inverse problems for the heat equation in the case when the unknown thermal coefficients are constant [12], time-dependent [75, 76], space-dependent [2], or temperature-dependent [85, 100, 101]. In these papers, the authors investigated the existence and uniqueness of the solution of the inverse problem, though no numerical method/solution was presented.

When solving an inverse problem the choice of additional information about the solution is crucial since this information enables us to determine the unknown parameters of the process under consideration uniquely. Usually, this additional information/observation is given by the boundary conditions or, the value of the solution on a specific subdomain or, at a certain time [78]. In [108], the authors proposed a new algorithm based on space decomposition in a reproducing kernel space for solving the inverse problem of finding the time-dependent thermal diffusivity. In [71, 74] the problem of finding the time-dependent leading coefficient and temperature distribution with Dirichlet boundary conditions and measured heat flux as the overdetermination condition was considered. In [36], the author considered retrieving lower-order time-dependent coefficients using the Trace-Type Functional approach [15], which assumes that the governing partial differential equation is valid at the boundary. However, this approach does not seem so stable [37], and it has never been applied to inverse coefficient identifica-

tion problems in which the unknown coefficients appear at the leading order in the heat operator.

In this chapter, we investigate the inverse problems of simultaneous determination of time-dependent leading and lower-order thermal coefficients. In the next section, we give the mathematical formulations of three inverse problems for which the unique solvability theorems of [58, 74, 75] are stated. The numerical finite-difference discretization of the direct problem is described in Section 4.3, whilst Section 4.4 introduces the regularized nonlinear minimization used for solving in a stable manner the inverse problems under investigation. In Section 4.5, we provide numerical results and discussion. Finally, conclusions are presented in Section 4.6.

4.2 Mathematical formulations of the inverse problems

Consider the linear one-dimensional parabolic equation with time-dependent coefficients

$$C(t)u_t(x,t) = K(t)u_{xx}(x,t) + Q(t)u_x(x,t),\ (x,t) \in (0,\ell) \times (0,T) =: \Omega \qquad (4.1)$$

where, in heat conduction, u represents the temperature in a finite slab of length $\ell > 0$ recorded over the time interval $(0,T)$ with $T > 0$, C and K represent the heat capacity and thermal conductivity of the heat conductor, respectively, $Q(t) = c(t)v(t)$ with c and v representing the heat capacity and velocity of a fluid flowing through the heat conducting body, [4, 33]. The first term in the right-hand side of equation (4.1) represents the diffusion, whilst the second term, if $v(t)$ is positive, represents the convection. A similar situation occurs in porous media, [26], where the properties are referred to as hydraulic rather than thermal as in heat transfer. For example, in the contaminant transport in groundwater the first term on the right-hand side of equation (4.1) represents the dispersion of the contaminant as it moves through the porous medium, whilst the second term with $v(t)$ negative describes the advection of the contaminant which flows along with the bulk movement of groundwater.

The initial condition is

$$u(x,0) = \phi(x), \qquad x \in [0,\ell], \qquad (4.2)$$

and the boundary and over-determination conditions are

$$u(0,t) = \mu_1(t), \qquad u(\ell,t) = \mu_2(t), \qquad t \in [0,T], \tag{4.3}$$

$$-K(t)u_x(0,t) = \nu_1(t), \qquad K(t)u_x(\ell,t) = \nu_2(t), \qquad t \in [0,T]. \tag{4.4}$$

Conditions (4.3) and (4.4) represent the specification of the boundary temperature and heat flux, respectively. Together they represent the Cauchy data for the inverse coefficient identification problems (ICIPs) which are described next.

We distinguish three ICIPs covering the simultaneous determination of a couple of coefficients in (4.1). The case of identifying all three coefficients in (4.1) is deferred to a future work.

4.2.1 Inverse Problem 1

Assuming that $c(t)v(t) = 0$, the inverse problem 1 (IP1) requires the simultaneous determination of the time-dependent thermal conductivity $K(t) > 0$, the heat capacity $C(t) > 0$ and the temperature $u(x,t)$ satisfying the one-dimensional heat equation

$$C(t)u_t(x,t) = K(t)u_{xx}(x,t), \qquad (x,t) \in \Omega \tag{4.5}$$

subject to the initial and boundary conditions (4.2)–(4.4).

For this IP1 we have the following existence and uniqueness of solution theorems [75].

Theorem 4.1. (Existence)
Suppose that:

1. $\phi \in C^2[0,\ell]$ *and* μ_i, $\nu_i \in C^1[0,T]$ *for* $i = 1,2$.

2. *The consistency conditions are satisfied:*

$$\mu_1(0) = \phi(0), \quad \mu_2(0) = \phi(\ell),$$
$$-\nu_1(0)\phi'(\ell) = \nu_2(0)\phi'(0), \quad \mu_1'(0)\phi''(\ell) = \mu_2'(0)\phi''(0).$$

3. *The following conditions are satisfied:*

$$\begin{aligned}
&\phi'(x) \geq 0, \quad x \in [0,\ell], \quad \phi''(x) + \phi''(\ell - x) > 0, \quad x \in [0, \ell/2),\\
&\nu_1^2(t) + \nu_2^2(t) > 0,\ \mu_2'(t) - \mu_1'(t) \geq 0,\ (1+\chi(t))\,\mu_1'(t) + (1-\chi(t))\,\mu_2'(t) > 0,\\
&\chi(t) > 0, \quad \chi'(t) \geq 0, \quad t \in [0,T],\\
&(1+\chi(t))\,\phi''(x) + (1-\chi(t))\,\phi''(\ell - x) > 0, \quad x \in [0,\ell/2],\ t \in [0,T],\\
&\phi''(x) - \phi''(\ell - x) \geq 0, \quad \textit{or} \quad \phi''(x) - \phi''(\ell - x) \leq 0, \quad x \in [0,\ell/2],
\end{aligned}$$

where $\chi(t) = \frac{\nu_2(t)+\nu_1(t)}{\nu_1(t)-\nu_2(t)}$. *Then, for a sufficiently small* $T > 0$, *the inverse problem (4.2)–(4.5) has at least one solution* $\{C(t), K(t), u(x,t)\}$, *where the functions* $C(t)$ *and* $K(t)$ *are continuous and positive on* $[0,T]$ *and* $u(x,t)$ *belongs to the class* $C^{2,1}(\Omega) \cap C^{1,0}(\overline{\Omega})$.

Theorem 4.2. (Uniqueness)
Suppose that the following conditions are satisfied:

1. $\phi \in C^2[0,\ell]$, $\mu_i \in C^1[0,T]$ *and* $\nu_i \in C[0,T]$ *for* $i = 1, 2$;
2. $\phi''(x) \geq 0$ *for* $x \in [0,\ell]$, $\phi''(0) > 0$, $\mu_1'(t) > 0$, $\mu_2'(t) > 0$, $\nu_1(t) < 0$, $\nu_2(t) > 0$ *for* $t \in [0,T]$.

If $\{C_j(t), K_j(t), u_j(x,t)\}$ *for* $j = 1, 2$, *are two solutions to the problem (4.2)–(4.5) such that* $a_j(t) = K_j(t)/C_j(t)$ *are piecewise analytic functions on* $(0,T)$, *then these solutions must coincide.*

4.2.2 Inverse Problem 2

Assuming that $K(t) > 0$ is known, we now wish to determine the time-dependent heat capacity $C(t) > 0$, the convection/advection coefficient $Q(t)$ and the temperature $u(x,t)$ satisfying equations (4.1)–(4.4). By dividing (4.1) with $C(t)$ and denoting with $a(t) := K(t)/C(t)$ the thermal diffusivity and $b(t) := Q(t)/C(t)$, we obtain

$$u_t(x,t) = a(t)u_{xx}(x,t) + b(t)u_x(x,t), \qquad (x,t) \in \Omega. \tag{4.6}$$

For simplicity, since $K(t) > 0$ is known we can divide with it in (4.4) and denote the right hand sides by

$$-u_x(0,t) = \nu_1(t)/K(t) =: \overline{\nu}_1(t),\ u_x(\ell,t) = \nu_2(t)/K(t) =: \overline{\nu}_2(t),\ t \in [0,T]. \tag{4.7}$$

For this inverse problem 2 (IP2), we have the existence and uniqueness of solution Theorems 4.3 and 4.4 below [76]. These are actually given for the more general reaction-convection-diffusion equation with a source term, namely,

$$u_t(x,t) = a(t)u_{xx}(x,t) + b(t)u_x(x,t) + d(x,t)u + f(x,t), \quad (x,t) \in \Omega, \tag{4.8}$$

where d and f are some given functions representing the reaction rate and source term, respectively. The triplet $(a(t), b(t), u(x,t))$ is called a solution to the IP2 given by equations (4.2), (4.3), (4.7) and (4.8) if it satisfies these equations and it belongs to the class $(H^{\gamma/2}[0,T])^2 \times H^{2+\gamma,1+\gamma/2}(\overline{\Omega})$ for some $\gamma \in (0,1)$, and $a(t) > 0$ for all $t \in [0,T]$. For the definition of the Hölder space, as well as other spaces of functions involved, see [87].

Theorem 4.3. (Existence)
Suppose that the following conditions are satisfied:

1. $\phi \in H^{2+\gamma}[0,\ell]$, μ_i, $\overline{\nu}_i \in H^{1+\gamma/2}[0,T]$ *for* $i = 1,2$, *and* d, f, $d_x, f_x \in H^{\gamma,\gamma/2}(\overline{\Omega})$;

2. $(\mu_1'(t) - f(0,t) - d(0,t)\mu_1(t))\overline{\nu}_2(t) + (\mu_2'(t) - f(\ell,t) - d(\ell,t)\mu_2(t))\overline{\nu}_1(t) > 0, \overline{\nu}_1(t) \geq 0, \overline{\nu}_2(t) \geq 0$, $\overline{\nu}_2(t)+\overline{\nu}_1(t) > 0$, $t \in [0,T]$, *and* $\phi''(x) > 0$, $x \in [0,\ell]$;

3. $\mu_1(0) = \phi(0)$, $\mu_2(0) = \phi(\ell)$, $-\overline{\nu}_1(0) = \phi'(0)$, *and* $\overline{\nu}_2(0) = \phi'(\ell)$.

Then the problem (4.2), (4.3), (4.7) and (4.8) has a (local) solution for $x \in [0,\ell]$ *and* $t \in [0,t_0]$, *where the time* $t_0 \in (0,T]$, *is determined by the input data of the problem.*

Theorem 4.4. (Uniqueness)
Suppose that the following condition is satisfied:
$(\mu_1'(t) - f(0,t) - d(0,t)\mu_1(t))\overline{\nu}_2(t) + (\mu_2'(t) - f(\ell,t) - d(\ell,t)\mu_2(t))\overline{\nu}_1(t) \neq 0$, $t \in [0,T]$. *Then a solution to (4.2), (4.3), (4.7) and (4.8) is unique.*

4.2.3 Inverse Problem 3

For completeness, we consider the inverse problem 3 (IP3) which consists of determining the thermal conductivity $K(t) > 0$, the convection/advection coefficient $Q(t)$ and the temperature $u(x,t)$ satisfying equations (4.1)–(4.4), when the heat capacity $C(t)$ is known. By dividing (4.1) with $C(t)$ we obtain equation (4.6). Also, dividing (4.4) by the known $C(t) > 0$ we obtain

$$-a(t)u_x(0,t) = \frac{\nu_1(t)}{C(t)} =: \tilde{\nu}_1(t), \quad a(t)u_x(\ell,t) = \frac{\nu_2(t)}{C(t)} =: \tilde{\nu}_2(t), \quad t \in [0,T]. \tag{4.9}$$

The following theorems proved in [58] give the unique solvability of the solution of the IP3 given by equations (4.2), (4.3), (4.8) and (4.9).

Theorem 4.5. (Existence)
Suppose that the following assumptions hold:

(A1) $\phi \in C^{2+\gamma}[0,\ell]$, $\mu_i \in C^1[0,T]$, $\tilde{\nu}_i \in C[0,T]$ *for* $i = 1,2$, $d, f \in C^{\gamma,0}(\Omega)$, *for some* $\gamma \in (0,1)$;

(A2) $\phi''(x) > 0$, $x \in [0,\ell]$, $\tilde{\nu}_1(t) \geq 0$, $\tilde{\nu}_2(t) \geq 0$, $\tilde{\nu}_2(t) + \tilde{\nu}_1(t) > 0$, $\mu_1'(t) - f(0,t) - d(0,t)\mu_1(t) > 0$, $\mu_2'(t) - f(\ell,t) - d(\ell,t)\mu_2(t) > 0$, $t \in [0,T]$;

(A3) $\phi(0) = \mu_1(0)$, $\phi(\ell) = \mu_2(0)$, $-\tilde{\nu}_1(0)\phi'(\ell) = \tilde{\nu}_2(0)\phi'(0)$.

Then there exists $t_0 \in (0,T]$ *such that the problem (4.2), (4.3), (4.8) and (4.9) has a (local) solution* $(a(t), b(t), u(x,t)) \in (C[0,t_0])^2 \times C^{2,1}([0,\ell] \times [0,t_0])$ *and* $a(t) > 0$, $t \in [0,t_0]$.

Theorem 4.6. (Uniqueness)
Suppose that the following assumptions hold:

(A4) $d \in C^{\gamma,0}(\Omega)$, *for some* $\gamma \in (0,1)$;

(A5) $\tilde{\nu}_1(t) \geq 0$, $\tilde{\nu}_2(t) \geq 0$, $\tilde{\nu}_2(t) + \tilde{\nu}_1(t) > 0$, $\mu_1'(t) - f(0,t) - d(0,t)\mu_1(t) > 0$, $\mu_2'(t) - f(\ell,t) - d(\ell,t)\mu_2(t) > 0$, $t \in [0,T]$.

Then the problem (4.2), (4.3), (4.8) and (4.9) can have at most one solution $(a(t), b(t), u(x,t)) \in (C[0,T])^2 \times C^{2+\gamma,1}(\overline{\Omega})$ *such that* $a(t) > 0, t \in [0,T]$.

4.3 Solution of direct problem

In this section, we consider the direct initial boundary value problem given by equations (4.2), (4.3) and (4.8), where $a(t)$, $b(t)$, $d(x,t)$, $f(x,t)$, $\phi(x)$ and $\mu_i(t)$, $i = 1,2$, are known and the solution $u(x,t)$ is to be determined. To achieve this, we use the Crank-Nicolson finite-difference scheme, as described in Section 2.4.

The discrete form of our problem is as follows. We divide the domain $\Omega = (0,\ell) \times (0,T)$ into M and N subintervals of equal step length Δx and Δt, where $\Delta x = \ell/M$ and $\Delta t = T/N$, respectively. So, the solution at the node (i,j) is $u_{i,j} := u(x_i, t_j)$, where $x_i = i\Delta x$, $t_j = j\Delta t$, for $i = \overline{0,M}$, $j = \overline{0,N}$.

Considering the general partial differential equation

$$u_t = G(x,t,u,u_x,u_{xx}), \tag{4.10}$$

the Crank-Nicolson approximation, [110], is given by

$$\frac{u_{i,j+1}-u_{i,j}}{\Delta t}=\frac{1}{2}\left(G_{i,j}+G_{i,j+1}\right),\ i=\overline{1,(M-1)},\ j=\overline{0,(N-1)}, \tag{4.11}$$

where $G_{i,j}=G\left(x_i,t_j,\frac{u_{i+1,j}-u_{i-1,j}}{2\Delta x},\frac{u_{i+1,j}-2u_{i,j}+u_{i-1,j}}{(\Delta x)^2}\right)$. Equations (4.2) and (4.3) can be collocated as:

$$u_{i,0}=\phi(x_i), \qquad i=\overline{0,M}, \tag{4.12}$$

$$u_{0,j}=\mu_1(t_j), \qquad j=\overline{0,N}, \tag{4.13}$$

$$u_{M,j}=\mu_2(t_j), \qquad j=\overline{0,N}. \tag{4.14}$$

For our problem, equation (4.8) can be discretized in the form of (4.11) as

$$\begin{aligned}-A_{j+1}u_{i-1,j+1}+(1-B_{i,j+1})u_{i,j+1}-C_{j+1}u_{i+1,j+1}=\\ -A_ju_{i-1,j}+(1+B_{i,j})u_{i,j}-C_ju_{i+1,j}+\frac{\Delta t}{2}\left(f_{i,j+1}+f_{i,j}\right)\end{aligned} \tag{4.15}$$

for $i=\overline{1,(M-1)}$, $j=\overline{0,N}$, where $f_{i,j}:=f(x_i,t_j)$,

$$A_j=\frac{\Delta t}{2(\Delta x)^2}a(t_j)-\frac{\Delta t}{4\Delta x}b(t_j),\quad B_{i,j}=-\frac{\Delta t}{(\Delta x)^2}a(t_j)+\frac{\Delta t}{2}d(x_i,t_j),$$
$$C_j=\frac{\Delta t}{2(\Delta x)^2}a(t_j)+\frac{\Delta t}{4\Delta x}b(t_j).$$

At each time step t_{j+1}, for $j=\overline{0,(N-1)}$, using the Dirichlet boundary conditions (4.3), the above difference equation can be reformulated as a $(M-1)\times(M-1)$ linear system of equations of the form,

$$L\mathbf{u}=\mathbf{b} \tag{4.16}$$

where

$$\mathbf{u}=(u_{1,j+1},u_{2,j+1},...,u_{M-1,j+1})^{\mathrm{T}},\quad \mathbf{b}=(b_1,b_2,...,b_{M-1})^{\mathrm{T}}.$$

and L is

$$\begin{pmatrix}1-B_{0,j+1} & -(A_{j+1}+C_{j+1}) & 0 & \cdots & 0 & 0 & 0\\ -A_{j+1} & 1-B_{1,j+1} & -C_{j+1} & \cdots & 0 & 0 & 0\\ \vdots & \vdots & \vdots & \ddots & \vdots & \vdots & \vdots\\ 0 & 0 & 0 & \cdots & -A_{j+1} & 1-B_{M-2,j+1} & -C_{j+1}\\ 0 & 0 & 0 & \cdots & 0 & -(A_{j+1}+C_{j+1}) & 1-B_{M-1,j+1}\end{pmatrix},$$

$$b_1 = (1+B_{0,j})u_{0,j} + (A_j + C_j)u_{1,j} - 2h(C_{j+1}\mu_1(t_{j+1}) + C_j\mu_1(t_j)) + \frac{\Delta t}{2}(f_{0,j+1} + f_{0,j}),$$

$$b_i = A_j u_{i-1,j} + (1+B_{i,j})u_{i,j} + C_j u_{i+1,j} + \frac{\Delta t}{2}(f_{i,j+1} + f_{i,j}), \quad i = \overline{2,(M-2)},$$

$$b_{M-1} = (A_j + C_j)u_{M-2,j} + (1+B_{M-1,j})u_{0,j} + 2h(A_{j+1}\mu_2(t_{j+1}) + A_j\mu_2(t_j)) + \frac{\Delta t}{2}(f_{M-1,j+1} + f_{M-1,j}).$$

As an example, consider the direct problem (4.2), (4.3) and (4.8) with $T = \ell = 1$ and

$$a(t) = 1+t, \quad b(t) = 1+2t, \quad d(x,t) = x^2 + t^2, \quad \phi(x) = (1-3x)^2, \quad \mu_1(t) = e^t,$$
$$\mu_2(t) = 4e^t, \; f(x,t) = (1-3x)^2 e^t - 18(1+t)e^t + (6+12t)(1-3x)e^t - (x^2+t^2)(1-3x)^2 e^t.$$

With this input data, the exact solution is given by $u(x,t) = (1-3x)^2 e^t$, and the desired heat fluxes (4.4), for $K(t) = 1$, are $\nu_1(t) = 6e^t$ and $\nu_2(t) = 12e^t$.

The numerical and exact solutions for $u(x,t)$ are shown in Figure 4.1 and a very good agreement is obtained. Tables 4.1 and 4.2 give the numerical heat fluxes in comparison with the exact ones. These have been calculated using the following $O(h^2)$ finite-difference approximations:

$$u_x(0,t_j) = \frac{4u_{1,j} - u_{2,j} - 3u_{0,j}}{2\Delta x}, \; u_x(\ell,t_j) = \frac{4u_{M-1,j} - u_{M-2,j} - 3u_{M,j}}{-2\Delta x}, \; j = \overline{1,N}. \tag{4.17}$$

From these tables it can be seen that the numerical results are in very good agreement with the exact solution and that a rapid monotonic increasing convergence is achieved.

Table 4.1: The exact and the numerical heat flux $-u_x(0,t)$ for $M = N \in \{10, 20, 40, 100\}$, for the direct problem.

t	0.1	0.2	...	0.8	0.9	1
$M = N = 10$	-6.6309	-7.3282	...	-13.3529	-14.7573	-16.3093
$M = N = 20$	-6.6310	-7.3284	...	-13.3532	-14.7575	-16.3096
$M = N = 40$	-6.6310	-7.3284	...	-13.3532	-14.7576	-16.3097
$M = N = 100$	-6.6310	-7.3284	...	-13.3532	-14.7576	-16.3097
exact	-6.6310	-7.3284	...	-13.3532	-14.7576	-16.3097

Table 4.2: The exact and the numerical heat flux $u_x(1,t)$ for $M = N \in \{10, 20, 40, 100\}$, for the direct problem.

t	0.1	0.2	...	0.8	0.9	1
$M = N = 10$	13.2614	14.6564	...	26.7059	29.5145	23.6187
$M = N = 20$	13.2620	14.6567	...	26.7063	29.5151	23.6192
$M = N = 40$	13.2620	14.6568	...	26.7064	29.5152	23.6193
$M = N = 100$	13.2620	14.6568	...	26.7065	29.5152	23.6194
exact	13.2620	14.6568	...	26.7065	29.5152	23.6194

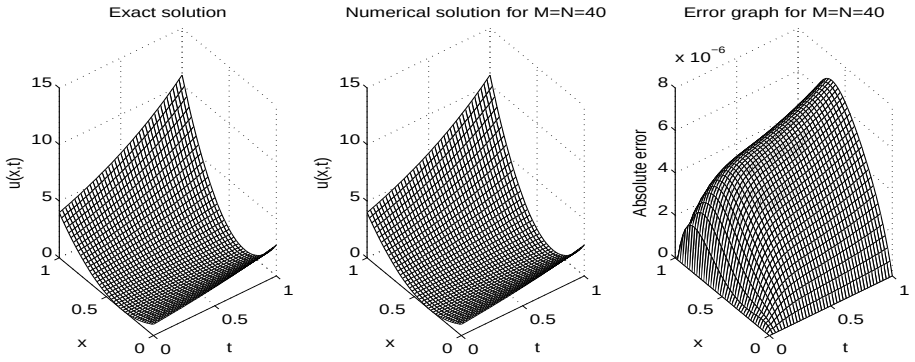

Figure 4.1: Exact and numerical solutions for $u(x,t)$ and the absolute error for the direct problem (4.2), (4.3) and (4.8) obtained with $M = N = 40$.

4.4 Solution of inverse problems

In our inverse problems we wish to obtain simultaneously stable reconstructions of two unknown coefficients in equation (4.1), satisfying the initial and boundary conditions (4.2)–(4.4). The most common Tikhonov-type regularization approach is to impose the measured input data (4.4) in a penalized least-squares sense. This recasts into minimizing the following regularized (penalized) nonlinear objective functions.

For the IP1 given by equations (4.2)–(4.5) we minimize the functional

$$F_1(K,C) := \| - K(t)u_x(0,t) - \nu_1(t)\|^2 + \|K(t)u_x(\ell,t) - \nu_2(t)\|^2 + \beta \left(\|K(t)\|^2 + \|C(t)\|^2 \right), \tag{4.18}$$

where $\beta \geq 0$ is a regularization parameter and the norm $\| \cdot \|$ is usually taken as the $L^2[0,T]$ norm. We note that in the regularization term we could have chosen different regularization parameters as $\beta_1 \|K(t)\|^2 + \beta_2 \|C(t)\|^2$, but this

more general regularization is deferred, for the time being, to the subsequent inverse problems investigated in the rest of the thesis.

Similarly, for the IP2 given by equations (4.2), (4.3), (4.7) and (4.8) we minimize the functional

$$F_2(a,b) := \| - u_x(0,t) - \overline{\nu}_1(t)\|^2 + \|u_x(\ell,t) - \overline{\nu}_2(t)\|^2 + \beta \left(\|a(t)\|^2 + \|b(t)\|^2 \right), \tag{4.19}$$

and for the IP3 given by equations (4.2)–(4.4) and (4.8) we minimize the functional

$$F_3(K,b) := \| - K(t)u_x(0,t) - \nu_1(t)\|^2 + \|K(t)u_x(\ell,t) - \nu_2(t)\|^2 + \beta \left(\|K(t)\|^2 + \|b(t)\|^2 \right). \tag{4.20}$$

The case $\beta = 0$ yields the ordinary nonlinear least-squares method which is usually unstable for noisy data. The physical constraints that the thermal conductivity and diffusivity are positive recast as a simple lower bound on these variables and is imposed as $K \geq 10^{-10}$ and $a \geq 10^{-10}$. The velocity v of the fluid is allowed to be either positive (convection) or negative (advection).

The discretizations of (4.18)–(4.20) are:

$$F_1(\underline{K},\underline{C}) = \sum_{j=0}^{N} [-K(t_j)u_x(0,t_j) - \nu_1(t_j)]^2 + \sum_{j=0}^{N} [K(t_j)u_x(\ell,t_j) - \nu_2(t_j)]^2 + \beta \left(\sum_{j=0}^{N} K^2(t_j) + \sum_{j=0}^{N} C^2(t_j) \right), \tag{4.21}$$

$$F_2(\underline{a},\underline{b}) = \sum_{j=0}^{N} [-u_x(0,t_j) - \overline{\nu}_1(t_j)]^2 + \sum_{j=0}^{N} [u_x(\ell,t_j) - \overline{\nu}_2(t_j)]^2 + \beta \left(\sum_{j=0}^{N} a^2(t_j) + \sum_{j=0}^{N} b^2(t_j) \right), \tag{4.22}$$

$$F_3(\underline{K},\underline{b}) = \sum_{j=0}^{N} [-K(t_j)u_x(0,t_j) - \nu_1(t_j)]^2 + \sum_{j=0}^{N} [K(t_j)u_x(\ell,t_j) - \nu_2(t_j)]^2 + \beta \left(\sum_{j=0}^{N} K^2(t_j) + \sum_{j=0}^{N} b^2(t_j) \right), \tag{4.23}$$

respectively.

It is worth mentioning that at the first time step, i.e. $j = 0$, the above equa-

tions (4.21)–(4.23) need the derivatives $u_x(0,0)$ and $u_x(\ell,0)$ which are obtained from the initial condition (4.2), using (4.17) as:

$$u_x(0,0) = \frac{4\phi_1 - \phi_2 - 3\phi_0}{2\Delta x}, \quad u_x(\ell,0) = \frac{4\phi_{M-1} - \phi_{M-2} - 3\phi_M}{-2\Delta x}, \tag{4.24}$$

where $\phi_i = \phi(x_i)$ for $i = \overline{0,M}$.

If there is noise in the measured data (4.4), we replace $\nu_1(t_j)$ and $\nu_2(t_j)$ in (4.21) and (4.23) by the noisy perturbations

$$\nu_1^{\epsilon 1}(t_j) = \nu_1(t_j) + \epsilon 1_j, \quad \nu_2^{\epsilon 2}(t_j) = \nu_2(t_j) + \epsilon 2_j, \quad j = \overline{0,N}, \tag{4.25}$$

where $\epsilon 1_j$ and $\epsilon 2_j$ are random variables generated from a Gaussian normal distribution with mean zero and standard deviations σ_1 and σ_2, respectively, given by

$$\sigma_1 = p \times \max_{t\in[0,T]} |\nu_1(t)|, \quad \sigma_2 = p \times \max_{t\in[0,T]} |\nu_2(t)|, \tag{4.26}$$

where p represents the percentage of noise. We use the MATLAB function *normrnd* to generate the random variables $\underline{\epsilon 1}$ and $\underline{\epsilon 2}$ as follows:

$$\underline{\epsilon 1} = normrnd(0, \sigma_1, N+1), \quad \underline{\epsilon 2} = normrnd(0, \sigma_2, N+1). \tag{4.27}$$

Note that via (4.7) we replace $\overline{\nu}_1$ and $\overline{\nu}_2$ in (4.22) by the noisy perturbations

$$\overline{\nu}_1^{\epsilon 1}(t_j) = \nu_1^{\epsilon 1}(t_j)/K(t_j), \quad \overline{\nu}_2^{\epsilon 2}(t_j) = \nu_2^{\epsilon 2}(t_j)/K(t_j), \quad j = \overline{0,N}. \tag{4.28}$$

4.4.1 Minimization Algorithms

Nevertheless, finding a global minimizer (even only approximately) to nonlinear (least-squares) problems is not an easy task. Numerical experience shows that the objective function which is, in general, non-convex has usually multiple local minima in which a descent method tends to get stuck if the underlying problem is ill-posed. Furthermore, the determination of an appropriate regularization parameter β requires additional computational effort.

In this section, we give brief description of the routines $fmincon$ and $lsqnonlin$ from the MATLAB Optimization Toolbox [95] that we have employed for the constrained nonlinear minimization of the functionals defined by equations (4.18)–(4.20). These routines are based on interior trust region methods for nonlinear minimization [9, 22].

The above routines attempt to find a minimum of a scalar objective function

of several variables, starting from an initial guess, subject to simple bounds on the variables. In all examples of the next section, the initial guess was $K^0 = 1$, $a^0 = 1$, $b^0 = 1$ and the lower and upper bounds were taken as $LB(K) = LB(a) = 10^{-10}$, $LB(b) = -10^3$, and $UB(K) = UB(a) = UB(b) = 10^3$.

Apart from the initial guess, and the upper and lower bounds the routines also require the user to input some parameters such as:

- Number of variables $M = N = 40$.
- Maximum number of iterations = $(10^2 \div 10^5) \times$ (number of variables).
- Maximum number of objective function evaluations = $(10^3 \div 10^7) \times$(number of variables).
- Solution and objective function tolerances= 10^{-10}.

It is also worth noting that the user does not need to supply the gradient of the objective function which is minimized, as this is calculated internally within the routines using finite differences. Further, the Broyden, Fletcher, Goldfarb and Shanno (BFGS) technique is used to compute the Hessian matrix.

We finally mention that we have also used a combination between a generalized pattern search algorithm for the poll method and a genetic algorithm for the search method, both of them from the MATLAB Global Optimization Toolbox. In comparison with the previously described interior-point algorithms the results were not significantly improved, but instead the computational time increased beyond purpose. For this reason, the numerical results obtained using this latter combined method are omitted.

4.5 Numerical results and discussion

Numerical results are presented for several test examples for the inverse problems IP1–IP3, and in each example we obtain the numerical solution of coefficient identification problems for various noise levels p. In these examples we take, for simplicity, $\ell = T = 1$.

We employ $fmincon$ for IP1 and $lsqnonlin$ for IP2 and IP3, for the minimization of the functionals (4.18)–(4.20). The other computational details have already been given in Subsection 4.4.1. We have also calculated the relative root mean square error ($rrmse$) to analyse the error between the exact and estimated

coefficients, defined as,

$$rrmse(K(t)) = \sqrt{\frac{1}{N+1}\sum_{j=0}^{N}\left(\frac{K_{numerical}(t_j) - K_{exact}(t_j)}{K_{exact}(t_j)}\right)^2}, \tag{4.29}$$

and similar expressions exist for $a(t)$, $b(t)$ and $C(t)$.

One of the main difficulties when we solve inverse and ill-posed problems is how to choose an appropriate regularization parameter β which must compromise between accuracy and stability. Nevertheless, one can use techniques such as the L-curve method [44] or, Morozov's discrepancy principle [96] to find such a parameter, but in our work we have used trial and error. As mentioned in [28], the regularization parameter β is selected based on experience by first choosing a small value and gradually increasing it until any numerical oscillations in the unknown coefficient are removed.

4.5.1 Example 1 for IP1

We first consider the problem IP1 given by equations (4.2)–(4.5), with unknown coefficients $C(t)$ and $K(t)$, and we solve this inverse problem with the following input data:

$$\begin{aligned}&\phi(x) = (1+x)^2,\ \mu_1(t) = t^2+t+1, \quad \mu_2(t) = t^2+t+4,\\ &\nu_1(t) = -(1+t)(1+2t), \quad \nu_2(t) = 2(1+t)(1+2t),\end{aligned}$$

for $x \in (0, \ell = 1)$ and $t \in (0, T = 1)$. The exact solution is given by

$$u(x,t) = (1+x)^2 + t^2 + t,\ C(t) = 1+t, \quad K(t) = (1+t)\left(t+\frac{1}{2}\right). \tag{4.30}$$

We also have that $a(t) = t + \frac{1}{2}$, and one can easily check that the conditions of Theorems 4.1 and 4.2 are satisfied such that we know beforehand for sure that the solution to the IP1 exists and is unique.

Table 4.3 gives the numerical coefficients obtained using $M = N \in \{10, 20, 40\}$ in comparison with the exact ones. From this table it can be seen that the numerical results are converging to the exact values, as the FDM mesh size decreases. In the remaining of this section, the FDM discretization with $M = N = 40$ is fixed in order to keep the accuracy good with reasonable computational effort.

In Figure 4.2, we present the regularized objective function (4.18) for $p = 0$ (no noise) and $p = 1\%$ noise included in input data $\nu_1(t)$ and $\nu_2(t)$ for several regularization parameters $\beta \in \{0, 10^{-3}, 10^{-2}, 10^{-1}\}$. From this figure, it can be

seen that convergence is achieved in a relatively small number of iterations. Also, it takes a slightly larger number of iterations when $p = 1\%$ noise contaminates the input data than when this data is errorless, i.e. $p = 0$.

Table 4.3: The exact and the numerical coefficients for $M = N \in \{10, 20, 40\}$, for the IP1 of Example 1 and without noise.

t	0.1	0.2	...	0.8	0.9	1	
	0.6600	0.8400	...	2.3400	2.6600	3.0000	$M = N = 10$
$K(t)$	0.6600	0.8400	...	2.3400	2.6600	3.0000	$M = N = 20$
	0.6600	0.8400	...	2.3400	2.6600	3.0000	$M = N = 40$
	0.6600	0.8400	...	2.3400	2.6600	3.0000	exact
	0.5769	0.7231	...	1.3231	1.3769	1.5231	$M = N = 10$
$a(t)$	0.6183	0.7183	...	1.3183	1.4183	1.5183	$M = N = 20$
	0.6119	0.7119	...	1.3119	1.4119	1.5119	$M = N = 40$
	0.6000	0.7000	...	1.3000	1.4000	1.5000	exact
	1.1441	1.1616	...	1.7686	1.9319	1.9696	$M = N = 10$
$C(t)$	1.0674	1.1694	...	1.7750	1.8755	1.9759	$M = N = 20$
	1.0787	1.1800	...	1.7837	1.8840	1.9843	$M = N = 40$
	1.1000	1.2000	...	1.8000	1.9000	2.0000	exact

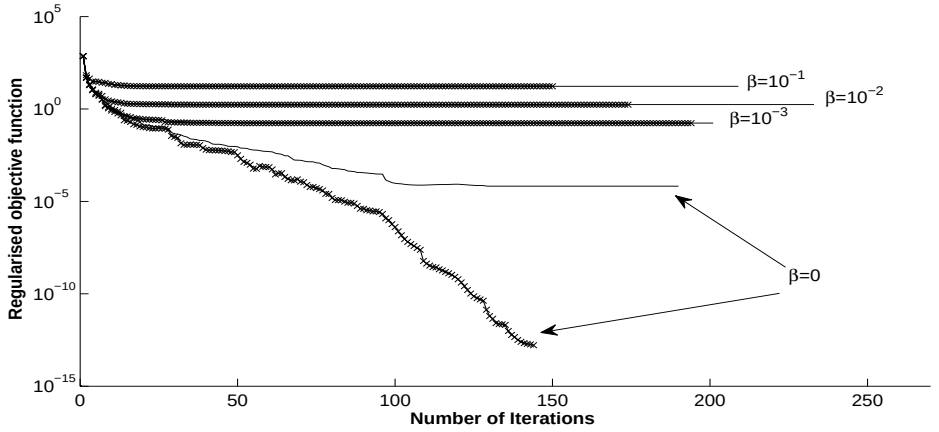

Figure 4.2: Regularized objective function (4.18), for Example 1 without noise (-×-) and with $p = 1\%$ noise (—).

In Figure 4.3 and Table 4.4, we present the identified coefficients and their *rrmse* values, respectively, for no noise, and with and without regularization. From this figure and table it can be seen that for exact data, when β decreases to zero, we obtain numerical results for the identified coefficients $K(t)$, $a(t)$ and $C(t)$ which are convergent to their exact values. In the case $\beta = 10^{-1}$ we observe that

the graphs of the identified coefficients slightly depart from the exact ones because we have added too much unwanted regularization to the objective function (4.18). In Figure 4.4 and Table 4.4 we present the retrieved coefficients and their $rrmse$ values, respectively, when $p = 1\%$ noise is included in the input data $\nu_1(t)$ and $\nu_2(t)$. It can be seen that the numerical retrieval of the thermal conductivity $K(t)$ is accurate; however, unstable results are obtained for $a(t)$ and $C(t)$ if no regularization, i.e. $\beta = 0$, is employed, or even if β is too small such as 10^{-3}. Clearly, one can observe the effect of the regularization parameter $\beta > 0$ in decreasing the oscillatory unstable behaviour of the retrieved coefficients. Overall, the numerical results obtained with $\beta = 10^{-1}$ seem the most stable and accurate.

Table 4.4: The $rrmse$ values for estimated coefficients in Example 1.

	$\beta = 0$	$\beta = 10^{-3}$	$\beta = 10^{-2}$	$\beta = 10^{-1}$
$p = 0$	$rrmse(K) = 8.5E-9$	$8.5E-5$	$8.3E-4$	0.0079
	$rrmse(a) = 0.0138$	0.0284	0.0352	0.0781
	$rrmse(C) = 0.0138$	0.0287	0.0385	0.1241
$p = 1\%$	$rrmse(K) = 0.0142$	0.0143	0.0146	0.0172
	$rrmse(a) = 0.2937$	0.2941	0.1654	0.0917
	$rrmse(C) = 0.4059$	0.6279	0.2080	0.1194

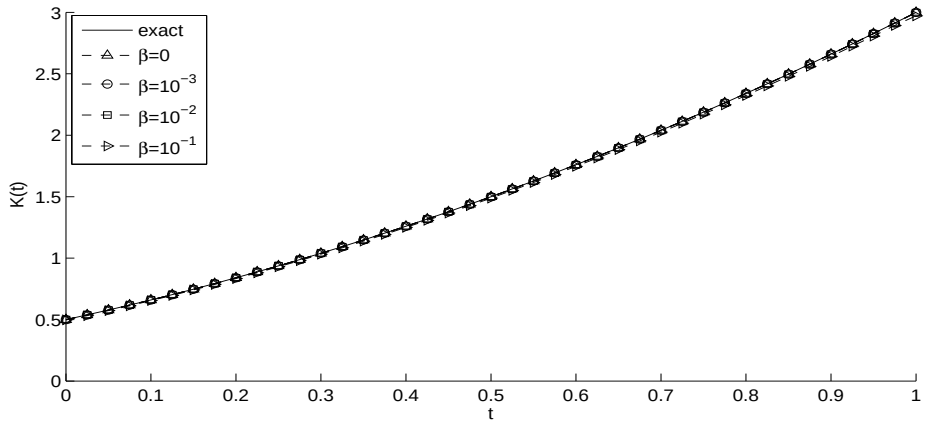

(a)

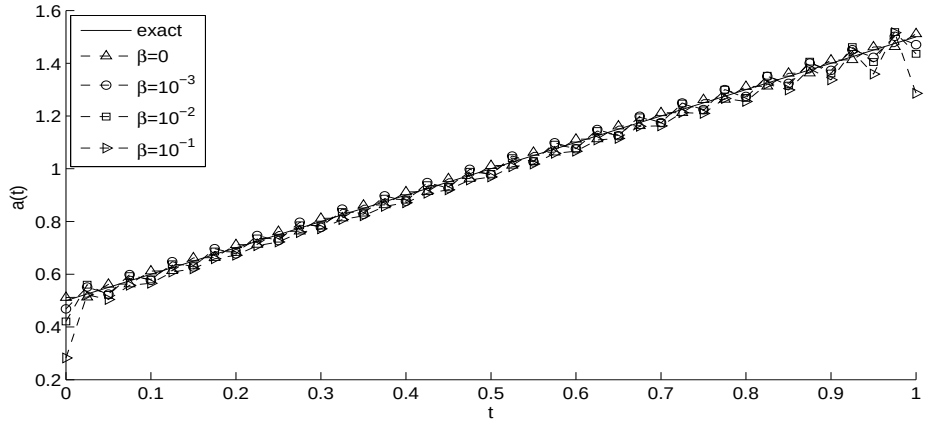

(b)

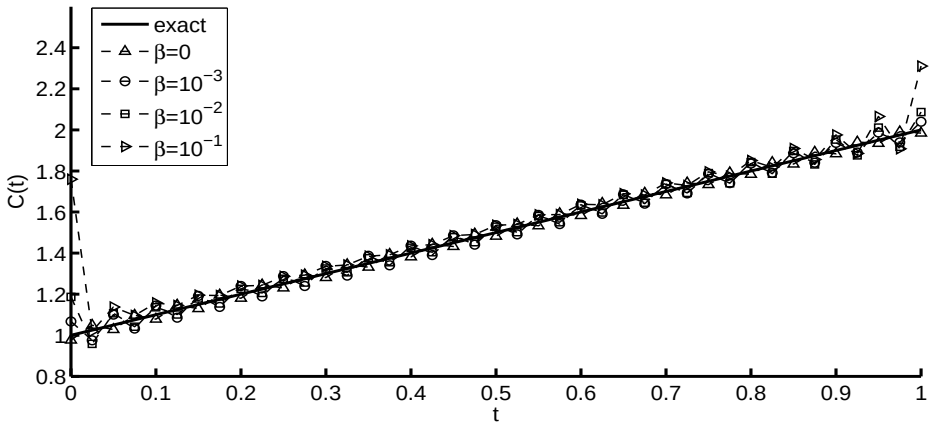

(c)

Figure 4.3: The identified coefficients: (a) Thermal conductivity, (b) Thermal diffusivity, and (c) Heat capacity, for Example 1 with no noise.

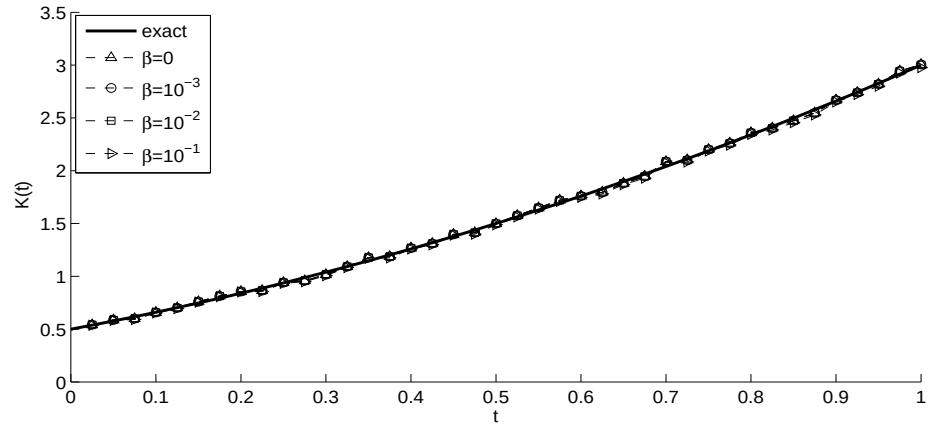

(a)

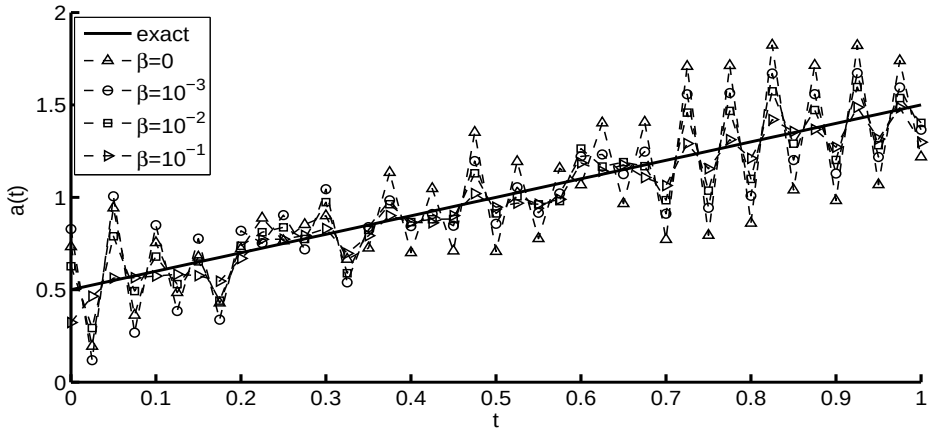

(b)

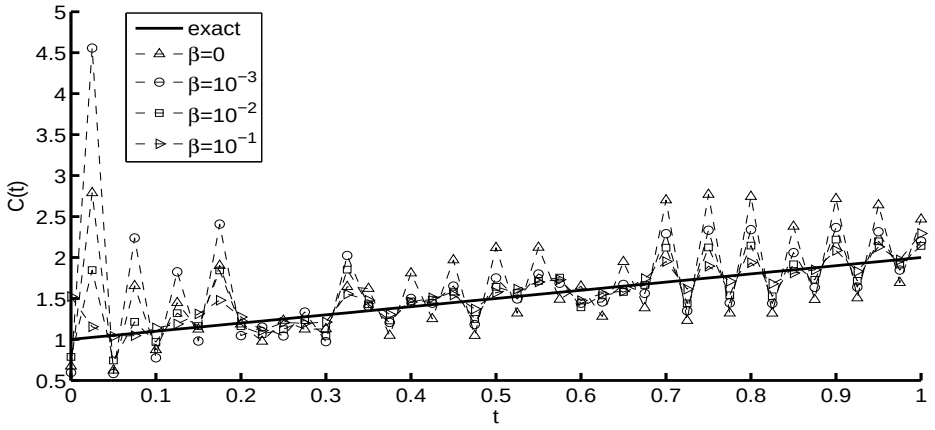

(c)

Figure 4.4: The identified coefficients: (a) Thermal conductivity, (b) Thermal diffusivity, and (c) Heat capacity, for Example 1 with $p = 1\%$ noise.

4.5.2 Example 2 for IP1

We next consider an example from [75] in which the input data satisfy the conditions of the existence of the solution of Theorem 4.1,

$$\phi(x) = \frac{x^4}{12} + 2x - 4,\ \mu_1(t) = t^4 + 2t^3 + t^2 - 4, \quad \mu_2(t) = t^4 + 2t^3 + 2t^2 + t - \frac{23}{12},$$
$$\nu_1(t) = -2t - 2, \qquad \nu_2(t) = (t+1)\left(2t^2 + 2t + \frac{7}{3}\right),$$

for $x \in (0, \ell = 1)$ and $t \in (0, T = 1)$. However, the conditions of the uniqueness of the solution of Theorem 4.2 are all satisfied, but for the condition $\phi''(0) > 0$ which is not satisfied. One can simply check by direct substitution that the solution

$$u(x,t) = t^4 + 2t^3 + t^2(x^2+1) + tx^2 + \frac{x^4}{12} + 2x - 4,$$
$$C(t) = \frac{1+t}{1+2t}, \quad K(t) = 1 + t. \tag{4.31}$$

satisfies the inverse problem (4.2)–(4.5). We also have that $a(t) = 1 + 2t$.

Figure 4.5 illustrates the objective function (4.18), as a function of the number of iterations for $p = 0$ (no noise) and $p = 1\%$ noise included in the input data $\nu_1(t)$ and $\nu_2(t)$. It is interesting to remark that for β small such as 0 to 10^{-3} the convergence is non-monotonic with respect to the number of iterations. Also, the unregularized ($\beta = 0$) objective function reduces rather non-smoothly to reach a stationary value of $O(10^{-7})$ for $p = 0$ and $O(10^{-4})$ for $p = 1\%$, whilst the curves obtained for $\beta > 0$ reach rapidly a stationary plateau.

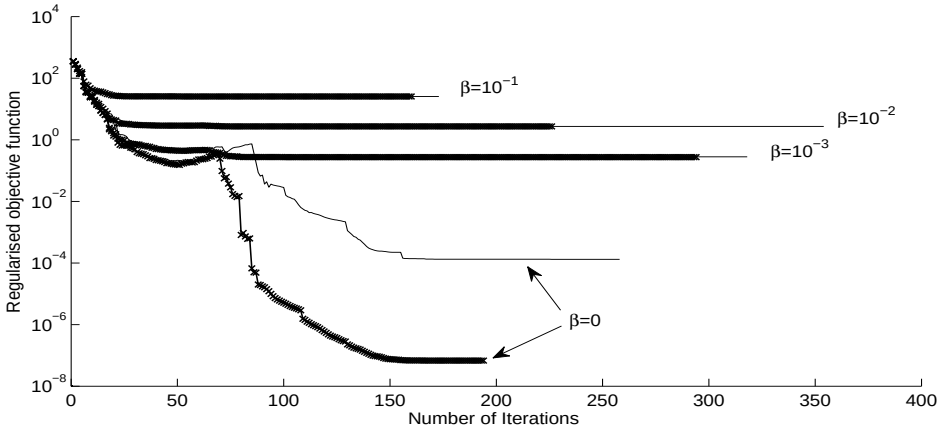

Figure 4.5: Regularized objective function (4.18), for Example 2 without noise (-×-) and with $p = 1\%$ noise (—).

Table 4.5: The *rrmse* values for estimated coefficients in Example 2.

	$\beta = 0$	$\beta = 10^{-3}$	$\beta = 10^{-2}$	$\beta = 10^{-1}$
$p = 0$	$rrmse(K) = 5.6E-5$	$6.8E-4$	0.0039	0.0223
	$rrmse(a) = 0.0078$	0.0449	0.1000	0.2239
	$rrmse(C) = 0.0078$	0.0552	0.2095	0.7778
$p = 1\%$	$rrmse(K) = 0.0123$	0.0125	0.0146	0.0276
	$rrmse(a) = 0.3066$	0.2301	0.1441	0.2321
	$rrmse(C) = 0.4350$	0.3677	0.2135	0.7993

Figures 4.6, 4.7 and Table 4.5 for Example 2 represent the same quantities as Figures 4.3, 4.4 and Table 4.4 for Example 1, and the same conclusions can be drawn. We also mention that the numerical results obtained with $\beta = 10^{-2}$ seem the most stable and accurate for $p = 1\%$ noisy data.

4.5.3 Example 3 for IP1

Finally, for IP1, we consider the case of a non-smooth coefficient and more complicated input data given by

$$\begin{aligned}
&\phi(x) = \frac{x^2+x}{2} - \frac{1}{4},\\
&\mu_1(t) = \begin{cases} \frac{3t-t^2}{2} - \frac{1}{4} & \text{if } t \in [0, \frac{1}{2}] \\ \frac{t+t^2}{2} & \text{if } t \in [\frac{1}{2}, 1] \end{cases}, \quad \mu_2(t) = \begin{cases} \frac{3t-t^2}{2} + \frac{3}{4} & \text{if } t \in [0, \frac{1}{2}] \\ \frac{t+t^2}{2} + 1 & \text{if } t \in [\frac{1}{2}, 1] \end{cases},\\
&\nu_1(t) = -\frac{1}{2}\left(1 + \left|t - \frac{1}{2}\right|\right), \qquad \nu_2(t) = \frac{3}{2}\left(1 + \left|t - \frac{1}{2}\right|\right),
\end{aligned}$$

for $x \in (0, \ell = 1)$ and $t \in (0, T = 1)$. One can remark that the conditions of Theorem 4.2 which ensure the uniqueness of the solution are satisfied. The exact solution is given by

$$\left.\begin{aligned}
u(x,t) &= \frac{x+x^2}{2} + \begin{cases} \frac{3t-t^2}{2} - \frac{1}{4} & \text{if } t \in [0, \frac{1}{2}] \\ \frac{t+t^2}{2} & \text{if } t \in [\frac{1}{2}, 1] \end{cases},\\
C(t) &= 1, \quad K(t) = 1 + \left|t - \frac{1}{2}\right|.
\end{aligned}\right\} \tag{4.32}$$

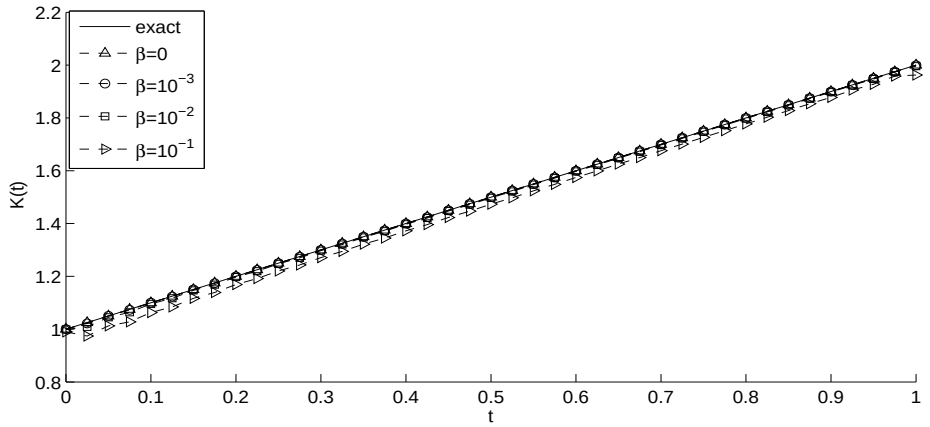

(a)

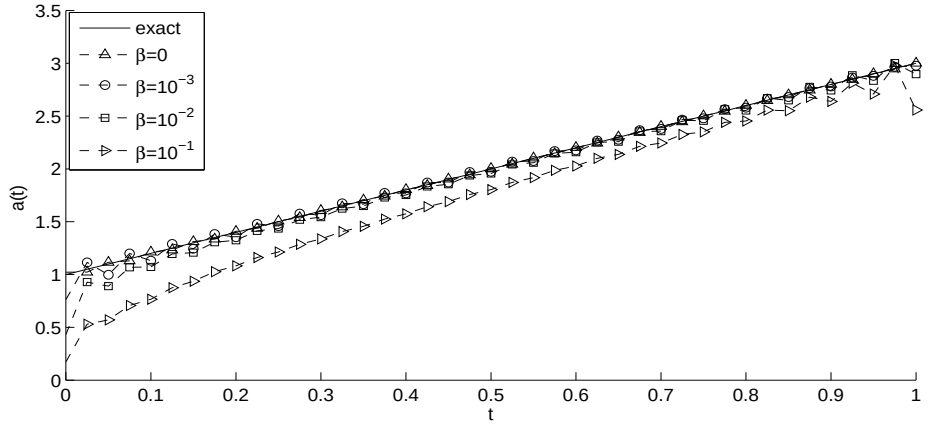

(b)

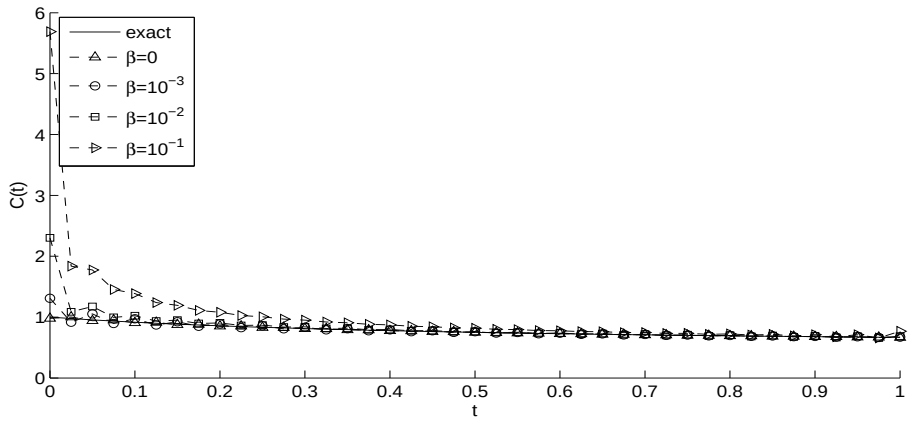

(c)

Figure 4.6: The identified coefficients: (a) Thermal conductivity, (b) Thermal diffusivity, and (c) Heat capacity, for Example 2 with no noise.

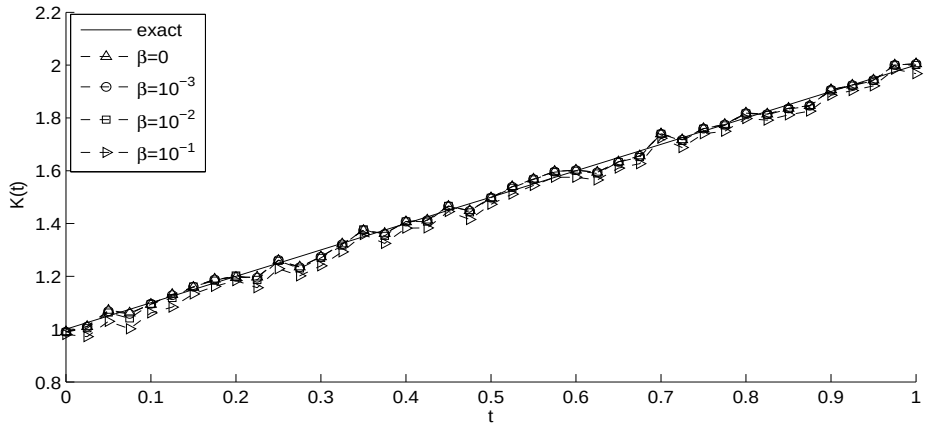

(a)

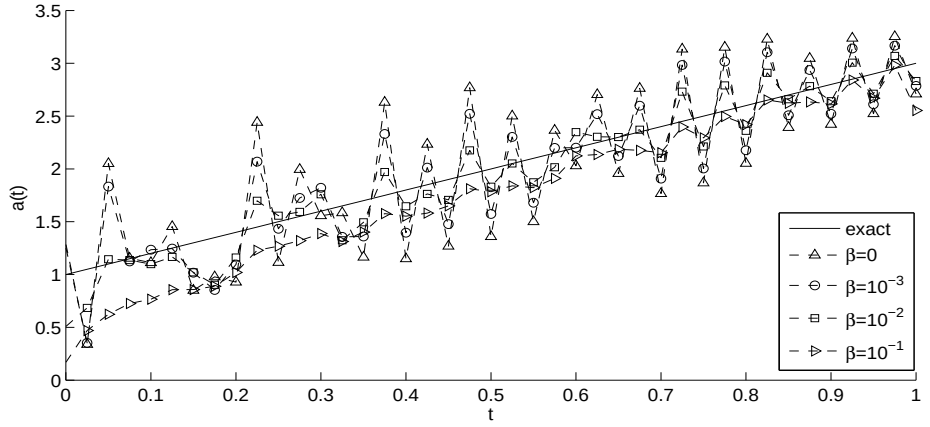

(b)

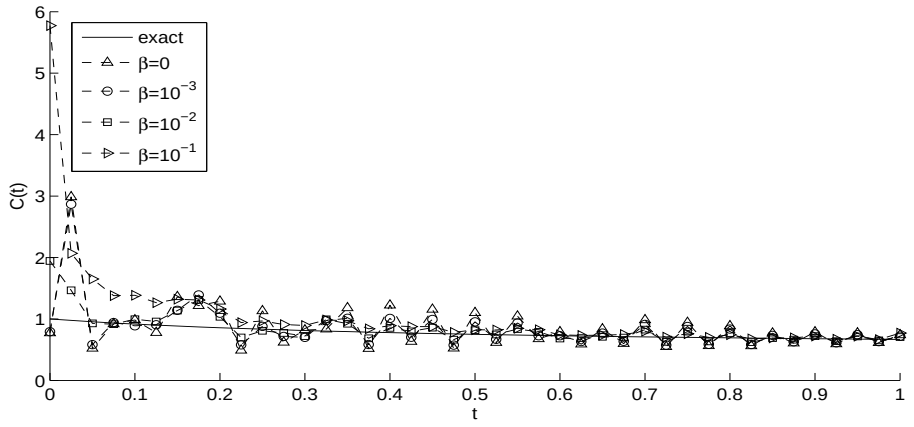

(c)

Figure 4.7: The identified coefficients: (a) Thermal conductivity, (b) Thermal diffusivity, and (c) Heat capacity, for Example 2 with $p = 1\%$ noise.

We start first with the case of exact data, i.e. $p = 0$. Figure 4.8 shows the objective function (4.18) without regularization, i.e. $\beta = 0$, as a function of

the number of iterations. It can be seen that the objective function decreases rapidly to a low level of $O(10^{-14})$ in 166 iterations. The corresponding exact and numerical coefficients $K(t)$, $a(t)$ and $C(t)$ are presented in Figure 4.9. From this figure, it can be seen that the recovered coefficients are in very good agreement with their corresponding analytical solutions.

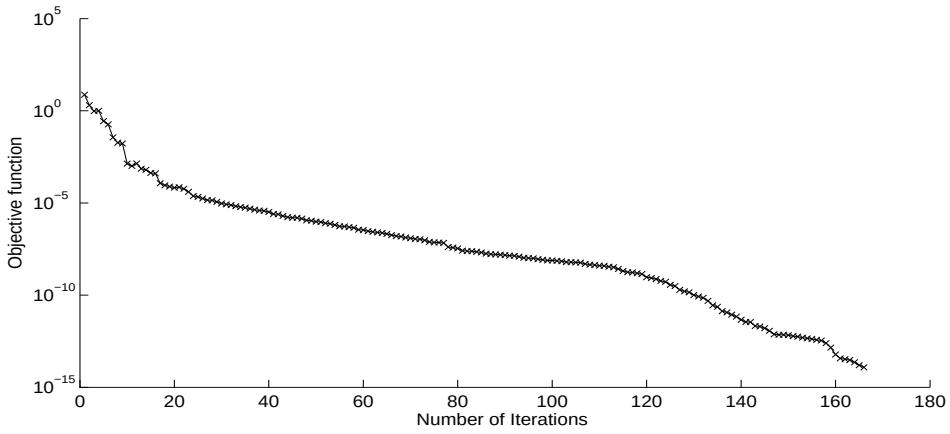

Figure 4.8: Objective function (4.18), for Example 3 with no noise (-×-) and no regularization.

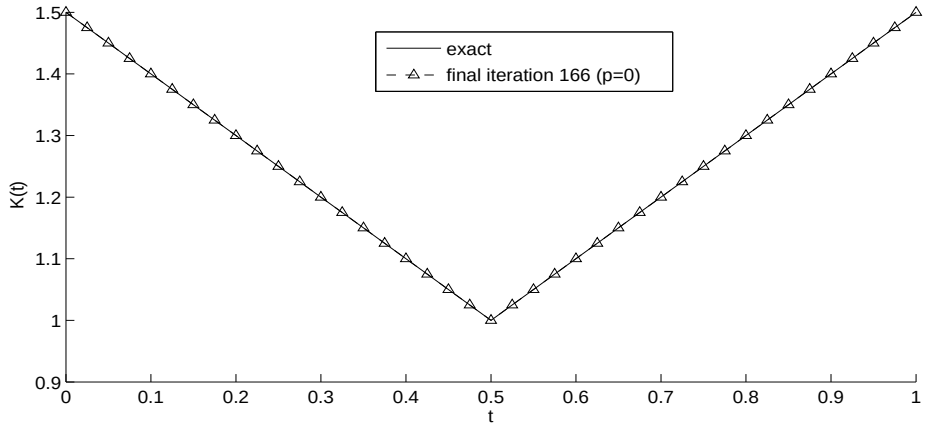

(a)

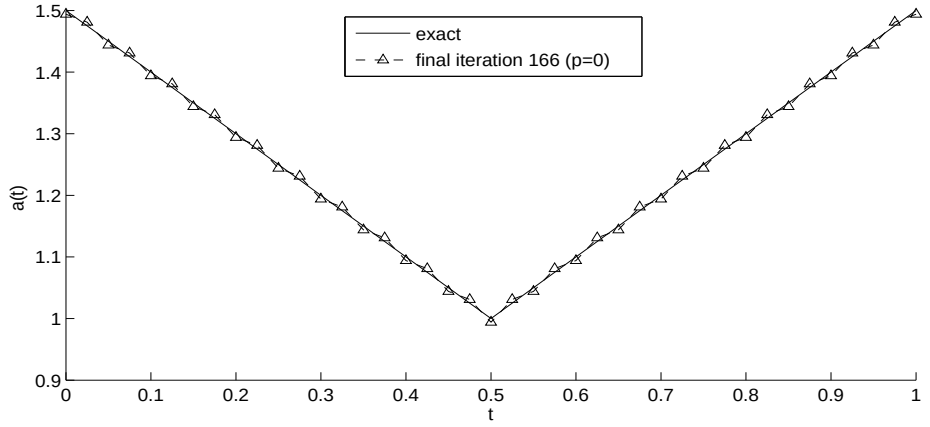

(b)

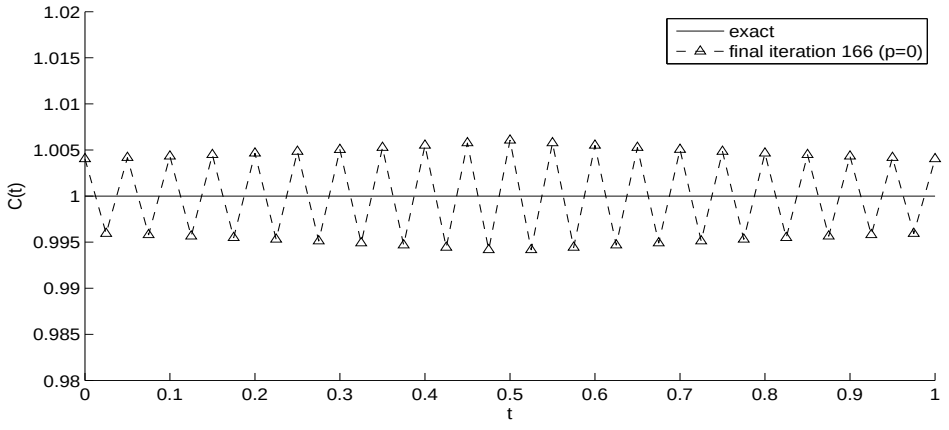

(c)

Figure 4.9: The identified coefficients: (a) Thermal conductivity, (b) Thermal diffusivity, and (c) Heat capacity, for Example 3 with no noise and no regularization.

We next include noise $p \in \{1\%,\ 2\%\}$ in the input fluxes $\nu_1(t)$ and $\nu_2(t)$, as in (4.25). In Figure 4.10, we can see that the regularized objective function becomes

a smooth decreasing curve and the convergence is achieved in a relatively small number of iterations, as β increases from 10^{-3} to 10^{-1}. The numerical results for $K(t)$, $a(t)$ and $C(t)$ when $p = 1\%$ and $p = 2\%$ are presented in Figures 4.11 and 4.12, respectively. Further, numerical outputs such as the number of iterations and function evaluations, as well as the final value of the converged objective function and the $rrmse$ values of the estimated coefficients are provided in Table 4.6. From these figures and table it can be seen that stable and reasonable accurate numerical results are obtained for $\beta = 10^{-3}$ when $p = 1\%$, and $\beta = 10^{-2}$ when $p = 2\%$ noise. The results for $\beta = 10^{-1}$ depart from the exact solution as too much regularization has been imposed, whilst the results for $\beta = 0$ seem only slightly unstable. In fact, from all examples presented in this section, see Tables 4.4–4.6, it seems that the retrieval of the thermal conductivity coefficient $K(t)$ is stable even if we do not use regularization and we may as well penalize only the thermal diffusivity $\beta\|a(t)\|^2$ in the last term of (4.18). Another reason for this stability of the solution in the $K(t)$-component might be that $K(t)$ appears explicitly in the nonlinear objective function (4.18). On the other hand the retrieval of the thermal diffusivity $a(t)$ (and hence the heat capacity $C(t)$) does require some regularization to be enforced in order to ensure stability.

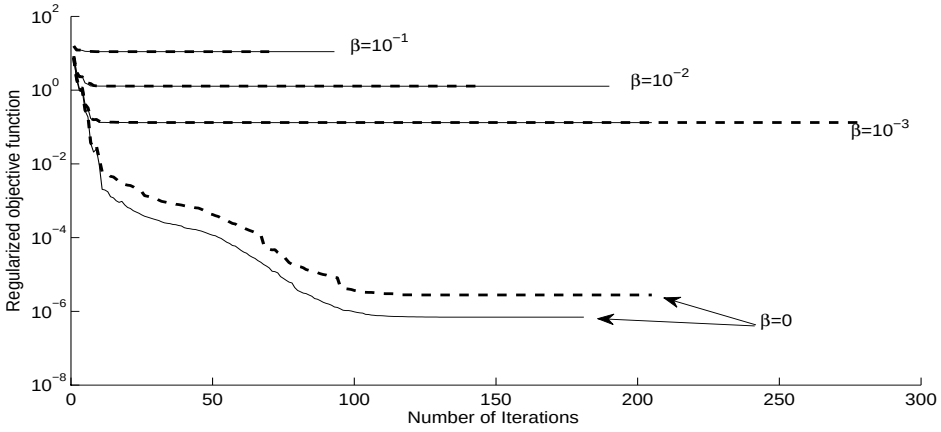

Figure 4.10: Regularized objective function (4.18), for Example 3 with $p = 1\%$ (—) and $p = 2\%$ (- - -) noise.

Table 4.6: Number of iterations, number of function evaluations, value of regularized objective function (4.18) at final iteration and $rrmse$ values for estimated coefficients, for Example 3.

Noise level		$\beta = 0$	$\beta = 10^{-3}$	$\beta = 10^{-2}$	$\beta = 10^{-1}$
$p = 1\%$	No. of iterations	181	205	190	93
	No. of function evaluations	15035	17120	16105	7889
	Function value	$6.9E-7$	0.1308	1.2778	11.03
	$rrmse(K)$	0.0090	0.0094	0.0143	0.0842
	$rrmse(a)$	0.0867	0.0619	0.0647	0.2232
	$rrmse(C)$	0.0899	0.0668	0.0740	0.3045
$p = 2\%$	No. of iterations	205	280	144	70
	No. of function evaluations	17047	23563	12210	5919
	Function value	$2.7E-6$	0.1316	1.2789	11.02
	$rrmse(K)$	0.0181	0.0186	0.0221	0.0860
	$rrmse(a)$	0.1710	0.1130	0.0794	0.2248
	$rrmse(C)$	0.1861	0.1237	0.0952	0.3120

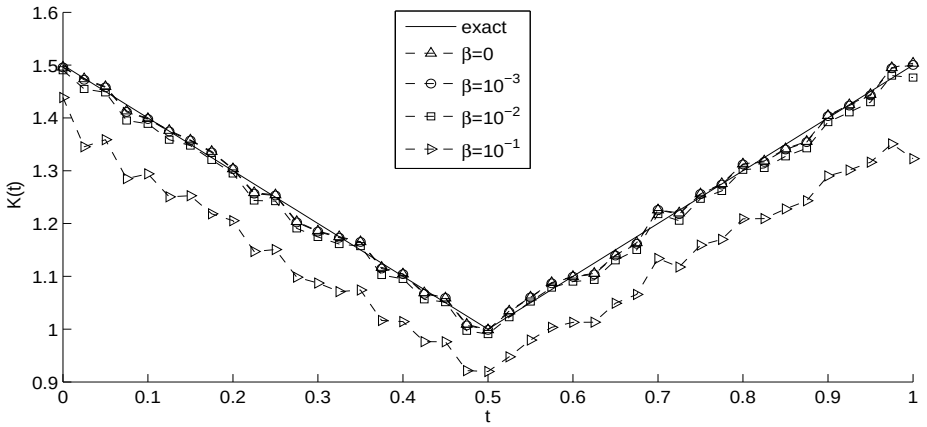

(a)

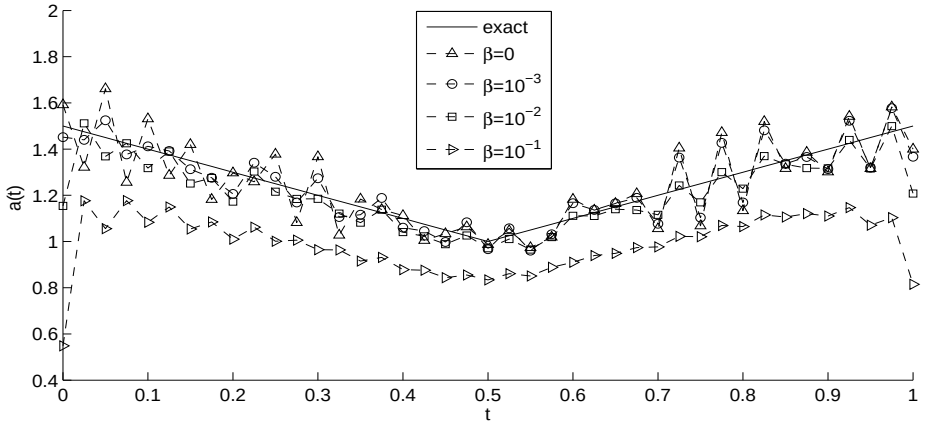

(b)

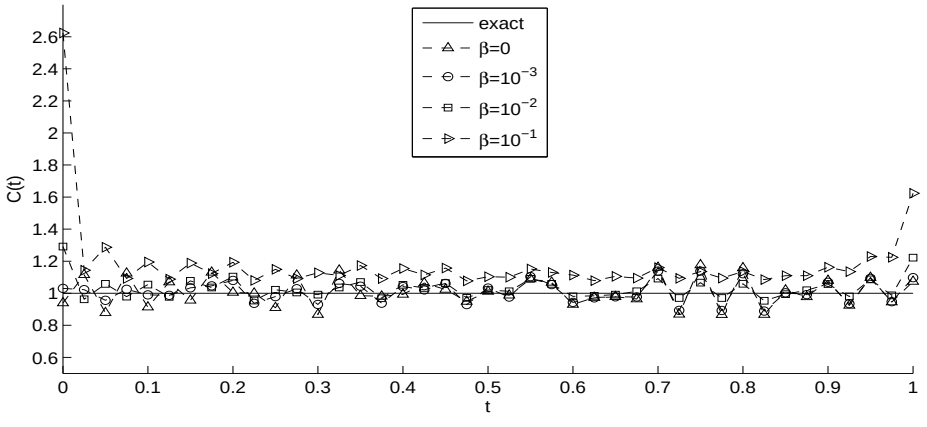

(c)

Figure 4.11: The identified coefficients: (a) Thermal conductivity, (b) Thermal diffusivity, and (c) Heat capacity, for Example 3 with $p = 1\%$ noise.

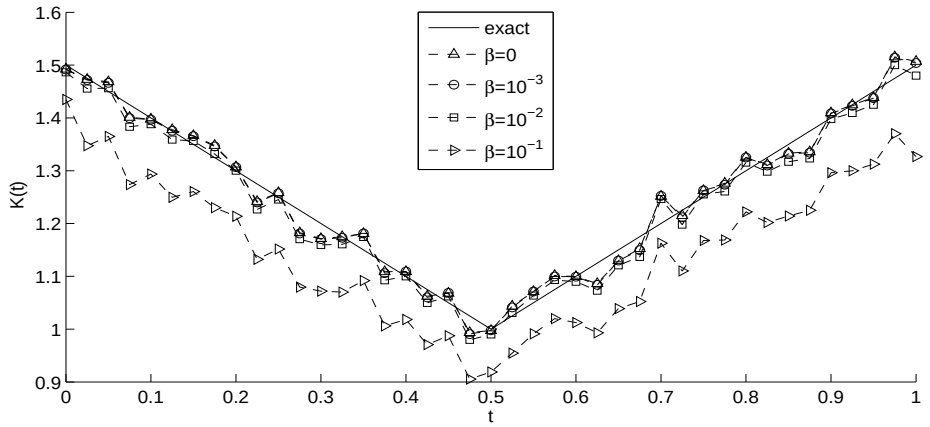

(a)

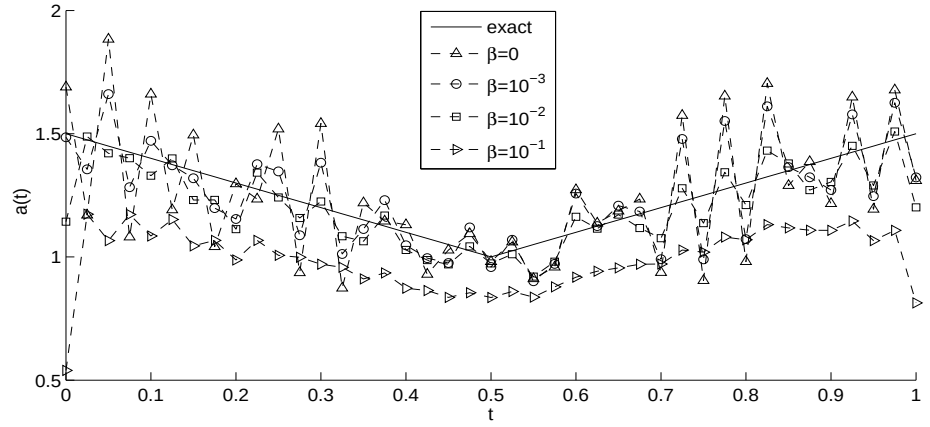

(b)

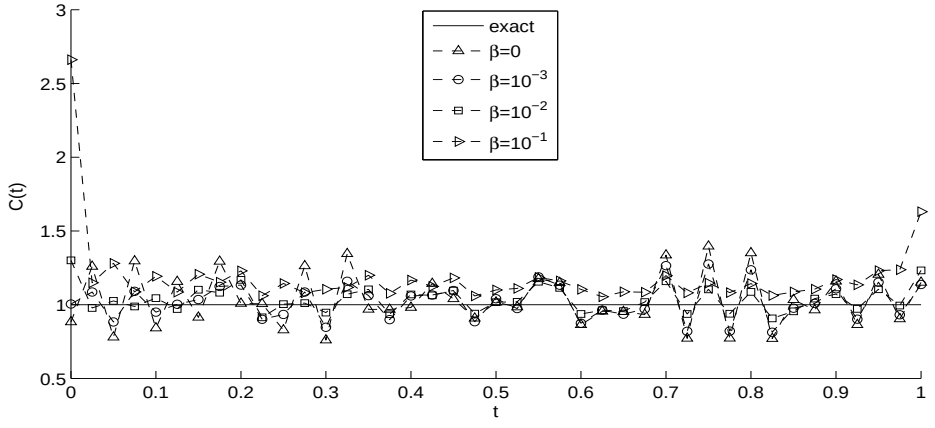

(c)

Figure 4.12: The identified coefficients: (a) Thermal conductivity, (b) Thermal diffusivity, and (c) Heat capacity, for Example 3 with $p = 2\%$ noise.

4.5.4 Example 4 for IP2

Consider now the IP2 given by equations (4.2), (4.3), (4.7) and (4.8) with unknown coefficients $a(t)$ and $b(t)$, and solve this inverse problem with the following input data:

$$\phi(x) = e^{-x} + x^2, \quad \mu_1(t) = e^t, \quad \mu_2(t) = (e^{-1} + 1)e^t, \quad \overline{\nu}_1(t) = e^t, \quad d(x,t) = 0,$$
$$\overline{\nu}_2(t) = (2 - e^{-1})e^t, \quad f(x,t) = e^t\left((1+t)e^{-x} + x^2 - 2(1+t) - 2x(1+2t)\right),$$

for $x \in (0, \ell = 1)$ and $t \in (0, T = 1)$. One can easily check that the condition of Theorem 4.4 which ensures the uniqueness of the solution is satisfied. The exact solution to this inverse problem is given by

$$a(t) = 1 + t, \quad b(t) = 1 + 2t, \qquad u(x,t) = (e^{-x} + x^2)e^t. \tag{4.33}$$

Consider first the case where there is no noise in the input data (4.7). The objective function (4.19), as a function of the number of iterations, is shown in Figure 4.13. From this figure, it can be seen that the convergence is achieved rapidly in a few iterations. The objective function (4.19) decreases rapidly and takes a stationary value of $O(10^{-8})$ in about 6 iterations. The numerical results for the corresponding coefficients $a(t)$ and $b(t)$ are presented in Figure 4.14. From this figure, it can be seen that the retrieved coefficients are in very good agreement with the exact ones.

Next, we add $p = 1\%$ noise to the heat fluxes $\overline{\nu}_1$ and $\overline{\nu}_2$, as in equation (4.28) via (4.25). The regularized objective function (4.19) is plotted, as a function of the number of iterations, in Figure 4.15 and convergence is rapidly achieved. Figure 4.16 presents the graphs of the recovered coefficients and further results are reported in Table 4.7. From this figure one can observe, as expected, that when $\beta = 0$ we obtain unstable and inaccurate solutions because the problem is ill-posed and sensitive to noise. So, regularization is needed in order to stabilize the solution. From all regularization parameters that were selected, we deduce that $\beta = 10^{-2}$ gives a stable and reasonable accurate approximation for the coefficients $a(t)$ and $b(t)$.

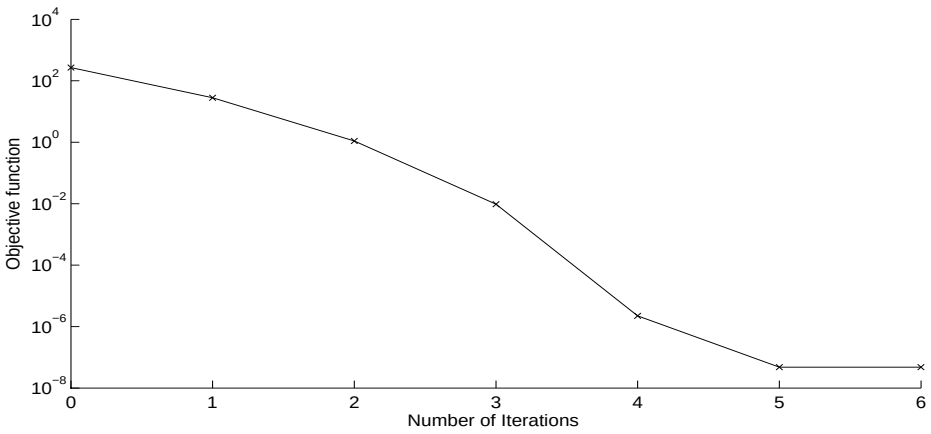

Figure 4.13: Objective function (4.19), for Example 4 with no noise and no regularization.

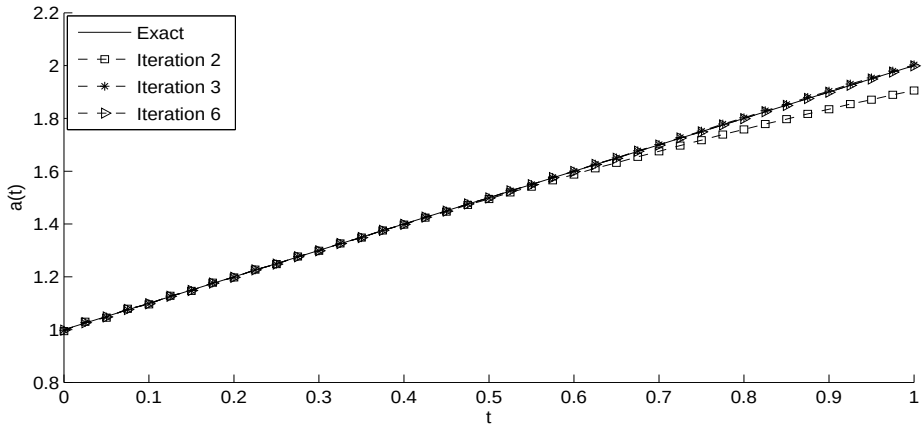

(a)

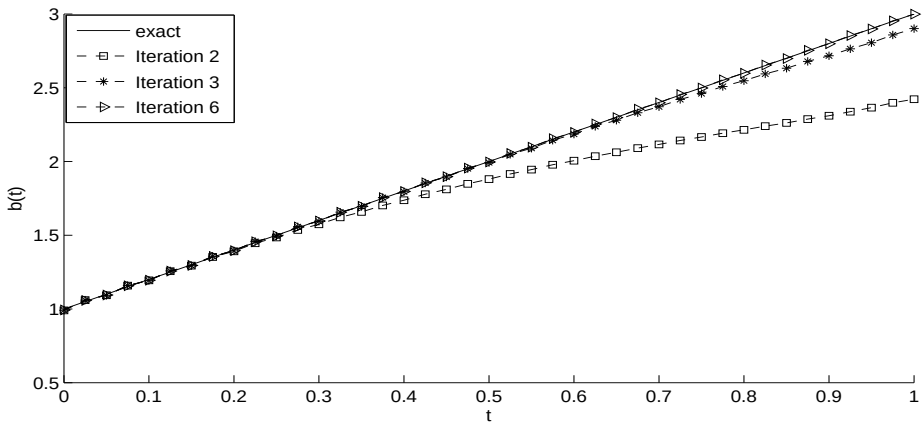

(b)

Figure 4.14: (a) Coefficient $a(t)$, and (b) Coefficient $b(t)$, for Example 4 with no noise and no regularization.

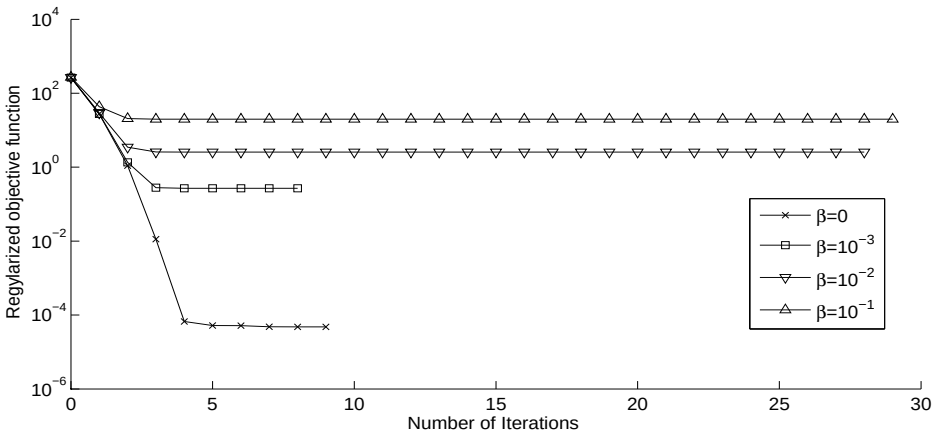

Figure 4.15: Regularized objective function (4.19), for Example 4 with $p = 1\%$ noise.

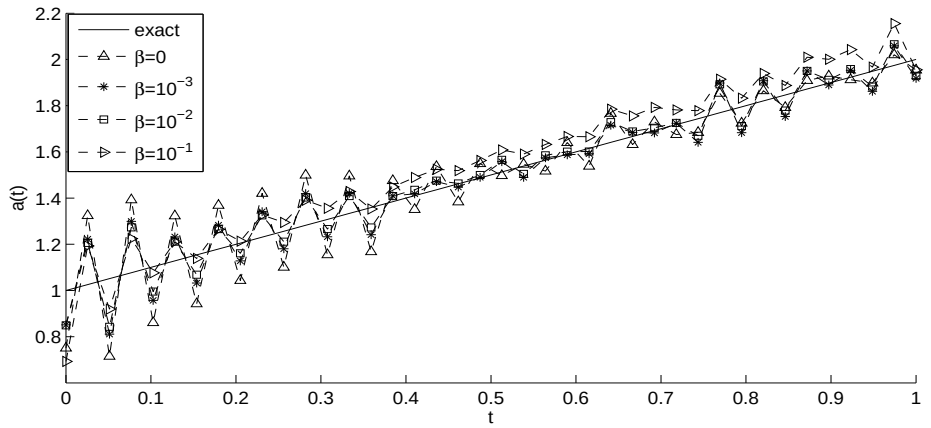

(a)

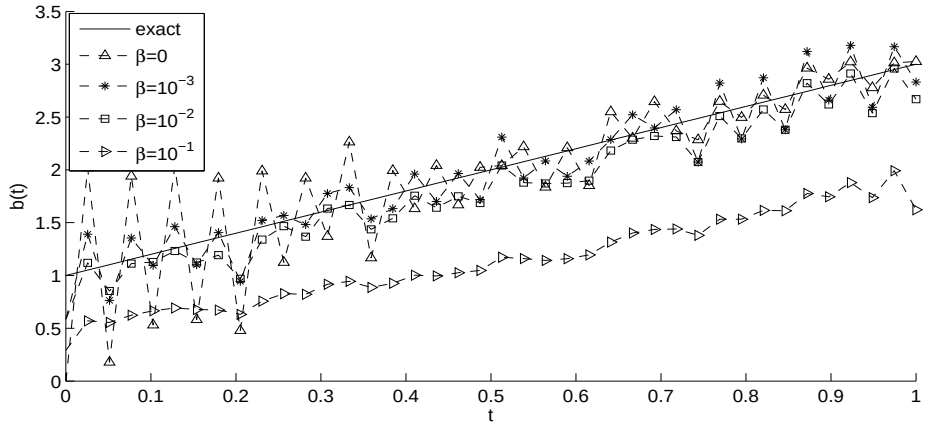

(b)

Figure 4.16: (b) Coefficient $a(t)$, and (b) Coefficient $b(t)$, for Example 4 with $p = 1\%$ noise and regularization.

4.5.5 Example 5 for IP2

In this example, we consider a more severe test case where the coefficients are non-smooth functions. Consider the IP2 with unknown coefficients $a(t)$ and $b(t)$, and solve this inverse problem with the following input data:

$$\phi(x) = e^{-x} + x^2,\ \mu_1(t) = e^t,\ \mu_2(t) = (e^{-1}+1)e^t,\ \overline{\nu}_1(t) = e^t,\ \overline{\nu}_2(t) = (2-e^{-1})e^t,$$
$$f(x,t) = (e^{-x}+x^2)e^t - \left(\left|t-\frac{1}{2}\right| + \frac{1}{2}\right)(e^{-x}+2)e^t - \left|t^2-\frac{1}{2}\right|(-e^{-x}+2x)e^t,$$
$$d(x,t) = 0,$$

for $x \in (0, \ell = 1)$ and $t \in (0, T = 1)$. One can remark that the condition of Theorem 4.4 which ensure the uniqueness of the solution is satisfied. The exact solution is given by

$$a(t) = \left|t-\frac{1}{2}\right| + \frac{1}{2}, \quad b(t) = \left|t^2-\frac{1}{2}\right|, \qquad u(x,t) = (e^{-x}+x^2)e^t. \tag{4.34}$$

The objective function (4.19), as a function of the number of iterations, with no noise and no regularization is presented in Figure 4.17. From this figure, it can be seen that the convergence is achieved in 11 iterations and it decreases rapidly to stationary value of $O(10^{-8})$. When no noise is included in the input data we obtain stable and accurate solutions for $a(t)$ and $b(t)$ which are shown in Figure 4.18. In these plots, beginning with the initial guess (-○-), one can observe that after 6 iterations the results are overlapping until reaching the final iteration 11.

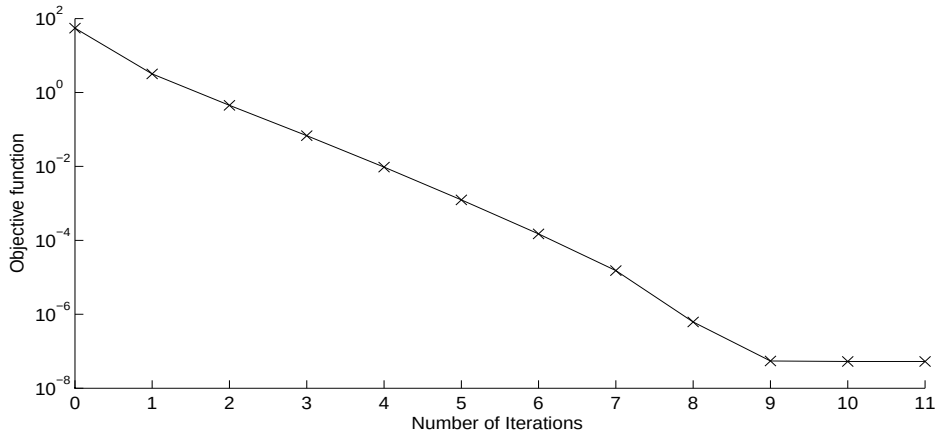

Figure 4.17: Objective function (4.19), for Example 5 with no noise and no regularization.

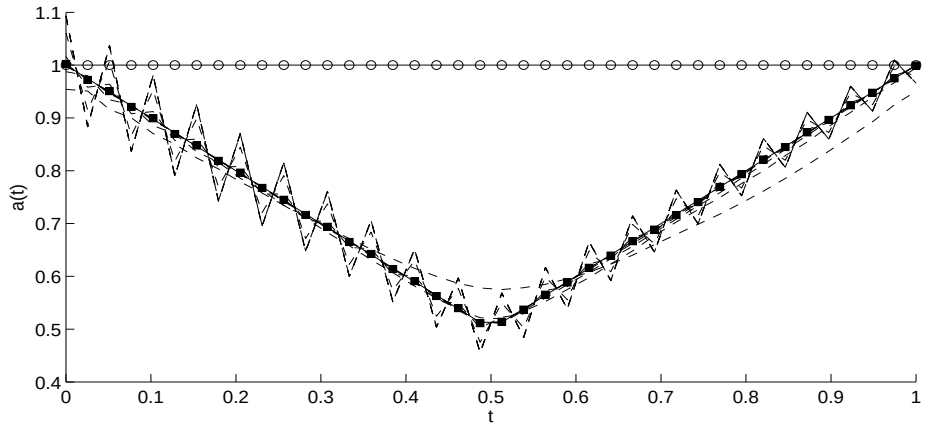

(a)

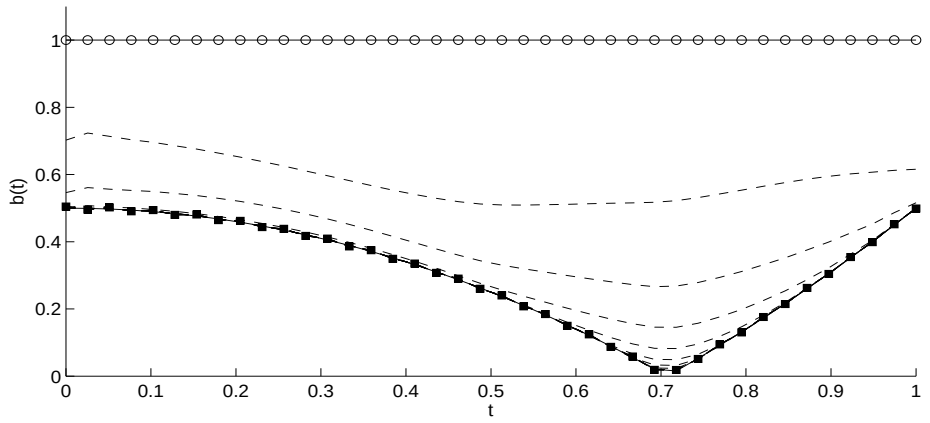

(b)

Figure 4.18: (a) Coefficient $a(t)$, and (b) Coefficient $b(t)$, for Example 5 with no noise and no regularization; (—) exact solution, (-○-) initial guess, (- - -) iterations 1, 2, ..., 10, and (-■-) the final iteration 11.

When $p = 1\%$ noise is included, regularization is needed to achieve stability. Figure 4.19 presents the regularized objective function (4.19), as a function of the number of iterations. From this figure, it can be seen that for no regularization the convergence is achieved in a relatively larger number of iterations than when regularization is applied with $\beta \in \{10^{-3}, 10^{-2}, 10^{-1}\}$.

Figure 4.20 shows the plots of the retrieved coefficients. From this figure and Table 4.7 it can be observed that we obtain stable and reasonable accurate solutions for $a(t)$ and $b(t)$ when we choose $\beta = 10^{-1}$ which has minimum $rrmse$ values for a and absolute error values for b. Note that $b(t)$ can vanish and therefore we have considered the absolute error instead of the $rrmse$ in Table 4.7 for Example 5.

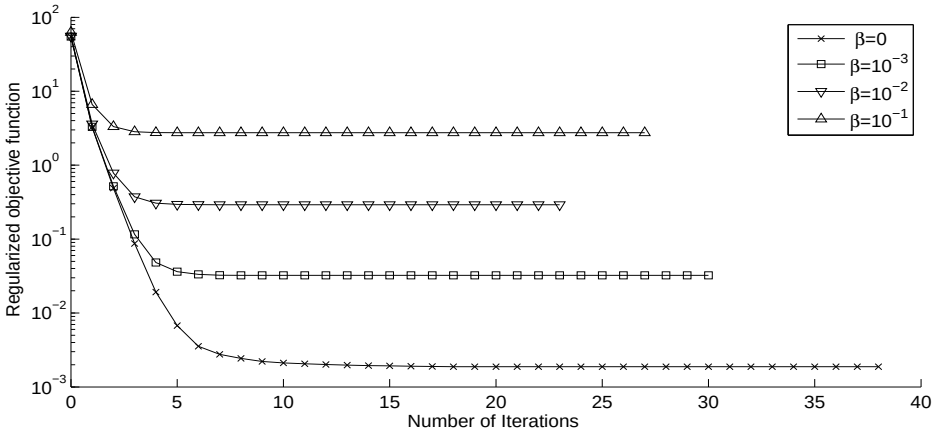

Figure 4.19: Regularized objective function (4.19), for Example 5 with $p = 1\%$ noise.

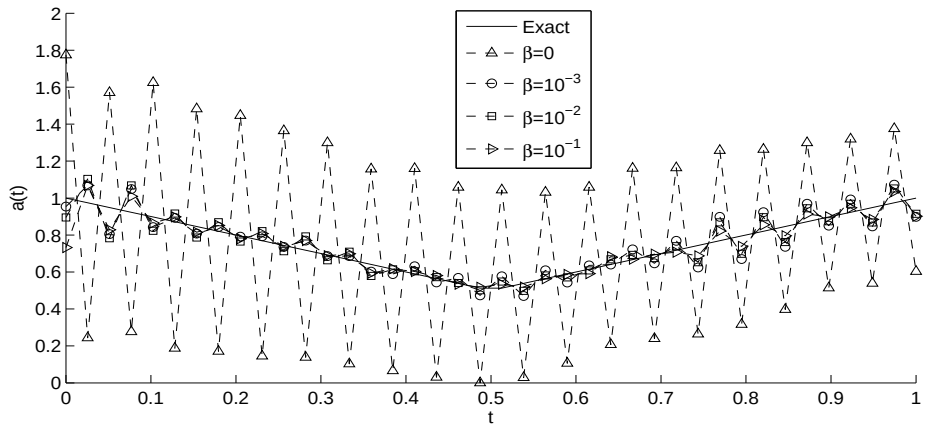

(a)

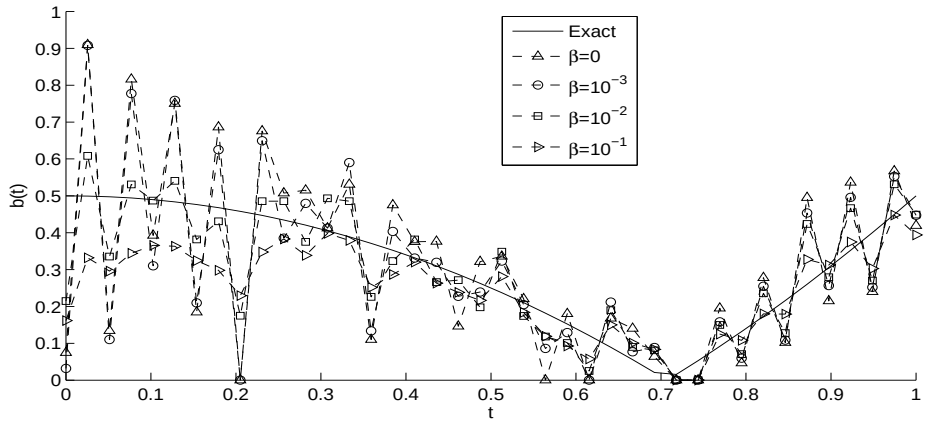

(b)

Figure 4.20: (a) Coefficient $a(t)$, and (b) Coefficient $b(t)$, for Example 5 with $p = 1\%$ noise and regularization.

Table 4.7: The *rrmse* values for the estimated coefficients for Examples 4 and 5 with $p = 1\%$ noise.

	$\beta = 0$	$\beta = 10^{-3}$	$\beta = 10^{-2}$	$\beta = 10^{-1}$
Example 4	$rrmse(a) = 0.1267$	0.0823	0.0713	0.0806
	$rrmse(b) = 0.3632$	0.1435	0.1263	0.4500
Example 5	$rrmse(a) = 0.7493$	0.0886	0.0791	0.0670
	$abs(b) = 0.1917$	0.1844	0.1003	0.1049

4.5.6 Example 6 for IP3

We finally consider the IP3 given by equations (4.2)–(4.4) and (4.8) with unknown coefficients $K(t)$ and $b(t)$, and solve this inverse problem with the following input data:

$$\begin{aligned}
&\phi(x) = e^{-x} + x^2, \quad \mu_1(t) = e^t, \quad \mu_2(t) = (e^{-1} + 1)e^t, \\
&\nu_1(t) = e^t \left(\left| t - \frac{1}{2} \right| + \frac{1}{2} \right), \quad \nu_2(t) = (2 - e^{-1})e^t \left(\left| t - \frac{1}{2} \right| + \frac{1}{2} \right), \\
&d(x,t) = 0, \quad C(t) = 1, \\
&f(x,t) = (e^{-x} + x^2)e^t - \left(\left| t - \frac{1}{2} \right| + \frac{1}{2} \right)(e^{-x} + 2)e^t - \left| t^2 - \frac{1}{2} \right| (-e^{-x} + 2x)e^t,
\end{aligned}$$

for $x \in (0, \ell = 1)$ and $t \in (0, T = 1)$. One can easily check that the conditions of Theorem 4.6 which ensure the uniqueness of the solution are satisfied. The exact solution is given by

$$K(t) = \left| t - \frac{1}{2} \right| + \frac{1}{2}, \quad b(t) = \left| t^2 - \frac{1}{2} \right|, \quad u(x,t) = (e^{-x} + x^2)e^t. \tag{4.35}$$

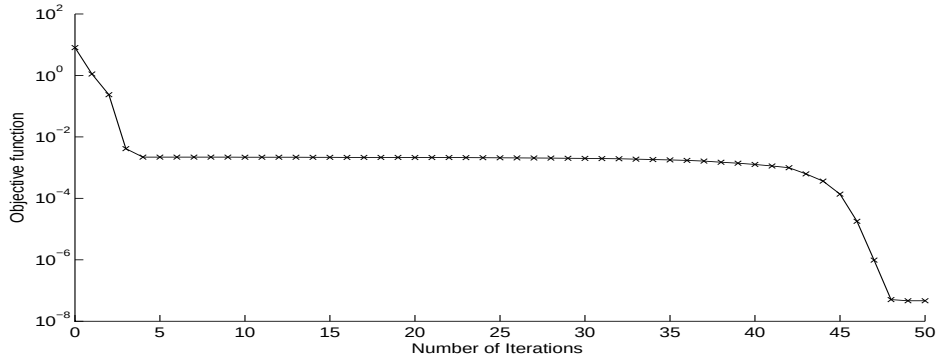

Figure 4.21: Objective function (4.20), for Example 6 with no noise and no regularization.

The objective function (4.20), as a function of the number of iterations, is shown in Figure 4.21. From this figure, it can be seen that the convergence is achieved in 50 iterations. It can also be observed that the objective function (4.20) decreases rapidly in the first 5 iterations, after which it takes a slow decrease until iteration 41, and finally it decreases rapidly to a stationary value of $O(10^{-8})$. When no noise is included in the input data we obtain stable and accurate solutions for $K(t)$ and $b(t)$ which are shown in Figure 4.22. In these plots, the numerically obtained coefficients show a very good agreement with the exact ones.

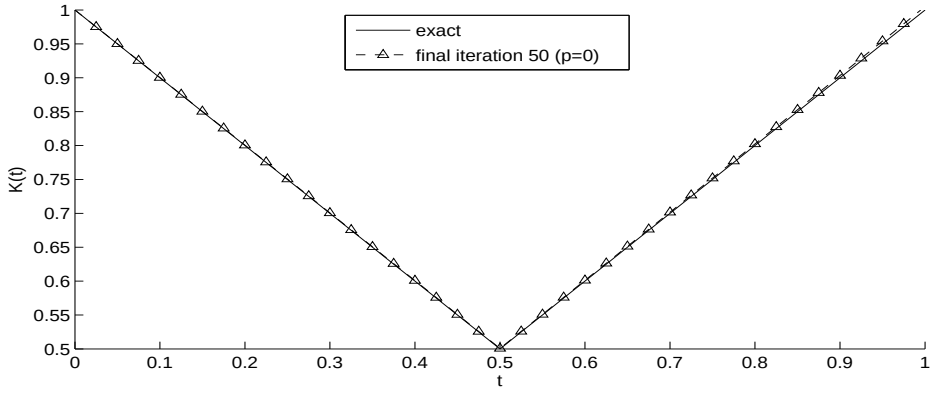

(a)

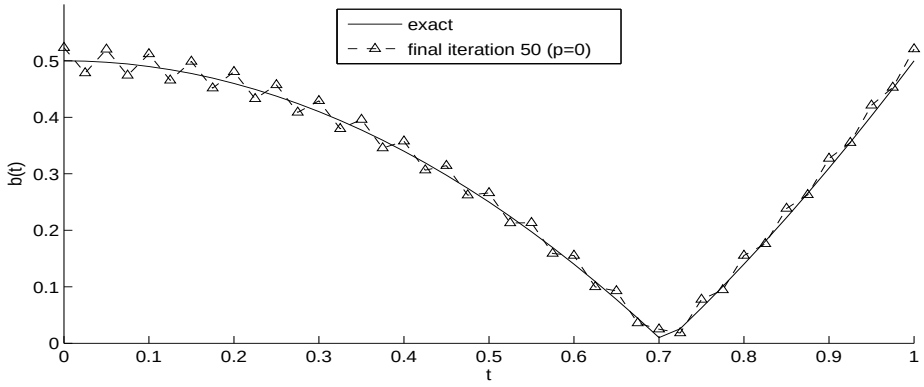

(b)

Figure 4.22: (a) Coefficient $K(t)$, and (b) Coefficient $b(t)$, for Example 6 with no noise and no regularization.

Next we include $p = 1\%$ noise to the heat fluxes ν_1 and ν_2, as in equation (4.25), and regularization is needed to achieve stability. Figure 4.23 presents the regularized objective function (4.20), as a function of the number of iterations. From this figure, it can be seen that for $\beta = 0$, i.e. no regularization, the convergence is achieved in a relatively larger number of iterations than when regularization is applied with $\beta \in \{10^{-3}, 10^{-2}, 10^{-1}\}$.

Figure 4.24 shows the plots of the retrieved coefficients. From this figure and it can be observed that in the case of non-smooth coefficients we still obtain stable and reasonable accurate solutions for $K(t)$ and $b(t)$.

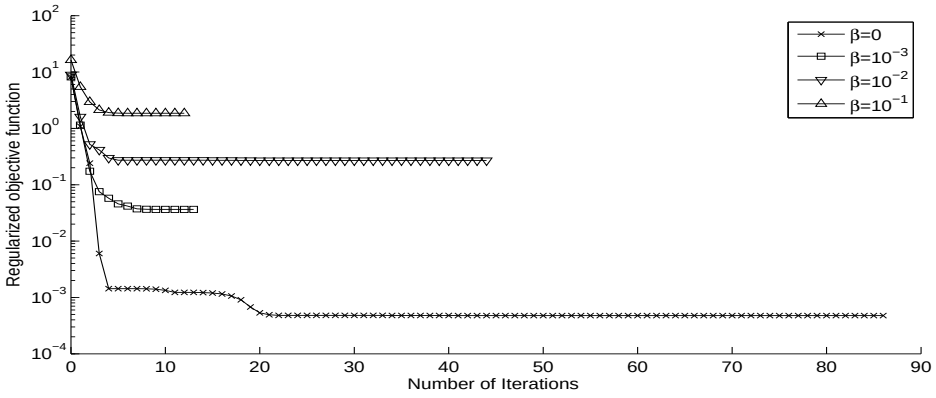

Figure 4.23: Regularized objective function (4.20), for Example 6 with $p = 1\%$ noise.

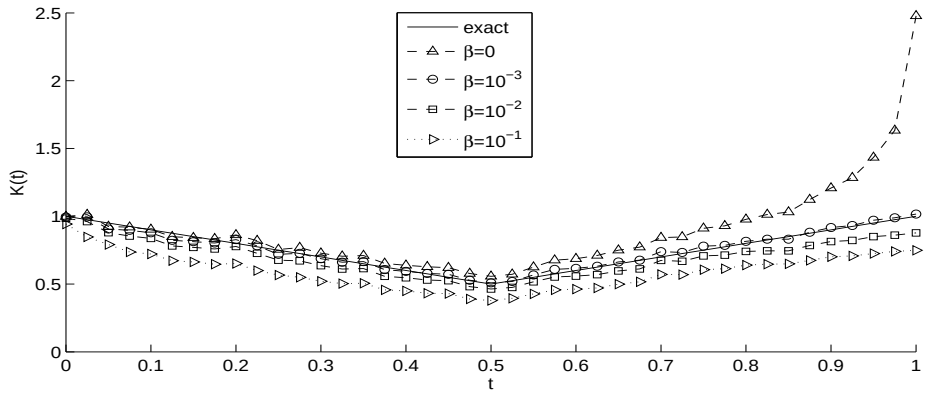

(a)

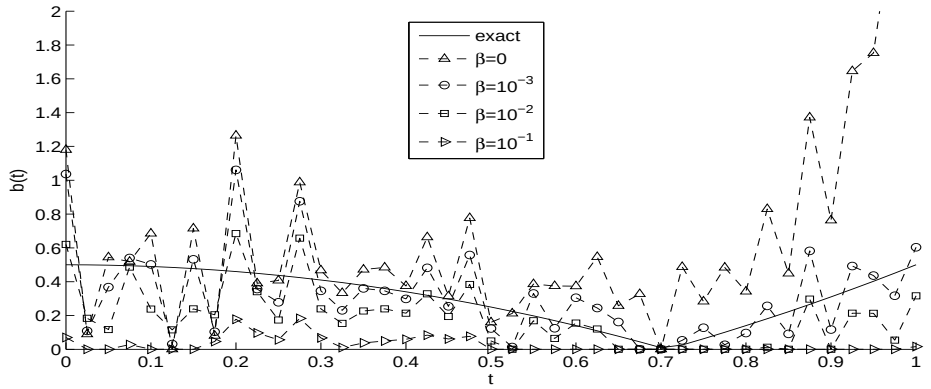

(b)

Figure 4.24: (a) Coefficient $K(t)$, and (b) Coefficient $b(t)$, for Example 6 with $p = 1\%$ noise and regularization.

4.6 Conclusions

This chapter has presented a numerical approach to identify simultaneously two time-dependent coefficients in the one-dimensional parabolic heat equation. The three resulting inverse problems have been reformulated as constrained regularized minimization problems which were solved using MATLAB optimization toolbox routines. The numerically obtained results are shown to be stable and accurate.

Multi-dimensional problems can easily be analysed as our unknowns depend on the temporal variable only.

Chapter 5

Simultaneous determination of time-dependent coefficients and heat source

5.1 Introduction

In the previous chapter and elsewhere in [8, 58, 72], the unknowns were mainly time-dependent coefficients multiplying the temperature and its partial derivatives, but more recent theoretical studies, [82, 83], allow for one of the time-dependent unknown to be in the free term heat source as well. And it is the purpose of this chapter to numerically solve a couple of such related multiple coefficient identification problems.

The structure of the chapter is as follows. In Section 5.2 we formulate the two inverse problems that we consider. In Section 5.3 we briefly describe the FDM used to discretise the direct problem, whilst Section 5.4 introduces the constrained regularized minimization problem that has to be solved using the MATLAB routine *lsqnonlin*. In Section 5.5, numerical results are presented and discussed and finally conclusions are given in Section 5.6.

5.2 Mathematical formulation

We study a couple of coefficient identification problems related to the second-order parabolic partial differential equation

$$u_t(x,t) = a(x,t)u_{xx}(x,t) - b(x,t)u_x(x,t) - d(x,t)u(x,t) + f(t)g(x,t),\ (x,t) \in Q_T. \tag{5.1}$$

where $Q_T = [-\ell, \ell] \times [0, T]$, with $\ell > 0$ and $T > 0$, represents the solution domain, $a(x,t)$ is a given positive function involving physical quantities of the medium $(-\ell, \ell)$ such as conductivity, capacity, storage, diffusivity, $u(x,t)$ is the unknown dependent variable, e.g. the temperature in heat conduction, the pressure in porous media or the piezometric head in groundwater flow, $f(t)g(x,t)$ with $f(t)$ unknown and $g(x,t)$ given function represents a source (heat or hydraulic), and either one of the coefficients b (representing an advection/convection coefficient) or d (representing a reaction or perfusion coefficient in bio-heat conduction) are unknown (though we shall further assume that, when unknown, the corresponding quantity b or d depends on time only). To be more explicit, let us particularize equation (5.1) to the following two cases, namely,

$$u_t(x,t) = a(x,t)u_{xx}(x,t) - b(t)u_x(x,t) - d(x,t)u(x,t) + f(t)g(x,t), \quad (x,t) \in Q_T \tag{5.2}$$

with unknown triplet $(u(x,t), f(t), b(t))$ and

$$u_t(x,t) = a(x,t)u_{xx}(x,t) - b(x,t)u_x(x,t) - d(t)u(x,t) + f(t)g(x,t), \quad (x,t) \in Q_T. \tag{5.3}$$

with unknown triplet $(u(x,t), f(t), d(t))$.

We emphasize that such particularizations are often necessary when seeking to establish the uniqueness of the solution. Together with (5.2) or (5.3) we impose the initial condition

$$u(x,0) = \phi(x), \quad x \in [-\ell, \ell], \tag{5.4}$$

and the homogenous Dirichlet boundary conditions

$$u(\pm\ell, t) = 0, \quad t \in [0,T]. \tag{5.5}$$

As over-determination conditions we consider, [82],

$$\int_{-\ell}^{\ell} \omega(x)u(x,t)dx = \varphi(t), \quad t \in [0,T], \tag{5.6}$$

$$\int_{-\ell}^{\ell} \omega(x)u_x(x,t)dx = \psi(t), \quad t \in [0,T], \tag{5.7}$$

where ω is given weight function. Integral observation such as (5.6) have been considered before in numerous studies, see e.g. [16, 18, 61] to mention only a few, and physically it represents the mass/energy specification obtained by measuring

the temperature $u(x,t)$ with thermocouples/ sources and then averaging over the space domain of the finite slab $[-\ell,\ell]$. This is because sometimes it might be practically impossible to measure the state of an object (or a process) at individual points and instead only the mean value of the state over the entire object can be specified, [1]. Remark also that if ω is differentiable then integration by parts in (5.7) and using (5.5) imply

$$\int_{-\ell}^{\ell}\omega'(x)u(x,t)dx=-\psi(t),\quad t\in[0,T], \tag{5.8}$$

so (5.7) may be thought to have the same physical meaning as (5.6) previously described.

The unique solvabilites of the inverse problems (5.2), (5.4)–(5.7) and (5.3)–(5.7) have been established in [82, 83].

5.3 Numerical solution of the direct problem

In this section, we consider the direct (forward) initial value problem given by equations (5.1), (5.4) and (5.5) when the coefficients $b(x,t)$, $d(x,t)$ and $f(t)$ are given and the dependent variable $u(x,t)$ is the solution to be determined. We use the Crank-Nicolson FDM, as described in Section 2.4.

The discrete form of the direct problem is as follows. Taking the positive integer numbers M and N, the solution domain $Q_T=[-\ell,\ell]\times[0,T]$ is divided by a $M\times N$ mesh with spatial step size $\Delta x=2\ell/M$ in x-direction and the time step size $\Delta t=T/N$. The solution at the node (i,j) is denoted by $u_{i,j}:=u(x_i,t_j)$, where $x_i=-\ell+i\Delta x$, $t_j=j\Delta t$, $a_{i,j}:=a(x_i,t_j)$, $b_{i,j}:=b(x_i,t_j)$, $f_j:=f(t_j)$, $d_{i,j}:=d(x_i,t_j)$ and $g_{i,j}:=g(x_i,t_j)$ for $i=\overline{0,M}$ and $j=\overline{0,N}$.

Considering the general form of partial differential equation (4.10), equations (5.1), (5.4) and (5.5) can be approximated as

$$\frac{u_{i,j+1}-u_{i,j}}{\Delta t}=\frac{1}{2}\left(G_{i,j}+G_{i,j+1}\right),\quad i=\overline{1,M},\ j=\overline{0,(N-1)}, \tag{5.9}$$

$$u_{i,0}=\phi(x_i),\quad i=\overline{0,M}, \tag{5.10}$$

$$u_{0,j}=0,\quad u_{M,j}=0,\quad j=\overline{0,N}, \tag{5.11}$$

where

$$G_{i,j}=G\left(x_i,t_j,\frac{u_{i+1,j}-u_{i-1,j}}{2(\Delta x)},\frac{u_{i+1,j}-2u_{i,j}+u_{i-1,j}}{(\Delta x)^2}\right),\ i=\overline{1,(M-1)},\ j=\overline{0,N}. \tag{5.12}$$

For our problem, equation (5.1) can be discretised in the form of (5.9) as

$$-A_{i,j+1}u_{i-1,j+1} + (1+B_{i,j+1})u_{i,j+1} - C_{i,j+1}u_{i+1,j+1} = A_{i,j}u_{i-1,j} + (1-B_{i,j})u_{i,j} + C_{i,j}u_{i+1,j} + \frac{\Delta t}{2}\left(f_j g_{i,j} + f_{j+1}g_{i,j+1}\right), \quad (5.13)$$

for $i = \overline{1,(M-1)}$, $j = \overline{0,(N-1)}$, where

$$A_{i,j} = \frac{(\Delta t)a_{i,j}}{2(\Delta x)^2} + \frac{b_{i,j}(\Delta t)}{4(\Delta x)},\ B_{i,j} = \frac{(\Delta t)a_{i,j}}{(\Delta x)^2} + \frac{\Delta t}{2}d_{i,j},\ C_{i,j} = \frac{(\Delta t)a_{i,j}}{2(\Delta x)^2} - \frac{b_{i,j}(\Delta t)}{4(\Delta x)}.$$

At each time step t_{j+1}, for $j = \overline{0,(N-1)}$, using the homogenous Dirichlet boundary conditions (5.11), the above difference equation can be reformulated as a $(M-1)\times(M-1)$ system of linear equations of the form (3.17), where

$$D = \begin{pmatrix} 1+B_{1,j+1} & -C_{1,j+1} & 0 & \cdots & 0 & 0 & 0 \\ -A_{2,j+1} & 1+B_{2,j+1} & -C_{2,j+1} & \cdots & 0 & 0 & 0 \\ \vdots & \vdots & \vdots & \ddots & \vdots & \vdots & \vdots \\ 0 & 0 & 0 & \cdots & -A_{M-2,j+1} & 1+B_{M-2,j+1} & -C_{M-2,j+1} \\ 0 & 0 & 0 & \cdots & 0 & -A_{M-1,j+1} & 1+B_{M-1,j+1} \end{pmatrix},$$

$$E = \begin{pmatrix} 1-B_{1,j} & C_{1,j} & 0 & \cdots & 0 & 0 & 0 \\ A_{2,j} & 1-B_{2,j} & C_{2,j} & \cdots & 0 & 0 & 0 \\ \vdots & \vdots & \vdots & \ddots & \vdots & \vdots & \vdots \\ 0 & 0 & 0 & \cdots & A_{M-2,j} & 1-B_{M-2,j} & C_{M-2,j} \\ 0 & 0 & 0 & \cdots & 0 & A_{M-1,j} & 1-B_{M-1,j} \end{pmatrix},$$

and

$$\mathbf{b} = \begin{pmatrix} \frac{\Delta t}{2}(f_j g_{1,j} + f_{j+1}g_{1,j+1}) \\ \frac{\Delta t}{2}(f_j g_{2,j} + f_{j+1}g_{2,j+1}) \\ \vdots \\ \frac{\Delta t}{2}(f_j g_{M-2,j} + f_{j+1}g_{M-2,j+1}) \\ \frac{\Delta t}{2}(f_j g_{M-1,j} + f_{j+1}g_{M-1,j+1}) \end{pmatrix}.$$

The numerical solutions for $\varphi(t)$ and $\psi(t)$ are calculated using the trapezoidal

rule for integrals in (5.6) and (5.7), namely,

$$\varphi(t_j) = \int_{-\ell}^{\ell} \omega(x)u(x,t_j)dx = \Delta x \left(\sum_{i=1}^{M-1} u_{i,j}\omega_i \right), \quad j = \overline{0,N}, \tag{5.14}$$

$$\psi(t_j) = \int_{-\ell}^{\ell} \omega(x)u_x(x,t_j)dx = \frac{\Delta x}{2} \left(u_{x0,j}\omega_0 + u_{xM,j}\omega_M + 2\sum_{i=1}^{M-1} u_{xi,j}\omega_i \right), \quad j = \overline{0,N}, \tag{5.15}$$

where $\omega_i := \omega(x_i)$ for $i = \overline{0,M}$, and

$$u_{x0,j} = \frac{4u_{1,j} - u_{2,j} - 3u_{0,j}}{2(\Delta x)}, \quad u_{xM,j} = -\frac{4u_{M-1,j} - u_{M-2,j} - 3u_{M,j}}{2(\Delta x)},$$
$$u_{xi,j} = \frac{u_{i+1,j} - u_{i-1,j}}{2(\Delta x)}, \quad i = \overline{1,(M-1)}, \quad j = \overline{0,N}.$$

5.4 Numerical solutions of the inverse problems

In this section, we aim to obtain accurate and stable simultaneous identifications for the temperature $u(x,t)$, source $f(t)$ and the coefficients $b(t)$ or $d(t)$ for the inverse problems (5.2), (5.4)–(5.7) or (5.3)–(5.7), respectively. In the former case we minimize the nonlinear Tikhonov functional

$$F_1(b,f) := \left\| \int_{-\ell}^{\ell} \omega(x)u(x,t)dx - \varphi(t) \right\|^2 + \left\| \int_{-\ell}^{\ell} \omega(x)u_x(x,t)dx - \psi(t) \right\|^2 + \beta_1 \left\| b(t) \right\|^2 + \beta_2 \left\| f(t) \right\|^2, \tag{5.16}$$

whilst in the latter case we minimize

$$F_2(d,f) := \left\| \int_{-\ell}^{\ell} \omega(x)u(x,t)dx - \varphi(t) \right\|^2 + \left\| \int_{-\ell}^{\ell} \omega(x)u_x(x,t)dx - \psi(t) \right\|^2 + \beta_3 \left\| d(t) \right\|^2 + \beta_2 \left\| f(t) \right\|^2, \tag{5.17}$$

where $\beta_i \geq 0$, $i = 1,2,3$, are regularization parameters which are introduced in order to stabilise the numerical solution and the norm is the $L^2[0,T]$ norm. Remark that we could have chosen a single regularization parameter $\beta = \beta_1 = \beta_2 = \beta_3$, as in Section 4.4. However, in the present case, we have found that the amount of regularization to be imposed on the solutions $b(t)$ and $f(t)$, or $d(t)$ and $f(t)$, has to be weighted in order to achieve stable reconstructions. However, allowing for two (instead of one) regularization parameters whilst enlarging the stability region it pays the penalty that their multiple choices can become cumbersome,

e.g. one would have to employ the L-surface method [6] instead of the L-curve method [44].

The discretizations of (5.16) and (5.17) are

$$F_1(\underline{b},\underline{f}) := \sum_{j=1}^{N}\Big[\int_{-\ell}^{\ell}\omega(x)u(x,t_j)dx-\varphi(t_j)\Big]^2+\sum_{j=1}^{N}\Big[\int_{-\ell}^{\ell}\omega(x)u_x(x,t_j)dx-\psi(t_j)\Big]^2 + \beta_1\sum_{j=1}^{N}b_j^2+\beta_2\sum_{j=1}^{N}f_j^2, \tag{5.18}$$

$$F_2(\underline{d},\underline{f}) := \sum_{j=1}^{N}\Big[\int_{-\ell}^{\ell}\omega(x)u(x,t_j)dx-\varphi(t_j)\Big]^2+\sum_{j=1}^{N}\Big[\int_{-\ell}^{\ell}\omega(x)u_x(x,t_j)dx-\psi(t_j)\Big]^2 + \beta_3\sum_{j=1}^{N}d_j^2+\beta_2\sum_{j=1}^{N}f_j^2. \tag{5.19}$$

respectively.

The unregularized case, i.e., $\beta_i = 0$ for $i = 1, 2, 3$, yields the ordinary nonlinear least-squares method which is usually producing unstable solutions when noisy data are inverted.

The noisy data is numerically simulated as

$$\varphi^{\epsilon 1}(t_j) = \varphi(t_j) + \epsilon 1_j, \quad \psi^{\epsilon 2}(t_j) = \psi(t_j) + \epsilon 2_j, \quad j = \overline{1,N}, \tag{5.20}$$

where $\epsilon 1_j$ and $\epsilon 2_j$ are random variables generated from a Gaussian normal distribution with mean zero and standard deviation $\sigma 1$ and $\sigma 2$, respectively, given by

$$\sigma 1 = p \times \max_{t\in[0,T]}|\varphi(t)|, \quad \sigma 2 = p \times \max_{t\in[0,T]}|\psi(t)|, \tag{5.21}$$

where p represents the percentage of noise. We use the MATLAB function *normrnd* to generate the random variables $\underline{\epsilon 1} = (\epsilon 1_j)_{j=\overline{1,N}}$ and $\underline{\epsilon 2} = (\epsilon 2_j)_{j=\overline{1,N}}$ as follows:

$$\underline{\epsilon 1} = normrnd(0, \sigma 1, N), \quad \underline{\epsilon 2} = normrnd(0, \sigma 2, N). \tag{5.22}$$

In the case of noisy data (5.6) and (5.7), we replace $\varphi(t_j)$ and $\psi(t_j)$ by $\varphi^{\epsilon 1}(t_j)$ and $\psi^{\epsilon 2}(t_j)$, respectively, in (5.18) and (5.19).

The minimization of F_1 or F_2 subject to simple bounds on the variables is accomplished using the MATLAB optimization toolbox routine *lsqnonlin*, as described in the previous chapters.

We take bounds for the quantities $b(t)$ and $f(t)$ say, we seek them in the interval $[-10^3, 10^3]$, whilst the non-negative quantity $d(t)$ is sought in the interval $[0, 10^3]$. We also take the parameters of the routine as follows:

- Maximum number of iterations = 10× (number of variables).
- Maximum number of objective function evaluations=10^5× (number of variables).
- Solution and object function tolerances = 10^{-10}.

5.5 Numerical results and discussion

In this section, we present numerical results for the recovery of the unknowns $f(t)$, $b(t)$ or $d(t)$, in the case of exact and noisy data (5.20). To measure the accuracy of the numerical solution we employ the root mean square error ($rmse$) defined by:

$$rmse(f) = \sqrt{\frac{1}{N}\sum_{j=1}^{N}\left(f_{numerical}(t_j) - f_{exact}(t_j)\right)^2}, \tag{5.23}$$

and similar expressions exist for $b(t)$ and $d(t)$.

During the computation we need the values of $f(0)$ and $b(0)$ or $d(0)$. One can easily derive these values from the governing equations (5.2) or (5.3) with the help of the initial and boundary conditions (5.4) and (5.5).

5.5.1 Example 1

Consider first the inverse problem (5.2), (5.4)–(5.7), with unknown coefficients $f(t)$ and $b(t)$, and the following input data:

$$a(x,t) = 1, \quad d(x,t) = 0, \quad g(x,t) = -x^3, \quad (x,t) \in Q_T, \tag{5.24}$$

$$\phi(x) = x(\ell^2 - x^2), \quad \omega(x) = (x^2 - \ell^2)^2, \quad x \in [-\ell, \ell], \tag{5.25}$$

$$\varphi(t) = \int_{-\ell}^{\ell} \omega(x)u(x,t)dx = 0, \quad t \in [0,T], \tag{5.26}$$

$$\psi(t) = \int_{-\ell}^{\ell} \omega(x)u_x(x,t)dx = \frac{64\ell^7 e^{-6t}}{105}, \quad t \in [0,T]. \tag{5.27}$$

It can easily be checked by direct substitution that the analytical solution is

given by

$$b(t) = 0, \quad f(t) = -\frac{6e^{\frac{-6t}{\ell^2}}}{\ell^2}, \quad t \in [0, T], \tag{5.28}$$

$$u(x,t) = e^{\frac{-6t}{\ell^2}} x(\ell^2 - x^2), \quad (x,t) \in Q_T. \tag{5.29}$$

We take for simplicity, $\ell = T = 1$ and employ the FDM described in Section 5.3 with $M = N = 40$ at each iteration of minimization procedure described in Section 5.4. By simple calculation we conclude that $b(0) = 0$ and $f(0) = -6$ and therefore, appropriate candidates for the initial guesses of b and f are $b^0 = 0$ and $f^0 = -6$. However, because the exact solution for $b(t)$ is actually the trivial zero function we also investigate another initial guess for b given by $b^0(t) = t$.

For exact data, i.e., $p = 0$ in (5.21), numerical results of the inversion with and without regularization in (5.18) and various initial guesses are presented in Figures 5.1–5.3 and Table 5.1. From Figure 5.1 and Table 5.1 it can be seen that, as expected, the farther the initial guess is, the more iterations and computational time are required to achieve convergence. However, for both initial guesses considered, the objective function (5.18) converges to the same minimum value which is of $O(10^{-10})$. Furthermore, from Figure 5.1(a) and Table 5.1 it can be seen that, in case of no regularization being employed, better results are obtained for the closer initial guess for $b(t)$. However, the results for $b(t)$ obtained for the farther initial guess in Figure 5.2(a) oscillate for the last 7-8 time steps near the final time showing that instability starts to manifest. In order to alleviate these oscillations some little regularization is recommended and these improvements over Figure 5.2 are clearly illustrated in Figure 5.3, see also the corresponding rows in Table 5.1 for further comparison. Observe in particular from Table 5.1 that including regularization also reduces the number of iterations and computational time in addition to achieving the stability of solution.

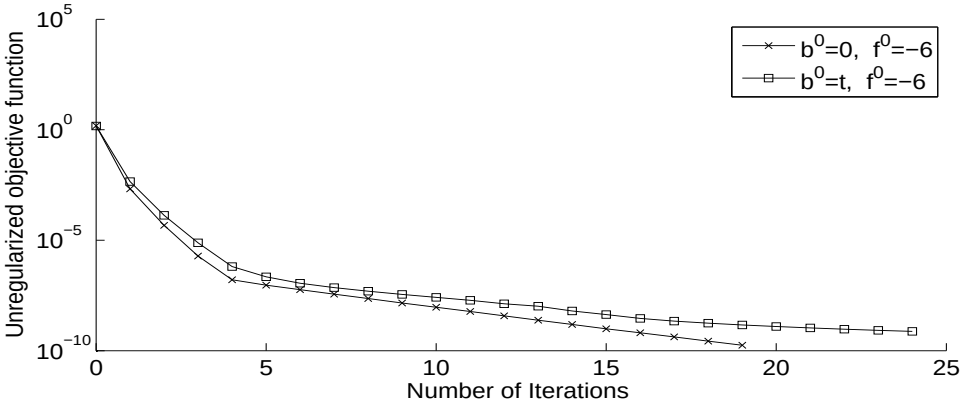

(a)

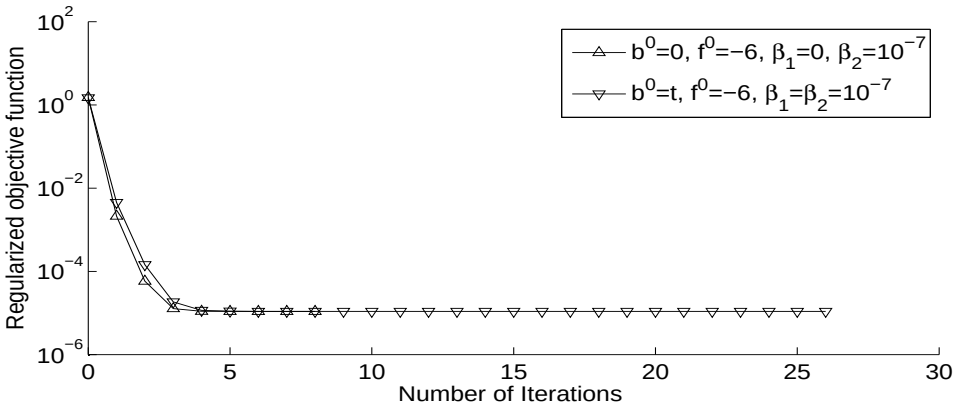

(b)

Figure 5.1: The objective function (5.18), (a) without and (b) with regularization, and various initial guesses, for Example 1 with exact data.

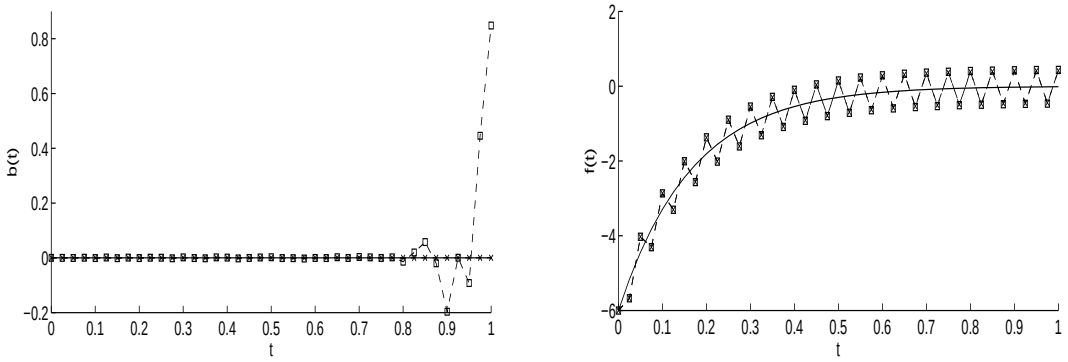

(a) (b)

Figure 5.2: The exact (—) and numerical solutions without regularization, and various initial guesses $b^0 = 0$ (- × -) and $b^0 = t$ (- □ -) for: (a) $b(t)$ and (b) $f(t)$, for Example 1 with exact data.

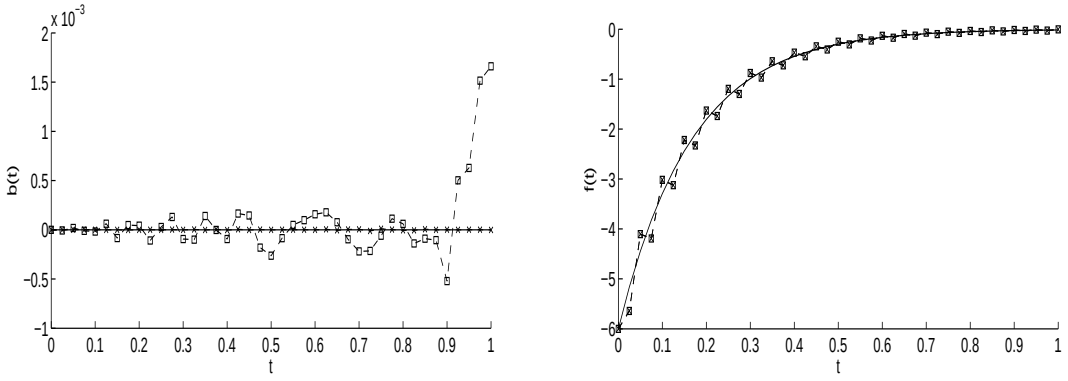

(a) (b)

Figure 5.3: The exact (—) and numerical solutions with regularization and various initial guesses $b^0 = 0$, $\beta_1 = 0$, $\beta_2 = 10^{-7}$ (- × -) and $b^0 = t$, $\beta_1 = \beta_2 = 10^{-7}$ (- □ -) for: (a) $b(t)$ and (b) $f(t)$, for Example 1 with exact data.

In the remaining of this subsection, for brevity, we only illustrate the results obtained with the initial guess $b^0 = t$ and $f^0 = -6$.

Table 5.1: Number of iterations, number of function evaluations, value of the objective function (5.18) at final iteration, the *rmse* values and the computational time with and without regularization and various initial guesses for Example 1 with exact data.

$\beta_1 = \beta_2 = 0$	$b^0 = 0$, $f^0 = -6$	$b^0 = t$, $f^0 = -6$
No. of iterations	19	24
No. of function evaluations	1660	2075
Value of objective function (5.18) at final iteration	1.7E-10	7.4E-10
$rmse(b)$	6.1E-6	0.1557
$rmse(f)$	0.4379	0.4536
Computational time	20 mins	24 mins
$\beta_2 = 10^{-7}$	$b^0 = 0$, $f^0 = -6$, $\beta_1 = 0$	$b^0 = t$, $f^0 = -6$, $\beta_1 = 10^{-7}$
No. of iterations	8	9
No. of function evaluations	747	830
Value of objective function (5.18) at final iteration	1.0E-5	1.0E-5
$rmse(b)$	3.5E-6	4.0E-4
$rmse(f)$	0.1514	0.1516
Computational time	9 mins	10 mins

In order to investigate the stability of the solution we add $p = 1\%$ noise to the input data (5.6) and (5.7), as in (5.20). The objective function (5.18), as a function of the number of iterations, is plotted in Figure 5.4. From this figure it can be seen that in the absence of regularization a slow and smooth convergence is recorded and, in fact, the process of minimization of the routine *lsqnonlin* is stopped when the prescribed tolerance of solution $= 10^{-10}$ is reached. The corresponding numerical results for the unknown coefficients are presented in Figure 5.5. From this figure it can be seen that unstable results are obtained for both coefficients $b(t)$ and $f(t)$ (compare with the results for exact data in Figure 5.2). This is expected since the problem under investigation is ill-posed. Consequently, regularization should be applied to restore the stability of the solution in the components $b(t)$ and $f(t)$.

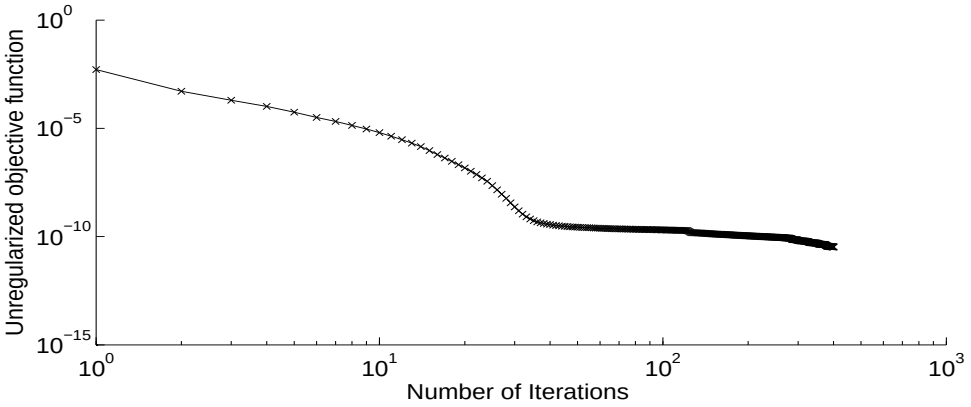

Figure 5.4: The objective function (5.18) without regularization for Example 1 with $p = 1\%$ noise data.

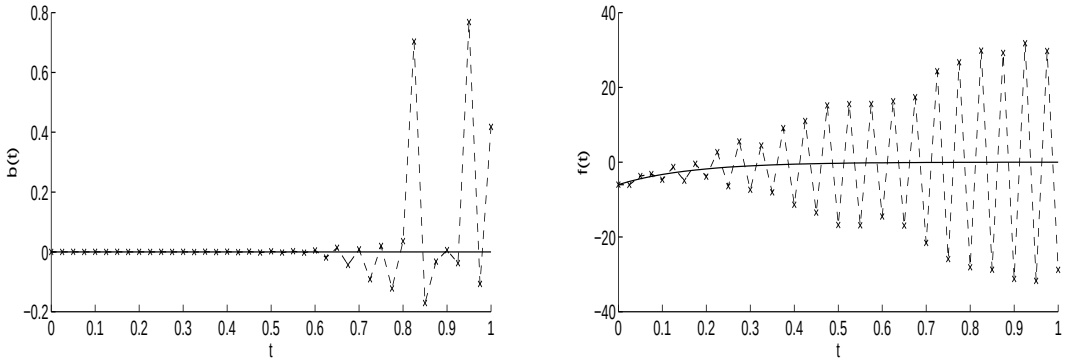

(a) (b)

Figure 5.5: The exact (—) and numerical (- × -) solutions without regularization for: (a) $b(t)$ and (b) $f(t)$, for Example 1 with $p = 1\%$ noisy data.

Regularization parameters have been chosen by trial and error and numerical

results obtained from some typical choices are given in Table 5.2 and Figures 5.6 and 5.7. Justifying more rigorously the choice of the regularization parameters β_1 and β_2 possibly using the L-surface method, [6], is nevertheless very important and will be the subject of future work. From Figure 5.6 it can be noticed that convergence in less than 8 iterations is achieved for each selection of regularization parameters. The corresponding numerical reconstructions for $b(t)$ and $f(t)$ are presented in Figure 5.7. By comparing Figure 5.5 with Figure 5.7 one can immediately notice the dramatic improvement in stability and accuracy which is achieved through the inclusion of regularization in the objective function (5.18).

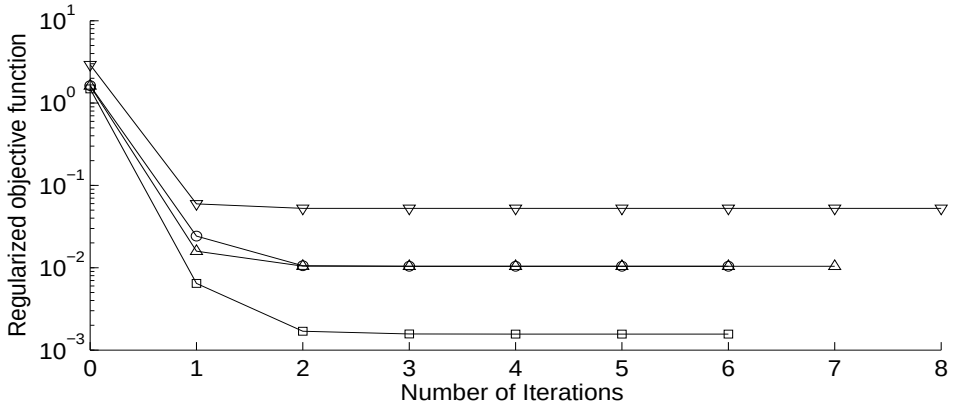

Figure 5.6: The objective function (5.18) with regularization parameters $\beta_1 = \beta_2 = 10^{-5}$ (-□-), $\beta_1 = \beta_2 = 10^{-4}$ (-△-), $\beta_1 = \beta_2 = 10^{-3}$ (-▽-) and $\beta_1 = 10^{-3}$, $\beta_2 = 10^{-4}$ (-○-), for Example 1 with $p = 1\%$ noisy data.

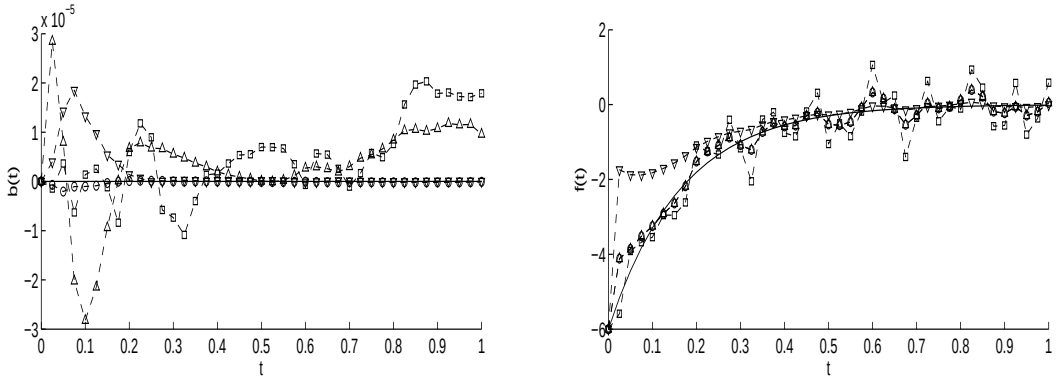

(a) (b)

Figure 5.7: The exact (—) and numerical solutions with regularization parameters $\beta_1 = \beta_2 = 10^{-5}$ (-□-), $\beta_1 = \beta_2 = 10^{-4}$ (-△-), $\beta_1 = \beta_2 = 10^{-3}$ (-▽-) and $\beta_1 = 10^{-3}$, $\beta_2 = 10^{-4}$ (-○-) for: (a) $b(t)$ and (b) $f(t)$, for Example 1 with $p = 1\%$ noisy data.

Table 5.2: Number of iterations, number of function evaluations, value of the objective function (5.18) at final iteration, the *rmse* values and the computational time, with regularization for Example 1 with $p = 1\%$ noisy data.

$p = 1\%$	β_1=β_2=10^{-5}	β_1=β_2=10^{-4}	β_1=β_2=10^{-3}	β_1=10^{-3}, β_2=10^{-4}
No. of iterations	6	7	8	6
No. of function evaluations	581	664	747	581
Value of objective function (5.18) at final iteration	0.0015	0.0104	0.0526	0.0104
$rmse(b)$	9.5E-6	1.0E-5	4.6E-6	4.5E-7
$rmse(f)$	0.5698	0.2884	0.8412	0.2884
Computational time	7 mins	8 mins	9 mins	7 mins

5.5.2 Example 2

In this example, we consider solving the second inverse problem given by equations (5.3)–(5.7) with unknown coefficients $f(t)$ and $d(t) \geq 0$, and the following input data:

$$b(x,t) = 1, \quad g(x,t) = \frac{(5-t)x^3}{\ell^2} - 3x^2 + (1+t)x + \ell^2, \quad (x,t) \in Q_T, \tag{5.30}$$

and a, ϕ, ω, φ, and ψ given by equations (5.25)–(5.27).

It can easily be checked by direct substitution that the analytical solution is given by

$$d(t) = \frac{1+t}{\ell^2}, \quad f(t) = e^{-\frac{6t}{\ell^2}}, \quad t \in [0,T], \tag{5.31}$$

and $u(x,t)$ is given by (5.29).

As in Example 1, we take $\ell = T = 1$ and employ the FDM with $M = N = 40$. By simple calculation we conclude that $f(0) = 1$ and $d(0) = 1$. So, we take the initial guesses $d^0 = f^0 = 1$ in the minimization of the functional (5.19).

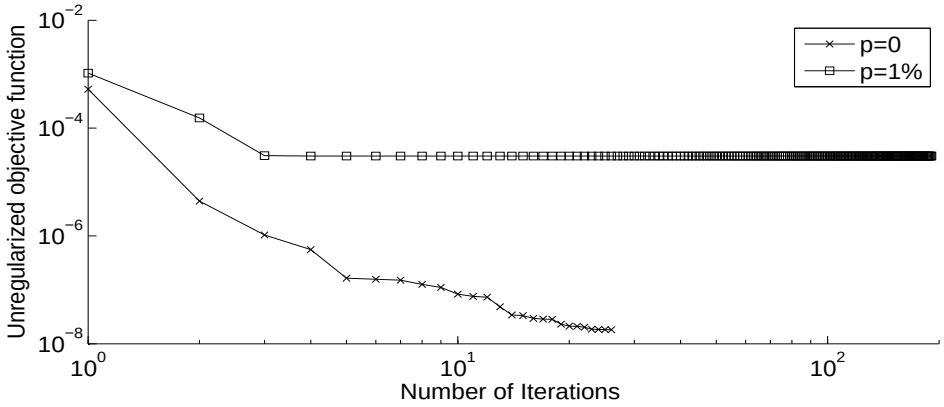

Figure 5.8: The objective function (5.19) without regularization, for Example 2 with exact data and $p = 1\%$ noisy data.

Figures 5.8 and 5.9 illustrate the convergence of the unregularized objective function (5.19) with $\beta_2 = \beta_3 = 0$ and the corresponding recovered coefficients $d(t)$ and $f(t)$, respectively, for exact data $p = 0$ and for $p = 1\%$ noisy data. First, from Figure 5.8 it can be seen that for exact data the unregularized objective function decreases rapidly in about 26 iterations to a low threshold of $O(10^{-8})$. However, for $p = 1\%$ noisy data, the number of iterations necessary to achieve the required degree of convergence with respect to the tolerance chosen increases to 191, see also the second column of Table 5.3 where, in particular, one can observe the long computational time recorded to be in excess of 4 hours. In Figure 5.9, reasonable good retrievals for the unknown coefficients can be observed for exact data, but the instability clearly manifests for noisy data. In order to stabilise the solution for noisy data, as in Example 5.5.1, regularization needs to be included in the functional (5.19) which is minimized.

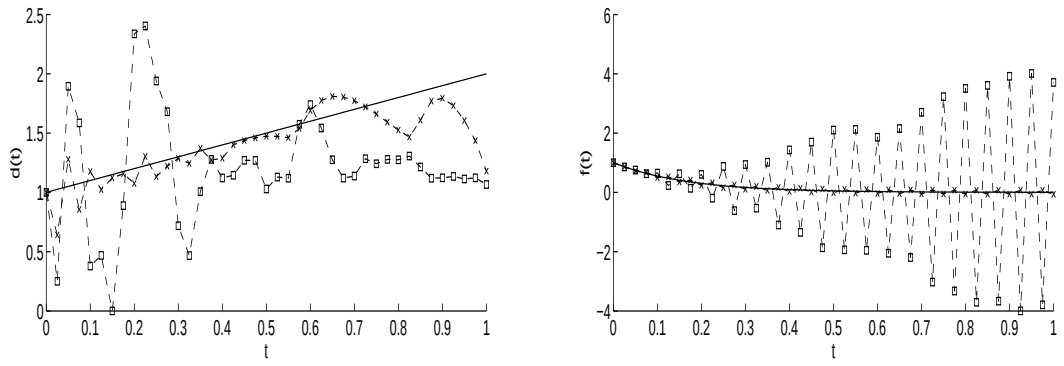

(a) (b)

Figure 5.9: The exact (—) and numerical solutions without regularization for: (a) $d(t)$ and (b) $f(t)$, for Example 2 with exact data (-×-) and with $p = 1\%$ noisy data (-□-).

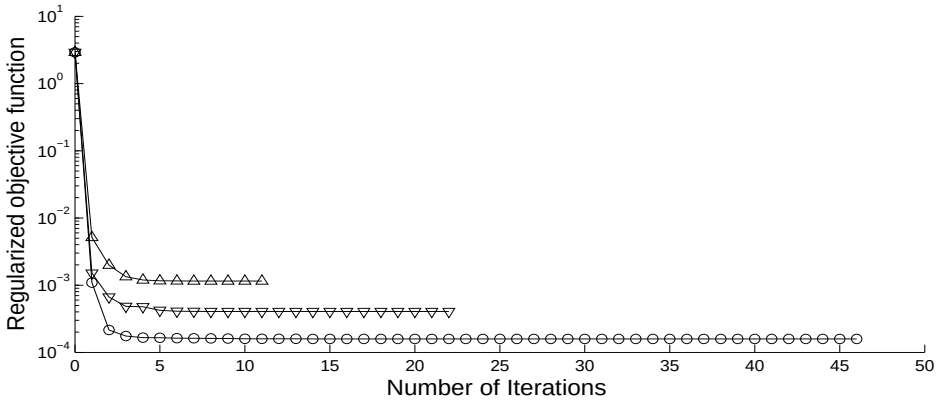

Figure 5.10: The objective function (5.19) with regularization parameters $\beta_2 = \beta_3 = 10^{-4}$ (-△-), $\beta_2 = \beta_3 = 10^{-5}$ (-▽-) and $\beta_2 = \beta_3 = 10^{-6}$ (-○-), for Example 2 with $p = 1\%$ noisy data.

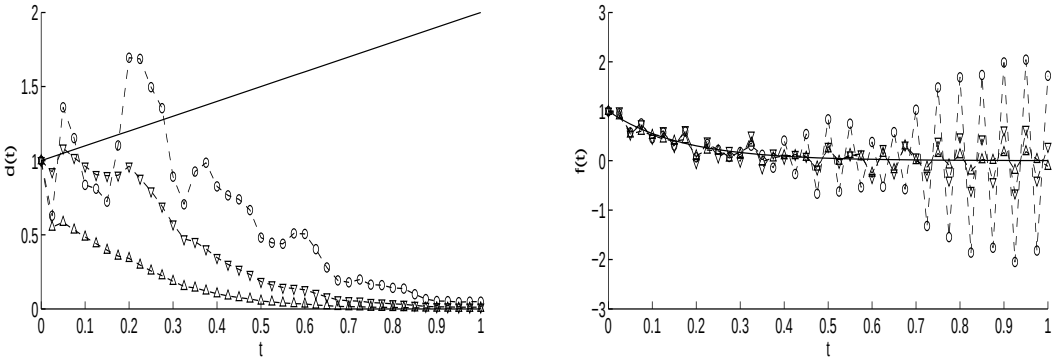

(a) (b)

Figure 5.11: The exact (—) and numerical solutions with regularization parameters $\beta_2 = \beta_3 = 10^{-4}$ (-△-), $\beta_2 = \beta_3 = 10^{-5}$ (-▽-) and $\beta_2 = \beta_3 = 10^{-6}$ (-○-) for: (a) $d(t)$ and (b) $f(t)$, for Example 2 with $p = 1\%$ noisy data.

Figure 5.10 shows the objective function (5.19), as a function of the number of the iterations, for various regularization parameters $\beta_2 = \beta_3 \in \{10^{-6}, 10^{-5}, 10^{-4}\}$, when the input data (5.6) and (5.7) is contaminated with $p = 1\%$ noise. From this figure it can be remarked that a rapid convergent is achieved for each selection of regularization parameters. The corresponding exact and numerical solutions for $d(t)$ and $f(t)$ are presented in Figure 5.11 and other numerical features of the solutions are summarised in Table 5.3. First, by comparing Figures 5.9 and 5.11 clearly the stabilisation benefit of employing regularization can be appreciated. It is also interesting to remark from Table 5.3 that retrieving accurately and simultaneously both the coefficients $d(t)$ and $f(t)$ requires an appropriate choice of the regularization parameters β_2 and β_3, e.g. for $\beta_2 = \beta_3 = 0$ the recovery of $d(t)$ is accurate in the detriment of that of $f(t)$, whilst for $\beta_2 = \beta_3 = 10^{-4}$ the accuracy

of the simultaneous recovery is viceversa. This situation has also been observed previously in cases where simultaneous identification of multiple coefficients has been attempted, [46, 56]. Therefore, a compromising but balancing choice would be to pick $\beta_2 = \beta_3$ in between, say between 10^{-5} and 10^{-4} as is common with ill-posed problems in which acceptable candidate solutions are those in the region where the accuracy and stability portions meet/ intersect.

Finally, for completeness, the exact and numerical reconstructions for the temperature $u(x,t)$ are presented in Figure 5.12 and the absolute error between them is also included. From this figure it can be observed that a stable and accurate reconstruction is obtained.

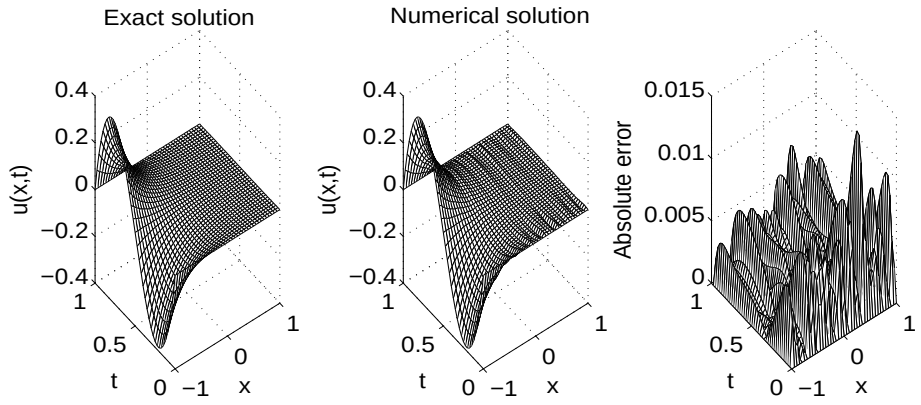

Figure 5.12: The exact (5.29) and numerical reconstructions for the temperature $u(x,t)$ with regularization parameters $\beta_1 = \beta_2 = 10^{-5}$, for Example 2 with $p = 1\%$ noisy data.

Table 5.3: Number of iterations, number of function evaluations, value of the objective function (5.19) at final iteration, $rmse$ values and the computational time, for various regularization parameters, for Example 2 with $p = 1\%$ noisy data.

$p = 1\%$	β_2=β_3=0	β_2=β_3=10^{-6}	β_2=β_3=10^{-5}	β_2=β_3=10^{-4}
No. of iterations	191	46	22	11
No. of function evaluations	15936	3901	1909	996
Value of objective function (5.19) at final iteration	3E-5	0.0001	0.0004	0.0011
$rmse(d)$	0.6283	1.1731	1.3207	1.4409
$rmse(f)$	2.3165	1.0330	0.3127	0.1325
Computational time	4 hours	57 mins	28 mins	15 mins

5.6 Conclusions

A couple of inverse problems consisting of finding the time-dependent coefficients and the time-dependent heat source term in the parabolic heat equation with integral overdetermination conditions have been numerically investigated. The MATLAB routine *lsqnonlin* has been employed effectively to solve the resulting nonlinear constraint optimization problems subject to both exact or noisy input data. Regularization has been imposed when the noisy data has been inverted. Numerical results presented and discussed for a couple test examples show that reasonably accurate and stable numerical solutions have been achieved.

Chapter 6

Simultaneous determination of time and space-dependent coefficients

6.1 Introduction

Choosing an appropriate additional information about what quantities to measure or supply is important since this data enables us to identify the unknown coefficients uniquely. For instance, an upper-base final temperature condition was chosen in [32] to identify a space-dependent heat source, and a similar version can be found in [27] where a Cauchy problem for a second-order parabolic equation was formulated for determining a space-dependent coefficient of a low-order derivative. Cauchy data have also been used in [35] for reconstructing numerically a temperature-dependent thermal conductivity or a heat source. The determination of the space-dependent thermal conductivity was studied in [102] using Kansa's method based on radial basis function techniques, and in [34] using a predictor-corrector iterative finite-difference method (FDM). While spacewise dependent perfusion coefficient identification in the transient bio-heat equation subjected to time-averaging temperature measurement was investigated in [118] using the Crank-Nicolson FDM scheme combined with the first-order Tikhonov regularization method. On the other hand, time-dependent coefficient identification problems have been investigated recently, just to mention a few, the time-dependent inverse source identification problem [45, 109, 119] and the thermal conductivity/diffusivity identification problem [65, 90] subjected to various kinds of overdetermination conditions.

In this chapter, we consider obtaining the numerical solution of a couple of related inverse time and space-dependent coefficient identification problems in the

parabolic heat equation subjected to nonlocal, time-averaging overdetermination conditions.

The organisation of this chapter is as follows. In Section 6.2, the mathematical formulations of the inverse problems are given. In Section 6.3, the Crank-Nicolson FDM is developed for solving the direct problem. In Section 6.4, the inverse problems are reformulated as nonlinear least-squares minimization problems further penalized with regularization terms in order to achive stable solutions with respect to noise in the input data. Numerical results illustrate that accurate and stable numerical solutions are obtained, as it is discussed in Section 6.5. Finally, the conclusions of this chapter are drawn in Section 6.6.

6.2 Mathematical formulation

Let $L > 0$ and $T > 0$ be fixed numbers representing the length of a one-dimensional finite slab and the time period, respectively, and denote by $Q_T := (0, L) \times (0, T)$ the solution domain. Let also f represent a given heat source. Then consider the inverse problem of finding the time-dependent thermal conductivity $a(t)$, the space-dependent component of the fluid velocity $b(x)$ or, of the absorbtion (perfusion) coefficient $c(x)$, together with the temperature $u(x, t)$, which satisfy the parabolic heat equation

$$u_t(x,t) = a(t)\left(u_{xx}(x,t) + b(x)u_x(x,t) - c(x)u(x,t)\right) + f(x,t),\ (x,t) \in Q_T, \quad (6.1)$$

the initial condition

$$u(x,0) = \phi(x), \qquad 0 \leq x \leq L, \quad (6.2)$$

the Dirichlet boundary conditions

$$u(0,t) = \mu_1(t), \qquad u(L,t) = \mu_2(t), \qquad 0 \leq t \leq T, \quad (6.3)$$

the heat flux Neumann condition

$$-a(t)u_x(0,t) = \mu_3(t), \qquad 0 \leq t \leq T. \quad (6.4)$$

and the time-average condition

$$\int_0^{T_0} a(t)u(x,t)dt = \psi(x), \qquad 0 \leq x \leq L, \quad (6.5)$$

where $T_0 \in (0, T]$ is a given fixed number. We note that the single identifications of the coefficient $b(x)$ or $c(x)$, when $a(t)$ is known and taken to be unity, have been investigated elsewhere in [80, 81].

Equation (6.5) is a new overdetermination condition that in the case of heat conduction, can be regarded as the total potential heat function whose derivative, if it exists,

$$\int_0^{T_0} a(t)u_x(x,t)dt = \psi'(x), \quad 0 \leq x \leq L, \tag{6.6}$$

yields the time-average of the heat flux over the time period $[0, T_0]$. We consider therefore the following two inverse problems concerning the simultaneous determination of the coefficients $a(t)$ and $b(x)$ when $c = 0$, termed the Inverse Problem I, and of the coefficients $a(t)$ and $c(x)$ when $b = 0$, termed the Inverse Problem II. These inverse problems have been previously investigated theoretically by Ivanchov [70, Chapter 5], who establish their existence and uniqueness, as follows.

6.2.1 Inverse problem I

In this case $c = 0$ and equation (6.1) becomes

$$u_t(x,t) = a(t)\left(u_{xx}(x,t) + b(x)u_x(x,t)\right) + f(x,t), \quad (x,t) \in Q_T. \tag{6.7}$$

Then the inverse problem I requires determining the triplet solution $(a(t), b(x), u(x,t)) \in C[0,T] \times H^{\gamma}[0,L] \times H^{2+\gamma,1}(\overline{Q}_T)$ for some $\gamma \in (0,1)$, $a(t) > 0$ for $t \in [0,T]$, that satisfies equations (6.2)–(6.4), (6.6) and (6.7). For the definition of the spaces involved, see [87]. In particular, $H^{\gamma}[0,L]$ denotes the space of Hölder continuous functions with exponent γ and $H^{2+\gamma,1}(\overline{Q}_T)$ denotes the space of continuous functions u along with their partial derivatives u_x, u_{xx}, u_t in $\overline{Q}_T$ and with u_{xx} being Hölder continuous with exponent γ in $x \in [0,L]$ uniformly with respect to $t \in [0,T]$.

Theorem 6.1 (Existence, see Theorem 5.2.1 of [70])**.** *Suppose that the following conditions hold:*

1. $\phi \in H^{2+\gamma}[0,L]$, $\psi \in H^{2+\gamma}[0,L]$, $\mu_i \in C^1[0,T]$ *for* $i = 1,2$, $\mu_3 \in C[0,T]$, $f \in H^{\gamma,0}(\overline{Q}_T)$;

2. $\phi'(x) > 0$, $\psi'(x) > 0$ *for* $x \in [0,L]$, $\mu_3(t) < 0$ *for* $t \in [0,T]$;

3. $\phi(0) = \mu_1(0)$, $\phi(L) = \mu_2(0)$, $\psi'(0) = -\int_0^{T_0} \mu_3(t)dt$, $\mu_1'(0) = a(0)(\phi''(0) + b(0)\phi'(0)) + f(0,0)$, $\mu_2'(0) = a(0)(\phi''(L) + b(L)\phi'(L)) + f(L,0)$, *where* $a(0)$, $b(0)$ *and* $b(L)$ *are determined by* $a(0) = -\mu_3(0)/\phi'(0)$,

$$b(0) = \frac{1}{\psi'(0)}\left(\mu_1(T_0) - \phi(0) - \psi''(0) - \int_0^{T_0} f(0,t)dt\right),$$
$$b(L) = \frac{1}{\psi'(L)}\Big(\mu_2(T_0) - \phi(L) - \psi''(L) - \int_0^{T_0} f(L,t)dt\Big).$$

Then, if T_0 *is sufficiently small, the inverse problem (6.2)–(6.4), (6.6) and (6.7) has a solution determined for* $(x,t) \in \overline{Q}_{T_0} := [0,L] \times [0,T_0]$.

In the above, $H^{2+\gamma}[0,L]$ denotes the space of twice continuously differentiable functions with the second-order derivative being Hölder continuous with exponent γ in $[0,L]$. Note that according to Theorem 1 of [67], the existence result in the above theorem also holds if $f \in C^{1,0}(\overline{Q}_T)$ and if condition 2 is replaced by:

2′. $\phi(x) \le 0$, $\phi'(x) \ge 0$, $\psi'(x) > 0$ *for* $x \in [0,L]$, $\phi'(0) > 0$, $\mu_3(t) < 0$, $\mu_1(t) \le 0$, $\mu_2(t) \le 0$, $\mu_1'(t) \le f(0,t)$, $\mu_2'(t) \ge f(L,t)$ *for* $t \in [0,T]$, $f(x,t) \le 0$, $f_x(x,t) \ge 0$ *for* $(x,t) \in \overline{Q}_T$.

Theorem 6.2 (Uniqueness, see Theorem 5.2.2 of [70])**.** *If the conditions*

$$\mu_3(t) \neq 0 \quad \textit{for } t \in [0,T], \quad \psi'(x) \neq 0 \quad \textit{for } x \in [0,L]$$

hold, then, if T_0 *is sufficiently small, the solution of the inverse problem (6.2)–(6.4), (6.6) and (6.7) is unique for* $(x,t) \in \overline{Q}_{T_0}$.

6.2.2 Inverse problem II

In this case $b = 0$ and equation (6.1) becomes

$$u_t(x,t) = a(t)\left(u_{xx}(x,t) - c(x)u(x,t)\right) + f(x,t), \quad (x,t) \in Q_T. \tag{6.8}$$

Then the inverse problem II requires determining the triplet solution $(a(t), c(x), u(x,t)) \in C[0,T] \times H^{\gamma}[0,L] \times H^{2+\gamma,1}(\overline{Q}_T)$, $a(t) > 0$ for $t \in [0,T]$, $c(x) \ge 0$ for $x \in [0,L]$, that satisfies equations (6.2)–(6.5) and (6.8).

Theorem 6.3 (Existence, see [66], and Theorem 5.1.1 of [70])**.** *Suppose that the following conditions hold:*

1. $\phi \in H^{2+\gamma}[0,L]$, $\psi \in H^{2+\gamma}[0,L]$, $\mu_i \in C^1[0,T]$ *for* $i = 1,2$, $\mu_3 \in C[0,T]$, $f \in C^{2,0}(\overline{Q}_T)$;

2. $\phi(x) \geq 0$, $\phi'(x) > 0$, $\phi''(x) \leq 0$, $\psi(x) > 0$, $\psi''(x) \geq 0$ *for* $x \in [0,L]$, $\mu_i(t) \geq 0$ *for* $i = 1,2$, $\mu_3(t) < 0$, $\mu_1(t) - \phi(0) - \int_0^t f(0,\tau)d\tau \leq 0$, $\mu_2(t) - \phi(L) - \int_0^t f(L,\tau)d\tau \leq 0$ *for* $t \in [0,T]$, $f(x,t) \geq 0$, $f_{xx}(x,t) \leq 0$ *for* $(x,t) \in \overline{Q}_T$;

3. $\phi(0) = \mu_1(0)$, $\phi(L) = \mu_2(0)$, $\psi'(0) = -\int_0^{T_0} \mu_3(t)dt$, $\mu_1'(0) = a(0)(\phi''(0) - c(0)\phi(0)) + f(0,0)$, $\mu_2'(0) = a(0)(\phi''(L) - c(L)\phi(L)) + f(L,0)$, *where* $a(0)$, $c(0)$ *and* $c(L)$ *are determined by* $a(0) = -\mu_3(0)/\phi'(0)$,

$$c(0) = -\frac{1}{\psi(0)}\left(\mu_1(T_0) - \phi(0) - \psi''(0) - \int_0^{T_0} f(0,t)dt\right),$$
$$c(L) = -\frac{1}{\psi(L)}\left(\mu_2(T_0) - \phi(L) - \psi''(L) - \int_0^{T_0} f(L,t)dt\right).$$

Then, if T_0 *is sufficiently small, the inverse problem (6.2)–(6.5) and (6.8) has a solution determined for* $(x,t) \in \overline{Q}_{T_0}$.

Theorem 6.4 (Uniqueness, see Theorem 5.1.2 of [70])**.** *If the conditions*

$$\mu_3(t) \neq 0 \quad \textit{for} \quad t \in [0,T], \quad \psi(x) \neq 0 \quad \textit{for} \quad x \in [0,L]$$

hold, then, if T_0 *is sufficiently small, the solution of the inverse problem (6.2)–(6.5) and (6.8) is unique for* $(x,t) \in \overline{Q}_{T_0}$.

6.3 Solution of direct problem

In this section, we consider the direct (forward) initial boundary value problem given by equations (6.1)–(6.3) in which the coefficients $a(t)$, $b(x)$ and $c(x)$ are known and $f(x,t)$, $\phi(x)$ and $\mu_i(t)$, for $i = 1,2$, are given, and the temperature $u(x,t)$ is the solution to be determined.

The discrete form of this direct problem is as follows. Take two positive integers M and N and let $\Delta x = L/M$ and $\Delta t = T/N$ be the uniform step lengths in space and time direction, respectively. We subdivide the solution domain $Q_T = (0,L) \times (0,T)$ into $M \times N$ subintervals of equal length. At the node (i,j) we denote $u_{i,j} = u(x_i,t_j)$, $a_j = a(t_j)$, $b_i = b(x_i)$, $c_i = c(x_i)$ and $f_{i,j} = f(x_i,t_j)$, where $x_i = i\Delta x$, $t_j = j\Delta t$ for $i = \overline{0,M}$, $j = \overline{0,N}$.

Considering the general form of partial differential equation (6.1) as (4.10), the Crank-Nicolson FDM, [51, 110], discretises (4.10), (6.2) and (6.3) as (4.11)–(4.14). For our problem, equation (6.1) can be discretised in the form of (4.11)

as

$$-A_{i,j+1}u_{i-1,j+1} + (1 + B_{i,j+1})u_{i,j+1} - C_{i,j+1}u_{i+1,j+1} = A_{i,j}u_{i-1,j} + (1 - B_{i,j})u_{i,j} + C_{i,j}u_{i+1,j} + \frac{\Delta t}{2}(f_{i,j} + f_{i,j+1}) \quad (6.9)$$

for $i = \overline{1,(M-1)}$, $j = \overline{0,N}$, where

$$A_{i,j} = \frac{(\Delta t)a_j}{2(\Delta x)^2} - \frac{a_j b_i(\Delta t)}{4(\Delta x)},\ B_{i,j} = \frac{(\Delta t)a_j}{(\Delta x)^2} + \frac{(\Delta t)a_j c_i}{2},\ C_{i,j} = \frac{(\Delta t)a_j}{2(\Delta x)^2} + \frac{a_j b_i(\Delta t)}{4(\Delta x)}.$$

At each time step t_{j+1} for $j = \overline{0,(N-1)}$, using the Dirichlet boundary conditions (4.13) and (4.14), the above difference equation can be reformulated as a $(M-1)\times(M-1)$ system of linear equations of the form (3.17), where

$$D = \begin{pmatrix} 1+B_{1,j+1} & -C_{1,j+1} & 0 & \cdots & 0 & 0 & 0 \\ -A_{2,j+1} & 1+B_{2,j+1} & -C_{2,j+1} & \cdots & 0 & 0 & 0 \\ \vdots & \vdots & \vdots & \ddots & \vdots & \vdots & \vdots \\ 0 & 0 & 0 & \cdots & -A_{M-2,j+1} & 1+B_{M-2,j+1} & -C_{M-2,j+1} \\ 0 & 0 & 0 & \cdots & 0 & -A_{M-1,j+1} & 1+B_{M-1,j+1} \end{pmatrix},$$

$$E = \begin{pmatrix} 1-B_{1,j} & C_{1,j} & 0 & \cdots & 0 & 0 & 0 \\ A_{2,j} & 1-B_{2,j} & C_{2,j} & \cdots & 0 & 0 & 0 \\ \vdots & \vdots & \vdots & \ddots & \vdots & \vdots & \vdots \\ 0 & 0 & 0 & \cdots & A_{M-2,j} & 1-B_{M-2,j} & C_{M-2,j} \\ 0 & 0 & 0 & \cdots & 0 & A_{M-1,j} & 1-B_{M-1,j} \end{pmatrix},$$

and

$$\mathbf{b} = \begin{pmatrix} \frac{\Delta t}{2}(f_{1,j} + f_{1,j+1}) + A_{1,j+1}\mu_1(t_{j+1}) \\ \frac{\Delta t}{2}(f_{2,j} + f_{2,j+1}) \\ \vdots \\ \frac{\Delta t}{2}(f_{M-2,j} + f_{M-2,j+1}) \\ \frac{\Delta t}{2}(f_{M-1,j} + f_{M-1,j+1}) + C_{M-1,j+1}\mu_2(t_{j+1}) \end{pmatrix}.$$

6.3.1 Example

As an example, consider the direct problem (6.1)–(6.3) and with $T = L = 1$ and

$$\begin{aligned} a(t) = e^t, \quad b(x) = 2 - x, \quad c(x) = \frac{1}{1+x}, \quad \phi(x) = u(x,0) = x^2 + x, \\ \mu_1(t) = u(0,t) = 2t, \quad \mu_2(t) = u(1,t) = 2 + 2t, \\ f(x,t) = 2 - 2e^t \left(2 + x - x^2 - \frac{t}{1+x}\right). \end{aligned}$$

The exact solution is given by

$$u(x,t) = x^2 + x + 2t, \quad (x,t) \in \overline{Q}_T. \tag{6.10}$$

Outputs of interest are the heat flux (6.4) and the total potential heat function (6.5) on the time period $[0, T_0]$, say $T_0 = 1$,

$$\mu_3(t) = -a(t)u_x(0,t) = -e^t, \quad t \in [0,1], \tag{6.11}$$

$$\psi(x) = \int_0^1 a(t)u(x,t)dt = (x^2 + x)(e-1) + 2, \quad x \in [0,1], \tag{6.12}$$

and its derivative (6.6) given by

$$\psi'(x) = \int_0^1 a(t)u_x(x,t)dt = (2x+1)(e-1), \quad x \in [0,1]. \tag{6.13}$$

The numerical and exact solutions for $u(x,t)$ at interior points are shown in Figure 6.1 and also the absolute error between them is included. One can notice that an excellent agreement is obtained. Figures 6.2(a)–(c) show the numerical solutions in comparison with the exact ones (6.11)–(6.13) for $\mu_3(t)$, $\psi(x)$ and $\psi'(x)$, respectively. These have been calculated using the following $O((\Delta x)^2)$ finite-difference approximation formula and trapezoidal rule for integrals:

$$\mu_3(t_j) = -a(t_j)u_x(0,t_j) = -\frac{(4u_{1,j} - u_{2,j} - 3u_{0,j})a_j}{2(\Delta x)}, \quad j = \overline{0,N}, \tag{6.14}$$

$$\psi(x_i) = \int_0^1 a(t)u(x_i,t)dt = \frac{1}{2N}\left(a_0u_{i,0} + a_Nu_{i,N} + 2\sum_{j=1}^{N-1} u_{i,j}\right), \quad i = \overline{0,M}, \tag{6.15}$$

$$\psi'(x_i) = \int_0^1 a(t)u_x(x_i,t)dt$$
$$= \frac{1}{2N}\begin{cases} a_0\phi'(0) + a_N u_x(0,t_N) + 2\sum_{j=1}^{N-1} a_j u_x(0,t_j), & \text{if } i=0; \\ a_0\phi'(x_i) + a_N u_x(x_i,t_N) + 2\sum_{j=1}^{N-1} a_j u_x(x_i,t_j), & \text{if } i=\overline{1,M-1}; \\ a_0\phi'(1) + a_N u_x(1,t_N) + 2\sum_{j=1}^{N-1} a_j u_x(1,j), & \text{if } i=M, \end{cases} \tag{6.16}$$

where, for $j=\overline{0,N}$,

$$u_x(0,t_j) = \frac{4u_{1,j} - u_{2,j} - 3u_{0,j}}{2(\Delta x)}, \tag{6.17}$$

$$u_x(1,t_j) = -\frac{4u_{M-1,j} - u_{M-2,j} - 3u_{M,j}}{2(\Delta x)}, \tag{6.18}$$

$$u_x(x_i,t_j) = \frac{u_{i+1,j} - u_{i-1,j}}{2(\Delta x)} \quad i=\overline{1,(M-1)}. \tag{6.19}$$

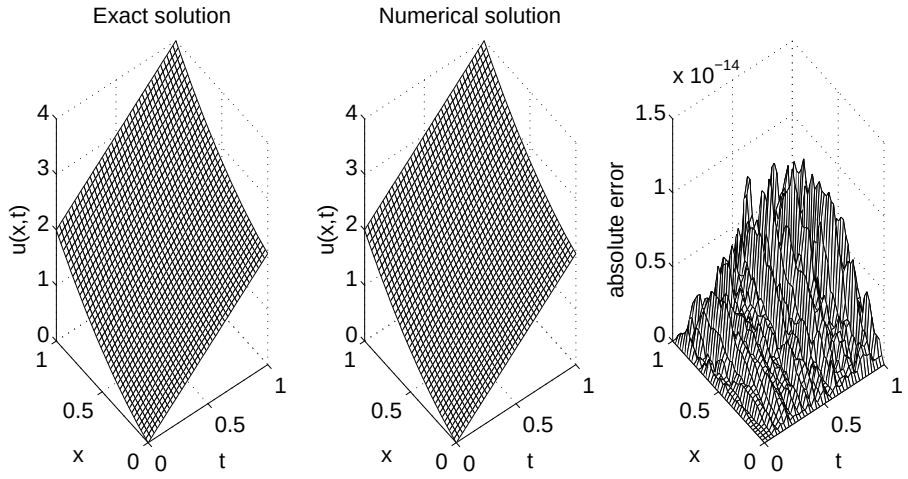

Figure 6.1: Exact and numerical solutions for the temperature $u(x,t)$, and the absolute error for the direct problem obtained with $M=N=40$.

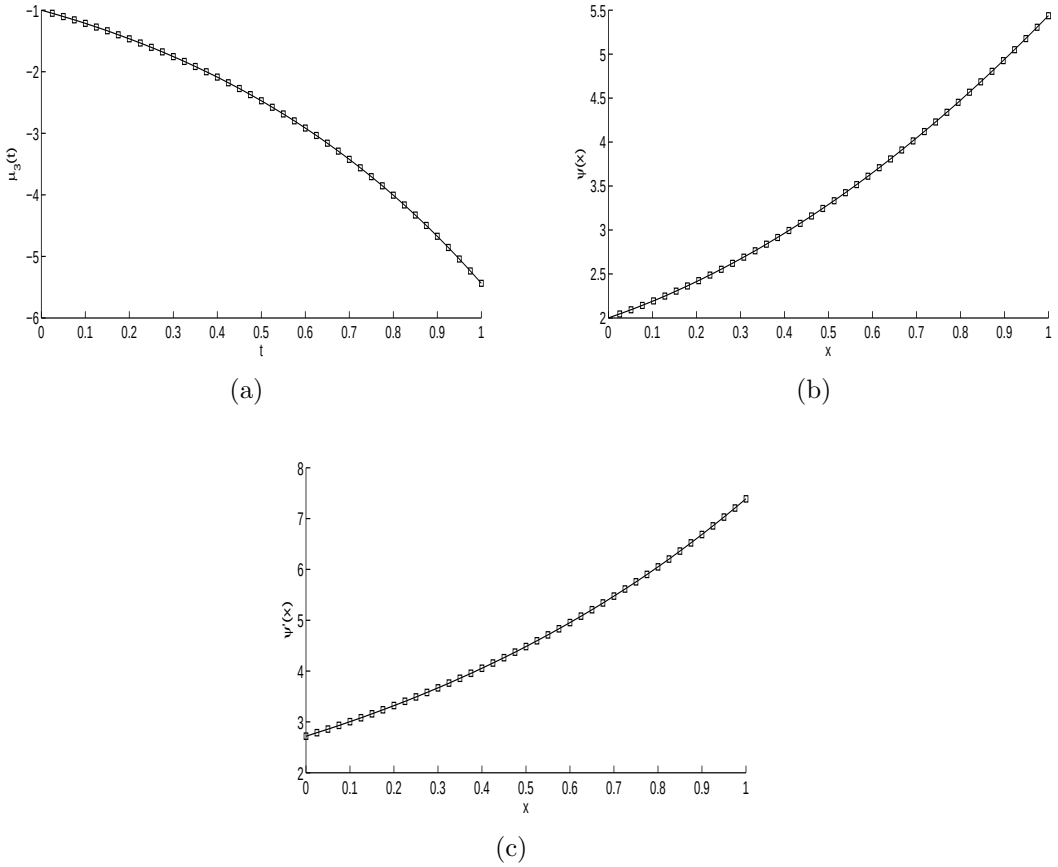

Figure 6.2: Exact (—) and numerical (□□□) solutions for: (a) the heat flux $\mu_3(t)$, (b) the total potential function $\psi(x)$, and (c) the time-average heat flux $\psi'(x)$, for the direct problem obtained with $M = N = 40$.

6.4 Numerical approach to the inverse problems

The inverse problems under investigation are nonlinear and the most common numerical approach is to impose the overdetermination conditions in a least-squares sense, based on minimizing the objective function

$$F_I(a,b) := \big\|a(t)u_x(0,t) + \mu_3(t)\big\|^2 + \Big\| \int_0^{T_0} a(t)u_x(x,t)dt - \psi'(x)\Big\|^2 + \beta_1\big\|a(t)\big\|^2 + \beta_2\big\|b(x)\big\|^2, \tag{6.20}$$

for the inverse problem I, and

$$F_{II}(a,c) := \big\|a(t)u_x(0,t) + \mu_3(t)\big\|^2 + \Big\| \int_0^{T_0} a(t)u(x,t)dt - \psi(x)\Big\|^2 + \beta_1\big\|a(t)\big\|^2 + \beta_3\big\|c(x)\big\|^2, \tag{6.21}$$

for the inverse problem II, where $\beta_i \geq 0$ for $i = 1, 2, 3$ are regularization parameters to be prescribed and the norms are understood in the L^2-sense. As in Chapter 5, Section 5.4, we choose different regularization parameters for $a(t)$, $b(x)$ and $c(x)$ because scaling their stabilities is not uniform. Moreover, in the case of this chapter, the coefficients $a(t)$ and $b(x)$ or $c(x)$ depend on the variables t and x, which are independent of each other, thus there is no reason beforehand why one can choose β_1, β_2 or β_3 equal.

Of course, finding a global minimizer to these nonlinear optimization problems is in general not an easy task. Since the inverse problems under investigation are nonlinear the functionals (6.20) and (6.21) are not convex and could have many local minima in which, depending on the initial guess, a descent-based method tends to get stuck if the underlying problems are ill-posed, [31, p.17]. A possible way to deal with this difficulty could be to develop a "global convergent method", [5, 106], whose convergence to a good approximation of the exact solution is independent of the initial guess but this challenging task is deferred to a future work.

Bearing in mind that the values of $a(0)$, $b(0)$, $b(L)$, $c(0)$ and $c(L)$ are determined *a priori* directly form the compatibility conditions in Theorems 6.1 and 6.3, the discretizations of (6.20) and (6.21) simplify as

$$F_I(\underline{a}, \underline{b}) = \sum_{j=1}^{N} \Big[a_j u_x(0, t_j) + \mu_3(t_j) \Big]^2 + \sum_{i=1}^{M-1} \Big[\int_0^{T_0} a(t) u_x(x_i, t) dt - \psi'(x_i) \Big]^2 + \beta_1 \sum_{j=1}^{N} a_j^2 + \beta_2 \sum_{i=1}^{M-1} b_i^2, \tag{6.22}$$

$$F_{II}(\underline{a}, \underline{c}) = \sum_{j=1}^{N} \Big[a_j u_x(0, t_j) + \mu_3(t_j) \Big]^2 + \sum_{i=1}^{M-1} \Big[\int_0^{T_0} a(t) u(x_i, t) dt - \psi(x_i) \Big]^2 + \beta_1 \sum_{j=1}^{N} a_j^2 + \beta_3 \sum_{i=1}^{M-1} c_i^2. \tag{6.23}$$

In the case when $\beta_1 = \beta_2 = \beta_3 = 0$, the above functions become the ordinary least-squares functionals which normally produce unstable solutions for noisy measurements (6.4)–(6.6). The minimization of the functions (6.22) and (6.23) subject to the physical simple lower bounds for $a(t) > 0$ and $c(x) \geq 0$ is accomplished via the MATLAB optimization toolbox *lsqnonlin*, [95], as described in the previous chapters. This initial guess, say $(a^0(t), b^0(x))$ for inverse problem I, could be included in (6.20) by replacing the last two terms in it by

$\beta_1\|a(t)-a^0(t)\|^2+\beta_2\|b(x)-b^0(x)\|^2$, but this is not necessary, see [31, p.18]. Alternatively, one could use a truncated Gauss-Newton method with simple bounds on the variables, [79], for solving the constrained nonlinear optimization problem. The positive components of the vector $\underline{a}$ and the non-negative components of the vector $\underline{c}$ are sought in the intervals $[10^{-10}, 10^3]$ and $[0, 10^3]$, respectively.

We also take the parameters of the routine as follows:

- Number of variables $M = N = 20$ for inverse problem I and $M = N = 40$ for inverse problem II.
- Maximum number of iterations = 20 × (number of variables).
- Maximum number of objective function evaluations = $10^3\times$ (number of variables).
- Solution (xTol) and object function (FunTol) tolerances = 10^{-20}.

The inverse problems under investigation are solved subject to both exact and noisy data which are numerically simulated as

$$\mu_3^{\epsilon 1}(t_j) = \mu_3(t_j) + \epsilon 1_j, \quad j = \overline{1, N}, \tag{6.24}$$

$$\psi'^{\epsilon 2}(x_i) = \psi'(x_i) + \epsilon 2_i, \quad i = \overline{1, (M-1)}, \tag{6.25}$$

$$\psi^{\epsilon 3}(x_i) = \psi(x_i) + \epsilon 3_i, \quad i = \overline{1, (M-1)}, \tag{6.26}$$

where $\epsilon 1_j$, $\epsilon 2_i$ and $\epsilon 3_i$ are random variables generated from Gaussian normal distributions with mean zero and standard deviations $\sigma 1$, $\sigma 2$ and $\sigma 3$ given by

$$\sigma 1 = p \times \max_{t\in[0,T]} |\mu_3(t)|, \quad \sigma 2 = p \times \max_{x\in[0,L]} |\psi'(x)|, \quad \sigma 3 = p \times \max_{x\in[0,L]} |\psi(x)|, \tag{6.27}$$

where p represents the percentage of noise. We use the MATLAB function *normrnd* to generate the random variables $\underline{\epsilon 1} = (\epsilon 1_j)_{j=\overline{1,N}}$, $\underline{\epsilon 2} = (\epsilon 2_i)_{i=\overline{1,M-1}}$ and $\underline{\epsilon 3} = (\epsilon 2_i)_{i=\overline{1,M-1}}$, as follows:

$$\left.\begin{aligned} \underline{\epsilon 1} = normrnd(0, \sigma 1, N), \quad \underline{\epsilon 2} = normrnd(0, \sigma 2, M-1), \\ \underline{\epsilon 3} = normrnd(0, \sigma 3, M-1). \end{aligned}\right\} \tag{6.28}$$

6.5 Numerical results and discussion

In this section we present, discuss and assess the numerically obtained results by employing the FDM combined with Tikhonov regularization method, as presented in previous section, for a couple of benchmark test examples for each of the inverse

problems I (Examples 1 and 2) and II (Examples 3 and 4). The root mean square errors ($rmse$)

$$rmse(a) = \sqrt{\frac{1}{N}\sum_{j=1}^{N}\left(a_{numerical}(t_j) - a_{exact}(t_j)\right)^2}, \tag{6.29}$$

$$rmse(b) = \sqrt{\frac{1}{M-1}\sum_{i=1}^{M-1}\left(b_{numerical}(x_i) - b_{exact}(x_i)\right)^2}, \tag{6.30}$$

$$rmse(c) = \sqrt{\frac{1}{M-1}\sum_{i=1}^{M-1}\left(c_{numerical}(x_i) - c_{exact}(x_i)\right)^2}, \tag{6.31}$$

were calculated in order to estimate the accuracy of the identified coefficients. In all examples we take $L = T_0 = T = 1$.

6.5.1 Example 1 (for inverse problem I)

In the first example, we consider the inverse problem I given by equations (6.2)–(6.4), (6.6) and (6.7) with the following input data:

$$\phi(x) = u(x,0) = x+1, \quad \mu_1(t) = u(0,t) = \frac{1}{1+t}, \quad \mu_2(t) = u(1,t) = \frac{2}{1+t},$$
$$\mu_3(t) = -a(t)u_x(0,t) = -1, \quad \psi'(x) = \int_0^1 a(t)u_x(x,t)dt = 1,$$
$$f(x,t) = -\frac{x+1}{(1+t)^2} + 2 - x.$$

One can observe that the conditions of Theorems 6.1 and 6.2 are satisfied, hence the problem is uniquely solvable. The analytical solution is given by

$$a(t) = 1+t, \quad b(x) = x-2, \quad u(x,t) = \frac{x+1}{1+t}. \tag{6.32}$$

The initial guess was $\underline{a}^0 = \underline{1}$ and $\underline{b}^0 = \underline{-2}$.

We consider first the case where there is no noise (i.e., $p = 0$) included in the input data $\mu_3(t)$ and $\psi'(x)$. In order to investigate the convergence of the numerical solutions for $a(t)$ and $b(x)$, the inverse problem was executed with various FDM mesh parameters, namely, $M = N \in \{10, 20, 40\}$ and the numerical results are compared with the exact ones in Table 6.1 and Figure 6.3. No regularization was included, i.e. $\beta_1 = \beta_2 = 0$ in (6.22). As illustrated in Figure 6.3 and more clearly in Table 6.1 one can be notice that, as $M = N$ increase, the numerical outputs converge to the exact values. The errors estimated through the $rmse(a)$

and $rmse(b)$ given by equations (6.29) and (6.30), respectively, are also included in Table 6.1. The decreasing behaviour of the errors with increasing the discretisation parameters clearly demonstrates the convergence and excellent accuracy of the numerically obtained solution. The number of iterations required to achieve the convergence of the objective functional (6.22) below a very low threshold of $O(10^{-20})$ also increases, as $M = N$ increase, as shown in Figure 6.4. From both Figures 6.3, 6.4 and Table 6.1, it can be seen that the independence of mesh is achieved with excellent accuracy and a rather coarse grid. Consequently, in what follows we fix $M = N = 20$ as a sufficiently fine mesh which ensures that a further refinement does not significantly affect the accuracy of the numerical results. Moreover, the rather low values for the number of variables result in a reasonable number of iterations and computational time to achieve the convergence of the objective function (6.22) which is minimized using the MATLAB toolbox routine *lsqnonlin*.

Table 6.1: The exact and the numerical coefficients $a(t)$ and $b(x)$, for Example 1 with no noise and no regularization, for $M = N \in \{10, 20, 40\}$. The $rmse(a)$ and $rmse(b)$ are also included.

t	0.1	0.2	...	0.9	1	M=N	$rmse(a)$
$a(t)$	1.1018	1.2016	...	1.8976	1.9971	10	1.7E-3
	1.1004	1.2004	...	1.8994	1.9993	20	4.0E-4
	1.1001	1.2001	...	1.8998	1.9998	40	9.8E-5
	1.1000	1.2000	...	1.9000	2.0000	exact	0
x	0.1	0.2	...	0.8	0.9	M=N	$rmse(b)$
$b(x)$	-1.8983	-1.7981	...	-1.1972	-1.0971	10	2.4E-3
	-1.8996	-1.7995	...	-1.1993	-1.0993	20	5.9E-4
	-1.8999	-1.7999	...	-1.1998	-1.0998	40	1.4E-4
	-1.9000	-1.8000	...	-1.2000	-1.1000	exact	0

Even though the Theorems 6.1 and 6.2 ensure the unique solvability of the inverse problem I, the problem is still ill-posed since small errors in input measurement can cause highly oscillating unbounded solutions. To overcome this instability, regularization such as the Tikhonov regularization method can be applied. The main difficulty in regularization of nonlinear ill-posed problems is the selection of regularization parameters. Many methods have been suggested to select such parameters which can be fairly applied to linear problems, but the selection in the nonlinear case is less reliable.

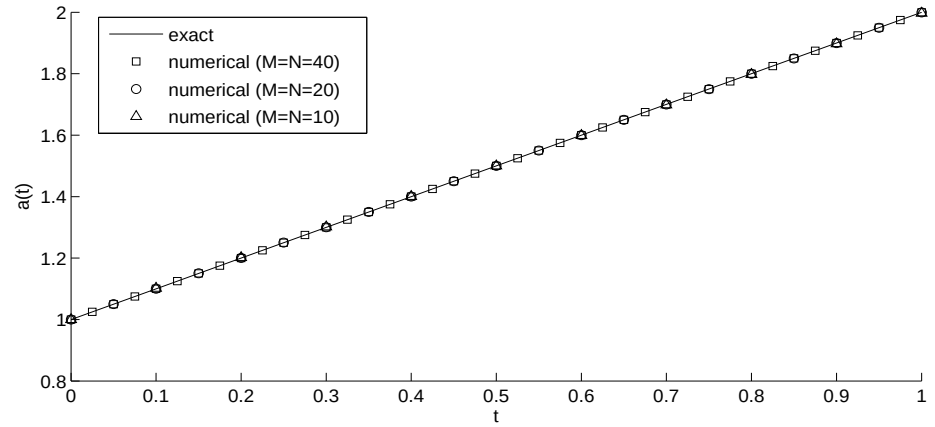

(a)

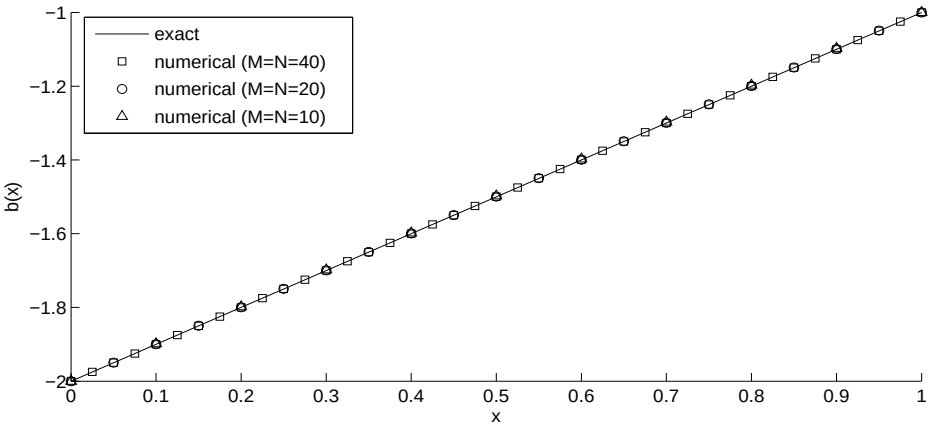

(b)

Figure 6.3: The coefficients (a) $a(t)$, and (b) $b(x)$ for Example 1 with no noise and no regularization, for $M = N \in \{10, 20, 40\}$.

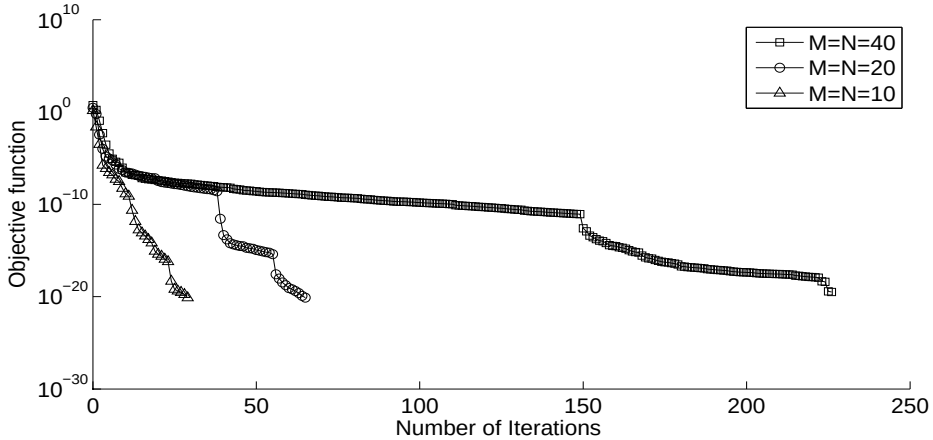

Figure 6.4: Objective function (6.22), for Example 1 with no noise and no regularization, for $M = N \in \{10, 20, 40\}$.

In this chapter, we choose the regularization parameters β_1 and β_2 by trial

and error. We start with small values for regularization parameters and gradually increase them until numerical oscillations in the unknown coefficients disappear.

We fix $M = N = 20$ and we add $p = 2\%$ noise to the heat flux measurement (6.4) and the integral average of heat flux (6.6), as in (6.24) and (6.25), respectively, to test the stability. Figure 6.5 shows the convergence of the objective function (6.22), as a function of the number of iterations, for $\beta_1 = 0$ and various $\beta_2 \in \{0, 10^{-3}, 10^{-2}, 10^{-1}\}$. The minimization process was stopped if the maximum number of iterations or, the permitted tolerance has been reached. The associated numerical results for $a(t)$ and $b(x)$ are presented in Figure 6.6. From this figure it can be seen that the unregularized, i.e. $\beta_1 = \beta_2 = 0$, numerical results are much more stable for $a(t)$ than for $b(x)$. Therefore, in what follows in order to simplify the investigation and discussion we can solely take $\beta_1 = 0$ and assess the stability of the solution with respect to the single regularization parameter β_2 only. Overall, from Figure 6.6 (see also the numerical features summarized in Table 6.4 for Example 1) it can be seen that accurate and stable solutions are reconstructed when we choose the regularization parameter β_2 between 10^{-3} and 10^{-2}.

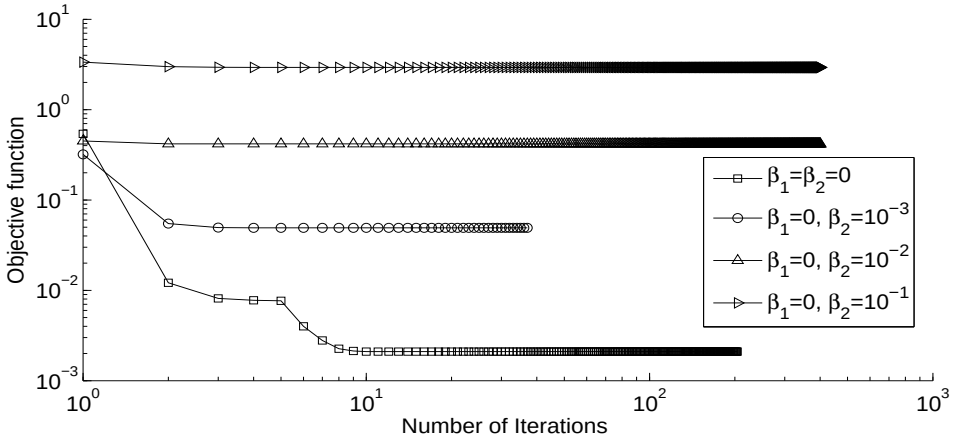

Figure 6.5: Objective function (6.22), for Example 1 with $p = 2\%$ noise and regularization.

The reconstructions of the temperature $u(x, t)$ are presented in Figure 6.7. From this figure one can observe that, in general, the temperature is not affected significantly in terms of stability by the inclusion of noise.

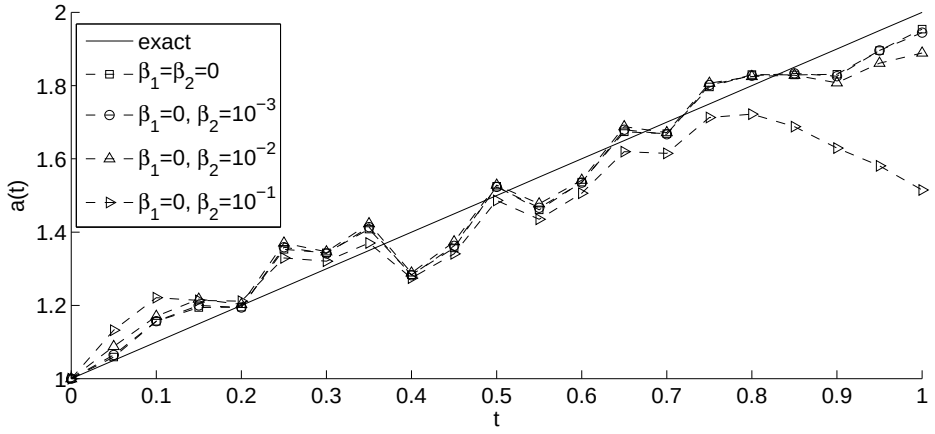

(a)

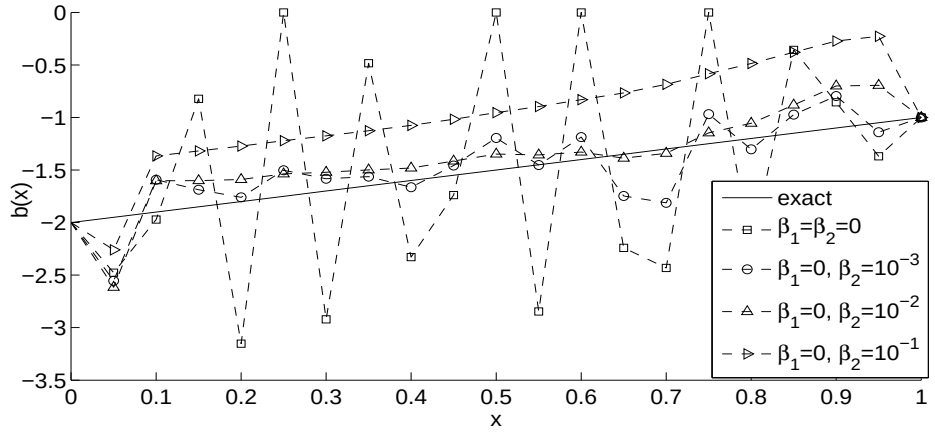

(b)

Figure 6.6: The coefficients (a) $a(t)$, and (b) $b(x)$ for Example 1 with $p = 2\%$ noise and regularization.

Next, in Table 6.2 we estimate the *rmse* errors (6.29) and (6.30) for various amounts of noise $p \in \{1, 2, 3\}\%$ and various regularization parameters $\beta_2 \in \{0, 10^{-3}, 10^{-2}, 10^{-1}\}$. From this table it can be seen that stable solutions are achieved if regularization is included. Furthermore, the results become more accurate as the amount of noise decreases.

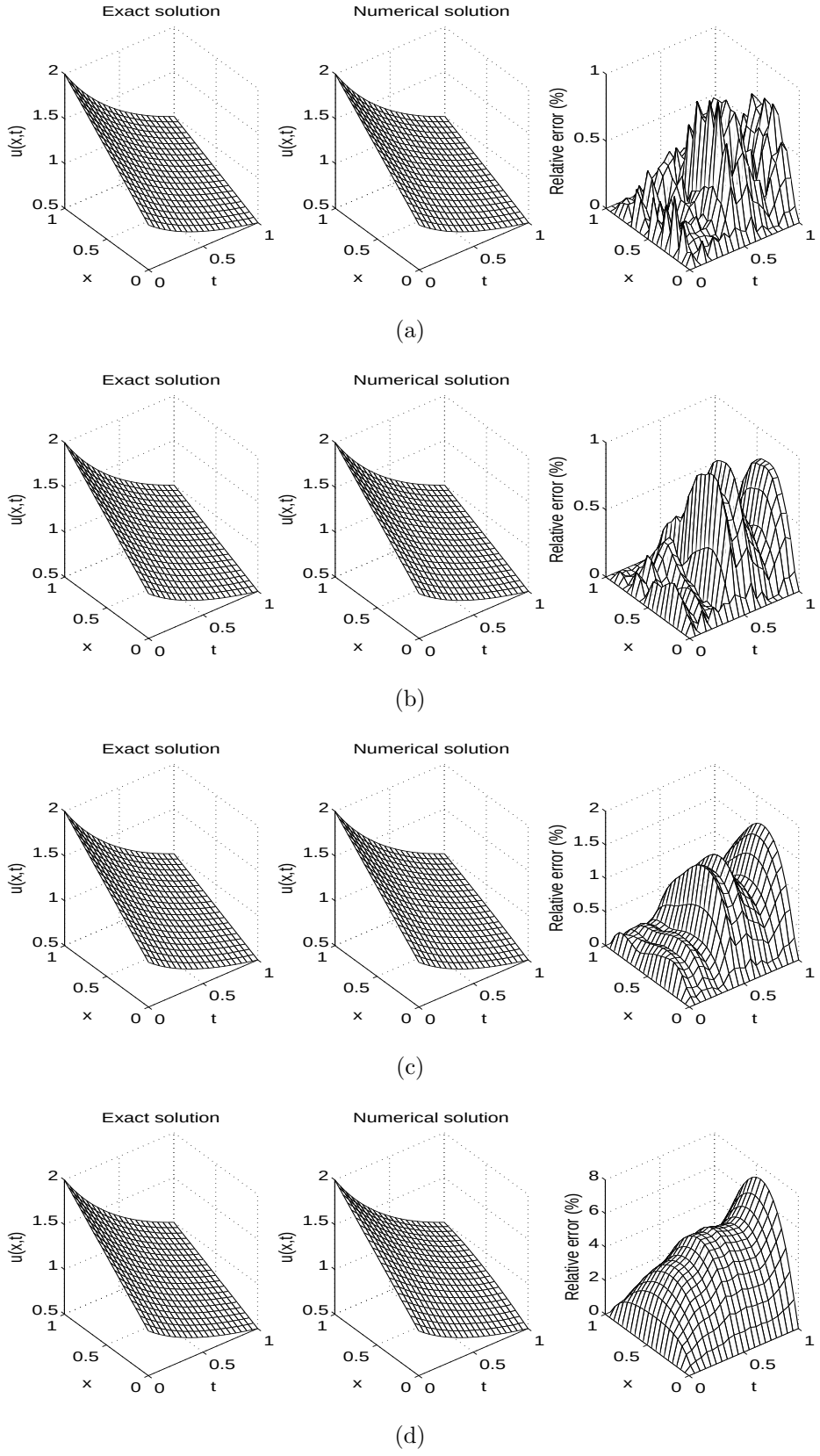

Figure 6.7: The exact and numerical temperatures $u(x,t)$, for Example 1, with $\beta_1 = 0$ and (a) $\beta_2 = 0$, (b) $\beta_2 = 10^{-3}$, (c) $\beta_2 = 10^{-2}$, and (d) $\beta_2 = 10^{-1}$, with $p = 2\%$ noise. The relative error between them is also included.

Table 6.2: The $rmse$ errors (6.29) and (6.30) for various amounts of noise $p \in \{1, 2, 3\}\%$ and various regularization parameters $\beta_1 = 0$ and $\beta_2 \in \{0, 10^{-3}, 10^{-2}, 10^{-1}\}$ for Example 1 .

	$rmse(a)$			$rmse(b)$		
$\beta_1 = 0$	$p = 1\%$	$p = 2\%$	$p = 3\%$	$p = 1\%$	$p = 2\%$	$p = 3\%$
$\beta_2 = 0$	0.0291	0.0595	0.0890	0.9507	1.0602	1.2718
$\beta_2 = 10^{-3}$	0.0322	0.0607	0.0907	0.1896	0.2668	0.3861
$\beta_2 = 10^{-2}$	0.0470	0.0691	0.0990	0.3105	0.2501	0.3539
$\beta_2 = 10^{-1}$	0.1775	0.1671	0.2082	0.6680	0.6043	0.6731

6.5.2 Example 2 (for inverse problem I)

In the previous example we have inverted linear and smooth coefficients given by equation (6.32). In this example, we consider the recovery of a smooth and nonlinear function for $a(t)$ and a non-smooth and piecewise linear function for $b(x)$ for the inverse problem I given by equations (6.2)–(6.4), (6.6) and (6.7) with the following input data:

$$\phi(x) = u(x,0) = x^3 + x, \quad \mu_1(t) = u(0,t) = t^2, \quad \mu_2(t) = u(1,t) = 2 + t + t^2,$$
$$\mu_3(t) = -a(t)u_x(0,t) = -(1+t)(1+\cos^2(2\pi t)),$$
$$\psi'(x) = \int_0^1 a(t)u_x(x,t)dt = \frac{9}{4}(1+2x^2),$$
$$f(x,t) = x + 2t - 6x(1+\cos^2(2\pi t)) - (1+\cos^2(2\pi t))\left(\left|x - \frac{1}{2}\right| - 2\right)(3x^2 + t + 1).$$

One can observe that the conditions of Theorem 6.2 are satisfied, hence the solution is unique. The analytical solution is given by

$$a(t) = 1 + \cos^2(2\pi t), \quad b(x) = \left|x - \frac{1}{2}\right| - 2, \quad u(x,t) = x^3 + x + xt + t^2. \quad (6.33)$$

The initial guess was $\underline{a}^0 = \underline{2}$ and $\underline{b}^0 = \underline{-1.5}$.

We consider first the case of exact data, i.e. $p = 0$. We solve this nonlinear problem by minimizing the functional (6.22) which minimize the gap between the measured and the modeled data in equations (6.4) and (6.6). The numerical results for the unknown coefficients $a(t)$, $b(x)$ and the objective function plotted against the number of iterations are displayed in Figures 6.8 and 6.9. From these figures it can be seen that the numerical solutions for the coefficients $a(t)$ and $b(x)$ are convergent and accurate, as the FDM mesh is increased.

It is convenient to choose $M = N = 20$ for the rest of computations due to the reasonable accuracy and acceptable number of iterations cost to achieve convergence, see Table 6.3. From this table it can also be seen that the estimated errors $rmse(a)$ and $rmse(b)$ decrease monotonically to zero, as the FDM mesh size decreases to zero. For comparison purposes, we have also employed the MATLAB toolbox routine $fmincon$ based on the interior point algorithm, [95], instead of the TRR algorithm on which the $lsqnonlin$ routine is based, and the numerically obtained results are also included in Table 6.3 in brackets. By comparing in Table 6.3 the numerical results obtained using the two MATLAB toolbox routines $lsqnonlin$ and $fmincon$ for minimizing the objective function (6.22) one can observe that the $rmse(a)$ and $rmse(b)$ values are identical at least up to 4 decimals after comma which is reassuring to conclude that possibly an optimal accuracy has been achieved. The minimum values of (6.22) in both cases are very small indicating that the global minimum has been obtained. Finally, as expected, because $fmincon$ is more general than $lsqnonlin$ it performs more function evaluations and iterations to achieve convergence.

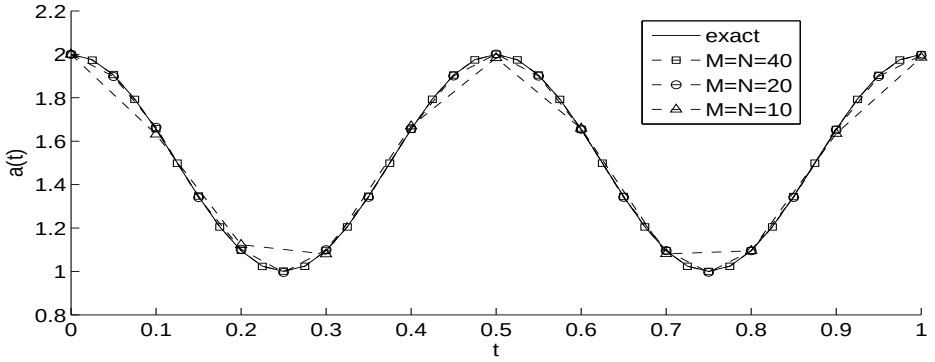

(a)

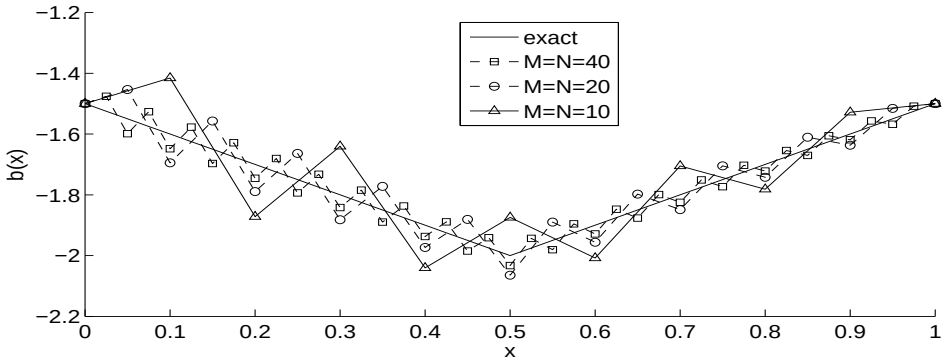

(b)

Figure 6.8: The coefficients (a) $a(t)$, and (b) $b(x)$ for Example 2 with no noise and no regularization, for $M = N \in \{10, 20, 40\}$.

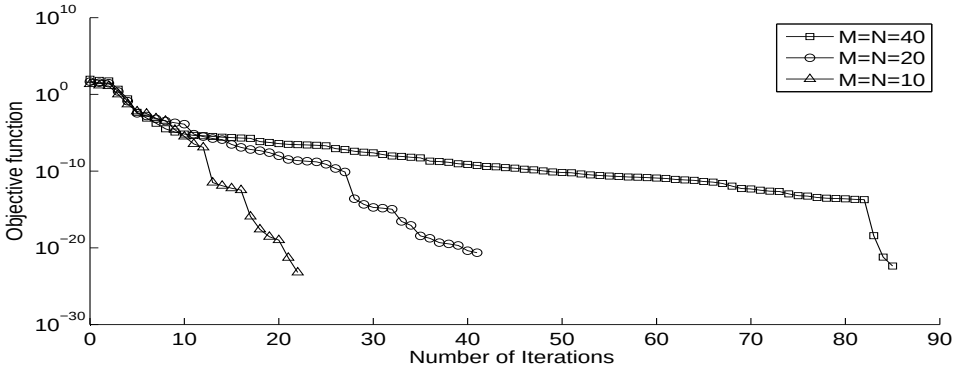

Figure 6.9: Objective function (6.22), for Example 2 with no noise no regularization, for $M = N \in \{10, 20, 40\}$.

Table 6.3: Number of iterations, number of function evaluations, value of objective function (6.22) at final iteration and the $rmse$ values (6.29) and (6.30), for Example 2 with no noise and no regularization, for $M = N \in \{10, 20, 40\}$, obtained using $lsqnonlin$ and $fmincon$ (in brackets).

$M = N$	10	20	40
No. of iterations	22 (85)	41 (167)	85 (446)
No. of function evaluations	529 (1986)	1806 (7254)	7138 (37142)
Minimum value of (6.22)	6.1E-24 (3.1E-15)	2.3E-21 (6E-15)	4.2E-23 (1.4E-14)
$rmse(a)$	0.0169 (0.0169)	0.0047 (0.0047)	0.0012 (0.0012)
$rmse(b)$	0.1321 (0.1321)	0.0685 (0.0685)	0.0349 (0.0349)

Next, the case of noise contamination with $p = 2\%$ is considered by adding Gaussian random noise into input data $\mu_3(t)$ and $\psi'(x)$ in (6.4) and (6.6), as in (6.24) and (6.25), respectively. As expected, without regularization, i.e., $\beta_1 = \beta_2 = 0$, the classical least-squares minimization produces an unstable solution. Hence, we employ the Tikhonov regularization method by adding stabilizing terms in (6.22) in order to restore the stability.

Figure 6.10 shows the objective function (6.22), as a function of the number of iterations. Form this figure it can be seen that convergence is achieved for each choice of regularization parameters. In case $\beta_1 = 0$ and $\beta_2 = 10^{-1}$, the minimization routine $lsqnonlin$ was stopped when the maximum number of iterations

(Maxiter=400) was reached. In the other cases the iterative process was stopped when the objective function tolerance, or the solution tolerance has been reached.

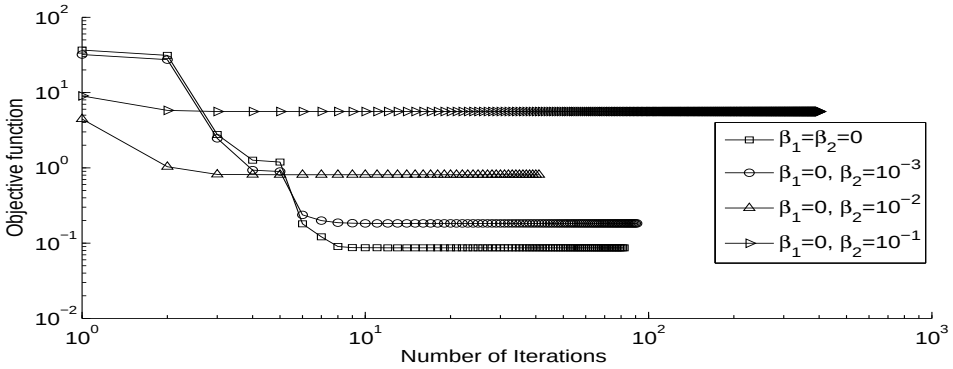

Figure 6.10: Objective function (6.22), for Example 2 with $p = 2\%$ noise and regularization.

Figure 6.11 displays the associated numerical results for the coefficients $a(t)$ and $b(x)$. From this figure and Table 6.4 it can be seen that accurate and stable results are obtained for $\beta_1 = 0$ and β_2 between 10^{-2} and 10^{-1}. As in Figure 6.6(a), one can notice once again that $\beta_1 = 0$ can be chosen because the retrieval of the thermal conductivity $a(t)$ is rather stable and is less influenced by noise, see Figures 6.8(a) and 6.11(a). Perhaps, this stability is due to the fact that this coefficient appears explicitly in the objective function (6.22), whilst $b(x)$ appears only implicitly.

Table 6.4: Number of iterations, number of function evaluations, value of regularized objective function (6.22) at final iteration, for Examples 1 and 2 with $\beta_1 = 0$ and $p = 2\%$ noise.

Example		$\beta_2 = 0$	$\beta_2 = 10^{-3}$	$\beta_2 = 10^{-2}$	$\beta_2 = 10^{-1}$
1	No. of iterations	204	37	401	401
	No. of function evaluations	8815	1634	17286	17286
	Minimum value of (6.22)	0.0020	0.0491	0.4178	2.9329
	$rmse(a)$	0.0602	0.0607	0.0691	0.1671
	$rmse(b)$	1.0602	0.2668	0.2501	0.6043
2	No. of iterations	82	91	41	401
	No. of function evaluations	3569	3956	1806	17286
	Minimum value of (6.22)	0.0865	0.1827	0.8105	5.5954
	$rmse(a)$	0.0501	0.0511	0.0483	0.0573
	$rmse(b)$	1.4860	1.3327	0.5415	0.3854

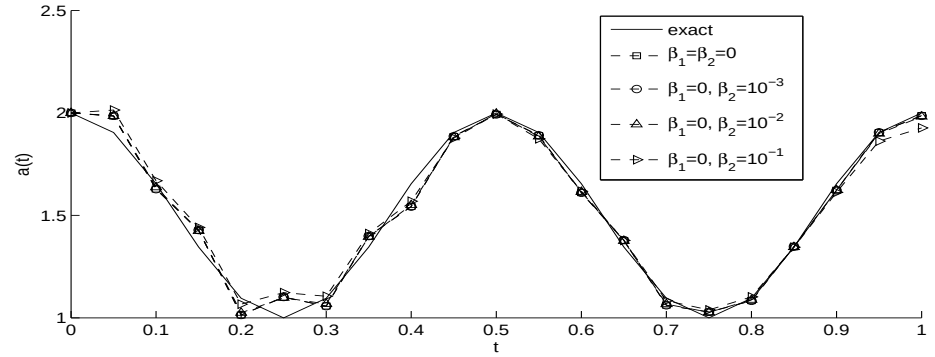

(a)

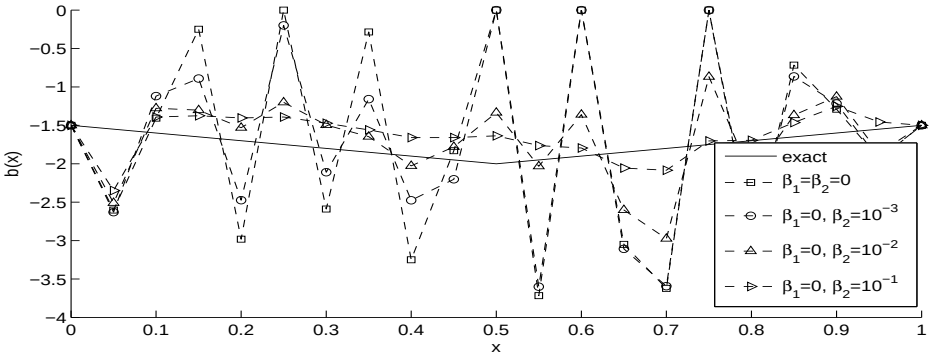

(b)

Figure 6.11: The coefficients (a) $a(t)$, and (b) $b(x)$ for Example 2 with $p = 2\%$ noise and regularization.

The exact and numerical temperatures are presented in Figure 6.12. As it also happened previously in Example 1 and illustrated in Figure 6.7, from Figure 6.12 it can be seen that the temperature reconstruction is not significantly affected by noise.

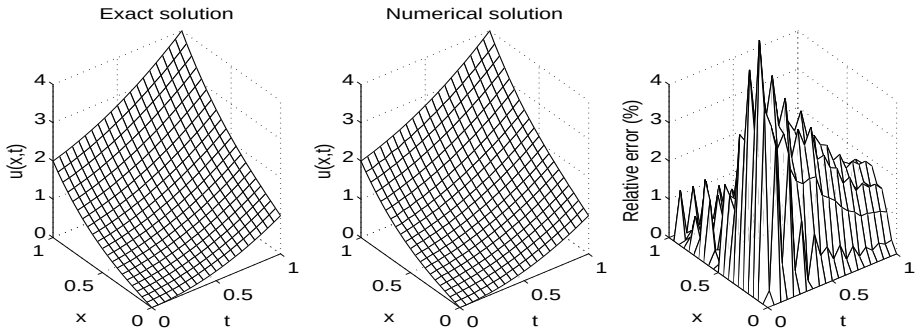

(a)

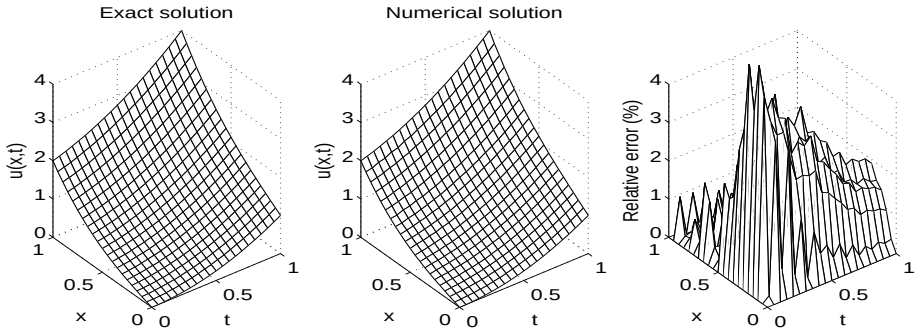

(b)

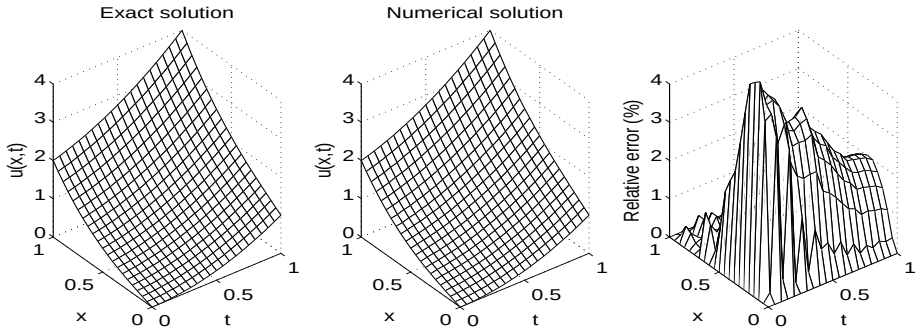

(c)

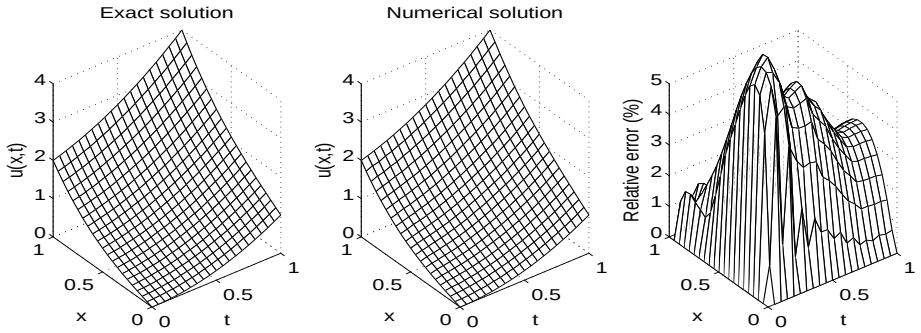

(d)

Figure 6.12: The exact and numerical temperatures $u(x,t)$, for Example 2, with $\beta_1 = 0$ and (a) $\beta_2 = 0$, (b) $\beta_2 = 10^{-3}$, (c) $\beta_2 = 10^{-2}$, and (d) $\beta_2 = 10^{-1}$, with $p = 2\%$ noise. The relative error between them is also included.

6.5.3 Example 3 (for inverse problem II)

We consider now the inverse problem II given by equations (6.2)–(6.5) and (6.8) with the following input data:

$$\phi(x) = u(x,0) = x+1, \quad \mu_1(t) = u(0,t) = \frac{1}{1+t}, \quad \mu_2(t) = u(1,t) = \frac{2}{1+t},$$
$$\mu_3(t) = -a(t)u_x(0,t) = -1, \quad \psi(x) = \int_0^1 a(t)u(x,t)dt = x+1,$$
$$f(x,t) = (x+1)(2-x) - \frac{x+1}{(1+t)^2}.$$

One can observe that the conditions of Theorems 6.3 and 6.4 are satisfied, hence the problem is uniquely solvable. The analytical solution is given by

$$a(t) = 1+t, \quad c(x) = 2-x, \quad u(x,t) = \frac{x+1}{1+t}. \tag{6.34}$$

The initial guess was $\underline{a}^0 = \underline{1}$ and $\underline{c}^0 = \underline{2}$.

The above example was mentioned in [70, p.176]. We start the investigation of finding the unknown coefficients $a(t)$, $c(x)$ and the temperature $u(x,t)$ without noise in input data (6.4) and (6.5). Figure 6.13 shows the objective function (6.23), as a function of the number of iterations. From this figure it can be seen that a monotonic decreasing convergence is achieved in 193 iterations to reach a very low prescribed tolerance of $O(10^{-21})$.

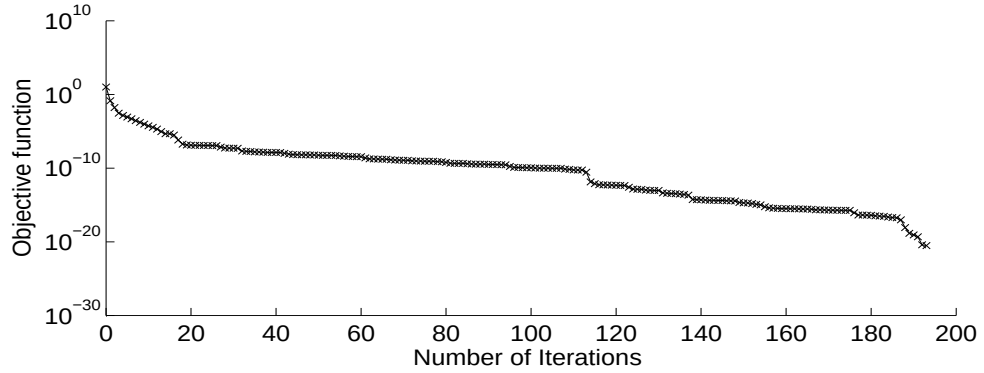

Figure 6.13: Objective function (6.23), for Example 3 with no noise and no regularization.

Figure 6.14 shows the numerical results for the associated time-dependent coefficient $a(t)$ and space-dependent coefficient $c(x)$ with no noise and no regularization. From this figure one can easily notice that there is an excellent agreement between the numerical and the exact solutions with $rmse(a) = 3.3E-4$ and $rmse(c) = 1.1E-4$.

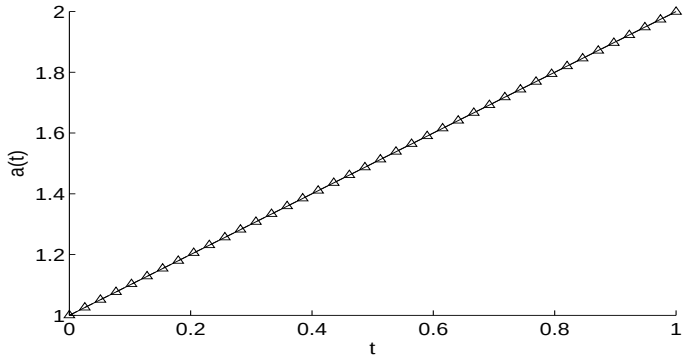

(a)

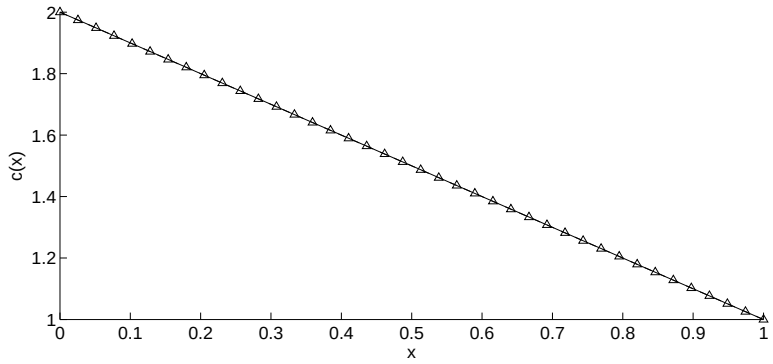

(b)

Figure 6.14: The exact (—) and numerical ($\triangle\triangle\triangle$) coefficients (a) $a(t)$, and (b) $c(x)$ for Example 3 with no noise and no regularization, obtained with $M = N = 40$.

Next, we investigate the stability of the solution with respect to noise. We include $p = 2\%$ additive Gaussian noise generated by equation (6.28). The input noisy data is therefore simulated numerically, via equation (6.24) for $\mu_3(t)$ and (6.26) for $\psi(x)$. Figure 6.15 shows the objective function (6.23), as a function of the number of iterations for various values of the regularization parameters. From this figure it can be seen that a monotonic decreasing convergence is achieved. Figure 6.16 shows the reconstructions of the coefficients $a(t)$ and $c(x)$. From this figure it can be seen that a very good estimation for $a(t)$ is obtained and less accurate for $c(x)$. Furthermore, one can be noticed that the coefficient $a(t)$ does not need to be regularized, i.e. we can take $\beta_1 = 0$ in (6.23). The $rmse$ (6.29) and (6.31), as well as other details, are included in Table 6.5.

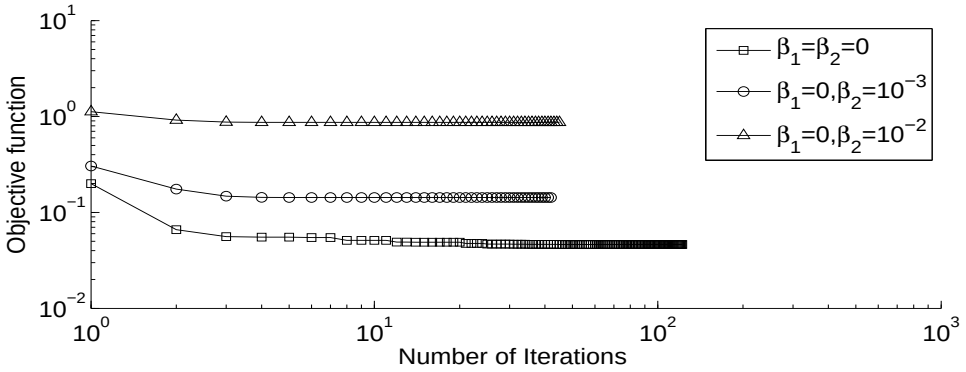

Figure 6.15: Objective function (6.23), for Example 3 with $p = 2\%$ noise and regularization.

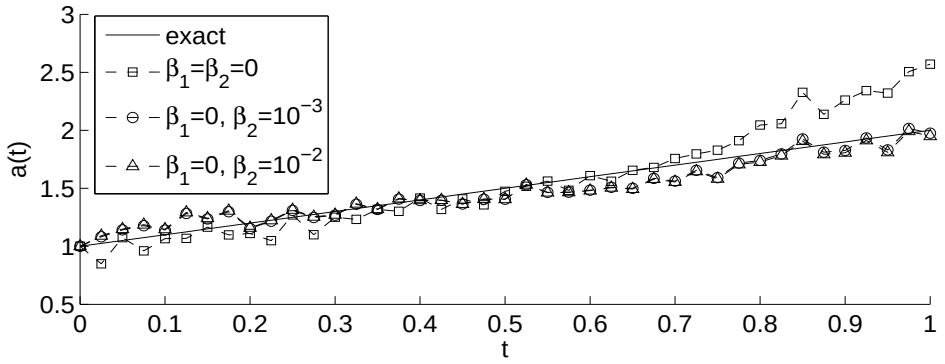

(a)

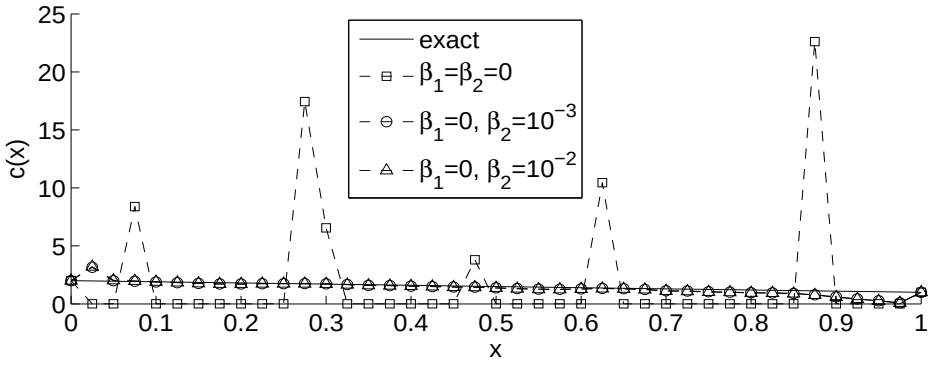

(b)

Figure 6.16: The coefficients (a) $a(t)$, and (b) $c(x)$ for Example 3 with $p = 2\%$ noise and regularization.

Figure 6.17 shows the exact and numerical solutions for the temperature $u(x,t)$ and the relative error between them. From this figure it can be seen that the numerical solution is stable and furthermore, its accuracy is consistent with the amount of noise included into the input data (6.4) and (6.5).

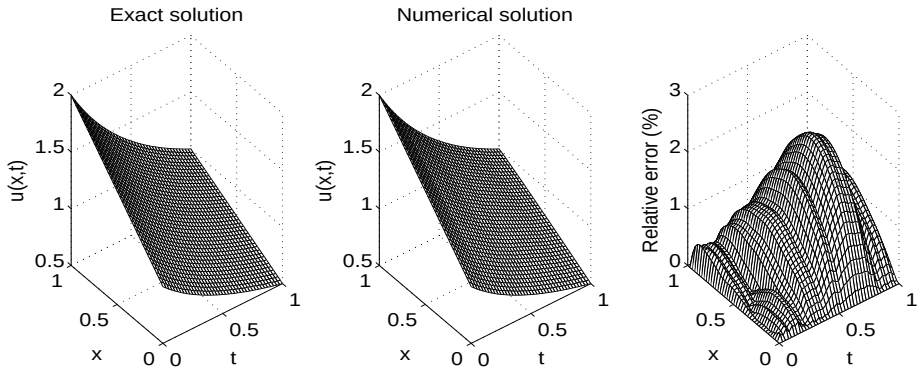

(a)

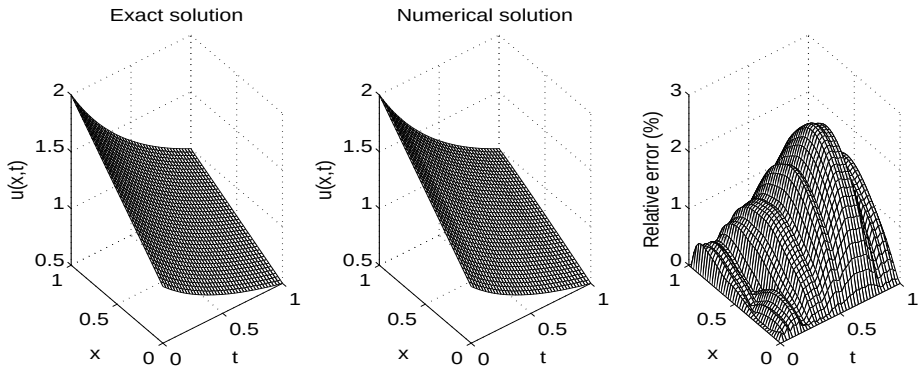

(b)

Figure 6.17: The exact and numerical temperature $u(x,t)$, for Example 3, with $\beta_1 = 0$ and (a) $\beta_2 = 10^{-3}$, and (b) $\beta_2 = 10^{-2}$, with $p = 2\%$ noise. The relative error between them is also included.

Table 6.5: Number of iterations, number of function evaluations, value of regularized objective function (6.23) at final iteration and the *rmse* values (6.29) and (6.31), for Example 3 with $p = 2\%$ noise.

$\beta_1 = 0$	$\beta_2 = 0$	$\beta_2 = 10^{-3}$	$\beta_2 = 10^{-2}$
No. of iterations	123	43	45
No. of function evaluations	10086	3526	3818
Minimum value of (6.23)	0.0463	0.1432	0.8684
$rmse(a)$	0.1705	0.0747	0.1761
$rmse(c)$	4.3624	0.3040	0.4554

6.5.4 Example 4 (for inverse problem II)

We now consider another test example for the inverse problem II given by equations (6.2)–(6.5) and (6.8), where the unknown coefficients $a(t)$ and $c(x)$ are not

linear, with the following input data:

$$\phi(x) = u(x,0) = e^x, \quad \mu_1(t) = u(0,t) = e^t, \quad \mu_2(t) = u(1,t) = e^{1+t},$$
$$\mu_3(t) = -a(t)u_x(0,t) = -(1+t^2)e^t, \quad \psi(x) = \int_0^1 a(t)u(x,t)dt = 2e^{1+x} - 3e^x,$$
$$f(x,t) = e^{x+t}(1-(1+t^2)(1-x^2)).$$

The condition of Theorem 6.4 are satisfied, hence the inverse problem has a unique solution. The analytical solution is given by

$$a(t) = 1 + t^2, \quad c(x) = x^2, \quad u(x,t) = e^{x+t}. \tag{6.35}$$

The initial guess was $\underline{a}^0 = \underline{1}$ and $\underline{c}^0 = \underline{0}$.

First we study the case of exact input data (6.4) and (6.5). The objective function (6.23) is plotted in Figure 6.18, as a function of the number of iterations. From this figure it can be seen that a nonsmooth decreasing convergence is obtained which levels to a stationary level of $O(10^{-9})$ in 302 iterations. The numerical results for the corresponding coefficients $a(t)$ and $c(x)$ are presented in Figure 6.19, and one can observe that the identified coefficients are in very good agreement with the exact ones in the absence of noise.

Next, we investigate the case of $p = 2\%$ noisy input data (6.4) and (6.5). The residual function (6.23) is plotted, as a function of number of iterations, in Figure 6.20 and a decreasing convergence can be observed. The corresponding coefficients are displayed in Figure 6.21 and good approximations are obtained for $a(t)$, but for $c(x)$ the numerical solution overshoots at various points and is unstable because no regularization has been employed yet.

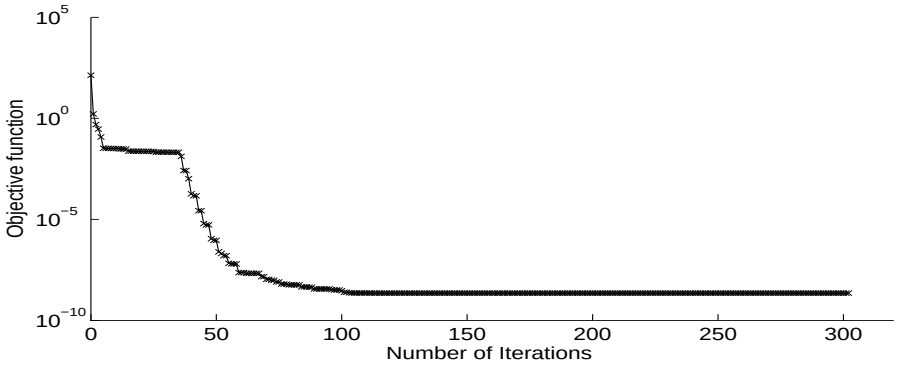

Figure 6.18: Objective function (6.23), for Example 4 with no noise and no regularization.

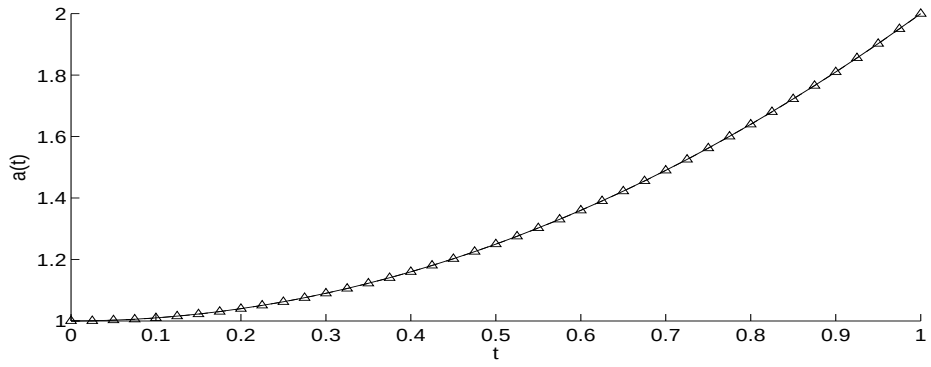

(a)

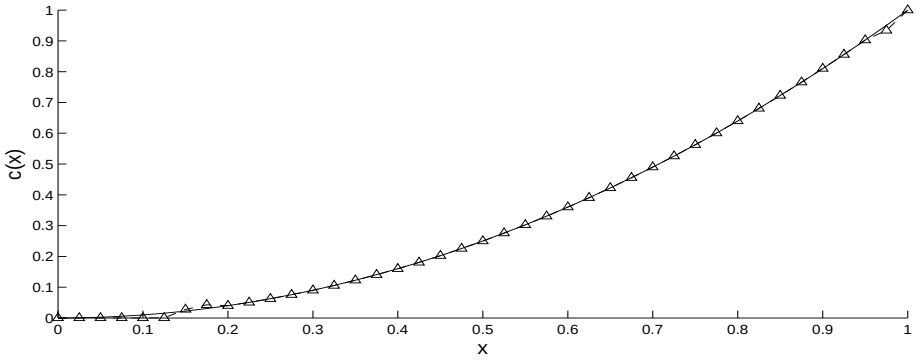

(b)

Figure 6.19: The exact (—) and numerical ($\triangle\triangle\triangle$) coefficients (a) $a(t)$, and (b) $c(x)$ for Example 4 with no noise and no regularization.

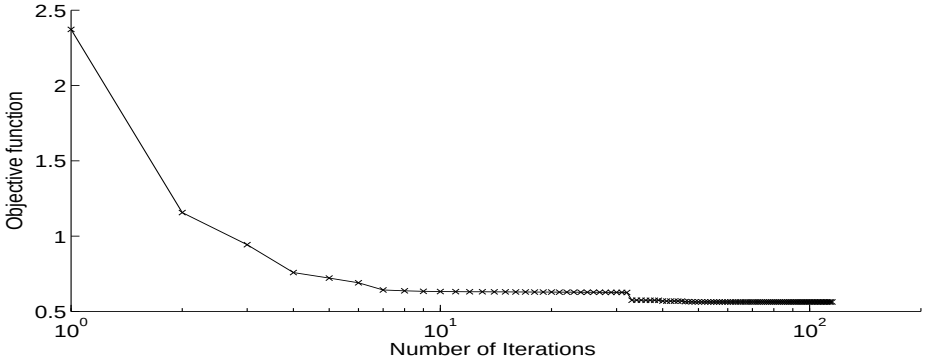

Figure 6.20: Objective function (6.23), for Example 4 with $p = 2\%$ noise and no regularization.

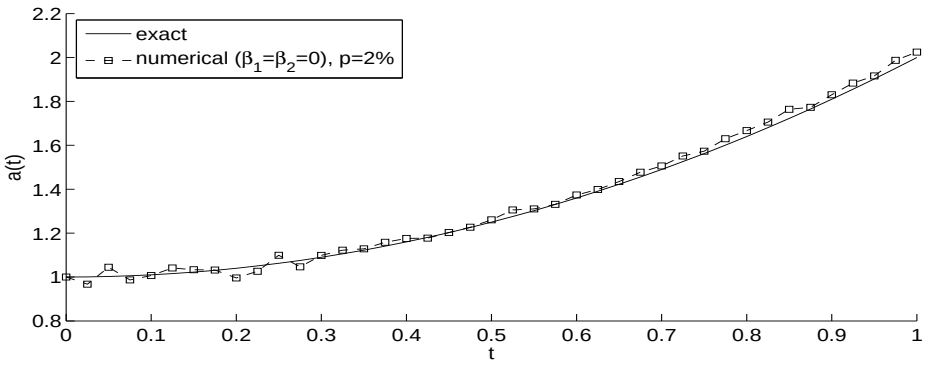

(a)

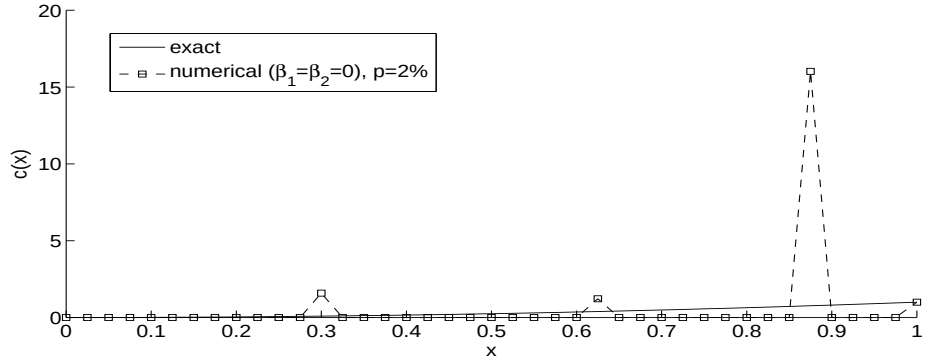

(b)

Figure 6.21: The coefficients (a) $a(t)$, and (b) $c(x)$ for Example 4 with $p = 2\%$ noise and no regularization.

As shown in Figure 6.21 the coefficient $a(t)$ seems rather stable. Therefore, we fix the value of β_1 to be zero and apply the regularization to the last term of objective function (6.23) for various values of the regularization parameter $\beta_2 \in \{10^{-3}, 10^{-2}, 10^{-1}\}$. Figure 6.22 shows the decreasing convergence of the objective function (6.23), as a function of the number of iterations. Figure 6.23 shows the retrieved coefficients for various values of β_2, and one can observe that the most accurate solution is obtained for $\beta_2 = 10^{-2}$, see also Table 6.6. In addition, as expected, the numerical solution for the temperature $u(x,t)$ is accurate, and stable, as illustrated in Figure 6.24.

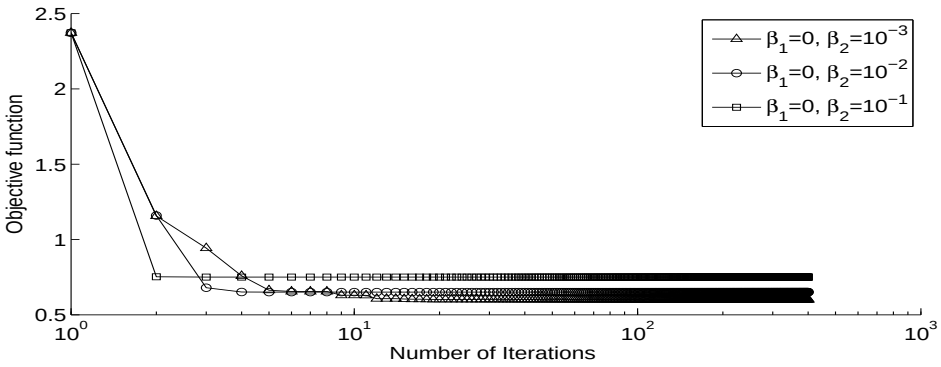

Figure 6.22: Objective function (6.23), for Example 4 with $p = 2\%$ noise and regularization.

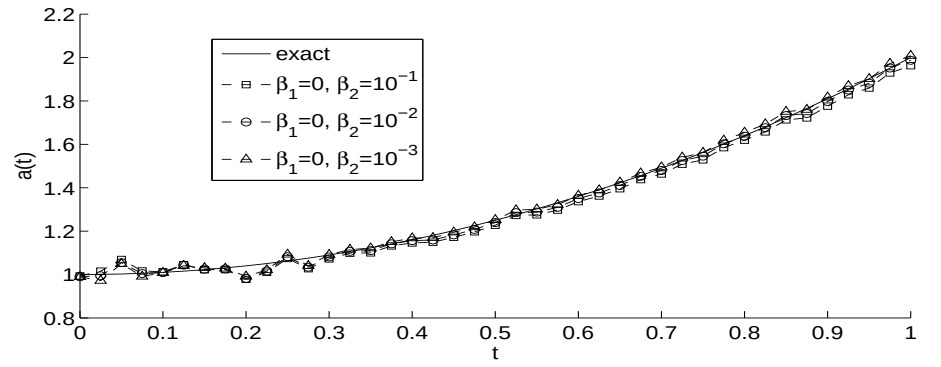

(a)

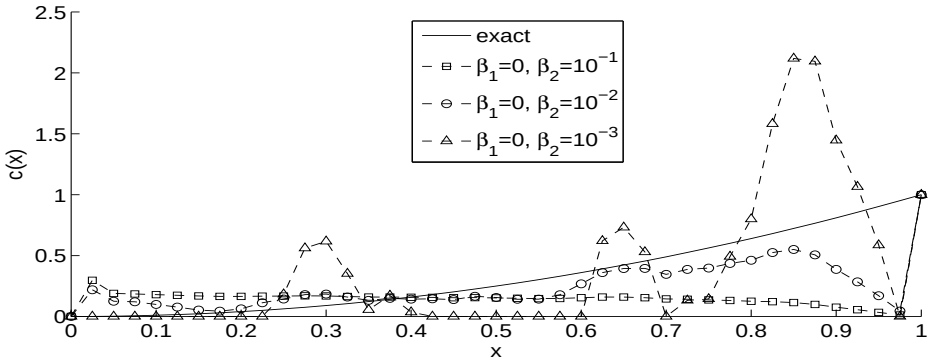

(b)

Figure 6.23: The coefficients (a) $a(t)$, and (b) $c(x)$ for Example 4 with $p = 2\%$ noise and regularization.

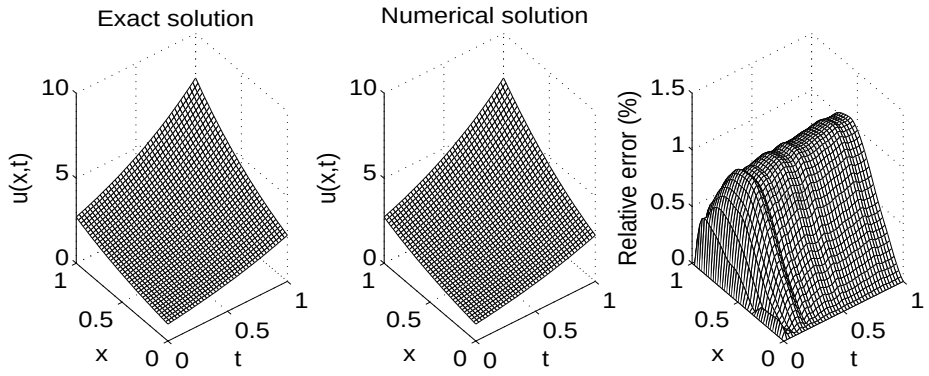

Figure 6.24: The exact and numerical temperatures $u(x,t)$, for Example 4, for $\beta_1 = 0$ and $\beta_2 = 10^{-2}$, with $p = 2\%$ noise. The relative error between them is also included.

Table 6.6: Number of iterations, number of function evaluations, value of regularized objective function (6.23) at final iteration and the *rmse* values (6.29) and (6.31), for Example 4 with $p = 2\%$ noise.

$\beta_1 = 0$	$\beta_2 = 10^{-3}$	$\beta_2 = 10^{-2}$	$\beta_2 = 10^{-1}$
No. of iterations	401	401	401
No. of function evaluations	33366	33366	33366
Minimum value of (6.23)	0.6023	0.6503	0.7501
$rmse(a)$	0.0181	0.0210	0.0313
$rmse(c)$	0.4498	0.2653	0.3848

6.6 Conclusions

This chapter has presented a numerical approach to identify simultaneously the time and space-dependent coefficients together with the temperature in a parabolic heat equation. The additional conditions which ensure a unique solution are given by the heat flux measurement (6.4) and the total potential heat function specification (6.5) or, the time-average heat flux (6.6). The direct solver based on a Crank-Nicolson finite difference scheme was employed. The resulting inverse problems have been reformulated as constrained regularized minimization problems which were solved using the MATLAB optimization toolbox routine *lsqnonlin*. The inverse problems have been found rather stable in the time-dependent thermal conductivity coefficient $a(t)$, but less stable in the space-dependent coefficient $b(x)$ or $c(x)$. Numerical results obtained for a wide range of typical test examples showed that accurate and stable numerical solutions have been achieved. Possible future work may consist of extending the analysis to the reconstruction of higher dimensional space-dependent coefficients.

Chapter 7

Free boundary determination in nonlinear diffusion

7.1 Introduction

In this chapter, we consider a novel inverse problem of determining a free boundary from the mass/energy specification in a one-dimensional nonlinear diffusion. In [13, 14], the authors investigated the problem of determining unknown coefficients for a nonlinear heat conduction problem together with temperature. While the problem of nonlinear diffusion with a free boundary was considered in [7], where the Stefan solidification problem was modelled as such. In addition, in [122] the authors developed a procedure to find an approximate stable solution to an unknown coefficient from over specification data based on the FDM combined with Tikhonov's regularization approach. In this work, we consider the problem of identifying the free boundary in a nonlinear diffusion problem.

This chapter is organized as follows. In the next section, we give the formulation of the inverse problem under investigation. The numerical methods for solving the direct and inverse problems are described in Sections 7.3 and 7.4, respectively. Furthermore, the numerical results and discussion are given in Section 7.5 and finally, conclusions are presented in Section 7.6.

7.2 Mathematical formulation

In this section we consider the nonlinear one-dimensional diffusion equation given by

$$u_t(x,t) = (a(u)u_x(x,t))_x + f(x,t), \quad (x,t) \in \Omega, \tag{7.1}$$

where the domain $\Omega = \{(x,t) : 0 < x < h(t), 0 < t < T < \infty\}$ with unknown free smooth boundary $x = h(t) > 0$. The initial condition is

$$u(x,0) = \phi(x), \quad 0 \le x \le h(0) =: h_0, \tag{7.2}$$

where $h_0 > 0$ is given, and the Dirichlet boundary conditions are

$$u(0,t) = \mu_1(t), \quad u(h(t),t) = \mu_2(t), \quad 0 \le t \le T, \tag{7.3}$$

In order to determine the unknown boundary $h(t)$ for $t \in (0,T]$ we impose the over-determination condition of integral type

$$\int_0^{h(t)} u(x,t)dx = \mu_3(t), \quad 0 \le t \le T, \tag{7.4}$$

which represents the specification of mass/energy of the diffusion system, [16]. In the above, the functions $a > 0$, ϕ, μ_i, $i \in \{1,2,3\}$ and f are given. In (7.1), u represents the concentration/ temperature, f represent a source/sink, and a represents the diffusivity.

The pair of functions $(h(t), u(x,t)) \in C^1[0,T] \times C^{2,1}(\overline{\Omega})$ with $h > 0$ is said to be a solution of problem if fulfills the equations (7.1)–(7.4).

The mathematical model (7.1)–(7.4) has been considered in [68] where the following existence and uniqueness of solution theorems are proved.

Theorem 7.1. (Existence)
Assume that the following assumptions are fulfilled:

1. $\phi \in C^2[0,h_0]$, $\mu_i \in C^1[0,T]$, $i \in \{1,2,3\}$, $f \in C^{1,0}([0,H_1] \times [0,T])$, $a \in C^1[M_0,M_1]$;

2. $\phi(x) > 0$ *for* $x \in [0,h_0]$, $\mu_i > 0$ *for* $t \in [0,T]$, $i \in \{1,2,3\}$, $f(x,t) \ge 0$ *for* $(x,t) \in [0,H_1] \times [0,T]$, $a(s) \ge a_0 > 0$ *for* $s \in [M_0,M_1]$, *where* a_0 *is some given constant;*

3. $\mu_1(0) = \phi(0), \quad \mu_2(0) = \phi(h_0), \quad \int_0^{h_0} \phi(x)dx = \mu_3(0),$
$\mu_1'(0) = a(\mu_1(0))\phi''(0) + a'(\mu_1(0))\phi'^2(0) + f(0,0),$
$\mu_2'(0) = a(\mu_2(0))\phi''(h_0) + a'(\mu_2(0))\phi'^2(h_0) + \phi'(h_0)h'(0) + f(h_0,0).$

Then the inverse problem (7.1)–(7.4) is locally solvable (in time).

Theorem 7.2. (Uniqueness)
Suppose that condition 2. of Theorem 7.1 and the following condition

$$a(s) \in C^1[M_0,M_1], \quad f(x,t) \in C^{1,0}([0,H_1] \times [0,T])$$

hold. Then a solution of the inverse problem (7.1)–(7.4) is unique.

In the above theorems, the constants H_1, M_0 and M_1 have the following meaning using the maximum principle [38] for the heat equation (7.1):

$$H_1 = \frac{1}{M_0}\max_{[0,T]}\mu_3(t), \quad M_0 = \min\{\min_{[0,h_0]}\phi(x), \ \min_{[0,T]}\mu_1(t), \ \min_{[0,T]}\mu_2(t)\},$$
$$M_1 = \max\{\max_{[0,h_0]}\phi(x), \ \max_{[0,T]}\mu_1(t), \ \max_{[0,T]}\mu_2(t), \ \max_{[0,H_1]\times[0,T]}f(x,t)\}.$$

We can also derive a formula for $h'(0)$ by differentiating equation (7.4) with time, and using equations (7.1)–(7.3) to obtain

$$h'(0) = \frac{\mu_3'(0) - a(\mu_2(0))\phi'(h_0) + a(\mu_1(0))\phi'(0) - \int_0^{h_0} f(x,0)dx}{\mu_2(0)}. \tag{7.5}$$

We perform the change of variable $y = x/h(t)$ to reduce the problem (7.1)–(7.4) to the following equivalent inverse problem in a rectangular domain for the unknowns $h(t)$ and $v(y,t) := u(yh(t),t)$, [68]:

$$v_t(y,t) = \frac{1}{h^2(t)}\left(a(v)v_y(y,t)\right)_y + \frac{yh'(t)}{h(t)}v_y(y,t) + f(yh(t),t), \ (y,t)\in Q \tag{7.6}$$

where $Q = \{(y,t) : 0 < y < 1, 0 < t < T\}$. The initial condition is

$$v(y,0) = \phi(h_0 y), \quad 0 \le y \le 1, \tag{7.7}$$

and the boundary and over-determination conditions are

$$v(0,t) = \mu_1(t), \quad v(1,t) = \mu_2(t), \quad 0 \le t \le T, \tag{7.8}$$
$$h(t)\int_0^1 v(y,t)dy = \mu_3(t), \quad 0 \le t \le T. \tag{7.9}$$

At the end of this section we state the theorem of continuous dependence of the free boundary $h(t)$ on the input energy data (7.4) which was proved in [57].

Theorem 7.3. (Stability)
Suppose that the conditions of Theorem 7.1 are satisfied. Let μ_3 and $\tilde{\mu}_3$ be two data (7.4) and let ($h(t)$,$u(x,t)$) and ($\tilde{h}(t)$,$\tilde{u}(x,t)$) be the corresponding solutions of the inverse problem (7.1)–(7.4). Then there is a positive constant C such that the following stability estimate holds:

$$\|h - \tilde{h}\|_{C^1[0,T]} + \|v - \tilde{v}\|_{C^{1,0}(\overline{\Omega})} \le C\|\mu_3 - \tilde{\mu_3}\|_{C^1[0,T]}, \tag{7.10}$$

where

$$v(y,t) = u(yh(t),t), \quad \tilde{v}(y,t) = \tilde{u}(y\tilde{h}(t),t), \quad (y,t) \in Q. \tag{7.11}$$

7.3 Solution of direct problem

In this section, we consider the direct initial-boundary value problem (7.6)–(7.8), where $h(t)$, $f(x,t)$, $a(u)$ and $\mu_i(t)$, $i \in \{1,2\}$ are known and the solution $u(x,t)$ is to be determined together with $\mu_3(t)$ defined by equation (7.4). To do so, we use the three-time levels finite difference scheme suggested by Lees [88].

The discrete form of our problem is as follows. We uniformly divide the fixed domain $Q = (0,1) \times (0,T)$ into M and N subintervals of equal step length Δy and Δt, where $\Delta y = 1/M$ and $\Delta t = T/N$, respectively. So, the solution at the node (i,j) is $v_{i,j} := v(y_i,t_j)$, where $y_i = i\Delta y$, $t_j = j\Delta t$, $h(t_j) = h_j$, $\phi(x_i) = \phi_i$, and $f(y_i,t_j) = f_{i,j}$ for $i = \overline{0,M}$, $j = \overline{0,N}$.

We develop the procedure described in [88] in order to solve the direct problem for the nonlinear parabolic equation (7.6), subject to the initial condition (7.7) and the Dirichlet boundary conditions (7.8). We need to define the standard difference operators D_+, D_-, and D_0, as follows:

$$D_+v(x_i,t_j) = \frac{v(x_{i+1},t_j) - v(x_i,t_j)}{\Delta y}, \quad D_-v(x_i,t_j) = \frac{v(x_i,t_j) - v(x_{i-1},t_j)}{\Delta y},$$
$$D_0v(x_i,t_j) = \frac{v(x_{i+1},t_j) - v(x_{i-1},t_j)}{2\Delta y}.$$

Finally, for any suitably defined function $k(x,t)$, we put

$$\bar{a}(k(x_i,t)) = a\left(\frac{k(x_i,t) + k(x_{i-1},t)}{2}\right).$$

For each $j = \overline{0,N}$ we put $v_{0,j} = \mu_1(j\Delta t)$ and $v_{M,j} = \mu_2(j\Delta t)$. Then the three time level scheme is given by

$$v_{i,0} = \phi_i, \quad i = \overline{0,M}, \tag{7.12}$$

where we have that $\phi_0 = \mu_1(0)$ and $\phi_M = \mu_2(0)$,

$$v_{i,1} = v_{i,0} + \frac{\Delta t}{h_0^2} D_+\left(\bar{a}(\phi_i)D_-\phi\right) + \frac{(\Delta t)y_ih_0'}{h_0}D_-\phi + (\Delta t)f_{i,0},\ i = \overline{1,M-1}, \tag{7.13}$$

where $h'_0 = h'(0)$ is given by (7.5),

$$v_{i,j+1} = v_{i,j-1} + \frac{2\Delta t}{h_j^2} D_+ \left(\bar{a}(v_{i,j}) D_- \hat{v}_{i,j}\right) + \frac{2(\Delta t) y_i h'_j}{h_j} D_- \hat{v}_{i,j} + 2(\Delta t) f_{i,j}, \quad i = \overline{1, M-1}, \quad j = \overline{1, N-1}, \tag{7.14}$$

where $h'_j = h'(t_j)$, and

$$\hat{v}_{i,j} = \frac{v_{i,j+1} + v_{i,j} + v_{i,j-1}}{3}. \tag{7.15}$$

It is clear that the three-level difference scheme determines $v_{i,j+1}$ uniquely as the solution of a linear, well-conditioned, tridiagonal system of equations which can be solved using traditional linear algebra methods to advance the solution to the next time step. The equations (7.12) and (7.13) provide the necessary starting values for (7.14). In [88], the author proved that the above scheme is stable, second-order accurate and convergent for sufficiently small values of Δy and Δt. Although, equation (7.1) or (7.6) is nonlinear, the linearity is achieved in $v_{i,j+1}$ by evaluating all coefficients at a time level of known solution values in previous steps. The stability is preserved by averaging $v_{i,j}$ over three time levels as (7.15) and the accuracy is maintained by using central-difference approximations, [110].

Equation (7.14) can be put in a simpler form as

$$v_{i,j+1} = \hat{v}_{i,j-1} + A_{i,j}\hat{v}_{i-1,j} - B_{i,j}\hat{v}_{i,j} + C_{i,j}\hat{v}_{i+1,j} + 2(\Delta t) f_{i,j}, \tag{7.16}$$

where,

$$A_{i,j} = \frac{2(\Delta t) a2_{i,j}}{h_j^2 (\Delta y)^2} - \frac{(\Delta t) y_i h'_j}{h_j \Delta y}, \quad B_{i,j} = \frac{2(\Delta t) a3_{i,j}}{h_j^2 \Delta y}, \quad C_{i,j} = \frac{2(\Delta t) a1_{i,j}}{h_j^2 (\Delta y)^2} + \frac{(\Delta t) y_i h'_j}{h_j \Delta y},$$
$$a1_{i,j} = \bar{a}(v(x_{i+1}, t_j)), \quad a2_{i,j} = \bar{a}(v(x_i, t_j)), \quad a3_{i,j} = a1_{i,j} + a2_{i,j}.$$

As mentioned before, to ensure the stability we average the solution over three levels as

$$\hat{v}_{i-1,j} = \frac{1}{3}\left(v_{i-1,j+1} + v_{i-1,j} + v_{i-1,j-1}\right),$$
$$\hat{v}_{i,j} = \frac{1}{3}\left(v_{i,j+1} + v_{i,j} + v_{i,j-1}\right),$$
$$\hat{v}_{i+1,j} = \frac{1}{3}\left(v_{i+1,j+1} + v_{i+1,j} + v_{i+1,j-1}\right).$$

Then the final version of (7.16) becomes

$$\begin{aligned}
&- A^*_{i,j}v_{i-1,j+1} + (1 + B^*_{i,j})v_{i,j+1} - C^*_{i,j}v_{i+1,j+1} = A^*_{i,j}v_{i-1,j} - B^*_{i,j}v_{i,j} + C^*_{i,j}v_{i+1,j} \\
&+ A^*_{i,j}v_{i-1,j-1} + (1 - B^*_{i,j})v_{i,j-1} + C^*_{i,j}v_{i+1,j-1} + 2(\Delta t)f_{i,j}, \\
&\qquad\qquad j = \overline{1, N}, \quad i = \overline{2, (M-1)},
\end{aligned} \tag{7.17}$$

where $A^* = \frac{A}{3}$, $B^* = \frac{B}{3}$ and $C^* = \frac{C}{3}$. At each time step t_j for $j = \overline{1, (N-1)}$, using the Dirichlet boundary conditions (7.8), the above difference equation can be reformulated as a $(M-2) \times (M-2)$ system of linear equations of the form,

$$L\mathbf{v} = \mathbf{b}, \tag{7.18}$$

where

$$\mathbf{v} = (v_{2,j+1}, v_{3,j+1}, ..., v_{M-1,j+1})^{\mathrm{T}}, \quad \mathbf{b} = (b_2, b_3, ..., b_{M-1})^{\mathrm{T}}.$$

and

$$L = \begin{pmatrix}
1 + B^*_{1,j} & -C^*_{1,j} & 0 & \cdots & 0 & 0 & 0 \\
-A^*_{2,j} & 1 + B^*_{2,j} & -C^*_{2,j} & \cdots & 0 & 0 & 0 \\
\vdots & \vdots & \vdots & \ddots & \vdots & \vdots & \vdots \\
0 & 0 & 0 & \cdots & -A^*_{M-2,j} & 1 + B^*_{M-2,j} & -C^*_{M-2,j} \\
0 & 0 & 0 & \cdots & 0 & -A^*_{M-1,j} & 1 + B^*_{M-1,j}
\end{pmatrix},$$

$$\begin{aligned}
b_2 &= A^*_{1,j}v_{0,j} - B^*_{1,j}v_{1,j} + C^*_{1,j}v_{2,j} + A^*_{1,j}v_{0,j-1} + (1 - B^*_{1,j})v_{1,j-1} + C^*_{1,j}v_{2,j-1} \\
&+ 2(\Delta t)f_{1,j} + A^*_{1,j}v_{0,j+1}, \\
b_i &= A^*_{i-1,j}v_{i,j} - B^*_{i,j}v_{i,j} + C^*_{i,j}v_{i+1,j} + A^*_{i,j}v_{i-1,j-1} + (1 - B^*_{i,j})v_{i,j-1} \\
&+ C^*_{i,j}v_{i+1,j-1} + 2(\Delta t)f_{i,j}, \quad i = \overline{3, (M-2)}, \\
b_{M-1} &= A^*_{M-1,j}v_{M-2,j} - B^*_{M-1,j}v_{M-1,j} + C^*_{M-1,j}v_{M,j} + A^*_{M-1,j}v_{M-2,j-1} \\
&+ (1 - B^*_{M-1,j})v_{M-1,j-1} + C^*_{M-1,j}v_{M+1,j-1} + 2(\Delta t)f_{M-1,j} + C^*_{M-1,j}v_{M,j+1}.
\end{aligned}$$

7.3.1 Example

As an example, consider the problem (7.6)–(7.8) with $T = 1$ and

$$a(v) = e^{-v}, \quad h(t) = 1 + t, \quad h_0 = h(0) = 1, \quad \phi(h_0 y) = 1 + (1 + y)^2,$$
$$\mu_1(t) = 1 + e^t, \quad \mu_2(t) = (2 + t)^2 + e^t,$$
$$f(h(t)y, t) = e^t + e^{-(1+y+yt)^2 - e^t}(4(1 + y + yt)^2 - 2).$$

The exact solution of the direct problem (7.6)–(7.8) is given by

$$v(y, t) = (1 + y + yt)^2 + e^t$$

and the desired output (7.4) is

$$\mu_3(t) = \frac{(2 + t)^3 - 1}{3} + (1 + t)e^t.$$

The numerical and the exact solution for the interior solution are shown in Figure 7.1 and one can notice that a very good agreement is obtained because the direct problem is well-posed. Figure 7.2 shows the numerical solution in comparison with exact one for μ_3. The trapezoidal rule is employed to compute the integral in (7.4) based on the formula

$$\int_0^1 v(y, t_j)dy = \frac{1}{2M}\left(\mu_1(t_j) + \mu_2(t_j) + 2\sum_{i=1}^{M-1} v(y_i, t_j)\right), \quad j = \overline{0, N}. \tag{7.19}$$

From this figure it can be seen that the numerical solution is in excellent agreement with the exact one.

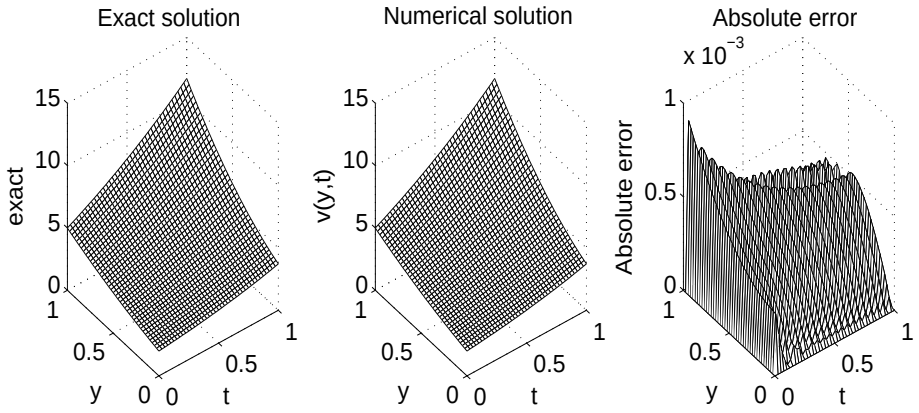

Figure 7.1: Exact and numerical solutions for $v(y, t)$ and the absolute error for the direct problem obtained with $M = N = 40$.

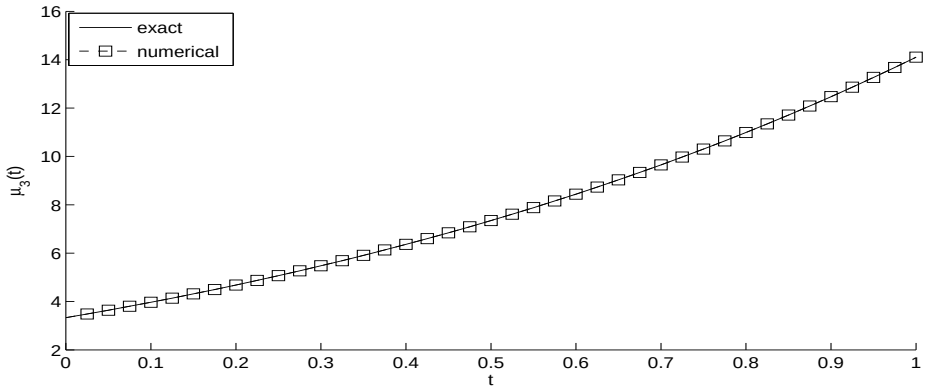

Figure 7.2: Exact and numerical integration for $\mu_3(t)$ for the direct problem obtained with $M = N = 40$.

7.4 Numerical approach to the inverse problem

In the inverse problem, we assume that the free boundary $h(t)$ is unknown. The nonlinear inverse problem (7.6)–(7.9) can be reformulated as a nonlinear least-squares minimization of

$$F(h) = \left\| h(t) \int_0^1 v(y,t)dy - \mu_3(t) \right\|^2_{L^2[0,T]}, \tag{7.20}$$

defined over the set of admissible functions

$$h \in \Lambda_{ad} := \{h \in C^1[0,T] \big| h(0) = h_0,\ h(t) > 0 \text{ for } t \in [0,T]\}. \tag{7.21}$$

The discretization of (7.20) is

$$F(\underline{h}) = \sum_{j=1}^{N} \left[h_j \int_0^1 v(y,t_j)dy - \mu_3(t_j) \right]^2, \tag{7.22}$$

where $\underline{h} = (h_j)_{j=\overline{1,N}}$. As it will be seen from the numerical results presented and discussed in the next section, it seems that there is no need to regularize the least-squares functional (7.20) by adding to it a Tikhonov penalty term of some norm of h, the problem being rather stable with respect to noise added in the input data $\mu_3(t)$.

The minimization of F subject to the physical constraints $\underline{h} > \underline{0}$ is accomplished using the MATLAB toolbox routine *lsqnonlin*.

We take bounds for the positive $h(t)$ say, we seek the components of the vector $\underline{h}$ in the interval $[10^{-10},10^3]$. We also take the parameters of the routine as follows:

- Number of variables $M = N = 40$.
- Maximum number of iterations = $10^2\times$ (number of variables).
- Maximum number of objective function evaluations = $10^3\times$(number of variables).
- Solution and objective function tolerances = 10^{-10}.

In addition, when we solve the inverse problem we approximate

$$h'(t_j) = \frac{h(t_j) - h(t_{j-1})}{\Delta t} = \frac{h_j - h_{j-1}}{\Delta t}, \quad j = \overline{1, N}, \tag{7.23}$$

and we express $h'_0 := h'(0)$ as in (7.5). If there is noise in the measured data (7.4), we replace $\mu_3(t_j)$ in (7.22) by $\mu_3^\epsilon(t_j)$ given by

$$\mu_3^\epsilon(t_j) = \mu_3(t_j) + \epsilon_j, \quad j = \overline{1, N}, \tag{7.24}$$

where ϵ_j are random variables generated from a Gaussian normal distribution with mean zero and standard deviation σ, given by

$$\sigma = p \times \max_{t\in[0,T]} |\mu_3(t)|, \tag{7.25}$$

where p represents the percentage of noise. We use the MATLAB function *normrnd* to generate the random variables $\underline{\epsilon} = (\epsilon_j)_{j=\overline{1,N}}$ as follows:

$$\underline{\epsilon} = normrnd(0, \sigma, N). \tag{7.26}$$

7.5 Numerical results and discussion

In this section, we will describe the numerical results for our nonlinear inverse problem for two different example according to the linear and nonlinear (rational) variation of free boundary. Moreover, we add noise to the measured input data (7.9) to mimic the reality situation by using (7.24) via (7.26). We also calculate the root mean square error ($rmse$) to analyse the error between the exact and numerically obtained coefficient, defined as,

$$rmse(h(t)) = \sqrt{\frac{1}{N}\sum_{j=1}^{N} \left(h_{numerical}(t_j) - h_{exact}(t_j)\right)^2}. \tag{7.27}$$

For simplicity, we take $T = 1$ and the initial guess $\underline{h}^{(0)} = \underline{1}$ for all examples.

7.5.1 Example 1

Consider the problem (7.1)–(7.4) with unknown coefficient $h(t)$, and solve this inverse problem with the following input data:

$$\begin{aligned}
&\phi(x) = (1+x)^2 + 1, \quad \mu_1(t) = 1 + e^t, \quad \mu_2(t) = (2+t)^2 + e^t, \\
&\mu_3(t) = \frac{(2+t)^3}{3} + (1+t)e^t - \frac{1}{3}, \quad a(u) = e^{-u}, \\
&f(x,t) = e^t + e^{-(1+x)^2 - e^t}(4x^2 + 8x + 2), \quad h_0 = 1,
\end{aligned}$$

One can remark that the conditions of Theorems 7.1 and 7.2 are satisfied hence, the existence and uniqueness of solution hold. With this data the analytical solution of inverse problem (7.1)–(7.4) is given by

$$h(t) = 1 + t, \quad u(x,t) = (1+x)^2 + e^t. \tag{7.28}$$

Then

$$h(t) = 1 + t, \quad v(y,t) = u(yh(t),t) = (1 + y + yt)^2 + e^t, \tag{7.29}$$

is the analytical solution of the problem (7.6)–(7.9).

We consider the case where there is no noise, i.e. $p = 0$, and when there is $p = 2\%$ noise in the input data (7.9).

The functional (7.22), as a function of the number of iterations, is represented in Figure 7.3. From this figure it can be seen that the convergence is very fast in five and seven iterations for $p = 0$ and $p = 2\%$, respectively. The objective function (7.22) decreases rapidly and takes a stationary value of $O(10^{-7})$ and 0.3411, for $p = 0$ and $p = 2\%$, respectively. The numerical results for the corresponding unknown free boundary $h(t)$ are presented in Figure 7.4. From this figure it can be seen that the retrieved free boundary $h(t)$ is in very good agreement with the exact one in the case where no noise in the input data. While, when the input data is contaminated by $p = 2\%$ noise then we can see that the retrieved solution is stable and within the same range of errors as the input data is.

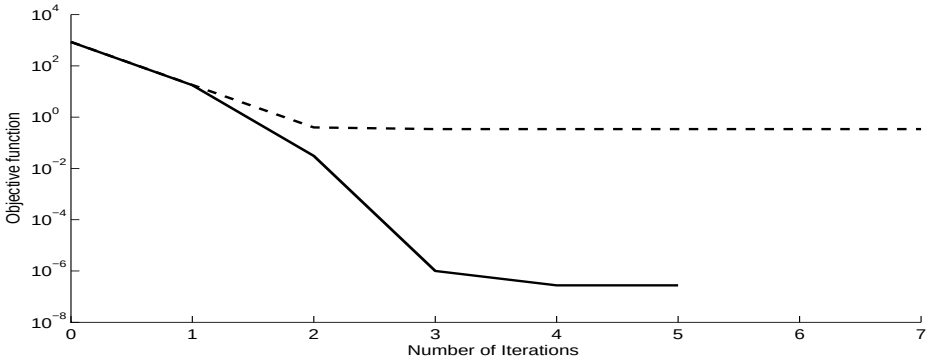

Figure 7.3: Objective function (7.22) without noise (—), and for $p = 2\%$ noise (- - -) for Example 1.

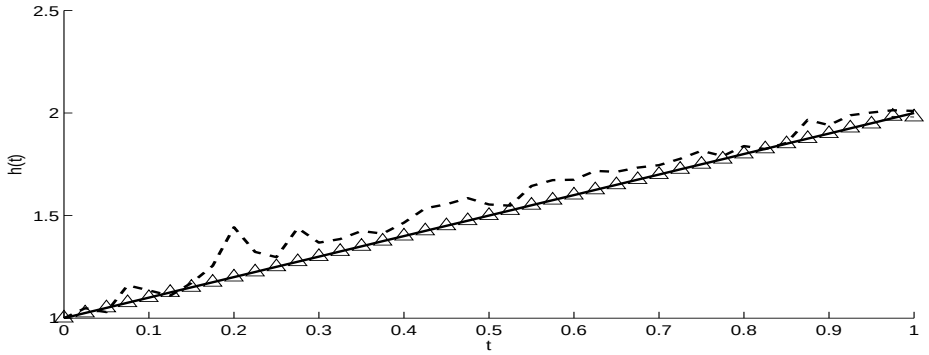

Figure 7.4: Free boundary $h(t)$, without noise (-△-), and for $p = 2\%$ noise (- - -) in comparison with the exact solution (—), for Example 1.

The restored temperatures $v(y,t)$ and $u(x,t)$ for $p = 2\%$ noise are shown in Figures 7.5 and 7.6, respectively. From these figures it can be seen that the solutions are stable by being free of high oscillations and unbounded behaviour.

Overall form the numerical results presented for this example it can be seen that the inverse problem seems to be well-posed and that the numerical solutions are accurate and stable with respect to noise in the input data for both the free boundary $h(t)$ and the temperature/concentration $v(y,t)$ or $u(x,t)$.

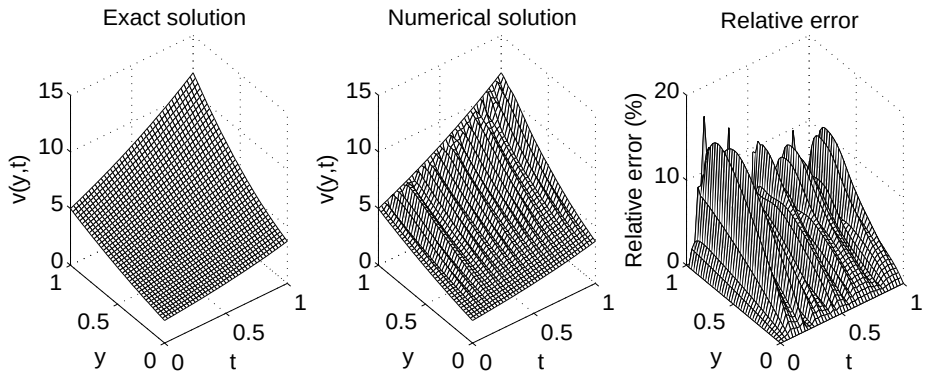

Figure 7.5: The analytical and numerical solutions, and the relative error for $v(y,t)$ for $p = 2\%$ noise for Example 1.

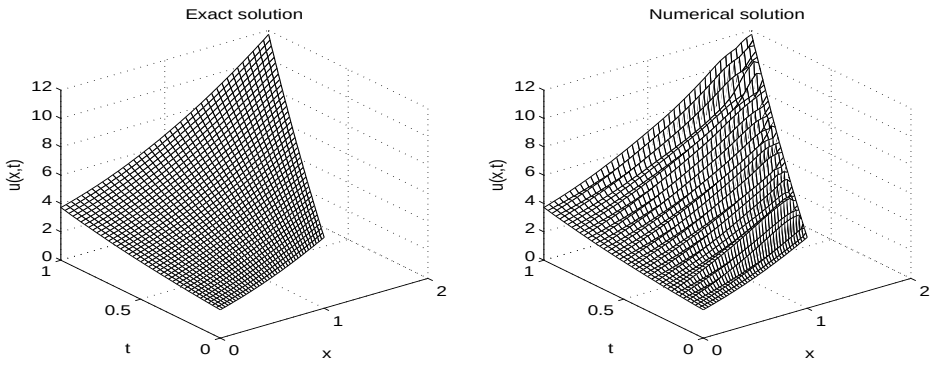

Figure 7.6: The analytical and numerical solutions for $u(x,t)$ for $p = 2\%$ noise for Example 1.

7.5.2 Example 2

In this example, we consider a more severe test case where the unknown function $h(t)$ is nonlinear with the following data

$$\phi(x) = (1+x)^2 + 1, \quad \mu_1(t) = 1 + e^t, \quad \mu_2(t) = \left(\frac{2+t}{1+t}\right)^2 + e^t,$$
$$\mu_3(t) = \frac{1}{3}\left(\frac{2+t}{1+t}\right)^3 + \frac{e^t}{1+t} - \frac{1}{3}, \quad a(u) = e^{-u},$$
$$f(x,t) = e^t + e^{-(1+x)^2 - e^t}\left(4x^2 + 8x + 2\right), \quad h_0 = 1.$$

One can notice that the conditions of Theorems 7.1 and 7.2 are satisfied hence, the existence and uniqueness of solution holds. With this data, the analytical solution of the inverse problem (7.1)–(7.4) is given by

$$h(t) = \frac{1}{1+t}, \quad u(x,t) = (1+x)^2 + e^t. \tag{7.30}$$

Then

$$h(t) = \frac{1}{1+t}, \quad v(y,t) = u(yh(t),t) = \left(1 + \frac{y}{1+t}\right)^2 + e^t, \tag{7.31}$$

is the analytical solution of the problem (7.6)–(7.9).

We study the case of exact and noisy input data (7.9). The objective function (7.22), as a function of the number of iterations is presented in Figure 7.7. From this figure it can be seen that the functional decreases very fast to stationary value at $O(10^{-7})$ and 0.0188 in about 7 and 12 iterations, for $p = 0$ and $p = 2\%$ noise, respectively.

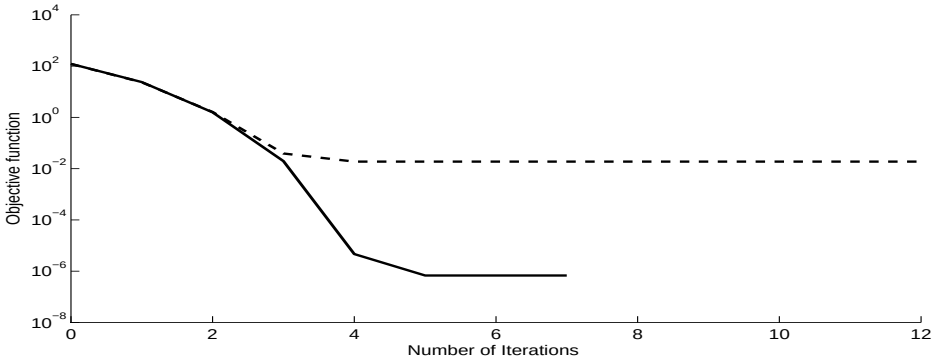

Figure 7.7: Objective function (7.22) without noise (—), and for $p = 2\%$ noise (- - -) for Example 2.

The numerical results for the corresponding free boundary $h(t)$ are presented in Figure 7.8. From this figure it can be seen that the identified free boundary is in very good agreement with the exact one in the absence of noise and this situation changes only a little when we perturb the input data by $p = 2\%$ noise.

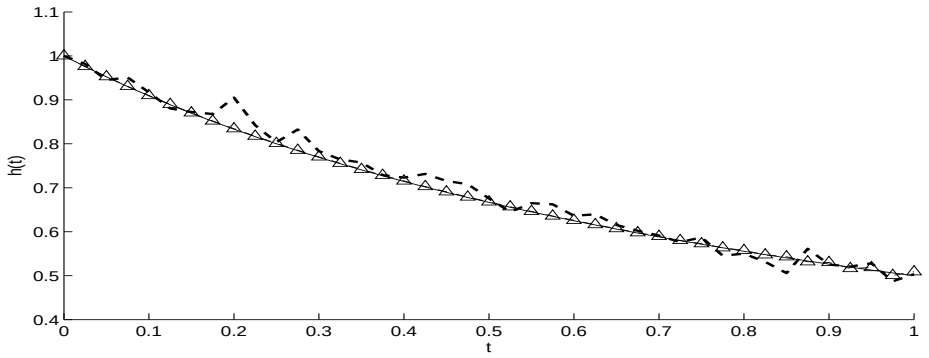

Figure 7.8: Free boundary $h(t)$, without noise (-△-), and with $p = 2\%$ noise (- - -) in comparison with the exact solution (—), for Example 2.

The numerical solutions for $v(y,t)$ and $u(x,t)$ are shown in Figure 7.9 and

7.10, respectively, in comparison with the exact solutions for $p = 2\%$ noise. As in Example 1, stable numerical solutions are obtained.

One can conclude that the inverse problem is well-posed since small errors in the measurement in (7.4) cause only small errors in the retrieved pair solution $(h(t),\, u(x,t))$. Consequently, we can say that the problem depends continuously on the input data.

Finally, for completeness, other details about the number of iterations, number of function evaluations, objective function value at final iteration and $rmse(h)$ for Examples 1 and 2 are given in Table 7.1. For this table it can be seen that accurate and stable numerical solutions are rapidly achieved by the iterative MATLAB toolbox routine *lsqnonlin*.

Table 7.1: Number of iterations, number of function evaluations, value of the objective function (7.22) at final iteration and $rmse$ values (7.27), for Examples 1 and 2.

		$p = 0$	$p = 2\%$
Example 1	No. of iterations	5	7
	No. of function evaluations	252	336
	Function value at final iteration	$2E-7$	0.3411
	$rmse(h)$	0.0035	0.0793
Example 2	No. of iterations	7	12
	No. of function evaluations	336	546
	Function value at final iteration	$6E-7$	0.0188
	$rmse(h)$	0.0023	0.0212

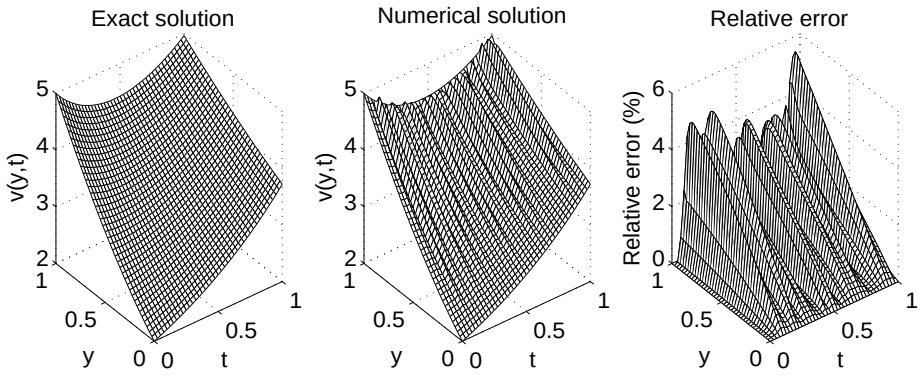

Figure 7.9: The analytical and numerical solutions and the relative error for $v(y,t)$ for $p = 2\%$ noise for Example 2.

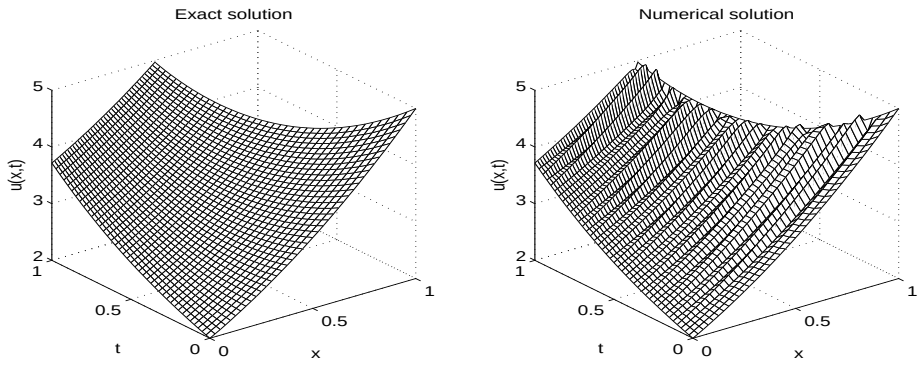

Figure 7.10: The analytical and numerical solutions for $u(x,t)$ for $p = 2\%$ noise for Example 2.

7.6 Conclusions

The inverse problem concerning the identification of free boundary $h(t)$ and the temperature $u(x,t)$ in the heat equation with nonlinear diffusivity $a(u)$ has been investigated. The additional condition which ensures a unique solution is given by the energy/mass specification $\mu_3(t)$ given by equation (7.4). As with other free surface problems, it turns out that the problem is well-posed if the data μ_3 is smooth. The direct solver based on a three-level finite difference scheme is developed. The inverse solver is based on a nonlinear least-squares minimization which is solved using the MATLAB toolbox routine *lsqnonlin*. As expected, for exact data, the numerical results obtained are very accurate. For noisy data μ_3^ϵ which consist of a random perturbation of the exact data μ_3, the results for $h(t)$, $v(y,t)$ and $u(x,t)$ are still stable and accurate. The instability is only manifested in the derivative $h'(t)$ for which the use of a regularization method would be warranted.

Chapter 8

Determination of the time-dependent thermal diffusivity and free boundary

8.1 Introduction

Many heat transfer applications can be modeled by the heat equation with a fixed boundary. However, there are numerous other problems for which the domain or the boundary varies with time and such problems are known as free boundary or Stefan problems [11]. For instance, when a conductor melts and the liquid is drained away as it appears, the heat conduction problem within the remaining solid involves the heat equation in a domain that is physically changing with time. In particular, the one-phase Stefan problem can be regarded as an inverse problem.

In [94], the author investigated the heat equation with an unknown heat source in a domain with a known moving boundary. In [48, 77], the authors investigated the numerical solution of inverse Stefan problems using the method of fundamental solutions. In [107], an inverse moving boundary problem is solved using the least-squares method. In this chapter, we consider the time-dependent nonlinear inverse one-dimensional and one-phase Stefan problem which consists in the simultaneous determination of the time-dependent thermal diffusivity and free boundary.

This chapter is organized as follows: In the next section, we give the formulation of the inverse problem under investigation. The numerical methods for solving the direct and inverse problems are described in Sections 8.3 and 8.4, respectively. Furthermore, the numerical results and discussion are given in Section 8.5 and finally, conclusions are presented in Section 8.6.

8.2 Mathematical formulation

Consider the one-dimensional time-dependent heat equation

$$u_t(x,t) = a(t)u_{xx}(x,t) + f(x,t), \quad (x,t) \in \Omega \tag{8.1}$$

in the domain $\Omega = \{(x,t) : 0 < x < h(t), 0 < t < T < \infty\}$ with unknown free smooth boundary $x = h(t) > 0$ and time-dependent thermal diffusivity $a(t) > 0$. The initial condition is

$$u(x,0) = \phi(x), \quad 0 \le x \le h(0) =: h_0, \tag{8.2}$$

where $h_0 > 0$ is given, and the boundary and over-determination conditions are

$$u(0,t) = \mu_1(t), \quad u(h(t),t) = \mu_2(t), \quad 0 \le t \le T, \tag{8.3}$$

$$-a(t)u_x(0,t) = \mu_3(t), \quad \int_0^{h(t)} u(x,t)dx = \mu_4(t), \quad 0 \le t \le T. \tag{8.4}$$

Note that μ_1 and μ_3 represent Cauchy data at the boundary end $x = 0$, whilst μ_4 represent the specification of the energy of the heat conducting system, [89].

First we perform the change of variable $y = x/h(t)$ to reduce the problem (8.1)–(8.4) to the following inverse problem for the unknowns $a(t)$, $h(t)$ and $v(y,t) := u(yh(t),t)$:

$$v_t(y,t) = \frac{a(t)}{h^2(t)}v_{yy}(y,t) + \frac{yh'(t)}{h(t)}v_y(y,t) + f(yh(t),t), \quad (y,t) \in Q \tag{8.5}$$

in the fixed domain $Q = \{(y,t) : 0 < y < 1, 0 < t < T\}$ with unknown time-dependent coefficients $a(t)$ and $h(t)$. The initial condition is

$$v(y,0) = \phi(h_0 y), \quad 0 \le y \le 1, \tag{8.6}$$

and the boundary and over-determination conditions are

$$v(0,t) = \mu_1(t), \quad v(1,t) = \mu_2(t), \quad 0 \le t \le T, \tag{8.7}$$

$$-a(t)v_y(0,t) = \mu_3(t)h(t), \quad h(t)\int_0^1 v(y,t)dy = \mu_4(t), \quad 0 \le t \le T. \tag{8.8}$$

This model has been considered in [69]. The triplet $(h(t), a(t), v(y,t))$ is called a solution to the inverse problem (8.5)–(8.8) if it belongs to the class $C^1[0,T] \times C[0,T] \times C^{2,1}(\overline{Q})$, $h(t) > 0$, $a(t) > 0$, $t \in [0,T]$, and satisfies the equations (8.5)–(8.8). For the input data we make the following regularity and compatibility

assumptions:

(A) $\mu_i(t) \in C^1[0,T]$, $\mu_i(t) > 0$ for $t \in [0,T]$, $i = 1,2,4$, $\mu_3(t) \in C^1[0,T]$, $\mu_3(t) < 0$ for $t \in [0,T]$, $\phi(x) \in C^2[0,h_0]$, $\phi(x) > 0$, $\phi'(x) > 0$ for $x \in [0,h_0]$, and $f(x,t) \in C^{1,0}([0,H_1] \times [0,T])$, $f(x,t) \geq 0$ for $(x,t) \in [0,H_1] \times [0,T]$, where

$$H_1 = \max_{[0,T]} \mu_4(t) \left(\min \left\{ \min_{[0,h_0]} \phi(x), \min_{[0,T]} \mu_1(t), \min_{[0,T]} \mu_2(t) \right\} \right)^{-1};$$

(B) $\phi(0) = \mu_1(0)$, $\phi(h_0) = \mu_2(0)$, and $\int_0^{h_0} \phi(x)dx = \mu_4(0)$.

The following existence and uniqueness of solution theorems are proved in [69].

Theorem 8.1. (Local existence)
If the conditions (A) and (B) are satisfied, then there exists $t_0 \in [0,T]$, (defined by the input data) such that a solution of problem (8.5)–(8.8) exists locally for $(y,t) \in [0,1] \times [0,t_0]$.

Theorem 8.2. (Uniqueness)
Suppose that the following conditions are satisfied:

(i) $0 \leq f(x,t) \in C^{1,0}([0,H_1] \times [0,T])$;

(ii) $\phi(x) > 0$ *for* $x \in [0,h_0]$, $\mu_1(t) > 0$, $\mu_2(t) > 0$, $\mu_3(t) < 0$, *and* $\mu_4(t) > 0$ *for* $t \in [0,T]$.

Then a solution to problem (8.5)–(8.8) is unique.

8.3 Solution of direct problem

In this section, we consider the direct initial boundary value problem (8.5)–(8.7), where $a(t)$, $h(t)$, $f(x,t)$, $\phi(x)$, and $\mu_i(t)$, $i = 1,2$, are known and the solution $u(x,t)$ is to be determined additionally with $\mu_i(t)$, $i = 3,4$. To achieve this, we use the Crank-Nicolson FDM, as described in the previous Chapters 2–6.

The discrete form of our problem is as follows. We divide the domain $Q = (0,1) \times (0,T)$ into M and N subintervals of equal step length Δy and Δt, where $\Delta y = 1/M$ and $\Delta t = T/N$, respectively. So, the solution at the node (i,j) is $v_{i,j} := v(y_i,t_j)$, where $y_i = i\Delta y$, $t_j = j\Delta t$, and $a(t_j) = a_j$, $h(t_j) = h_j$ and

$f(y_i, t_j) = f_{i,j}$ for $i = \overline{0, M}$, $j = \overline{0, N}$. Based on the Crank-Nicolson FDM, equation (8.5) can be approximated as:

$$\begin{aligned} &- A_{i,j+1}v_{i+1,j+1} + (1 + B_{j+1})v_{i,j+1} - C_{i,j+1}v_{i-1,j+1} \\ &\qquad = A_{i,j}v_{i+1,j} + (1 - B_j)v_{i,j} + C_{i,j}v_{i-1,j} + \frac{\Delta t}{2}\left(f_{i,j} + f_{i,j+1}\right) \end{aligned} \tag{8.9}$$

for $i = \overline{1, (M-1)}$, $j = \overline{0, N}$, where

$$A_{i,j} = \frac{(\Delta t)\alpha_j}{2(\Delta y)^2} - \frac{(\Delta t)\gamma_j y_i}{4\Delta y}, \quad B_j = \frac{(\Delta t)\alpha_j}{(\Delta y)^2}, \quad C_j = \frac{(\Delta t)\alpha_j}{2(\Delta y)^2} + \frac{(\Delta t)\gamma_j y_i}{4\Delta y},$$
$$\alpha_j = \frac{a_j}{h_j^2}, \quad \gamma_j = \frac{h'(t_j)}{h_j}.$$

The initial and boundary conditions (8.6) and (8.7) can also be collocated as:

$$v_{i,0} = \phi(h_0 y_i), \quad i = \overline{0, M}, \tag{8.10}$$
$$v_{0,j} = \mu_1(t_j), \quad v_{M,j} = \mu_2(t_j), \quad j = \overline{0, N}. \tag{8.11}$$

At each time step t_j, for $j = \overline{0, (N-1)}$, using the Dirichlet boundary conditions (8.11), the above difference equation (8.9) can be reformulated as a $(M-1) \times (M-1)$ system of linear equations of the form,

$$L\mathbf{v} = \mathbf{b}, \tag{8.12}$$

where

$$\mathbf{v} = (v_{1,j+1}, v_{2,j+1}, ..., v_{M-1,j+1})^{\mathrm{T}}, \quad \mathbf{b} = (b_1, b_2, ..., b_{M-1})^{\mathrm{T}}$$

and

$$L = \begin{pmatrix} 1 + B_{j+1} & -C_{1,j+1} & 0 & \cdots & 0 & 0 & 0 \\ -A_{2,j+1} & 1 + B_{j+1} & -C_{2,j+1} & \cdots & 0 & 0 & 0 \\ \vdots & \vdots & \vdots & \ddots & \vdots & \vdots & \vdots \\ 0 & 0 & 0 & \cdots & -A_{M-2,j+1} & 1 + B_{j+1} & -C_{M-2,j+1} \\ 0 & 0 & 0 & \cdots & 0 & -A_{M-1,j+1} & 1 + B_{j+1} \end{pmatrix},$$

$$b_1 = A_{1,j}v_{0,j} + (1 - B_j)v_{1,j} + C_{1,j}v_{2,j} + A_{1,j+1}v_{0,j+1} + \frac{\Delta t}{2}(f_{1,j+1} + f_{1,j}),$$

$$b_i = A_{i,j}v_{i-1,j} + (1 - B_j)v_{i,j} + C_{i,j}v_{i+1,j} + \frac{\Delta t}{2}(f_{i,j+1} + f_{i,j}), \quad i = \overline{2, (M-2)},$$

$$b_{M-1} = A_{M-1,j}v_{M-2,j} + (1 - B_j)v_{M-1,j} + C_{M-1,j}v_{M,j} + C_{M-1,j+1}v_{M,j+1} + \frac{\Delta t}{2}(f_{M-1,j+1} + f_{M-1,j}).$$

As an example, consider the problem (8.5)–(8.7) with $T = 1$ and

$$a(t) = 1 + t, \quad h(t) = 1 + 2t, \quad h_0 = h(0) = 1, \quad \phi(h_0 y) = (1 + y)^2,$$
$$\mu_1(t) = 1 + 8t, \quad \mu_2(t) = (2 + 2t)^2 + 8t, \quad f(h(t)y, t) = 6 - 2t.$$

The exact solution of the direct problem (8.5)–(8.7) is given by $v(y,t) = (1 + y + 2yt)^2 + 8t$, and the desired outputs are $\mu_3(t) = -2(1 + t)$ and $\mu_4(t) = \frac{(2+2t)^3-1}{3} + 8t(1 + 2t)$. The numerical and exact solutions for $v(y,t)$ are shown in Figure 8.1 and very good agreement is obtained. Tables 8.1 and 8.2 give the numerical heat flux at $y = 0$ and the numerical integral in comparison with the exact values, i.e. μ_3 and μ_4. These have been calculated using the following $O(h^2)$ finite-difference approximations for derivative and trapezoidal rule for integration:

$$v_y(0, t_j) = \frac{4v_{1,j} - v_{2,j} - 3v_{0,j}}{2\Delta y}, \quad j = \overline{1, N}, \tag{8.13}$$

$$\int_0^1 v(y, t_j)dy = \frac{\Delta y}{2}\left(v(0, t_j) + v(1, t_j) + 2\sum_{i=1}^{M-1} v(y_i, t_j)\right), \; j = \overline{0, N}. \tag{8.14}$$

From these tables it can be seen that the numerical results are in very good agreement with the exact ones and that a rapid monotonic decreasing convergence is achieved.

Table 8.1: The exact and the numerical heat flux $-a(t)v_y(0,t)/h(t)$ for $M = N \in \{10, 20\}$, for the direct problem.

t	0.1	0.2	...	0.8	0.9	1
$M = N = 10$	-2.2000	-2.4000	...	-3.6000	-3.8000	-4.0000
$M = N = 20$	-2.2000	-2.4000	...	-3.6000	-3.8000	-4.0000
exact	-2.2000	-2.4000	...	-3.6000	-3.8000	-4.0000

Table 8.2: The exact and the numerical integral $h(t)\int_0^1 v(y,t)dy$ for $M = N \in \{10, 20, 40, 100\}$, for the direct problem.

t	0.1	0.2	...	0.8	0.9	1
$M = N = 10$	4.1789	6.5192	...	31.8880	38.1539	45.0450
$M = N = 20$	4.1767	6.5158	...	31.8660	38.1265	45.0113
$M = N = 40$	4.1762	6.5150	...	31.8605	38.1196	45.0028
$M = N = 100$	4.1760	6.5147	...	31.8590	38.1177	45.0005
exact	4.1760	6.5147	...	31.8587	38.1173	45.0000

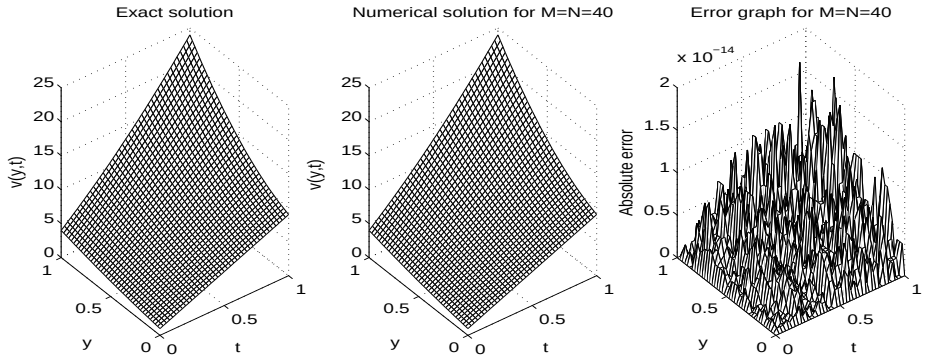

Figure 8.1: Exact and numerical solutions for $v(y,t)$ and the absolute error for the direct problem obtained with $M = N = 40$.

8.4 Numerical approach for the inverse problem

In the inverse problem, we assume that the thermal diffusivity $a(t)$ and free boundary $h(t)$ are unknown. Usually, the nonlinear inverse problem (8.5)–(8.8) can be formulated as a nonlinear least-squares minimization. The regularized objective function which is minimized is given by

$$F(a,h) = \left\| -\frac{a(t)}{h(t)} v_y(0,t) - \mu_3(t) \right\|^2 + \left\| h(t)\int_0^1 v(y,t)dy - \mu_4(t) \right\|^2 + \beta\left(\|a(t)\|^2 + \|h(t)\|^2\right), \tag{8.15}$$

where $\beta \geq 0$ is a regularization parameter and the norm is usually the $L^2[0,T]$-norm. For the simplicity of explanation, as in Chapter 4, Section 4.4, we choose the same regularization parameter for regularizing both $a(t)$ and $h(t)$ in (8.16) because, as it turns out, it was found a posteriori that regularization might, in fact, not be necessary, as it happened with the inverse problem of Chapter 7.

The discretization of (8.15) is

$$F(\underline{a},\underline{h}) = \sum_{j=0}^{N}\Big[-\frac{a_j}{h_j}v_y(0,t_j)-\mu_3(t_j)\Big]^2+\sum_{j=0}^{N}\Big[h_j\int_0^1 v(y,t_j)dy-\mu_4(t_j)\Big]^2 + \beta\left(\sum_{j=0}^{N}a_j^2+\sum_{j=1}^{N}h_j^2\right). \tag{8.16}$$

The minimization of F subject to the physical constraints $\underline{a} > \underline{0}$ and $\underline{h} > \underline{0}$ is accomplished using the MATLAB toolbox routine *lsqnonlin*, as described in the previous chapters. We take bounds for the positive quantities $a(t)$ and $h(t)$ say, we seek them in the interval $[10^{-10},10^3]$. We also take the parameters of the routine as follows:

- Number of variables $M = N = 40$.
- Maximum number of iterations = $10^2\times$(number of variables).
- Maximum number of objective function evaluations = $10^3\times$(number of variables).
- Solution and objective function tolerances = 10^{-10}.

We take the initial guess as $\underline{a}^{(0)} = \underline{h}^{(0)} = \underline{1}$. It is worth mentioning that at the first time step, i.e. $j = 0$, the derivative $v_y(0,0)$ is obtained from (8.10) and (8.13), as

$$v_y(0,0) = \frac{4\phi_1-\phi_2-3\phi_0}{2\Delta y}, \tag{8.17}$$

where $\phi_i = \phi(h_0 y_i)$ for $i = \overline{0,M}$. In addition, when we solve the inverse problem we approximate

$$h'(t_j) = \frac{h(t_j)-h(t_{j-1})}{\Delta t} = \frac{h_j-h_{j-1}}{\Delta t}, \quad j = \overline{1,N}. \tag{8.18}$$

We also express $h'(0)$ as

$$h'(0) = \frac{\mu_2'(0)-a(0)\phi''(h_0)-f(h_0,0)}{\phi'(h_0)}, \tag{8.19}$$

which can easily be derived from equation (8.3) using the chain rule technique. In (8.19), $a(0)$ is unknown.

If there is noise in the measured data (8.8), we replace $\mu_3(t_j)$ and $\mu_4(t_j)$ in (8.16) by $\mu_3^{\epsilon 1}(t_j)$ and $\mu_4^{\epsilon 2}(t_j)$, namely,

$$\mu_3^{\epsilon 1}(t_j) = \mu_3(t_j)+\epsilon 1_j, \quad \mu_4^{\epsilon 2}(t_j) = \mu_4(t_j)+\epsilon 2_j, \quad j = \overline{0,N}, \tag{8.20}$$

where $\epsilon 1_j$ and $\epsilon 2_j$ are random variables generated from a Gaussian normal distribution with mean zero and standard deviations σ_1 and σ_2, respectively, given by

$$\sigma_1 = p \times \max_{t\in[0,T]} |\mu_3(t)|, \quad \sigma_2 = p \times \max_{t\in[0,T]} |\mu_4(t)|, \tag{8.21}$$

where p represents the percentage of noise. We use the MATLAB function *normrnd* to generate the random variables $\underline{\epsilon 1}$ and $\underline{\epsilon 2}$ as follows:

$$\underline{\epsilon 1} = normrnd(0, \sigma_1, N+1), \quad \underline{\epsilon 2} = normrnd(0, \sigma_2, N+1). \tag{8.22}$$

8.5 Numerical results and discussion

The numerical results are illustrated for two different examples according to the linear or nonlinear variation of estimated coefficients. In addition, we add noise, as in (8.20), to the measured input data (8.8). We have also calculated the root mean square error ($rmse$) to analyse the error between the exact and estimated solution, defined as,

$$rmse(a(t)) = \sqrt{\frac{1}{N+1}\sum_{j=0}^{N} \left(a_{numerical}(t_j) - a_{exact}(t_j)\right)^2}, \tag{8.23}$$

$$rmse(h(t)) = \sqrt{\frac{1}{N}\sum_{j=1}^{N} \left(h_{numerical}(t_j) - h_{exact}(t_j)\right)^2}. \tag{8.24}$$

For simplicity, we take $T = 1$.

8.5.1 Example 1

Consider the problem (8.1)–(8.4) with unknown coefficients $a(t)$ and $h(t)$, and solve this inverse problem with the following input data:

$$\mu_1(t) = 1 + 8t, \quad \mu_2(t) = (2+2t)^2 + 8t, \quad \mu_3(t) = -2(1+t),$$
$$\mu_4(t) = \frac{(2+2t)^3 - 1}{3} + 8t(1+2t), \quad h_0 = 1,\ \phi(x) = (1+x)^2,\ f(x,t) = 6 - 2t.$$

One can remark that the conditions of Theorem 8.2 are satisfied hence, the uniqueness of solution holds. With this data the analytical solution is given by

$$a(t) = 1 + t, \quad h(t) = 1 + 2t, \quad u(x,t) = (1+x)^2 + 8t. \tag{8.25}$$

Then

$$a(t) = 1 + t,\ h(t) = 1 + 2t,\ v(y,t) = u(yh(t),t) = (1 + y(1 + 2t))^2 + 8t, \quad (8.26)$$

is the analytical solution of the problem (8.5)–(8.8).

Consider first the case where there is no noise in the input data (8.8). The objective function (8.16), as a function of the number of iterations, is represented in Figure 8.2. From this figure it can be seen that the convergence is rapidly achieved in a few iterations. The objective function (8.16) decreases rapidly and takes a stationary value of $O(10^{-8})$ in about 7 iterations. The numerical results for the corresponding unknowns $a(t)$ and $h(t)$ are presented in Figure 8.3. From this figure it can be seen that the retrieved thermal diffusivity $a(t)$ and free surface $h(t)$ are in very good agreement with the exact values from (8.26).

Next, we add $p = 2\%$ noise to the measured data μ_3 and μ_4, as in equation (8.20). The regularized objective function (8.16) is plotted, as a function of the number of iterations, in Figure 8.4 and convergence is again rapidly achieved. Figure 8.5 presents the graphs of the recovered functions, whilst the $rmse$ values are given in Table 8.3. From this figure and table it can be seen that there is not much difference between the numerical solution obtained with $\beta = 0$ or $\beta = 10^{-3}$, but there is some slight improvement in accuracy obtained for $\beta = 10^{-1}$.

The recovered temperatures for $\beta \in \{0, 10^{-3}, 10^{-1}\}$ are shown in Figure 8.6. From this figure it can be seen that the temperature component of the solution is stable and is not significantly affected by the inclusion of noise in the input data.

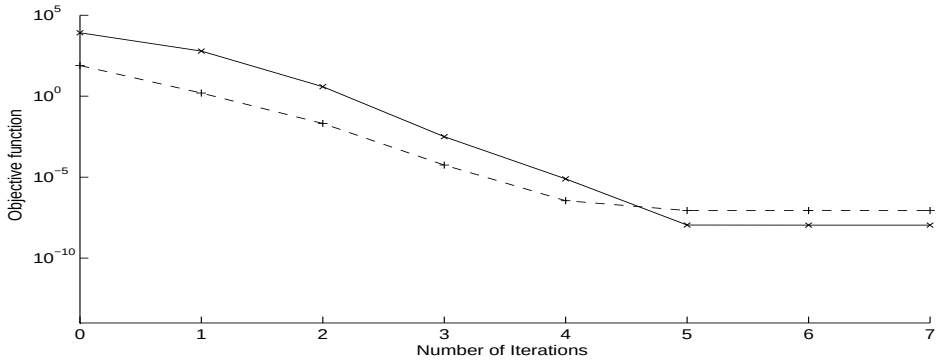

Figure 8.2: Unregularized objective function (8.16), for Example 1 (—) and Example 2 (- - -) with no noise and no regularization.

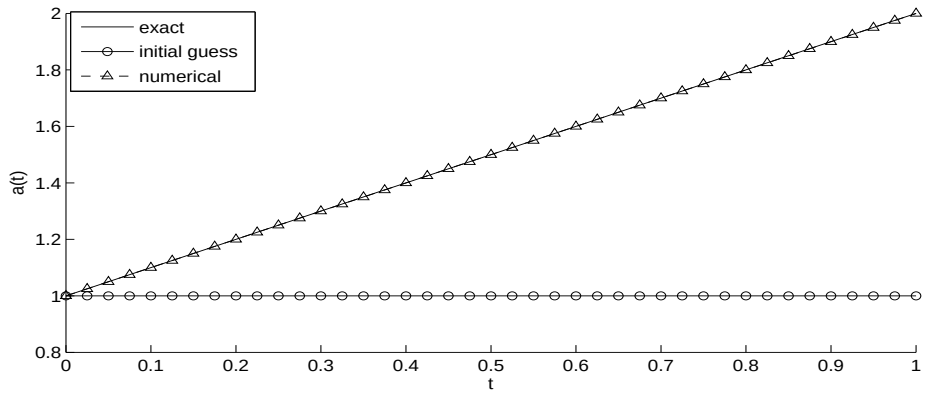

(a)

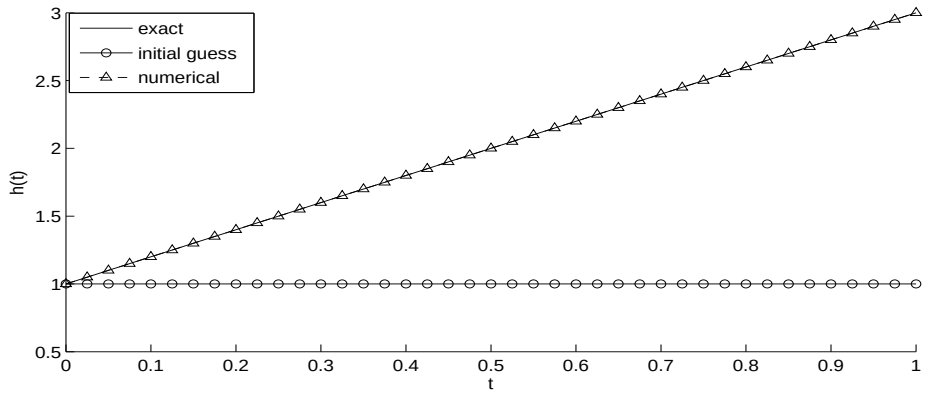

(b)

Figure 8.3: (a) Thermal diffusivity $a(t)$, and (b) Free surface $h(t)$, for Example 1 with no noise and no regularization.

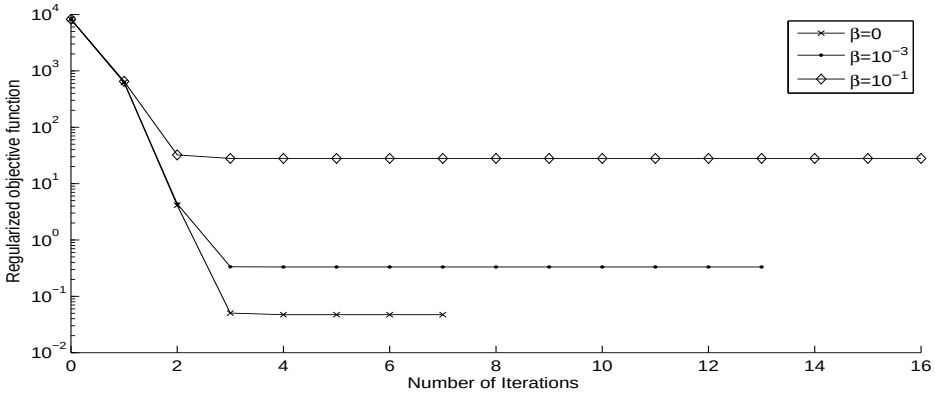

Figure 8.4: Regularized objective function (8.16), for Example 1 with $p = 2\%$ noise.

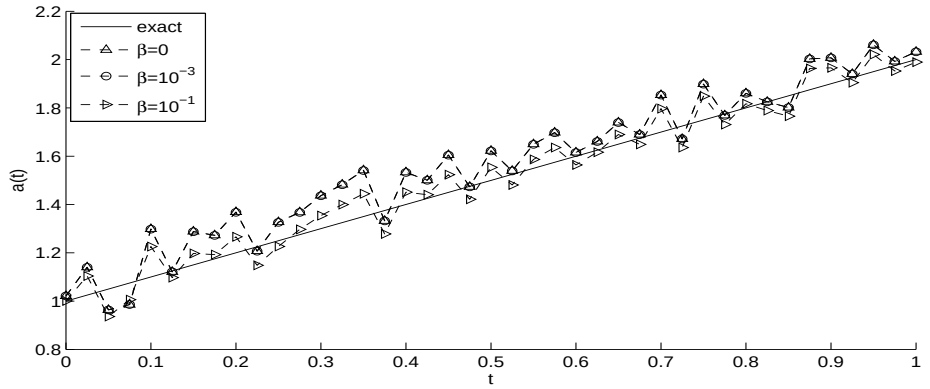

(a)

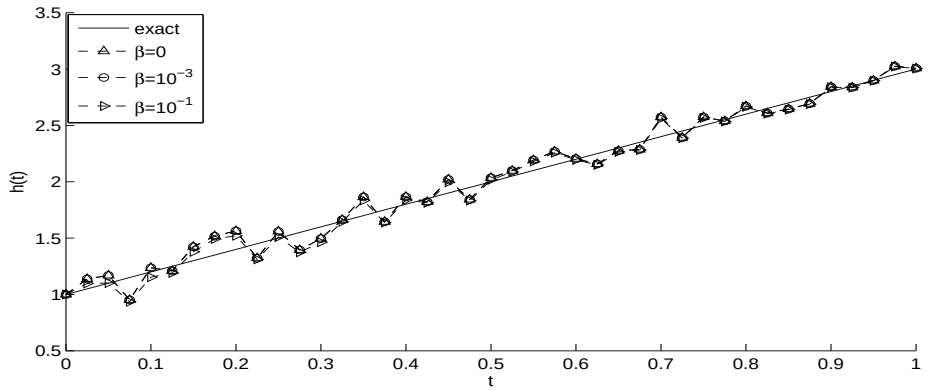

(b)

Figure 8.5: (a) Thermal diffusivity $a(t)$, and (b) Free surface $h(t)$, for Example 1 with $p = 2\%$ noise and regularization.

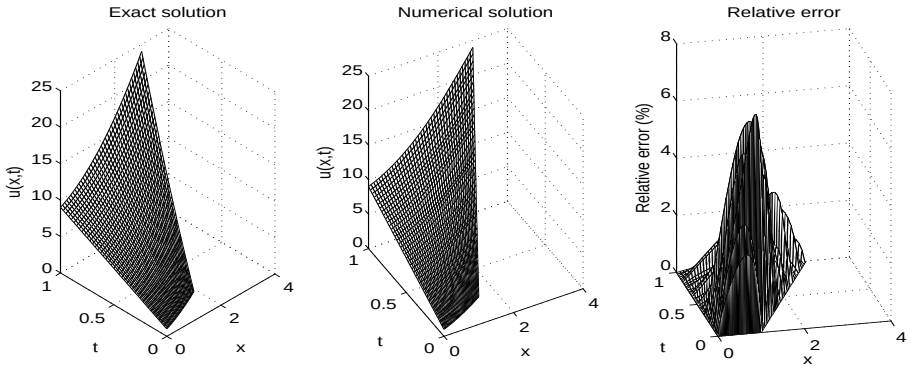

(a)

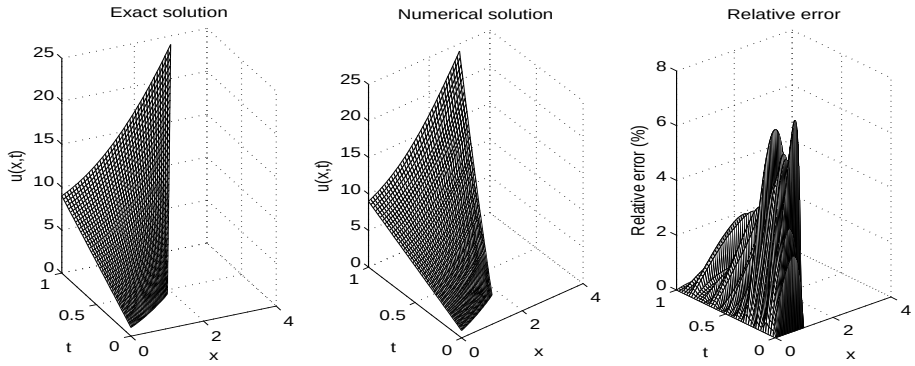

(b)

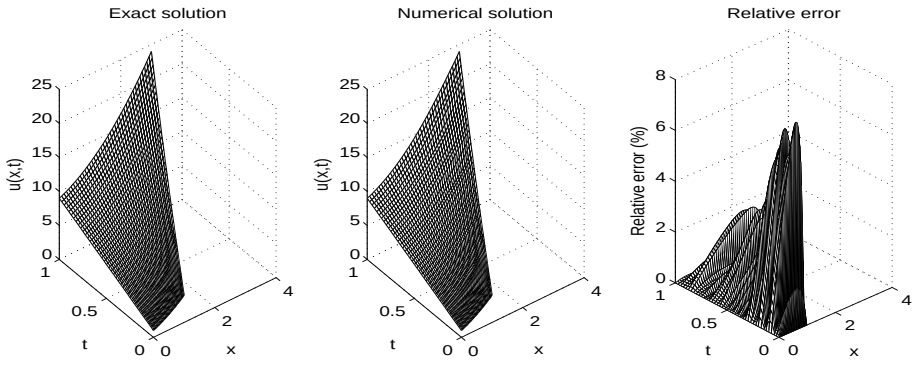

(c)

Figure 8.6: (a) Temperature for $\beta = 0$, (b) $\beta = 10^{-3}$, and (c) $\beta = 10^{-1}$, for Example 1 with $p = 2\%$ noise.

8.5.2 Example 2

In this example we consider the inverse problem (8.5)–(8.8) with the following input data:

$$\begin{aligned}
\mu_1(t) &= 1+8t, \quad \mu_2(t) = (1+\sqrt{2-t})^2 + 8t, \quad \mu_3(t) = -2\sqrt{1+t}, \\
\mu_4(t) &= \frac{(1+\sqrt{2-t})^3 - 1}{3} + 8t\sqrt{2-t}, \quad h_0 = \sqrt{2},\ \phi(x) = (1+\sqrt{2}x)^2, \\
f(x,t) &= 8 - 2\sqrt{1+t}.
\end{aligned}$$

One can remark that the conditions of Theorem 8.2 are satisfied hence, the uniqueness of solution holds. The solution to this inverse problem is given by

$$a(t) = \sqrt{1+t}, \quad h(t) = \sqrt{2-t}, \quad u(x,t) = (1+x)^2 + 8t. \tag{8.27}$$

Then

$$a(t) = \sqrt{1+t},\ h(t) = \sqrt{2-t},\ v(y,t) = u(yh(t),t) = (1+y\sqrt{2-t})^2 + 8t, \tag{8.28}$$

is the analytical solution of the problem (8.5)–(8.8). In this example the moving boundary is given by a nonlinear function.

Initially, we consider the case of noise free in the input data (8.8). The objective function (8.16), as a function of the number of iterations, is presented in Figure 8.2. From this figure it can be seen that the convergence is rapidly achieved in a few iterations. The objective function (8.16) decreases dramatically and takes a stationary value of $O(10^{-7})$ in about 7 iterations, the same as in Example 1. The numerical results for the corresponding coefficients $a(t)$ and $h(t)$ are presented in Figure 8.7. From this figure it can be seen that the identified coefficients are in very good agreement with the exact values from (8.28).

Next, we add $p = 2\%$ noise to the measured data μ_3 and μ_4, as in equation (8.20). The regularized objective function (8.16) is plotted, as a function of the number of iterations, in Figure 8.8 and convergence is again rapidly achieved. Figures 8.9 and 8.10 show the numerical solution $(a(t), h(t), u(x,t))$ and the $rmse$ values are given in Table 8.3. As in Example 1, one can observe that the inverse problem is rather stable with respect to noise included in the input data.

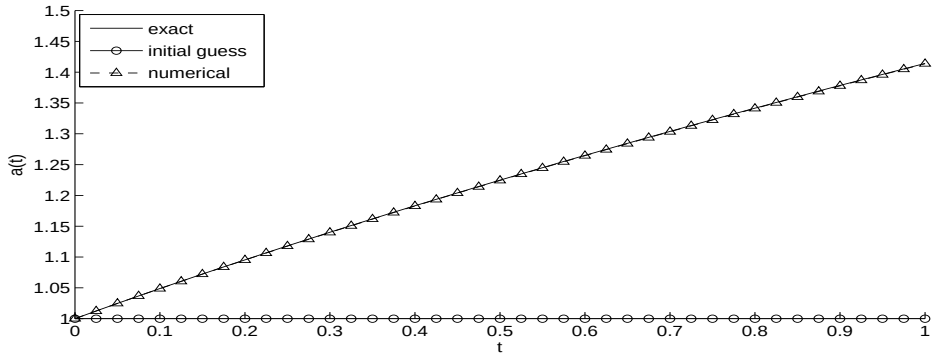

(a)

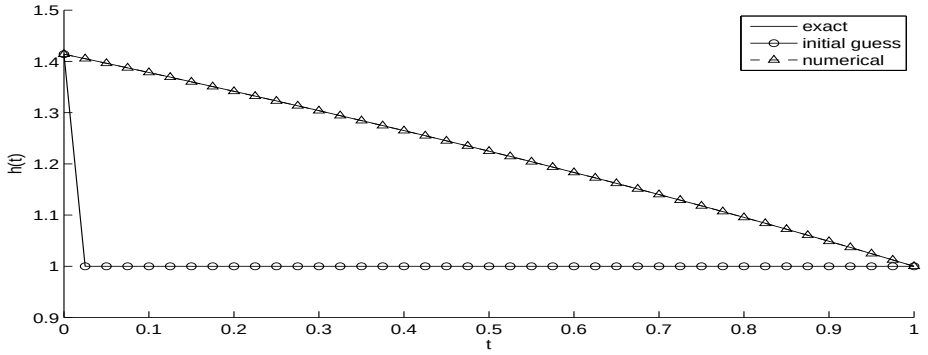

(b)

Figure 8.7: (a) Thermal diffusivity $a(t)$, and (b) Free surface $h(t)$, for Example 2 with no noise and no regularization.

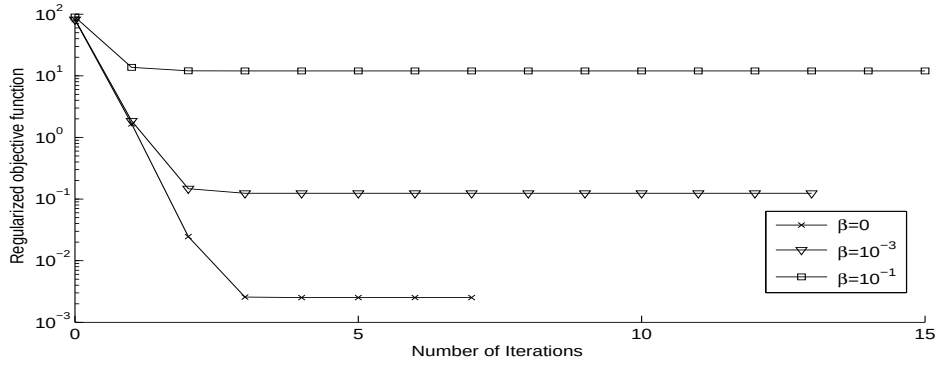

Figure 8.8: Regularized objective function (8.16), for Example 2 with $p = 2\%$ noise.

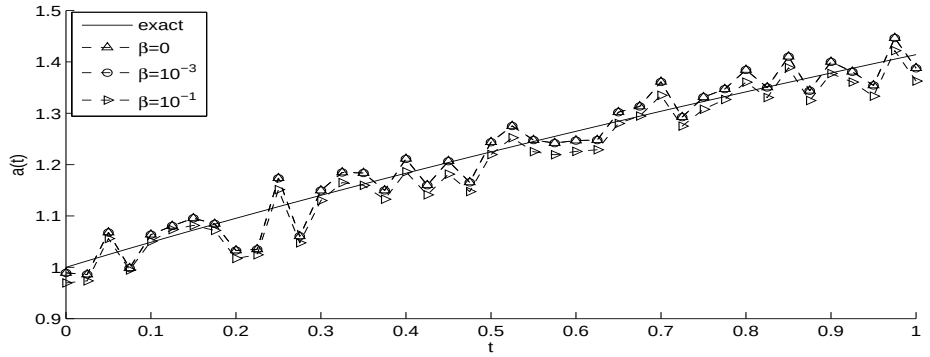

(a)

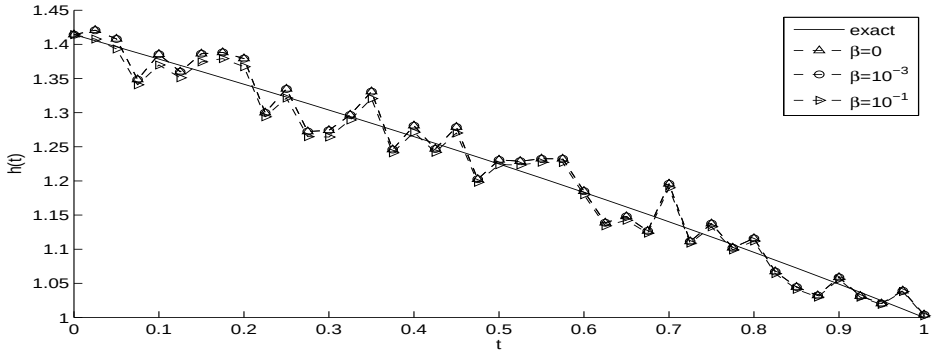

(b)

Figure 8.9: (a) Thermal diffusivity $a(t)$, and (b) Free surface $h(t)$, for Example 2 with $p = 2\%$ noise and regularization.

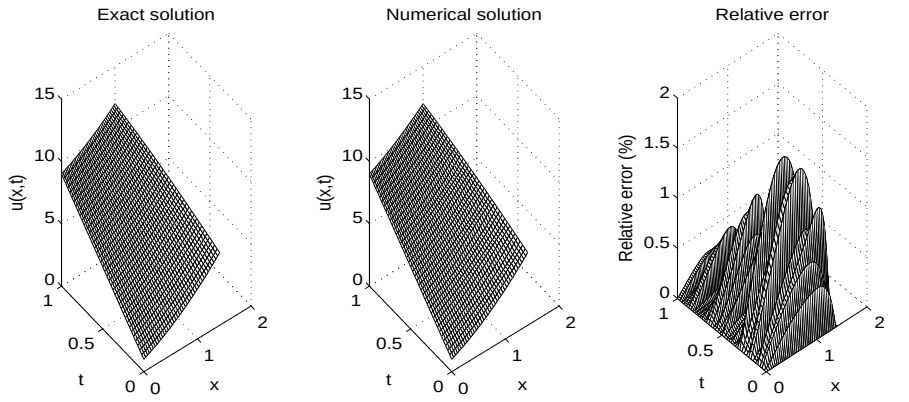

(a)

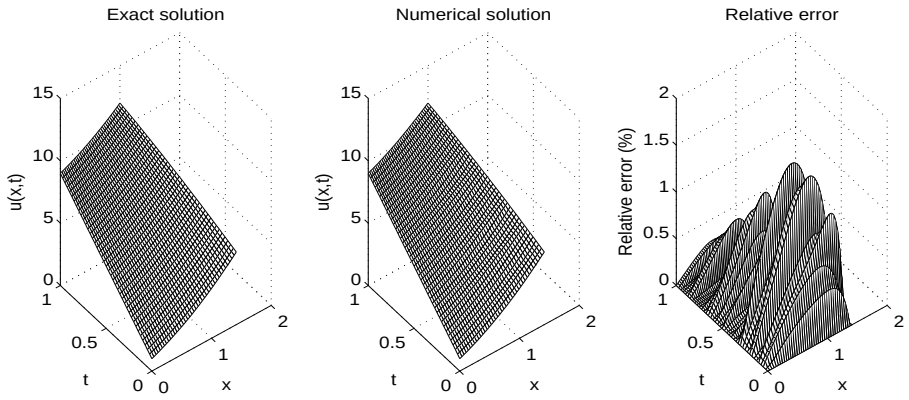

(b)

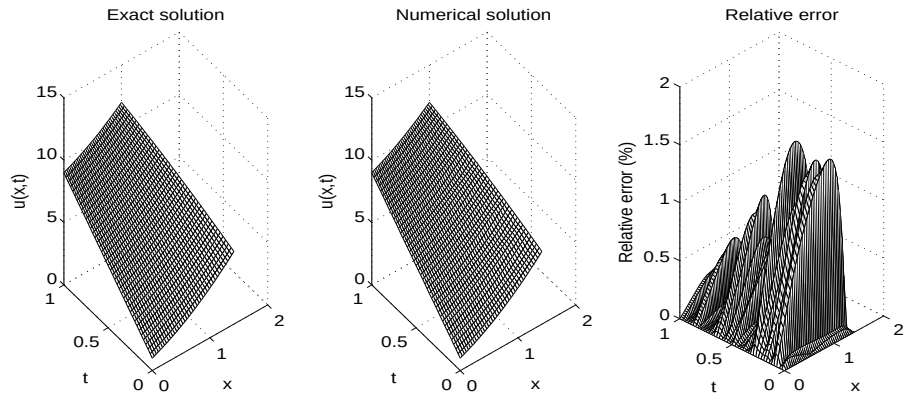

(c)

Figure 8.10: (a) Temperature for $\beta = 0$, (b) $\beta = 10^{-3}$, and (c) $\beta = 10^{-1}$, for Example 2 with $p = 2\%$ noise.

Table 8.3: The *rmse* values for Examples 1 and 2 with $p = 2\%$ noise.

Example	$\beta = 0$	$\beta = 10^{-3}$	$\beta = 10^{-1}$
1	$rmse(a) = 0.1010$	0.1004	0.0628
	$rmse(h) = 0.0932$	0.0922	0.0872
2	$rrmse(a) = 0.0336$	0.0336	0.0368
	$rrmse(h) = 0.0253$	0.0253	0.0248

8.6 Conclusion

The inverse nonlinear problem which requires simultaneously determining the time-dependent thermal diffusivity and free boundary in the parabolic heat equation has been investigated. The resulting inverse problem has been reformulated as a nonlinear least-squares optimization problem which produced stable and reasonably accurate numerical results. Extension of the present work to include the determination of unknown convection $b(t)u_x$ and reaction $c(t)u$ coefficients in the heat equation (8.1), in addition to the unknowns $a(t)$ and $h(t)$, [113], will be considered in the next chapter.

Chapter 9

Multiple time-dependent coefficient identification thermal problems with a free boundary

9.1 Introduction

Prior to this study, references [53, 57, 69] investigated both theoretically and numerically several combined formulations for the retrieval of the free boundary together with the thermal diffusivity both which are unknown time-dependent functions. The theoretical investigation has been extended recently to the case of several multiple coefficients in [112, 113] and it the purpose of this chapter to, apart from some theoretical clarifications which are elaborated in Section 9.2, perform the numerical realization using the FDM combined with a nonlinear least-squares toolbox MATLAB routine, see Sections 9.3 and 9.4. In Section 9.5, we provide numerical results and discussion, whilst Section 9.6 presents an extension to a triple unknown coefficient identification. Finally, conclusions are highlighted in Section 9.7.

9.2 Mathematical formulation

Consider the one-dimensional time-dependent heat equation

$$u_t(x,t) = a(x,t)u_{xx}(x,t) + b(t)u_x(x,t) + c(t)u(x,t) + f(x,t),\ (x,t) \in \Omega \quad (9.1)$$

for the unknown temperature $u(x,t)$ in the domain $\Omega = \{(x,t)|\ 0 < x < h(t), 0 < t < T < \infty\}$ with unknown free smooth boundary $x = h(t) > 0$ and time-dependent coefficients $b(t)$ and $c(t)$ representing the convection/advection and

reaction coefficients, respectively. Also in (9.1), $f(x,t)$ represents a given heat source, whilst $a(x,t) > 0$ is the given thermal diffusivity. In many applications, [53, 113, 125], the thermal diffusivity depends on time only, but here we envisage a more general physical situation in which the thermal conductivity depends on time and the heat capacity depends on space such that their ratio defined as the thermal diffusivity depends on both space and time. To give more physical meaning to the inverse problem, we have in mind a process in which a finite slab is undertaking radioactive decay such that its diffusivity, convection and reaction coefficients are unknown but they depend on time [11, Chap.13], [90]. We finally mention that extensions to cases when the time-dependent heat source is also unknown or when some unknown coefficients may depend on space as well have recently been considered elsewhere, [55, 52].

The initial condition is

$$u(x,0) = \phi(x), \quad 0 \le x \le h(0) =: h_0, \tag{9.2}$$

where $h_0 > 0$ is given, and the Dirichlet boundary conditions are

$$u(0,t) = \mu_1(t), \quad u(h(t),t) = \mu_2(t), \quad t \in [0,T]. \tag{9.3}$$

As over-determination conditions we consider, [112],

$$h'(t) + u_x(h(t),t) = \mu_3(t), \quad t \in [0,T], \tag{9.4}$$

$$\int_0^{h(t)} u(x,t)dx = \mu_4(t), \quad t \in [0,T], \tag{9.5}$$

$$\int_0^{h(t)} xu(x,t)dx = \mu_5(t), \quad t \in [0,T]. \tag{9.6}$$

Note that $\mu_4(t)$ and $\mu_5(t)$ represent the specification of the energy or, mass of the heat conducting system and heat momentum, respectively, [16, 72, 89]. Also, equation (9.4) represents a Stefan interface moving boundary condition.

Now we perform the change of variable $y = x/h(t)$ to reduce the problem (9.1)–(9.6) to the following inverse problem for the unknowns $h(t)$, $b(t)$, $c(t)$ and $v(y,t) := u(yh(t),t)$:

$$v_t(y,t) = \frac{a(yh(t),t)}{h^2(t)} v_{yy}(y,t) + \frac{b(t) + yh'(t)}{h(t)} v_y(y,t) + c(t)v(y,t) + f(yh(t),t), \quad (y,t) \in Q_T \tag{9.7}$$

in the fixed domain $Q_T := \{(y,t) : 0 < y < 1, 0 < t < T\} = (0,1) \times (0,T)$,

$$v(y,0) = \phi(h_0 y), \quad y \in [0,1], \tag{9.8}$$

$$v(0,t) = \mu_1(t), \quad v(1,t) = \mu_2(t), \quad t \in [0,T], \tag{9.9}$$

$$h'(t) + \frac{1}{h(t)} v_y(1,t) = \mu_3(t), \quad t \in [0,T], \tag{9.10}$$

$$h(t) \int_0^1 v(y,t)dy = \mu_4(t), \quad t \in [0,T], \tag{9.11}$$

$$h^2(t) \int_0^1 yv(y,t)dy = \mu_5(t), \quad t \in [0,T]. \tag{9.12}$$

A variant of the theorem proved in [112] (under the additional assumption that $h(0) = h_0 > 0$ is known) ensures the unique solvability (locally in time) of the inverse problem (9.7)–(9.12), proved in [60], as follows.

Theorem 9.1. *Suppose that:*
$0 < a \in C^{2,0}([0,\infty) \times [0,T])$, $[0,f_0] \ni f \in C^{1,0}([0,\infty) \times [0,T])$, *where* $f_0 \geq 0$ *is a given constant,* $0 < \phi \in C^1[0,h_0]$, $0 < \mu_i \in C^1[0,T]$ *for* $i = 1,2,4,5$, $\mu_3 \in C[0,T]$,

$$(\mu_2(0) - \mu_1(0))\mu_5(0) - (h_0\mu_2(0) - \mu_4(0))\mu_4(0) \neq 0, \tag{9.13}$$

$\phi(0) = \mu_1(0)$, $\phi(h_0) = \mu_2(0)$, $\int_0^{h_0} \phi(x)dx = \mu_4(0)$, *and* $\int_0^{h_0} x\phi(x)dx = \mu_5(0)$. *Then, there is* $T_0 \in (0,T]$, *such that there exists a unique solution* $(h(t), b(t), c(t), v(y,t)) \in C^1[0,T_0] \times (C[0,T_0])^2 \times (C^{2,1}(Q_{T_0}) \cap C^{1,0}(\overline{Q}_{T_0}))$, $h(t) > 0$ *for* $t \in [0,T_0]$, *of the inverse problem (9.7)–(9.12).*

Once the unique local solvability to the inverse problem (9.7)–(9.12) has been provided by Theorem 9.1, the next three Sections 9.3–9.5 explain, discuss and illustrate the procedures for obtaining an accurate and stable numerical solution. But before we do that, in the next subsection we introduce another related problem in which the Stefan condition (9.10) is replaced by the second-order heat moment condition (9.14).

9.2.1 Another related inverse problem formulation

It was pointed out in [112] that the Stefan condition (9.4), or (9.10), may be replaced by the second-order heat moment measurement

$$\int_0^{h(t)} x^2 u(x,t)dx = \mu_6(t), \quad t \in [0,T], \tag{9.14}$$

or, in terms of the variable $y = x/h(t)$,

$$h^3(t)\int_0^1 y^2 v(y,t)dy = \mu_6(t), \quad t \in [0,T], \tag{9.15}$$

respectively. Then, we can formulate the following theorem, see [60], on the local unique solvability of the inverse problem (9.7)–(9.9), (9.11), (9.12) and (9.15), which is a variant of Theorem 2 of [112] when $h(0) = h_0 > 0$ is assumed to be known.

Theorem 9.2. *Suppose that:*
$0 < a \in C^{2,0}([0,\infty)\times[0,T])$, $[0,f_0] \ni f \in C^{1,0}([0,\infty)\times[0,T])$, *where* $f_0 \geq 0$ *is a given constant,* $0 < \phi \in C^1[0,h_0]$, $0 < \mu_i \in C^1[0,T]$ *for* $i = 1,2,4,5,6$,

$$\begin{aligned}&\mu_4(0)\mu_6(0) - 2\mu_5^2(0) - h_0(\mu_6(0)\mu_1(0) - 2\mu_4(0)\mu_5(0))\\ &- h_0^2(\mu_4^2(0) - \mu_1(0)\mu_5(0)) \neq 0,\end{aligned} \tag{9.16}$$

$\phi(0) = \mu_1(0)$, $\phi(h_0) = \mu_2(0)$, $\int_0^{h_0}\phi(x)dx = \mu_4(0)$, $\int_0^{h_0} x\phi(x)dx = \mu_5(0)$, *and* $\int_0^{h_0} x^2\phi(x)dx = \mu_6(0)$. *Then, there is* $T_0 \in (0,T]$, *such that there exists a unique solution* $(h(t),b(t),c(t),v(y,t)) \in C^1[0,T_0]\times(C[0,T_0])^2\times(C^{2,1}(Q_{T_0})\cap C^{1,0}(\overline{Q}_{T_0}))$, $h(t) > 0$ *for* $t \in [0,T_0]$, *of the inverse problem (9.7)–(9.9), (9.11), (9.12) and (9.15).*

9.3 Solution of direct problem

In this section, we consider the direct initial boundary value problem (9.1)–(9.3), where $h(t)$, $b(t)$, $c(t)$, $a(x,t)$, $f(x,t)$, $\phi(x)$, and $\mu_i(t)$, $i = 1,2$, are known and the solution $u(x,t)$ is to be determined, additionally to the quantities of interest $\mu_i(t)$, $i = \overline{3,6}$. To achieve this, we use the Crank-Nicolson FDM based on subdividing the solution domain $Q_T = (0,1)\times(0,T)$ into M and N subintervals of equal step lengths Δy and Δt, where $\Delta y = 1/M$ and $\Delta t = T/N$, respectively. At the node (i,j) we denote $v_{i,j} := v(y_i,t_j)$, where $y_i = i\Delta y$, $t_j = j\Delta t$, $a_{i,j} := a(y_i,t_j)$, $h_j := h(t_j)$, $b_j := b(t_j)$, $c_j := c(t_j)$ and $f_{i,j} := f(y_i,t_j)$ for $i = \overline{0,M}$ and $j = \overline{0,N}$.

Once the solution $v_{i,j}$ for $i = \overline{0,M}$, $j = \overline{0,N}$ has been determined accurately, the data (9.10)–(9.12) and (9.15) can be calculated using the following finite-

difference approximation formula and trapezoidal rule for integrals:

$$\mu_3(t_j) = \frac{h_j - h_{j-1}}{\Delta t} - \frac{4v_{M-1,j} - v_{M-2,j} - 3v_{M,j}}{2(\Delta y)h_j}, \quad j = \overline{1,N}, \tag{9.17}$$

$$\mu_{k+3}(t_j) = \frac{h_j^k}{2N}\left(y_0^{k-1}v_{0,j} + y_M^{k-1}v_{M,j} + 2\sum_{i=1}^{M-1} y_i^{k-1}v_{i,j}\right), \; j = \overline{1,N}, \; k = 1,2,3. \tag{9.18}$$

9.4 Numerical approach to the inverse problems

In the inverse problems stated in Section 9.2, we wish to obtain simultaneously stable reconstructions of the two unknown coefficients $b(t)$ and $c(t)$, together with the free boundary $h(t)$ and the transformed temperature $v(y,t)$, satisfying equations (9.7)–(9.12) or, (9.7)–(9.9), (9.11), (9.12) and (9.15), by minimizing the Tikhonov regularized nonlinear objective function

$$\begin{aligned} F(\underline{h},\underline{b},\underline{c}) = &\sum_{j=1}^{N}\left[h_j' + \frac{v_y(1,t_j)}{h_j} - \mu_3(t_j)\right]^2 + \sum_{j=1}^{N}\left[h_j\int_0^1 v(y,t_j)dy - \mu_4(t_j)\right]^2 \\ &+ \sum_{j=1}^{N}\left[h_j^2\int_0^1 yv(y,t_j)dy - \mu_5(t_j)\right]^2 + \beta_1\sum_{j=1}^{N}h_j^2 + \beta_2\sum_{j=1}^{N}b_j^2 \\ &+ \beta_3\sum_{j=1}^{N}c_j^2, \end{aligned} \tag{9.19}$$

or,

$$\begin{aligned} F_1(\underline{h},\underline{b},\underline{c}) = &\sum_{j=1}^{N}\left[h_j\int_0^1 v(y,t_j)dy - \mu_4(t_j)\right]^2 + \sum_{j=1}^{N}\left[h_j^2\int_0^1 yv(y,t_j)dy - \mu_5(t_j)\right]^2 \\ &+ \sum_{j=1}^{N}\left[h_j^3\int_0^1 y^2v(y,t_j)dy - \mu_6(t_j)\right]^2 + \beta_1\sum_{j=1}^{N}h_j^2 + \beta_2\sum_{j=1}^{N}b_j^2 \\ &+ \beta_3\sum_{j=1}^{N}c_j^2, \end{aligned} \tag{9.20}$$

respectively. In this case, we choose the most general regularization terms $(\beta_i)_{i=1,2,3}$ in order to allow for different weightings of the multiple parameters $h(t)$, $b(t)$ and $c(t)$. The unregularized case, i.e., $\beta_i = 0$ for $i = 1,2,3$, yields the ordinary nonlinear least-squares method which usually produces unstable solutions for noisy data. The minimization of F or (F_1) subject to the physical constraint for the free boundary $\underline{h} > \underline{0}$ is performed using the MATLAB optimization toolbox routine *lsqnonlin*. We take bounds for the positive quantity $h(t)$ say, we seek it in the

interval $[10^{-10}, 10^2]$ and the bounds for the quantities $b(t)$ and $c(t)$ say, we seek them in the interval $[-10^2, 10^2]$. We also take the parameters of the routine as follows:

- Number of variables $M = N$.
- Maximum number of iterations = $10\times$ (number of variables).
- Maximum number of objective function evaluations = $10^5\times$ (number of variables).
- Solution and object function tolerances = 10^{-15}.

In (9.19), we approximate the derivative of $h(t)$ as in (8.18).

Condition (9.4) represents a Stefan condition of melting between a solid and a fluid and, in general, μ_3 is taken to be zero (or is assumed to be prescribed exactly). Therefore, practically the experimental measurement errors are likely to be only in the heat moments (9.5), (9.6) and (9.14). In order to model these errors, we replace $\mu_{k+3}(t_j)$, $k = 1, 2, 3$, in equations (9.11), (9.12) and (9.14) by $\mu_{k+3}^{\epsilon k}(t_j)$, as

$$\mu_{k+3}^{\epsilon k}(t_j) = \mu_{k+3}(t_j) + \epsilon k_j, \quad k = 1, 2, 3, \quad j = \overline{1, N}, \tag{9.21}$$

where ϵk_j are random variables generated from a Gaussian normal distribution with mean zero and standard deviation σ_k, given by

$$\sigma_k = p \times \max_{t\in[0,T]} |\mu_{k+3}(t)|, \quad k = 1, 2, 3, \tag{9.22}$$

where p represents the percentage of noise.

9.5 Numerical results and discussion

In this section, we present a couple of typical test examples to illustrate the accuracy and stability of the numerical scheme based on the FDM with $M = N = 40$ combined with minimization of the nonlinear objective function (9.19) or (9.20), as described in Section 9.4. To assess the accuracy of the approximate

solutions, let us introduce the root mean squares error ($rmse$) defined as

$$rmse(h) = \sqrt{\frac{T}{N}\sum_{j=1}^{N}\left(h_{numerical}(t_j) - h_{exact}(t_j)\right)^2}, \tag{9.23}$$

$$rmse(b) = \sqrt{\frac{T}{N}\sum_{j=1}^{N}\left(b_{numerical}(t_j) - b_{exact}(t_j)\right)^2}, \tag{9.24}$$

$$rmse(c) = \sqrt{\frac{T}{N}\sum_{j=1}^{N}\left(c_{numerical}(t_j) - c_{exact}(t_j)\right)^2}. \tag{9.25}$$

9.5.1 Example 1

We consider the first inverse problem (9.1)–(9.6) with unknown coefficients $h(t)$, $b(t)$ and $c(t)$, and the following input data:

$$a(x,t) = \frac{(1+x)(1+t)}{2}, \quad \phi(x) = \frac{1}{1+x}, \quad \mu_1(t) = e^{3t}, \quad \mu_2(t) = \frac{e^{3t}}{2+t},$$
$$\mu_3(t) = 1 - \frac{e^{3t}}{(2+t)^2}, \quad \mu_4(t) = e^{3t}\ln(2+t), \quad \mu_5(t) = e^{3t}(1+t-\ln(2+t)),$$
$$f(x,t) = \frac{e^{3t}(2-t)}{1+x}, \quad h_0 = 1, \quad T = 1.$$

One can remark that conditions of Theorem 9.1 are satisfied hence, the local uniqueness of this solution is guaranteed.

With the above data the analytical solution of the inverse problem (9.1)–(9.6) is given by

$$h(t) = 1+t, \quad b(t) = 1+t, \quad c(t) = 1+t, \tag{9.26}$$

$$u(x,t) = \frac{e^{3t}}{1+x}. \tag{9.27}$$

We also have that the analytical solution of the transformed inverse problem (9.7)–(9.12) is given by equation (9.26) and

$$v(y,t) = u(yh(t),t) = \frac{e^{3t}}{1+y+yt}. \tag{9.28}$$

The initial guesses for the vectors $\underline{h}$, $\underline{b}$ and $\underline{c}$ are taken as $\underline{1}$, namely,

$$h_j^0 = b_j^0 = c_j^0 = 1, \quad j = \overline{1,N}. \tag{9.29}$$

We consider first the case where there is no noise in the input data (9.10)–(9.12),

i.e. $p = 0$ in (9.22). The objective function (9.19), as a function of the number of iterations is presented in Figure 9.1. From this figure it can be seen that a monotonic decreasing convergence is rapidly achieved in a few iterations. The objective function (9.19) decreases rapidly and takes a stationary value of $O(10^{-15})$ in about 95 iterations by the (-×-) line with initial guess (9.29) when we do not employ any regularization, i.e. $\beta_i = 0$, $i = 1, 2, 3$. In order to investigate the robustness of the nonlinear iterative routine *lsqnonlin* employed for minimizing the objective function (9.19), in Figure 9.1 we also include the convergence history for a different than (9.29) initial guess for the unknowns $\underline{h}$, $\underline{b}$ and $\underline{c}$ namely,

$$h_j^0 = b_j^0 = c_j^0 = 1 - \frac{t_j}{2}, \quad j = \overline{1, N}. \tag{9.30}$$

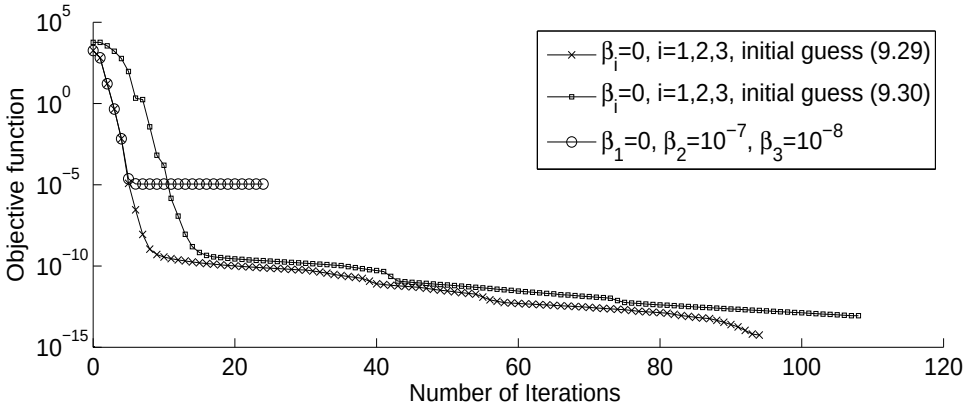

Figure 9.1: The objective function (9.19) without noise for Example 1.

As expected, from this farther initial guess (9.30) to the exact solution (9.26) than (9.29) is it takes a slighter larger number of iterations (108 instead of 95), but the minimization of the objective function (9.19) converges to similar very small minimum values which are of $O(10^{-15})$ to $O(10^{-14})$. This means that the routine used is robust by being quite insensitive to the initial guess for the unknowns. In the remaining of this subsection and the next subsection 9.5.2, figures are illustrated only for the initial guess (9.29). Although not illustrated, we report that similar numerical results have been obtained for the other initial guess (9.30).

The corresponding numerical results for the unknowns $h(t)$, $b(t)$ and $c(t)$ are presented in Figure 9.2. From this figure it can be noticed that a stable and very accurate retrieval for the free boundary $h(t)$ is obtained with a small $rmse(h) = 1.7E-4$. Consequently, there is no need to regularize h and therefore, in what follows, we take $\beta_1 = 0$ in (9.19). The numerical reconstructions for $b(t)$ and $c(t)$ are stable, but with less accurate values of $rmse(b) = 0.0472$ and $rmse(c) =$

0.0260, respectively. However, when we add a little regularization with $\beta_2 = 10^{-7}$, $\beta_3 = 10^{-8}$ to (9.19) we obtain a faster convergence in about 25 iterations to reach a stationary value of $O(10^{-5})$, see Figure 9.1 by the (-○-) line, and even more stable and accurate results for $b(t)$ and $c(t)$ with $rmse$ values decreasing to $rmse(b) = 0.0394$ and $rmse(c) = 0.0213$, respectively, see Figure 9.2.

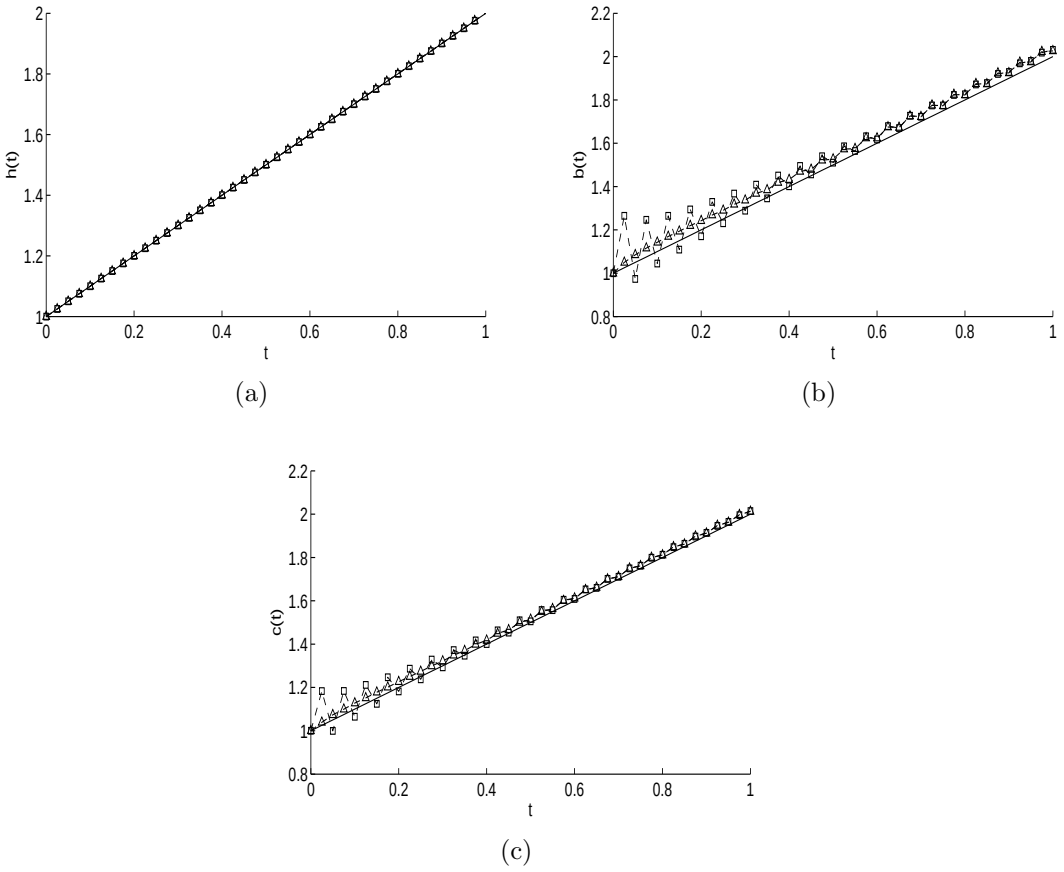

(a) (b) (c)

Figure 9.2: The exact (—) and numerical solutions without regularization (-□-), and with regularization parameters $\beta_1 = 0$, $\beta_2 = 10^{-7}$ and $\beta_3 = 10^{-8}$ (-△-) for: (a) the free boundary $h(t)$, (b) the coefficient $b(t)$, and (c) the coefficient $c(t)$, without noise for Example 1.

Next, in order to investigate the stability of the numerical solution we add some small percentage $p = 0.1\%$ of noise to the input data (9.11) and (9.12), as in (9.21) for $k = 1, 2$. We have also investigated higher amounts of noise p, but the results obtained were less accurate hence, they are not presented. However, similar qualitative conclusions, regarding achieving stability through regularization, maintain. Details regarding the number of iterations, number of function evaluations, value of the objective function (9.19) at the final iteration, the $rmse$ values (9.23)–(9.25) and the computational time taken for running the iterative minimization routine *lsqnonlin* are summarised in Table 9.1. One can

notice that it takes almost one day to run the program without regularization.

The objective function (9.19), as a function of the number of iterations, is plotted in Figure 9.3. From this figure it can be seen that in the absence of regularization, see the graph for $\beta_i = 0$, $i = 1, 2, 3$, a slow convergence is recorded and, in fact, the process of minimization of the routine *lsqnonlin* is stopped when the prescribed maximum number of 400 iterations is reached. The corresponding numerical results for the unknown coefficients are presented in Figure 9.4. From Figure 9.4(a) it can be seen that stable and accurate numerical results are obtained for the free boundary $h(t)$. However, from Figures 9.4(b) and 9.4(c) one can observe that unstable (highly oscillatory and unbounded) and very inaccurate solutions for $b(t)$ and $c(t)$ are obtained. This is expected since the problem under investigation is ill-posed and small errors in the measurement data (9.11) and (9.12) lead to a drastic amount of error in the output coefficients $b(t)$ and $c(t)$. Therefore, regularization should be applied to restore the stability of the solution in the components $b(t)$ and $c(t)$. Since in Figure 9.4(a) the free boundary has been obtained accurately, we fix $\beta_1 = 0$ and we only take β_2 and β_3 as positive regularization parameters in (9.19). These regularization parameters have been chosen by trial and error, and some numerical results obtained from a couple of choices are given in Table 9.1, and Figures 9.3 and 9.5. Justifying more rigorously the choice of multiple regularization parameters in the nonlinear Tikhonov regularization method is very challenging and will be the object of future numerical investigations. At this stage, we only mention the idea of extending to the nonlinear case some possible strategies of multi-parameter selection for the linear Tikhonov regularization suggested in [20]. From Figure 9.3 it can be noticed that a rapid convergence in less than 30 iterations is achieved for each selection of regularization parameters. Furthermore, from Table 9.1 it can be seen that the computational time is reduced from 1 day to less than an hour by the inclusion of regularization in (9.19).

Table 9.1: Number of iterations, number of function evaluations, value of the objective function (9.19) at final iteration, $rmse$ values (9.23)-(9.25) and the computational time, for $p = 0.1\%$ noise for Example 1.

$\beta_1 = 0$	$\beta_2 = \beta_3 = 0$	$\beta_2 = \beta_3 = 10^{-4}$	$\beta_2 = \beta_3 = 10^{-3}$
No. of iterations	401	23	28
No. of function evaluations	49446	2976	3596
Value of objective function (9.19) at final iteration	0.0026	0.0345	0.1412
$rmse(h)$	0.0108	0.0026	0.0040
$rmse(b)$	105.34	1.1044	1.0787
$rmse(c)$	61.838	0.8184	0.6558
Computational time	23 hours	40 min	45 min

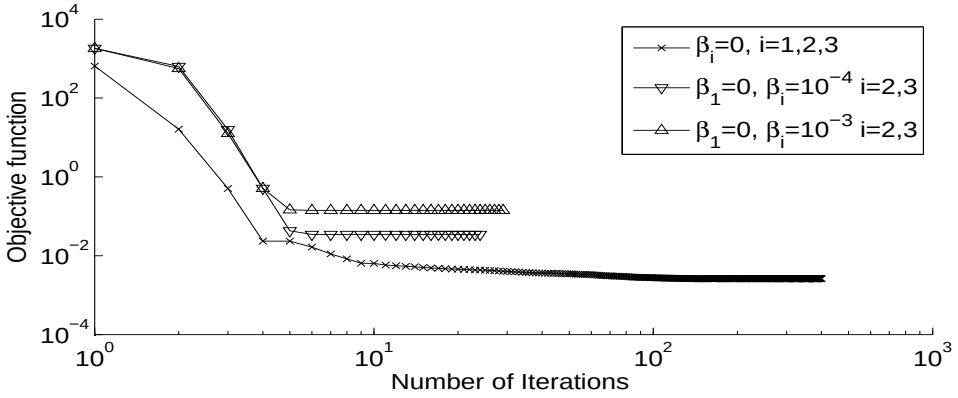

Figure 9.3: The objective function (9.19) for $p = 0.1\%$ noise for Example 1.

The corresponding numerical reconstructions for the unknown free boundary $h(t)$ and the coefficients $b(t)$ and $c(t)$ are presented in Figures 9.5(a)-(c), respectively. By comparing Figures 9.4(b) and 9.4(c) with 9.5(b) and 9.5(c) one can immediately observe the dramatic improvement in stability and accuracy which is achieved through the inclusion of regularization in the objective function (9.19).

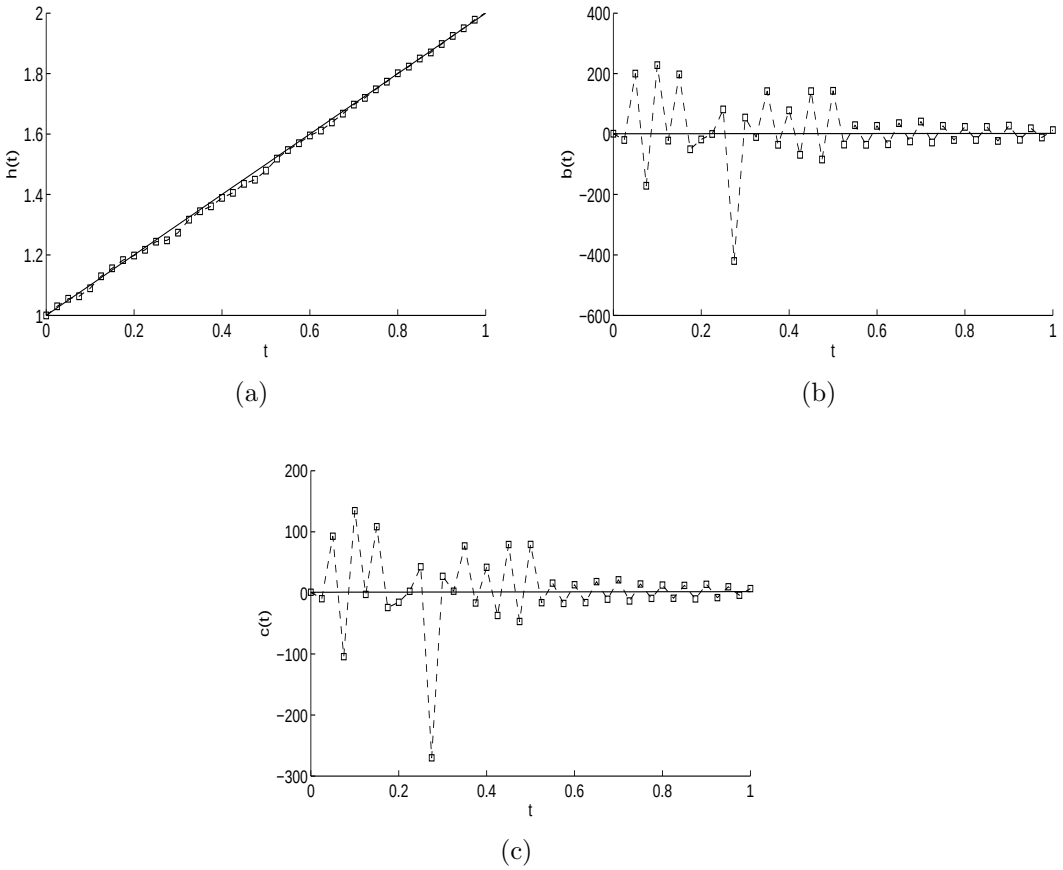

(a) (b) (c)

Figure 9.4: The exact (—) and numerical (−□−) solutions for: (a) the free boundary $h(t)$, (b) the coefficient $b(t)$, and (c) the coefficient $c(t)$, with $p = 0.1\%$ noise and no regularization for Example 1.

9.5.2 Example 2

We consider now the second inverse problem (9.1)–(9.3), (9.5), (9.6) and (9.14) with unknown coefficients $h(t)$, $b(t)$ and $c(t)$, with the same input data as in Example 1 of Subsection 9.5.1, but in which the Stefan condition data $\mu_3(t)$ given by equation (9.4) is replaced by the second-order heat moment $\mu_6(t)$ given by equation (9.15) as

$$\mu_6(t) = \frac{e^{3t}}{2}(t^2 - 1 + 2\ln(2+t)), \quad t \in [0,1].$$

One can remark that conditions of Theorem 9.2 are satisfied and therefore, the local existence of a unique solution is guaranteed.

The analytical solution is the same as that given by equations (9.26) and (9.27). All the computational details are the same as for Example 1.

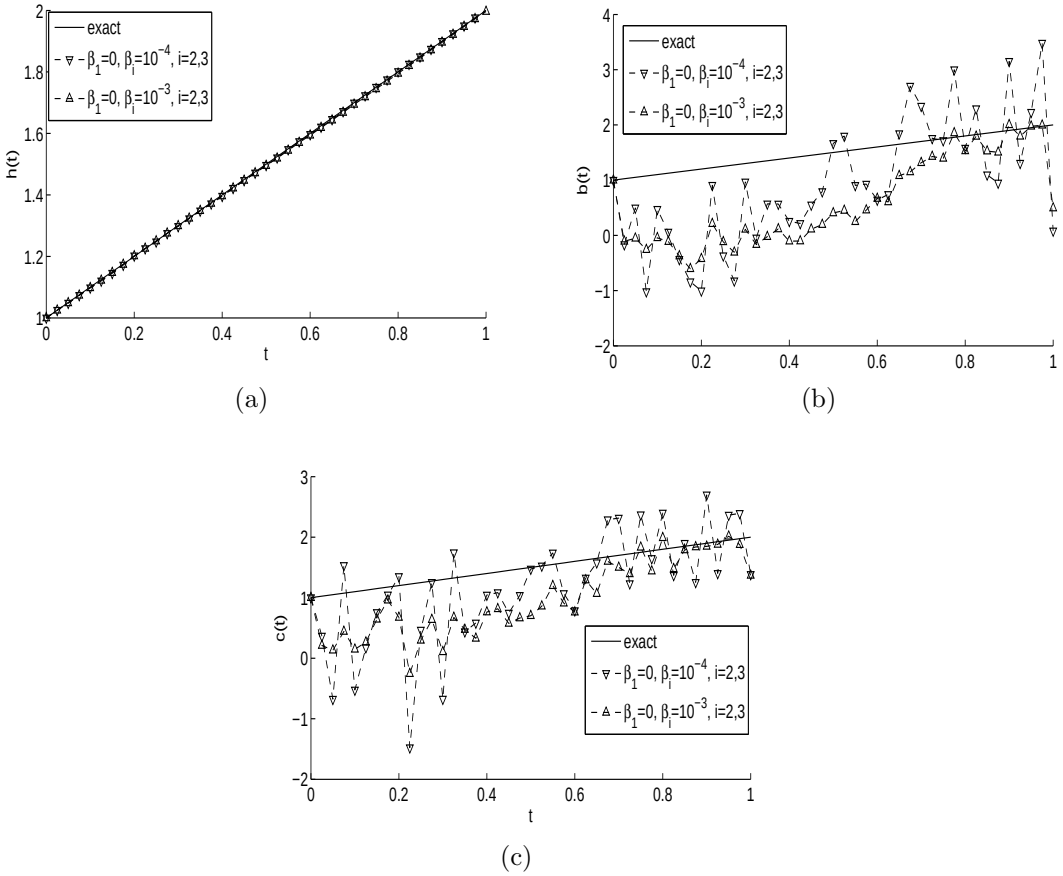

Figure 9.5: The exact and numerical solutions for: (a) the free boundary $h(t)$, (b) the coefficient $b(t)$, and (c) the coefficient $c(t)$, with $p = 0.1\%$ noise and regularization for Example 1.

As we did in Example 1, we start with the case of exact input data (9.11), (9.12) and (9.15), i.e. $p = 0$ in (9.22). The objective function (9.20), as a function of the number of iterations is displayed in Figure 9.6. From this figure it can be noticed that a monotonic convergence is rapidly achieved (in the early few iterations) and then turn to a steady slow convergence. The objective function (9.20) decreases and takes stationary values of $O(10^{-11})$ and $O(10^{-6})$ in about 401 and 112 iterations for $\beta_i = 0$, $i = 1, 2, 3$, and $\beta_1 = 0$, $\beta_2 = \beta_3 = 10^{-8}$, respectively. The numerical results for the unknown coefficients are illustrated in Figure 9.7. From this figure it can be noticed that, as in Example 1, a stable and very accurate recovery for the free boundary $h(t)$ is obtained with a small $rmse(h) = 0.001$. With no regularization, the numerical results for $b(t)$ and $c(t)$ are quite unstable and inaccurate with $rmse$ values of 0.5962 and 0.4279, respectively. However, when we apply the regularization with $\beta_1 = 0$, and $\beta_2 = \beta_3 = 10^{-8}$ to (9.20) we obtain more stable and accurate reconstructions for $b(t)$ and $c(t)$ with $rmse$ values decreasing to 0.2908 and 0.1838, respectively.

Next, we consider the case of noisy input data (9.11), (9.12) and (9.15) and perturb them with $p = 0.01\%$ as in (9.21). Remark that in Example 2 we include noise in all the input data μ_4, μ_5 and μ_6, whilst in Example 1 noise was included only in μ_4 and μ_5. Therefore, in Example 2 we take a smaller percentage of noise than in Example 1. In addition, the investigation of the inversion of noisy data performed in this subsection, when compared with that of Example 1, indicates that the second inverse problem (9.1)–(9.3), (9.5), (9.6) and (9.14) is more ill-posed than the first inverse problem (9.1)–(9.6). The case when no regularization is included, i.e. $\beta_i = 0$ for $i = 1, 2, 3$, is omitted since a similar unstable behaviour to Example 1 shown in Figures 9.4(b) and 9.4(c) was obtained. The regularized objective function (9.20) with $\beta_1 = 0$, $\beta_2 = \beta_3 = 10^{-6}$ shown in Figure 9.6 decreases rapidly and takes a stationary value of $O(10^{-3})$ in 63 iterations. With this selection of regularization parameters, the unknown coefficients are plotted in Figure 9.7 using the dashed line style (**- - -**). The coefficients are reconstructed with reasonable accuracy having the *rmse* values of 0.0022, 0.9498 and 0.6781 for $h(t)$, $b(t)$ and $c(t)$, respectively.

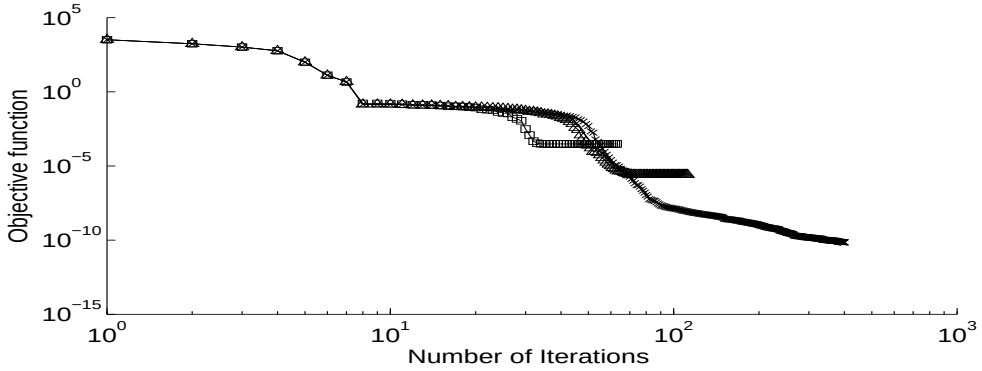

Figure 9.6: The objective function (9.20) with no regularization (-×-) and with regularization parameters $\beta_1 = 0$, $\beta_2 = \beta_3 = 10^{-8}$ (-△-), without noise for Example 2. We also include with (-□-) the results for $p = 0.01\%$ noise, with regularization parameters $\beta_1 = 0$, $\beta_2 = \beta_3 = 10^{-6}$.

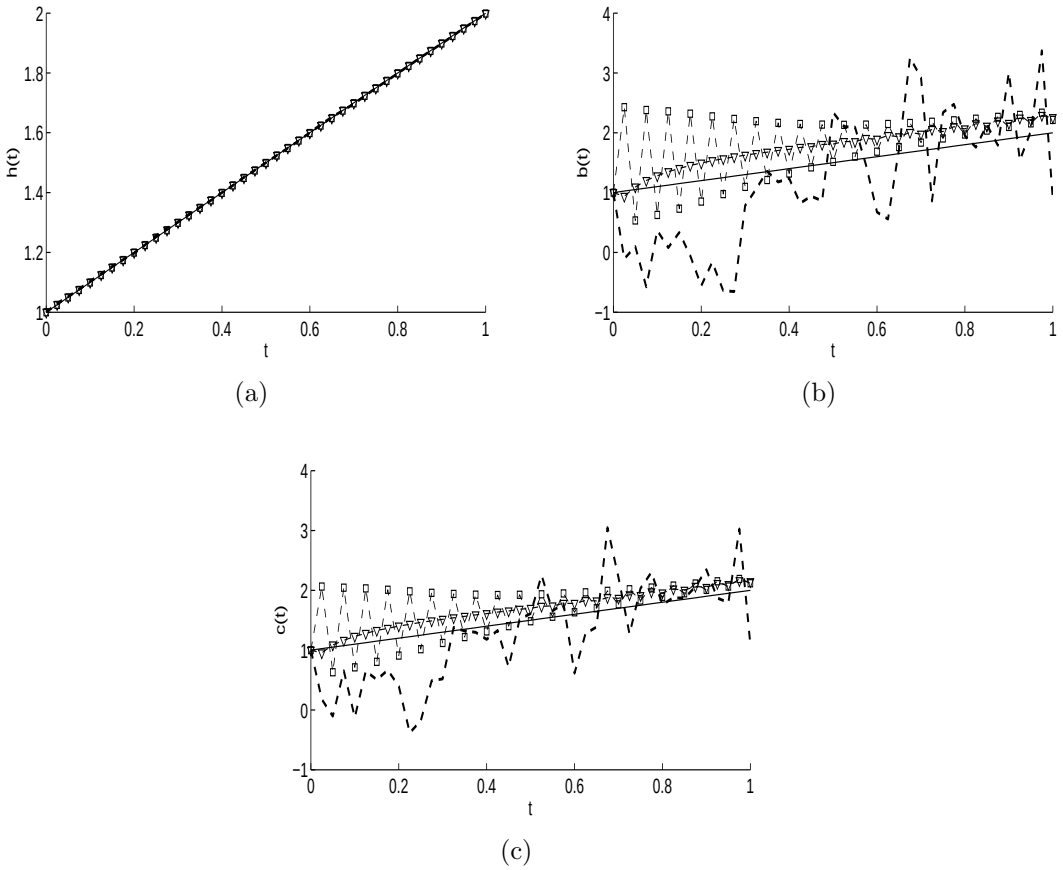

Figure 9.7: The exact (—) and numerical solutions with no regularization (-□-), and with regularization parameters $\beta_1 = 0$, $\beta_2 = \beta_3 = 10^{-8}$ (-△-) without noise for Example 2. We also include with (**- - -**) the numerical results for $p = 0.01\%$ noise with regularization parameters $\beta_1 = 0$, $\beta_2 = \beta_3 = 10^{-6}$ for: (a) the free boundary $h(t)$, (b) the coefficient $b(t)$, and (c) the coefficient $c(t)$.

The next section investigates inverse problems similar to those of Sections 9.2, 9.4 and 9.5, but in which the time-dependent thermal conductivity is an additional unknown.

9.6 Triple coefficient extension

Consider the one-dimensional time-dependent heat equation

$$u_t(x,t) = a(t)u_{xx}(x,t) + b(t)u_x(x,t) + c(t)u(x,t) + f(x,t),\ (x,t) \in \Omega \qquad (9.31)$$

for the unknown temperature $u(x,t)$ with unknown free smooth boundary $x = h(t) > 0$ and time-dependent coefficients $a(t) > 0$, $b(t)$ and $c(t)$. The initial and Dirichlet boundary conditions are (9.2) and (9.3), respectively, and the overdetermination conditions are (9.4)–(9.6), together with the heat flux specification

at $x = 0$, namely,

$$-a(t)u_x(0,t) = \tilde{\mu}_3(t), \quad t \in [0,T]. \tag{9.32}$$

As in Section 9.2, by performing the change of variable $y = x/h(t)$ we reduce the problem (9.2)–(9.6), (9.31) and (9.32) to the inverse problem for the unknowns $h(t)$, $a(t)$, $b(t)$, $c(t)$ and $v(y,t) := u(yh(t),t)$ given by:

$$v_t(y,t) = \frac{a(t)}{h^2(t)}v_{yy}(y,t) + \frac{b(t)+yh'(t)}{h(t)}v_y(y,t) + c(t)v(y,t) + f(yh(t),t), \quad (y,t) \in Q_T, \tag{9.33}$$

equations (9.8)–(9.12) and

$$-\frac{a(t)v_y(0,t)}{h(t)} = \tilde{\mu}_3(t), \quad t \in [0,T]. \tag{9.34}$$

A slightly corrected version of the theorem proved in [113] which ensures the unique solvability (locally in time) for the inverse problem (9.8)–(9.12), (9.33) and (9.34), has been provided in [60].

Theorem 9.3. *Suppose that:*
$0 \leq f \in C^{1,0}([0,\infty) \times [0,T])$, $0 < \mu_i \in C^1[0,T]$ *for* $i = 1,2,4,5$, $\mu_3 \in C[0,T]$, $0 > \tilde{\mu}_3 \in C[0,T]$, $0 < \phi \in C^2[0,h_0]$, $\phi' > 0$,

$$(\ln \phi)'' \neq 0, \tag{9.35}$$

the compatibility conditions of the zero order:

$\phi(0) = \mu_1(0)$, $\phi(h_0) = \mu_2(0)$, $\int_0^{h_0} \phi(x)dx = \mu_4(0)$, $\int_0^{h_0} x\phi(x)dx = \mu_5(0)$,
and of the first-order:

$$\left.\begin{aligned} \mu_1'(0) &= a(0)\phi''(0) + b(0)\phi'(0) + c(0)\phi(0) + f(0,0), \\ \mu_2'(0) &= a(0)\phi''(h_0) + b(0)\phi'(h_0) + c(0)\phi(h_0) + f(h_0,0), \end{aligned}\right\} \tag{9.36}$$

are satisfied. Then, there is $T_0 \in (0,T]$, *such that there exists a unique solution* $(h(t), a(t), b(t), c(t), v(y,t)) \in C^1[0,T_0] \times (C[0,T_0])^3 \times C^{2,1}(\overline{Q}_{T_0})$, $h(t) > 0$, $a(t) > 0$ *for* $t \in [0,T_0]$, *of the inverse problem (9.8)–(9.12), (9.33) and (9.34).*

Remark. We can obtain the values of $a(0)$, $b(0)$ and $c(0)$ directly from equations (9.32) and (9.36). First, from (9.32) applied at $t = 0$ we have

$$a(0) = -\frac{\tilde{\mu}_3(0)}{\phi'(0)}. \tag{9.37}$$

Then, introducing (9.37) into (9.36) and solving the resulting system of equations for $b(0)$ and $c(0)$ we obtain

$$b(0) = \frac{\phi(h_0)\left(\mu_1'(0) + \frac{\tilde{\mu}_3(0)\phi''(0)}{\phi'(0)} - f(0,0)\right) - \phi(0)\left(\mu_2'(0) + \frac{\tilde{\mu}_3(0)\phi''(h_0)}{\phi'(0)} - f(h_0,0)\right)}{\phi(0)\phi(h_0)\left(\frac{\phi'(0)}{\phi(0)} - \frac{\phi'(h_0)}{\phi(h_0)}\right)}, \tag{9.38}$$

$$c(0) = \frac{\phi'(0)\left(\mu_2'(0) + \frac{\tilde{\mu}_3(0)\phi''(h_0)}{\phi'(0)} - f(h_0,0)\right) - \phi'(h_0)\left(\mu_1'(0) + \frac{\tilde{\mu}_3(0)\phi''(0)}{\phi'(0)} - f(0,0)\right)}{\phi(0)\phi(h_0)\left(\frac{\phi'(0)}{\phi(0)} - \frac{\phi'(h_0)}{\phi(h_0)}\right)}. \tag{9.39}$$

One can easily remark that the conditions on ϕ given in Theorem 9.3 ensure that expressions (9.38) and (9.39) are well-defined. In particular, condition (9.35) implies that the function ϕ'/ϕ is strictly monotone.

9.6.1 Another related inverse problem formulation

It was point out in [73] that the Stefan condition (9.4), or (9.10), may be replaced by the second-order heat moment measurement (9.14), or (9.15), respectively. Then we have the following local existence and uniqueness theorem, see [73] with appropriate corrections.

Theorem 9.4. *Let the assumptions of Theorem 9.3 be satisfied, except for the condition on μ_3 being replaced by the condition $0 < \mu_6 \in C^1[0,T]$. Then, there exists $T_0 \in (0,T]$, such that there exists a unique solution $(h(t), a(t), b(t), c(t), v(y,t)) \in C^1[0,T_0] \times (C[0,T_0])^3 \times C^{2,1}(\overline{Q}_{T_0})$, $h(t) > 0$, $a(t) > 0$ for $t \in [0,T_0]$, of the inverse problem (9.8), (9.9), (9.11), (9.12), (9.33) and (9.34).*

9.6.2 Numerical implementation, results and discussion

The solution of the direct problem is based on the same FDM described in Section 9.3 with the simplification that the thermal conductivity coefficient a depends now on t only. For the inverse problems under investigation in Section 9.6 we

minimize the functionals

$$\tilde{F}(\underline{h},\underline{a},\underline{b},\underline{c}) = \sum_{j=1}^{N}\Big[\frac{a_j v_y(0,t_j)}{h_j} + \tilde{\mu}_3(t_j)\Big]^2 + \sum_{j=1}^{N}\Big[h_j' + \frac{v_y(1,t_j)}{h_j} - \mu_3(t_j)\Big]^2$$
$$+ \sum_{j=1}^{N}\Big[h_j\int_0^1 v(y,t_j)dy - \mu_4(t_j)\Big]^2 + \sum_{j=1}^{N}\Big[h_j^2\int_0^1 y^2 v(y,t_j)dy - \mu_5(t_j)\Big]^2$$
$$+ \beta_1\sum_{j=1}^{N}h_j^2 + \beta_2\sum_{j=1}^{N}a_j^2 + \beta_3\sum_{j=1}^{N}b_j^2 + \beta_4\sum_{j=1}^{N}c_j^2, \tag{9.40}$$

and

$$\tilde{F}_1(\underline{h},\underline{a},\underline{b},\underline{c}) = \sum_{j=1}^{N}\Big[\frac{a_j v_y(0,t_j)}{h_j} + \tilde{\mu}_3(t_j)\Big]^2 + \sum_{j=1}^{N}\Big[h_j\int_0^1 v(y,t_j)dy - \mu_4(t_j)\Big]^2$$
$$+ \sum_{j=1}^{N}\Big[h_j^2\int_0^1 y v(y,t_j)dy - \mu_5(t_j)\Big]^2 + \sum_{j=1}^{N}\Big[h_j^3\int_0^1 y^2 v(y,t_j)dy - \mu_6(t_j)\Big]^2$$
$$+ \beta_1\sum_{j=1}^{N}h_j^2 + \beta_2\sum_{j=1}^{N}a_j^2 + \beta_3\sum_{j=1}^{N}b_j^2 + \beta_4\sum_{j=1}^{N}c_j^2. \tag{9.41}$$

The minimization of $\tilde{F}$ and $\tilde{F}_1$ subject to the physical constraints $\underline{h} > \underline{0}$ and $\underline{a} > \underline{0}$ are preformed using the MATLAB optimization toolbox routine *lsqnonlin*, as described in Section 9.4. We also add noise in the heat flux (9.34), as described at the end of Section 9.4.

9.6.2.1 Example 3

We consider first the inverse problem (9.2)–(9.6), (9.31) and (9.32) with unknown coefficients $h(t)$, $a(t)$, $b(t)$ and $c(t)$, and solve this problem with the following input data:

$$\phi(x) = u(x,0) = (1+x)^2,\ \mu_1(t) = u(0,t) = 1+t,\ \mu_2(t) = u(h(t),t)$$
$$= (1+t)(2+t)^2,\ \tilde{\mu}_3(t) = -a(t)u_x(0,t) = -2(1+t)^2,\ \mu_3(t) = h'(t) + u_x(h(t),t)$$
$$= 1 + 2(1+t)(2+t),\ \mu_4(t) = \int_0^{h(t)} u(x,t)dx = \frac{1}{3}(1+t)^2(7+5t+t^2),$$
$$\mu_5(t) = \int_0^{h(t)} xu(x,t)dx = \frac{1}{12}(1+t)^3(17+14t+3t^2)$$
$$f(x,t) = 2+5t+4t^2+6x+12tx+8t^2x+2x^2+3tx^2+2t^2x^2,\ h_0 = 1,\ T = 1.$$

One can remark that the conditions of Theorem 9.3 are satisfied and hence, the local unique solvability of the inverse problem holds. With the data above, the

analytical solution is given by

$$h(t) = 1 + t, \quad a(t) = 1 + t, \quad b(t) = -1 - 2t, \quad c(t) = -1 - 2t, \tag{9.42}$$

$$u(x, t) = (1 + t)(1 + x)^2. \tag{9.43}$$

Then, (9.42) and

$$v(y, t) = u(yh(t), t) = (1 + t)(1 + y + yt)^2, \tag{9.44}$$

is the analytical solution of the problem (9.8)–(9.12), (9.33) and (9.34).

The initial guess for the vectors $\underline{h}$, $\underline{a}$, $\underline{b}$ and $\underline{c}$ are taken as $\underline{1}$, $\underline{1}$, $\underline{-1}$ and $\underline{-1}$, respectively.

We start the numerical discussion with the case of exact data, i.e. $p = 0$ in (9.22). The objective function (9.40), as a function of the number of iterations, is shown in Figure 9.8. From this figure it can be seen that a monotonic convergence is achieved in 50 iterations if no regularization is applied. The unregularized objective function (9.40) decreases rapidly in the first 10 iterations and then steadily reaches a stationary low value of $O(10^{-16})$. The numerical results for the unknowns coefficients $h(t)$, $c(t)$, $b(t)$ and $c(t)$ are represented in Figures 9.9(a)–(d) by the (−x−) lines. From these figures it can be observed that we obtain accurate and stable reconstructions for free boundary $h(t)$ and the thermal conductivity $a(t)$, whilst for the coefficients $b(t)$ and $c(t)$ some very slight instabilities appear. Consequently, we do not need to regularize $h(t)$ and $a(t)$ and therefore, we are take $\beta_1 = \beta_2 = 0$ in (9.40) and apply the Tikhonov regularization method with some small regularization parameters $\beta_3 = \beta_4 = 10^{-5}$. The accurate and stable numerically obtained results are shown in Figures 9.9(a)–(d) by the (-□-) line. The regularized objective function (9.40) for this case is also plotted in Figure 9.8 and a rapid monotone convergence is obtained in 26 iterations. A summary of all details is presented in Table 9.2, where the $rmse(a)$ is defined, similarly as in (9.23)–(9.25), as

$$rmse(a) = \sqrt{\frac{T}{N} \sum_{j=1}^{N} (a_{numerical}(t_j) - a_{exact}(t_j))^2}. \tag{9.45}$$

Table 9.2: Number of iterations, number of function evaluations, value of the objective function (9.40) at final iteration, *rmse* values (9.23)-(9.25) and (9.45), and the computational time, without noise for Example 3.

$\beta_1 = \beta_2 = 0$	$\beta_3 = \beta_4 = 0$	$\beta_3 = \beta_4 = 10^{-5}$
No. of iterations	50	26
No. of function evaluations	8415	4455
Value of objective function (9.40) at final iteration	6.2E-16	0.0035
$rmse(h)$	3.3E-4	3.3E-4
$rmse(a)$	0.0021	0.0021
$rmse(b)$	0.0333	0.0207
$rmse(c)$	0.0335	0.0149
Computational time	90 min	50 min

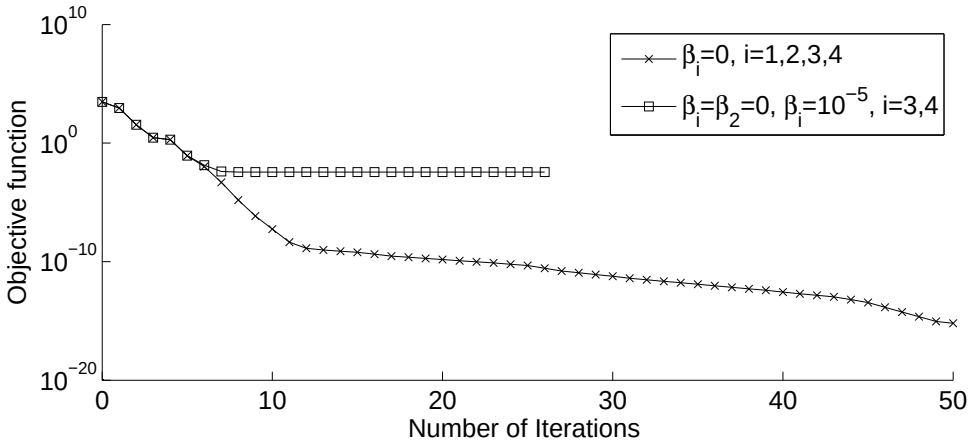

Figure 9.8: The objective function (9.40) without noise for Example 3.

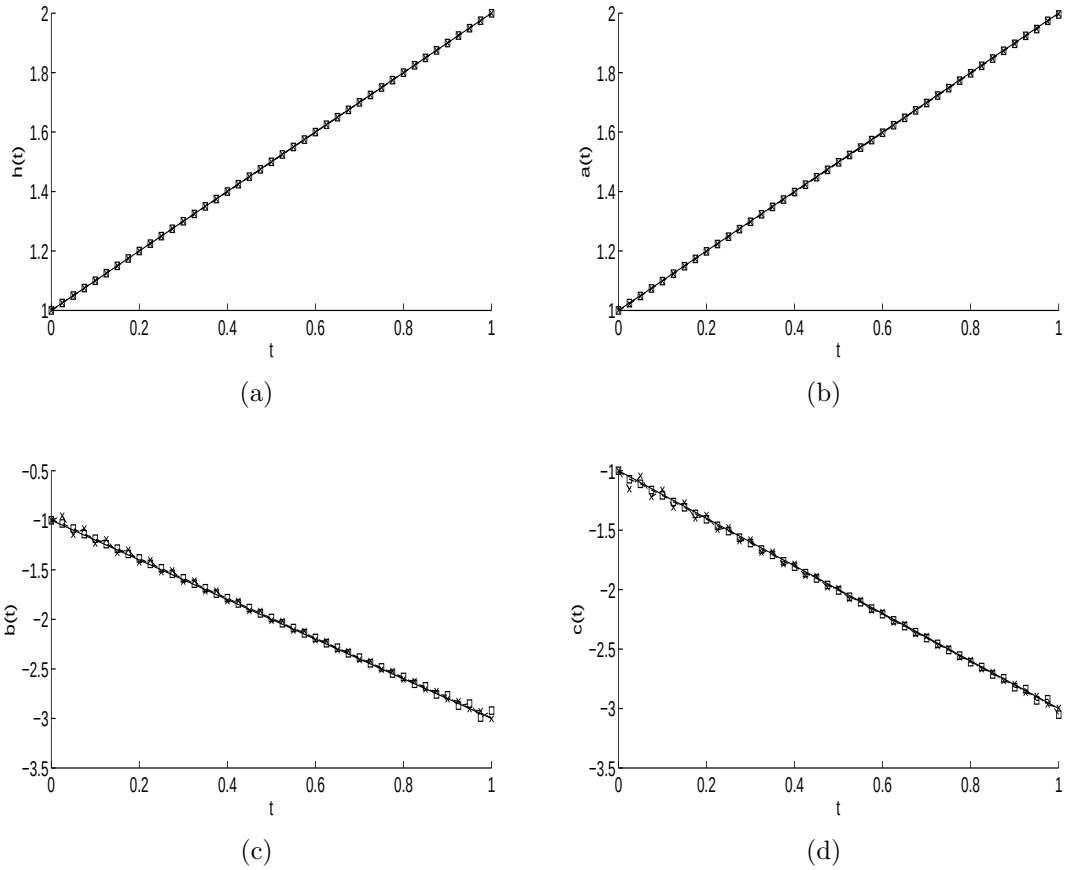

Figure 9.9: The exact (—) and numerical solutions (−x−) without regularization, and (−□−) with regularization parameters $\beta_1 = \beta_2 = 0$, and $\beta_3 = \beta_4 = 10^{-5}$ for: (a) the free boundary $h(t)$, (b) the coefficient $a(t)$, (c) the coefficient $b(t)$, and (d) the coefficient $c(t)$, without noise for Example 3.

Next, we investigate the stability of the numerical solution with respect to some small percentage $p = 0.1\%$ of noise included in the input data $\tilde{\mu}_3(t)$, $\mu_4(t)$ and $\mu_5(t)$. The objective function (9.40), as a function of the number of iterations in the case of no regularization employed is plotted in Figure 9.10. Form this figure it can be noticed that a monotonic decreasing convergence is achieved and the minimization process stops when the allowed tolerance is reached. On the other hand, the numerical solutions for the unknown coefficients plotted in Figure 9.11 are oscillatory and highly unstable except for the free boundary $h(t)$ which is accurate and stable. There is also some slight instability manifested in Figure 9.11(b) in estimating the coefficient $a(t)$, but the magnitude of these oscillations is significantly much smaller than the highly unbounded and unstable behaviour shown in Figures 9.11(c) and 9.11(d) illustrating the estimation of the unregularized coefficients $b(t)$ and $c(t)$, respectively. As a result, we can take $\beta_1 = \beta_2 = 0$ and then minimize (9.40) with various regularization parameters

$\beta_3 = \beta_4 \in \{10^{-4}, 10^{-3}, 10^{-2}\}$. Figure 9.12 shows the rapid monotonic decreasing convergence of the regularized objective function, as the number of iterations increases. The corresponding numerical results for the unknown time-dependent coefficients are shown in Figures 9.13. A summary of the computational details, as well as the *rmse* errors are included in Table 9.3. Overall, by comparing Figures 9.11 and 9.13 it can be observed some remarkable stability restored through the inclusion of regularization. It is also interesting to remark that although we take $\beta_2 = 0$ and hence we do not penalise the coefficient $a(t)$ in (9.40), some of the regularization of the other two coefficients $b(t)$ and $c(t)$ is transferred to the former unregularized coefficient $a(t)$, compare Figures 9.11(b) and 9.13(b).

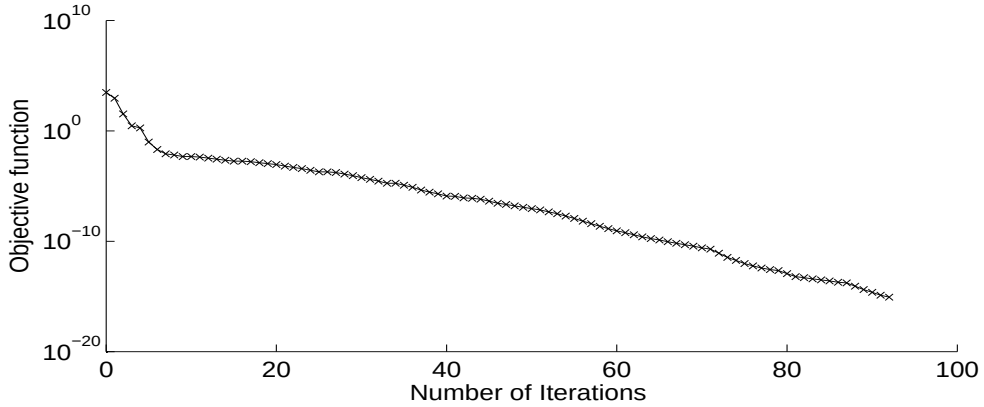

Figure 9.10: The objective function (9.40) with $p = 0.1\%$ noise and no regularization for Example 3.

Table 9.3: Number of iterations, number of function evaluations, value of the objective function (9.40) at final iteration, *rmse* values (9.23)-(9.25) and (9.45), and the computational time, for $p = 0.1\%$ noise for Example 3.

β_1=β_2=0	β_3=β_4=0	β_3=β_4=10^{-4}	β_3=β_4=10^{-3}	β_3=β_4=10^{-2}
No. of iterations	92	27	25	30
No. of function evaluations	15354	4620	4290	5115
Value of objective function (9.40) at final iteration	8.4E-16	0.0449	0.3660	3.5102
$rmse(h)$	0.0043	0.0026	0.0022	0.0032
$rmse(a)$	0.2508	0.0487	0.0253	0.0398
$rmse(b)$	8.3489	0.5420	0.1991	0.2276
$rmse(c)$	7.8212	0.4354	0.1563	0.1646
Computational time	168 min	52 min	48 min	58 min

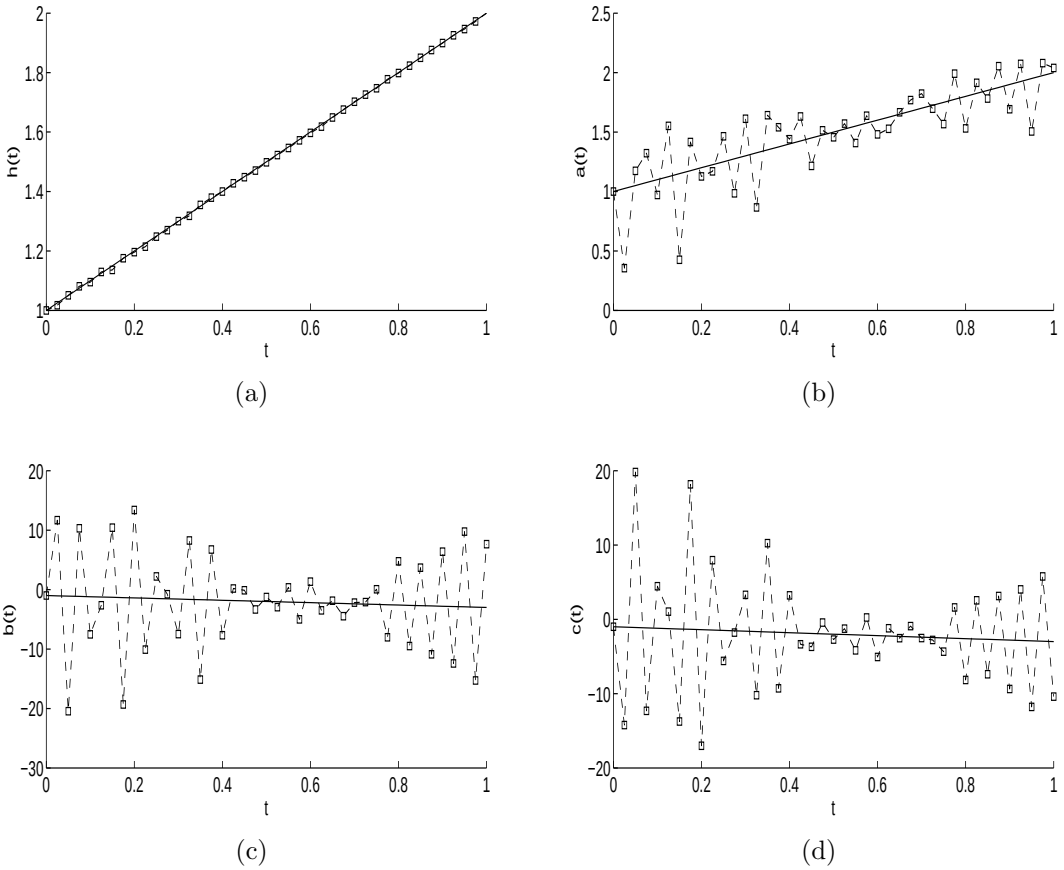

Figure 9.11: The exact (—) and numerical solution ($-\square-$) for: (a) the free boundary $h(t)$, (b) the coefficient $a(t)$, (c) the coefficient $b(t)$, and (d) the coefficient $c(t)$, with $p = 0.1\%$ noise and no regularization for Example 3.

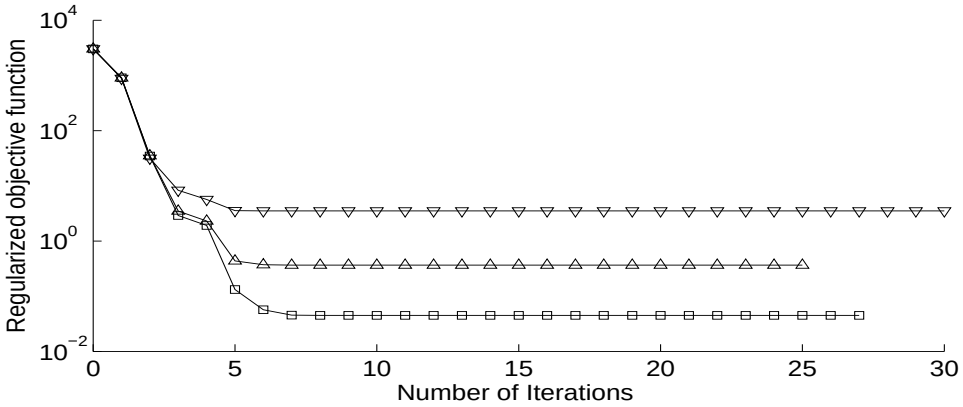

Figure 9.12: The regularized objective function (9.40), with regularization parameters $\beta_1 = \beta_2 = 0$, and $\beta_i = 10^{-4}$ $(-\square-)$, $\beta_i = 10^{-3}$ $(-\bigtriangledown-)$, $\beta_i = 10^{-2}$ $(-\bigtriangleup-)$, $i = 3, 4$, with $p = 0.1\%$ noise for Example 3.

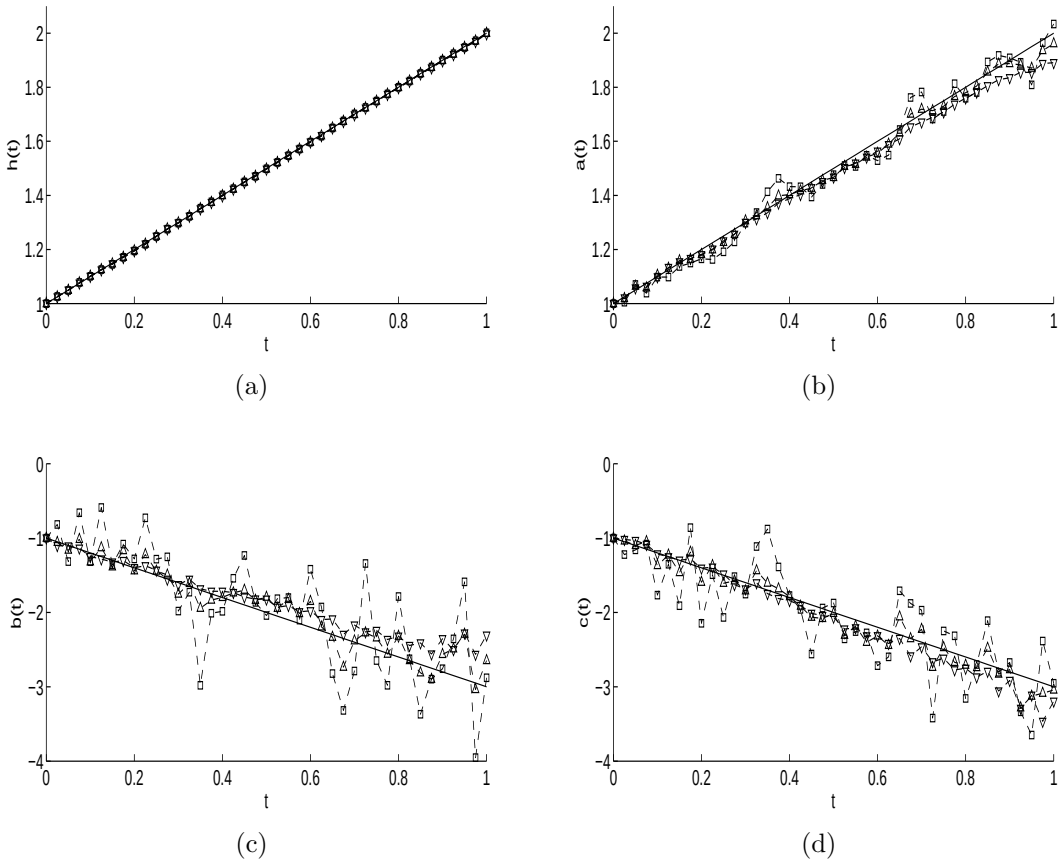

Figure 9.13: The exact (—) and numerical solutions for: (a) the free boundary $h(t)$, (b) the coefficient $a(t)$, (c) the coefficient $b(t)$, and (d) the coefficient $c(t)$, with regularization parameters $\beta_1 = \beta_2 = 0$, and $\beta_i = 10^{-4}$ $(-\square-)$, $\beta_i = 10^{-3}$ $(-\bigtriangledown-)$, $\beta_i = 10^{-2}$ $(-\bigtriangleup-)$, $i = 3, 4$, with $p = 0.1\%$ noise for Example 3.

9.6.2.2 Example 4

Consider now the second inverse problem given by equations (9.2), (9.3), (9.5), (9.6), (9.14), (9.31) and (9.32) with unknown coefficients $h(t)$, $a(t)$, $b(t)$ and $c(t)$, and solve this problem with the same input data as in Example 3 but replacing $\mu_3(t)$ by $\mu_6(t)$ given by

$$\mu_6(t) = \int_0^{h(t)} x^2 u(x,t)dx = \frac{1}{30}(1+t)^4(31+27t+6t^2), \quad t \in [0,1].$$

One can remark that the conditions of Theorem 9.4 are satisfied hence, the unique local solvability of solution holds. The analytical solution is given by equations (9.42) and (9.43). All the computational details and numerical representation are the same as those for Example 3 except that noise is now included in the input data $\mu_6(t)$, as well. Figures 9.14–9.19, and Tables 9.4 and 9.5 represent/ illustrate analogous quantities as Figures 9.8–9.13 and Tables 9.2 and 9.3 for Example 3

and similar conclusions can be obtained.

It is also possible to compare, at least for the case without noise, the level of information provided to the inverse problem by the Stefan condition (9.4) in comparison with the second-order heat moment specification (9.14). Indeed, by comparing Figure 9.8 and Table 9.2 with Figure 9.14 and Table 9.4, respectively, it can be seen that the rate of convergence is much higher for Example 3 than for Example 4. Moreover, the computational time required to achieve the converge of the objective functions (9.40) and (9.41) is much higher for Example 4 than for Example 3. Finally, by comparing the accuracy of the numerical results presented in Figure 9.9 and Table 9.2 of Example 3 with Figure 9.15 and Table 9.4 of Example 4, respectively, one can clearly conclude that the Stefan condition (9.4) provides significantly more information than the second-order heat moment specification (9.14), especially in predicting the coefficients $b(t)$ and $c(t)$. Similar considerations can also be made for the case of $p = 0.1\%$ noisy data, by comparing Figures 9.10–9.13 and Table 9.3 of Example 3 with Figures 9.16–9.19 and Table 9.5 of Example 4, but this comparison is less reliable because in the latter example we include noise in all the four input data $\tilde{\mu}_3$, μ_4, μ_5 and μ_6, whilst in the former example we include noise only in three input data $\tilde{\mu}_3$, μ_4 and μ_5, having the forth one μ_3 uncontaminated.

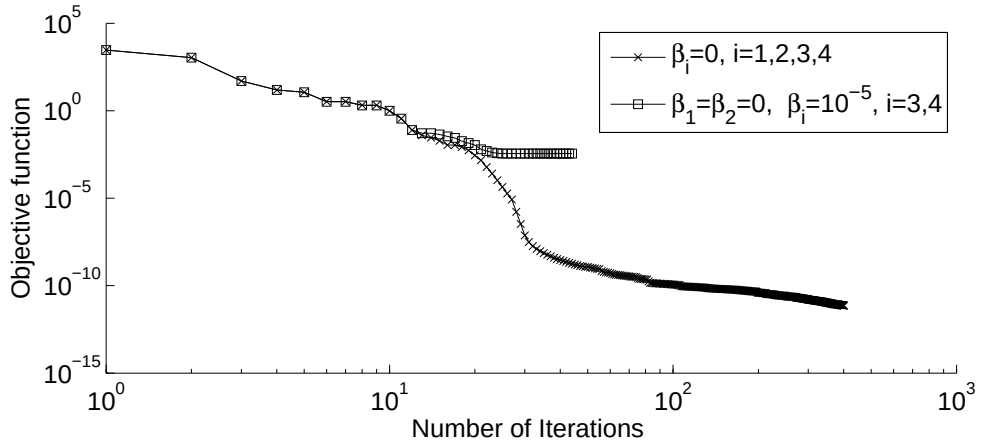

Figure 9.14: The objective function (9.41) without noise for Example 4.

Table 9.4: Number of iterations, number of function evaluations, value of the objective function (9.41) at final iteration, *rmse* values (9.23)-(9.25) and (9.45), and the computational time with no noise for Example 4.

$\beta_1 = \beta_2 = 0$	$\beta_3 = \beta_4 = 0$	$\beta_3 = \beta_4 = 10^{-5}$
No. of iterations	401	44
No. of function evaluations	66330	7425
Value of objective function (9.41) at final iteration	7.2E-12	0.0035
$rmse(h)$	6.1E-4	5.9E-4
$rmse(a)$	0.0058	0.0048
$rmse(b)$	0.1289	0.0847
$rmse(c)$	0.1672	0.0999
Computational time	23 hours	138 min

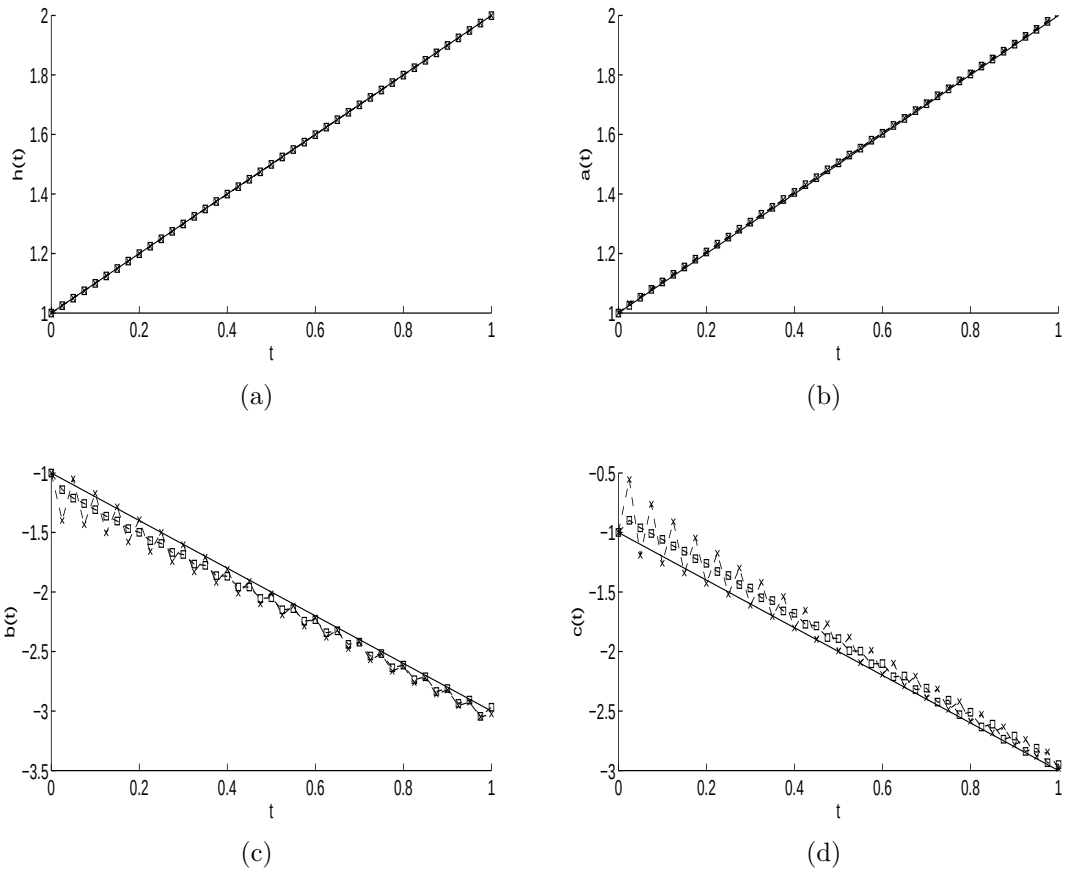

Figure 9.15: The exact (—) and numerical solutions (−x−) without regularization, and (−□−) with regularization parameters $\beta_1 = \beta_2 = 0$, and $\beta_3 = \beta_4 = 10^{-5}$ for: (a) the free boundary $h(t)$, (b) the coefficient $a(t)$, (c) the coefficient $b(t)$, and (d) the coefficient $c(t)$, without noise for Example 4.

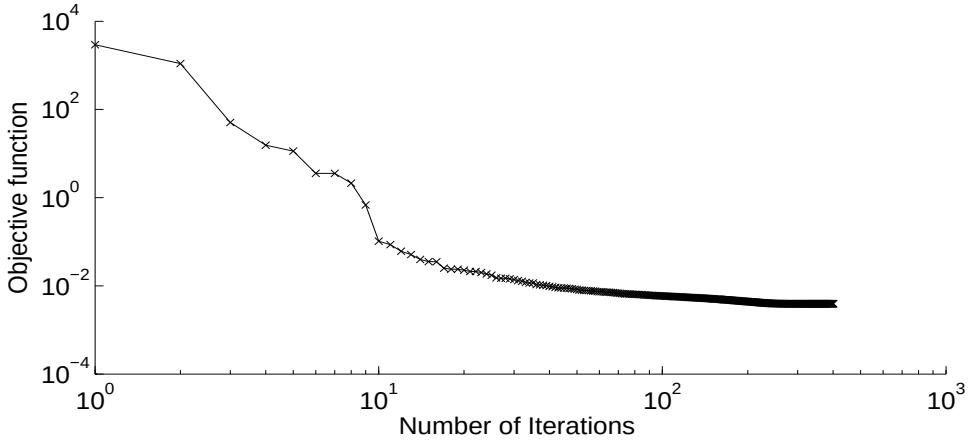

Figure 9.16: The objective function (9.41) with $p = 0.1\%$ noise and no regularization for Example 4.

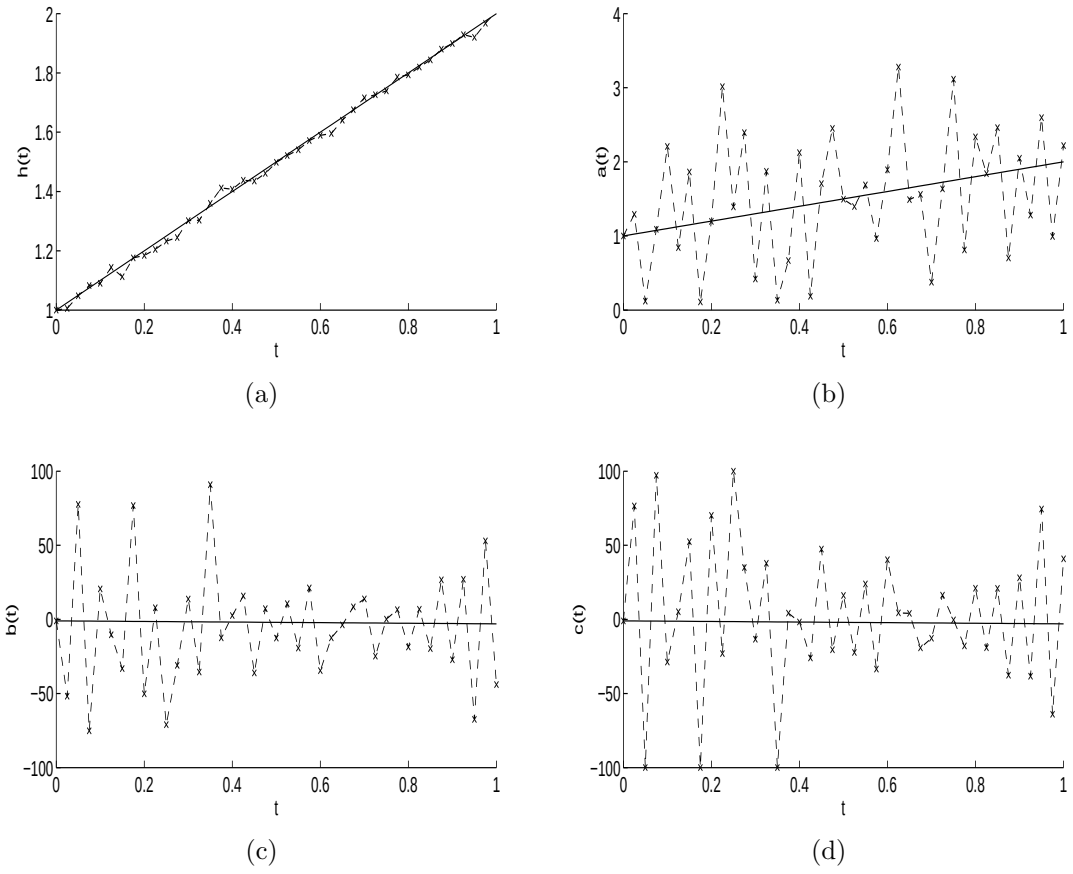

(a) (b) (c) (d)

Figure 9.17: The exact (—) and numerical solutions (−x−) without regularization for: (a) the free boundary $h(t)$, (b) the coefficient $a(t)$, (c) the coefficient $b(t)$, and (d) the coefficient $c(t)$, with $p = 0.1\%$ noise for Example 4.

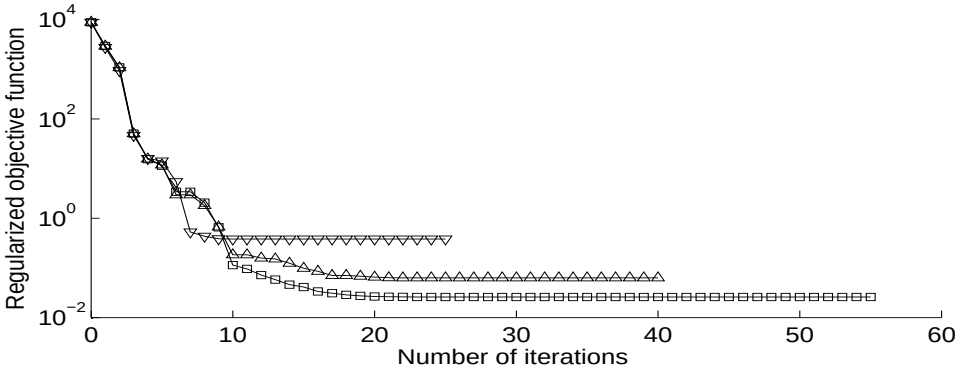

Figure 9.18: The regularized objective function (9.41), with regularization parameters $\beta_1 = \beta_2 = 0$, and $\beta_i = 10^{-5}$ (-□-), $\beta_i = 10^{-4}$ (-△-), $\beta_i = 10^{-3}$ (-▽-), $i = 3, 4$, with $p = 0.1\%$ noise for Example 4.

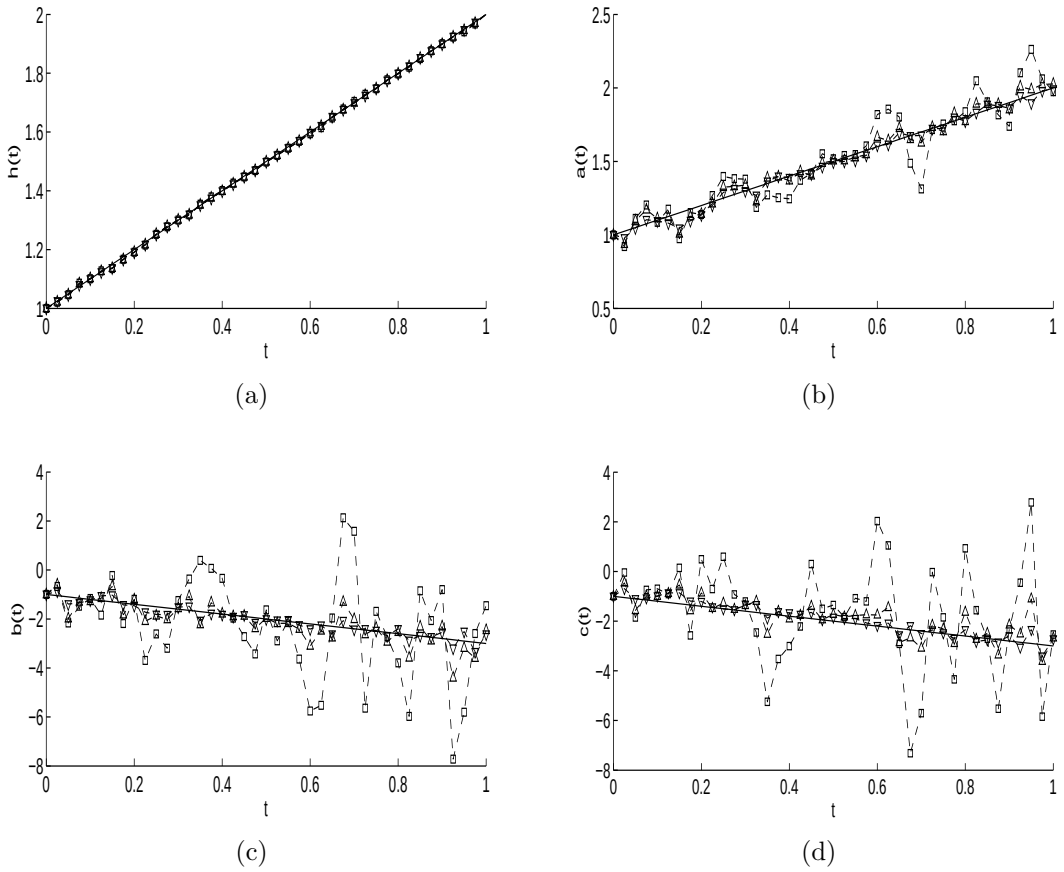

(a) (b) (c) (d)

Figure 9.19: The exact (—) and numerical solutions for: (a) the free boundary $h(t)$, (b) the coefficient $a(t)$, (c) the coefficient $b(t)$, and (d) the coefficient $c(t)$, with regularization parameters $\beta_1 = \beta_2 = 0$, and $\beta_i = 10^{-5}$(-□-), $\beta_i = 10^{-4}$ (-△-), $\beta_i = 10^{-3}$ (-▽-), $i = 3, 4$, with $p = 0.1\%$ noise for Example 4.

Table 9.5: Number of iterations, number of function evaluations, value of the objective function (9.41) at final iteration, *rmse* values (9.23)-(9.25) and (9.45), and computational time, for $p = 0.1\%$ noise for Example 4.

β_1=0, β_2=0	β_3=β_4=0	β_3=β_4=10^{-5}	β_3=β_4=10^{-4}	β_3=β_4=10^{-3}
No. of iterations	401	55	40	25
No. of function evaluations	66330	9240	6765	5610
Value of objective function (9.41) at final iteration	0.0039	0.0260	0.0632	0.3820
$rmse(h)$	0.0156	0.0055	0.0044	0.0041
$rmse(a)$	0.8098	0.1338	0.0535	0.0354
$rmse(b)$	37.739	1.9712	0.5126	0.2073
$rmse(c)$	48.118	2.1369	0.5245	0.2218
Computational time	24 hours	150 min	81 min	48 min

9.7 Conclusions

In this chapter, a numerical investigation for the recovery of multiple time-dependent coefficients entering the parabolic heat equation with a free boundary has been presented. The moving boundary value problem has been first transformed, by a simple change of variables, to a problem formulated in a fixed domain. The analysis can also be extended to the case when both sides of the finite slab are free, [111, 114].

Numerically, we discretised the governing equation using the FDM and solved the inverse problem as a constrained regularized minimization using the MATLAB optimization routine *lsqnonlin*. Notably, we report that the inclusion of regularization, apart from restoring the stability of the numerical solution, it also reduces the computational time for the minimization using the *lsqnonlin* routine from several hours to several minutes, see Tables 9.1, 9.4 and 9.5. Numerical results presented and discussed for several test examples show that accurate and stable numerical solutions have been achieved. It is also interesting to conclude that, based on the comparison between the Examples 3 and 4, the Stefan condition (9.4) contains more information than the second-order moment (9.14).

Chapter 10

Identification of a heterogeneous orthotropic conductivity in a rectangular domain

10.1 Introduction

The determination of coefficients in inverse heat conduction problems for the parabolic heat equation, [70], continues to receive significant attention in a variety of fields, such as heat transfer, oil recovery, groundwater flow, and finance. Some researchers investigated the case of simultaneous identification of coefficients in two-dimensional heat conduction problems, [23, 24, 124].

The identification of physical properties such as thermal conductivity using measured temperature or heat flux values at wall sites is an important inverse problem. A common identification strategy is the indirect one where one can minimize the gap between a computed solution and the measured data (observations) via an iterative process, [115].

The main obstacle in this kind of problem is that there are usually so few observations that one finds hard to evaluate the spatial derivative of temperature by simple numerical differentiation. Therefore, heavier and more time-consuming optimization techniques are needed to obtain reliable results.

The estimation of thermal properties for the multi-dimensional inhomogeneous and anisotropic media is rather scarce in the literature [17, 86]. The aim of this chapter is to consider a two-dimensional coefficient identification problem to estimate the space and time varying principal direction components of an orthotropic conductivity in a rectangular domain.

The structure of the chapter is as follows. In Section 10.2 we give the mathematical formulation of the two-dimensional inverse problem and state its unique

solvability. In Section 10.3 we briefly describe the explicit FDM used to discretise the direct problem, whilst Section 10.4 introduces the constrained nonlinear minimization problem that has to be solved using the MATLAB routine *lsqnonlin*. In Section 10.5, numerical results are presented and discussed and finally conclusions are given in Section 10.6.

10.2 Statement of the inverse problem

Consider the nonlinear inverse coefficient identification problem which requires determining the principal direction components $a(y,t) > 0$ and $b(x,t) > 0$ of the two-dimensional heterogeneous orthotropic rectangular medium $D = (0,h)\times(0,\ell)$ together with the temperature $u(x,y,t)$ satisfying the heat equation

$$u_t = a(y,t)u_{xx} + b(x,t)u_{yy} + f(x,y,t), \quad (x,y,t) \in Q_T := D \times (0,T), \quad (10.1)$$

where f is a given heat source, subject to initial, boundary and overdetermination conditions

$$u(x,y,0) = \phi(x,y), \quad (x,y) \in \overline{D}, \quad (10.2)$$

$$u(0,y,t) = \mu_1(y,t), \quad u(h,y,t) = \mu_2(y,t), \quad (y,t) \in [0,l] \times [0,T], \quad (10.3)$$

$$u(x,0,t) = \mu_3(x,t), \quad u(x,l,t) = \mu_4(x,t), \quad (x,t) \in [0,h] \times [0,T], \quad (10.4)$$

$$a(y,t)u_x(0,y,t) = \mu_5(y,t), \quad (y,t) \in [0,l] \times [0,T], \quad (10.5)$$

$$b(x,t)u_y(x,0,t) = \mu_6(x,t), \quad (x,t) \in [0,h] \times [0,T]. \quad (10.6)$$

In the above setting one can see that Cauchy data are prescribed over the boundaries $x = 0$ and $y = 0$. Also by restricting the conductivity components $a(y,t)$ and $b(x,t)$ be independent of x and y, respectively, it then makes sense to study the injectivity/surjectivity of the mapping $(a,b) \mapsto (\mu_5,\mu_6)$. We finally mention that in the general case when $a(x,y,t)$ and $b(x,y,t)$ depend on all coordinates then the right hand side of (10.1) modifies as $(a(x,y,t)u_x)_x + (b(x,y,t)u_y)_y + f(x,y,t)$.

There is no theory available for this general orthotropic inverse coefficient identification, but at least in the isotropic case when $a = b$, all the knowledge of the temperature $u(x,y,t)$ for $(x,y,t) \in Q_T$ is necessary in order to render a unique solution, [49]. All this discussion warrants and justifies our assumption that $a(y,t)$ and $b(x,t)$ are independent on the variables x and y, respectively. Then, the measurements (10.5) and (10.6) are supplied as the correct traces of functionals, according to the illuminating discussion of Cannon et al. [15].

Suppose that the following assumptions hold:

(A1) $\phi \in C^{2+\gamma}(\overline{D})$, $\mu_i \in C^{2+\gamma,1+\gamma/2}([0,l]\times[0,T])$, $i \in \{1,2\}$, $\mu_k \in C^{2+\gamma,1+\gamma/2}([0,h] \times[0,T])$, $k \in \{3,4\}$, $\mu_5 \in C^{\gamma,\gamma/2}([0,l] \times [0,T])$, $\mu_6 \in C^{\gamma,\gamma/2}([0,h] \times [0,T])$, $f \in C^{\gamma,\gamma/2}(\overline{Q}_T)$ for some $\gamma \in (0,1)$;

(A2) $\phi_x(x,y) > 0$, $\phi_y(x,y) > 0$, $(x,y) \in \overline{D}$, $\mu_5(y,t) > 0$, $(y,t) \in [0,l] \times [0,T]$, $\mu_6(x,t) > 0$, $(x,t) \in [0,h] \times [0,T]$;

(A3) consistency conditions of the zero and the first orders.

We remark that a formal elimination of $a(y,t)$ and $b(x,t)$ in (10.5) and (10.6), respectively, and substitution into (10.1) result in the nonlinear partial differential equation

$$u_t(x,y,t) = \frac{\mu_5(y,t)}{u_x(0,y,t)}u_{xx} + \frac{\mu_6(x,t)}{u_y(x,0,t)}u_{yy} + f(x,y,t), \quad (x,y,t) \in Q_T \qquad (10.7)$$

to be solved for the temperature $u(x,y,t)$ subject to the initial and boundary conditions (10.2)–(10.4).

The following theorems, [59], state the unique solvability of the inverse problem (10.1)–(10.6).

Theorem 10.1. *Suppose that the assumptions* **(A1)-(A3)** *hold. Then for some* $T_0 \in (0,T]$ *there exists a solution of the problem (10.1)-(10.6) such that* $(a,b,u) \in C^{\gamma,\gamma/2}([0,l]\times[0,T_0]) \times C^{\gamma,\gamma/2}([0,h]\times[0,T_0]) \times C^{2+\gamma,1+\gamma/2}(\overline{Q}_{T_0})$, $a(y,t) > 0, (y,t) \in [0,l]\times[0,T_0], b(x,t) > 0, (x,t) \in [0,h]\times[0,T_0]$.

Theorem 10.2. *Suppose that* $\mu_5(y,t) \neq 0, (y,t) \in [0,l]\times[0,T], \mu_6(x,t) \neq 0, (x,t) \in [0,h] \times [0,T]$. *Then a solution* $(a(y,t), b(x,t), u(x,y,t))$ *of the problem (10.1)-(10.6) is unique in the space* $C^{\gamma,\gamma/2}([0,l]\times[0,T]) \times C^{\gamma,\gamma/2}([0,h]\times[0,T]) \times C^{2+\gamma,1+\gamma/2}(\overline{Q}_T)$, $a(y,t) > 0$, $(y,t) \in [0,l] \times [0,T]$, $b(x,t) > 0$, $(x,t) \in [0,h] \times [0,T]$.

10.3 Solution of direct problem

In this section, we consider the direct initial boundary value problem (10.1)–(10.4) where $a(y,t)$, $b(x,t)$, $f(x,y,t)$, $\phi(x,y)$, and μ_i, $i = 1,2,3,4$, are known and the solution $u(x,y,t)$ is to be determined. To achieve this, we use the Forward-Time-Central-Space (FTCS) finite-difference scheme which is conditionally stable, [92, p.195].

We subdivide the solution domain Q_T into M_x, M_y and N subintervals of equal step lengths Δx and Δy, and uniform time step Δt, where $\Delta x = h/M_x$, $\Delta y = \ell/M_y$ and $\Delta t = T/N$, for space and time, respectively. At the node (i,j,k) we denote $u^k_{i,j} := u(x_i, y_j, t_k)$, where $x_i = i\Delta x$, $y_j = j\Delta y$, $t_k = k\Delta t$,

$a_j^k := a(y_j, t_k)$, $b_i^k := b(x_i, t_k)$ and $f_{i,j}^k := f(x_i, y_j, t_k)$ for $i = \overline{0, M_x}$, $j = \overline{0, M_y}$ and $k = \overline{0, N}$.

The simplest explicit difference scheme for equation (10.1) is given by

$$\frac{u_{i,j}^{k+1} - u_{i,j}^k}{\Delta t} = a_j^k \frac{u_{i+1,j}^k - 2u_{i,j}^k + u_{i-1,j}^k}{(\Delta x)^2} + b_i^k \frac{u_{i,j+1}^k - 2u_{i,j}^k + u_{i,j-1}^k}{(\Delta y)^2} + f_{i,j}^k \tag{10.8}$$

for $i = \overline{1, M_x - 1}$, $j = \overline{1, M_y - 1}$ and $k = \overline{0, N}$. The initial and boundary conditions (10.2)–(10.4) give

$$u_{i,j}^0 = \phi_{i,j}, \quad i = \overline{0, M_x}, \quad j = \overline{0, M_y}, \tag{10.9}$$

$$u_{0,j}^k = \mu_1(y_j, t_k), \quad u_{M_x,j}^k = \mu_2(y_j, t_k), \quad j = \overline{0, M_y}, \quad k = \overline{1, N}, \tag{10.10}$$

$$u_{i,0}^k = \mu_3(x_i, t_k), \quad u_{i,M_y}^k = \mu_4(x_i, t_k), \quad i = \overline{0, M_x}, \quad k = \overline{1, N}. \tag{10.11}$$

Let $\tilde{a}$ and $\tilde{b}$ be the maximum values of $a(y, t)$ and $b(x, t)$, respectively, then, the stability condition for the explicit FDM scheme (10.8) will be [97].

$$\frac{\tilde{a}\Delta t}{(\Delta x)^2} + \frac{\tilde{b}\Delta t}{(\Delta y)^2} \leq \frac{1}{2}. \tag{10.12}$$

The heat fluxes (10.5) and (10.6) can be calculated using the second-order FDM approximations:

$$\mu_5(y_j, t_k) = a_j^k \frac{4u_{1,j}^k - u_{2,j}^k - 3u_{0,j}^k}{2\Delta x}, \quad j = \overline{1, M_y - 1}, \quad k = \overline{1, N}, \tag{10.13}$$

$$\mu_6(x_i, t_k) = b_i^k \frac{4u_{i,1}^k - u_{i,2}^k - 3u_{i,0}^k}{2\Delta y}, \quad i = \overline{1, M_x - 1}, \quad k = \overline{1, N}. \tag{10.14}$$

10.4 Numerical solution of inverse problem

In this section we aim to obtain stable reconstructions for the principal direction components $a(y, t) > 0$ and $b(x, t) > 0$ of the two-dimensional heterogeneous orthotropic rectangular medium together with the temperature $u(x, y, t)$ satisfying the equations (10.1)–(10.6). One can remark that at initial time $t = 0$ the values of the principal direction components are known and they can easily be obtained form the overdetermination conditions (10.5) and (10.6) as

$$a(y, 0) = \frac{\mu_5(y, 0)}{\phi_x(0, y)}, \quad b(x, 0) = \frac{\mu_6(x, 0)}{\phi_y(x, 0)}, \quad y \in [0, \ell], \quad x \in [0, h]. \tag{10.15}$$

The inverse problem is solved based on the nonlinear minimization of the least-squares objective function

$$F(a,b) := \left\|a(y,t)u_x(0,y,t) - \mu_5(y,t)\right\|^2 + \left\|b(x,t)u_y(x,0,t) - \mu_6(x,t)\right\|^2, \quad (10.16)$$

or, in discretised form

$$\begin{aligned} F(\underline{a},\underline{b}) = &\sum_{k=1}^{N}\sum_{j=0}^{M_y}\Big[a_{j,k}u_x(0,y_j,t_k) - \mu_5(y_j,t_k)\Big]^2 \\ &+ \sum_{k=1}^{N}\sum_{i=0}^{M_x}\Big[b_{i,k}u_y(x_i,0,t_k) - \mu_6(x_i,t_k)\Big]^2. \end{aligned} \quad (10.17)$$

Regularization terms may also be included to enhance the stability of numerical results but in this case, as in Chapter 2, regularization was not found necessary, see later on the numerical results of Section 10.5.

The minimization of the objective functional (10.17), subjected to the physical simple bound constraints $\underline{a} > \underline{0}$ and $\underline{b} > \underline{0}$ is accomplished using the MATLAB optimization toolbox routine *lsqnonlin*.

Upper and lower bounds on the thermal conductivities a and b can be specified according to *a priori* information on these physical parameters.

In the numerical computation, we take the parameters of the routine *lsqnonlin* as follows:

- Maximum number of iterations = $10^5\times$ (number of variables).
- Maximum number of objective function evaluations = $10^6\times$ (number of variables).
- Solution and objective function tolerances = 10^{-10}.

The inverse problem (10.1)–(10.6) is solved subject to both exact and noisy measurements (10.5) and (10.6). The noisy data is numerically simulated as

$$\mu_5^{\epsilon 1}(y_j,t_k) = \mu_5(y_j,t_k) + \epsilon 1_{j,k}, \quad j = \overline{0,M_y}, \quad k = \overline{1,N}, \quad (10.18)$$

$$\mu_6^{\epsilon 2}(x_i,t_k) = \mu_6(x_i,t_k) + \epsilon 2_{i,k}, \quad i = \overline{0,M_x}, \quad k = \overline{1,N}, \quad (10.19)$$

where $\epsilon 1_{j,k}$ and $\epsilon 2_{i,k}$ are random variables generated from a Gaussian normal distribution with mean zero and standard deviation $\sigma 1$ and $\sigma 2$ given by

$$\sigma 1 = p \times \max_{(y,t)\in[0,\ell]\times[0,T]} |\mu_5(y,t)|, \quad \sigma 2 = p \times \max_{(x,t)\in[0,h]\times[0,T]} |\mu_6(x,t)|, \quad (10.20)$$

where p represents the percentage of noise. We use the MATLAB function *normrnd* to generate the random variables $\underline{\epsilon 1} = (\epsilon 1_{j,k})_{j=\overline{0,M_y},k=\overline{1,N}}$ and $\underline{\epsilon 2} = (\epsilon 2_{i,k})_{i=\overline{0,M_x},k=\overline{1,N}}$ as follows:

$$\underline{\epsilon 1} = normrnd(0, \sigma 1, M_y + 1, N), \quad \underline{\epsilon 2} = normrnd(0, \sigma 2, M_x + 1, N). \quad (10.21)$$

In the case of noisy data (10.18) and (10.19), we replace $\mu_5(y_j, t_k)$ and $\mu_6(x_i, t_k)$ by $\mu_5^{\epsilon 1}(y_j, t_k)$ and $\mu_6^{\epsilon 2}(x_i, t_k)$, respectively, in (10.17).

10.5 Numerical results and discussion

In this section, we present numerical results for the orthotropic thermal conductivity components $a(y,t)$, $b(x,t)$ and the temperature $u(x,y,t)$, in the case of exact and noisy data (10.18) and (10.19). To assess the accuracy of the numerical solution we employ the root mean square errors ($rmse$) defined by:

$$rmse(a) = \left[\frac{1}{N(M_y+1)}\sum_{k=1}^{N}\sum_{j=0}^{M_y}\left(a_{numerical}(y_j,t_k) - a_{exact}(y_j,t_k)\right)^2\right]^{1/2}, \quad (10.22)$$

$$rmse(b) = \left[\frac{1}{N(M_x+1)}\sum_{k=1}^{N}\sum_{i=0}^{M_x}\left(b_{numerical}(x_i,t_k) - b_{exact}(x_i,t_k)\right)^2\right]^{1/2}. \quad (10.23)$$

For simplicity, we take $h = \ell = T = 1$.

10.5.1 Example 1

Consider the inverse problem (10.1)–(10.6) with unknown coefficients $a(y,t)$ and $b(y,t)$, with the input data ϕ and μ_i, $i = \overline{1,6}$, as follows:

$$\begin{aligned}
\phi(x,y) &= u(x,y,0) = -(-2+x)^2 - (-2+y)^2,\\
f(x,y,t) &= \frac{101.5 + 3t + x + y}{50},\\
\mu_1(y,t) &= u(0,y,t) = -4 + 2t - (-2+y)^2,\\
\mu_2(y,t) &= u(h,y,t) = -1 + 2t - (-2+y)^2,\\
\mu_3(x,t) &= u(x,0,t) = -4 + 2t - (-2+x)^2,\\
\mu_4(x,t) &= u(x,\ell,t) = -1 + 2t - (-2+x)^2,\\
\mu_5(y,t) &= a(y,t)u_x(0,y,t) = \frac{y+t+1}{25},\\
\mu_6(x,t) &= b(x,t)u_y(x,0,t) = \frac{x+2t+0.5}{25}.
\end{aligned}$$

One can remark that conditions of Theorems 10.1 and 10.2 are satisfied and therefore, the local solvability of the solution is guaranteed. In fact, it can easily be checked by direct substitution that the analytical solution is given by

$$a(y,t) = \frac{y+t+1}{100}, \quad (y,t) \in [0,1] \times [0,1], \tag{10.24}$$

$$b(x,t) = \frac{x+2t+0.5}{100}, \quad (x,t) \in [0,1] \times [0,1], \tag{10.25}$$

$$u(x,y,t) = -(x-2)^2 - (y-2)^2 + 2t, \quad (x,y,t) \in \overline{Q}_T. \tag{10.26}$$

We take a coarse mesh size with $N = M_x = M_y = 5$, i.e. $\Delta x = \Delta y = \Delta t = 1/5 = 0.2$. Then we need to choose an upper bound UB for a and b such that the stability condition (10.12) is satisfied. This yields $UB = 1/20 = 0.05$. Also since a and b represent positive physical quantities we take a lower bound for a and b be given by $LB = 0.01$. Keeping the sought parameters inside the lower and upper prescribed bounds through all the minimization process increases the performance of identification, [50].

We start our investigation for simultaneously determining the principal direction components $a(y,t)$ and $b(x,t)$ in a heterogeneous orthotropic with the case of exact input data, i.e. $p = 0$ in (10.20). To test the robustness of the iterative method with respect to the independence on the initial guess, we take three different initial guesses namely:

$$\begin{aligned}
\text{initial A: } a^0 &= a_{exact} + 3 \times 10^{-4}\text{randn(size(a))}, \\
b^0 &= b_{exact} + 3 \times 10^{-4}\text{randn(size(b))}, \\
\text{initial B: } a^0 &= a_{exact} + 3 \times 10^{-3}\text{randn(size(a))}, \\
b^0 &= b_{exact} + 3 \times 10^{-3}\text{randn(size(b))}, \\
\text{initial C: } a^0 &= \text{ones(size(a))}, \; b^0 = \text{ones(size(b))}.
\end{aligned}$$

where `randn(:)` is a MATLAB function.

Figure 10.1 shows the convergence of the objective function (10.17) with exact input data (10.5) and (10.6) for the various initial guesses A, B and C. Table 10.1 gives more details of these computations including the computational time and the *rmse* values (10.22) and (10.23). From Figure 10.1 and Table 10.1, it can be seen that, as expected, the farther the initial guess is, e.g. initial C, the more iterations and longer computational time are required to achieve convergence. However, for all initial guesses, the objective function (10.17) converges to the same very small minimum value of $O(10^{-20})$. This shows robustness with respect to the independence on the initial guess. Furthermore, one can notice that a rapid

convergence is achieved for each initial guesses in more than eight iterations within no more than 64 seconds. Moreover, from Table 10.1 it can be seen that there is an excellent agreement between exact and numerically obtained solutions for all initial guesses with $rmse$ values being very low of $O(10^{-12})$ to $O(10^{-11})$ for $a(y,t)$ and $b(x,t)$.

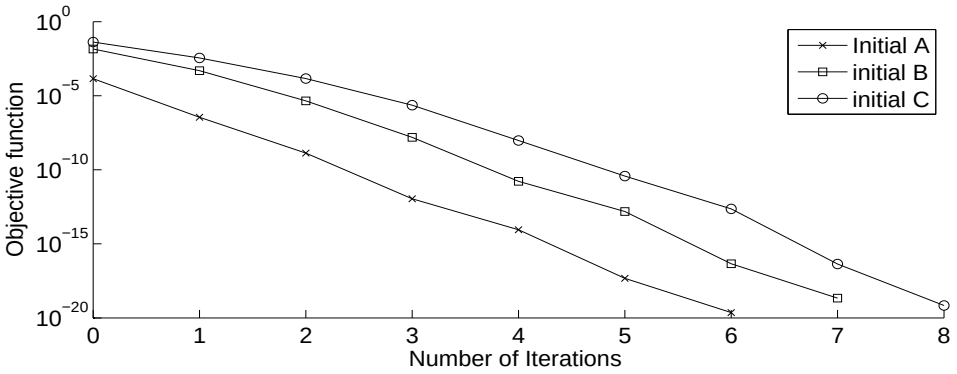

Figure 10.1: The objective function (10.17) with no noise, for various initial guesses, for Example 1.

Table 10.1: Number of iterations, number of function evaluations, value of the objective function (10.17) at final iteration, the $rmse$ values and the computational time, with no regularization and no noise for Example 1 for various initial guesses.

	initial A	initial B	initial C
No. of iterations	6	7	8
No. of function evaluations	511	584	657
Value of objective function (10.17) at final iteration	2.3E-20	2.1E-19	6.9E-20
$rmse(a)$	3.6E-12	1.1E-11	2.9E-12
$rmse(b)$	5.8E-12	1.7E-11	1.1E-11
Computational time	49 sec	57 sec	64 sec

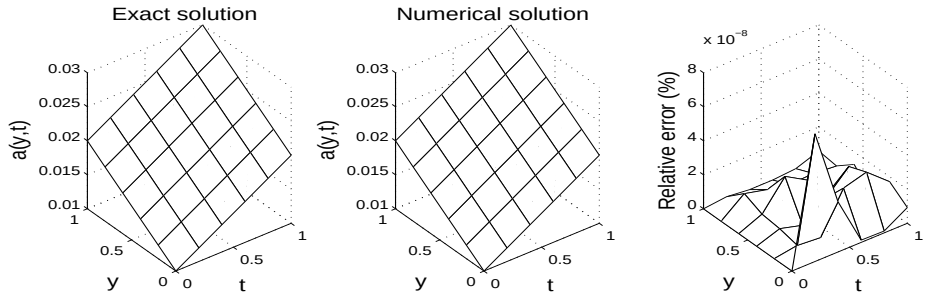

(a)

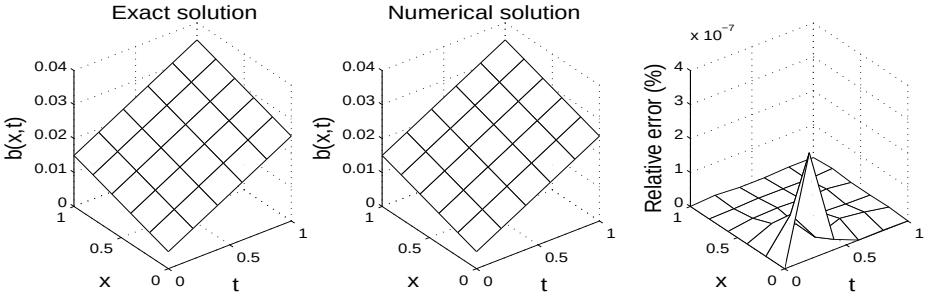

(b)

Figure 10.2: The exact solution (left), numerical solution (middle), error between them (right), with initial guess C, for: (a) $a(y,t)$ and (b) $b(x,t)$, with no noise, for Example 1.

In what follows, we take the initial guess for the unknown coefficients equal to the constant matrix of ones, i.e. we choose the initial guess C. The numerically obtained results for a and b are illustrated in Figure 10.2 and an excellent agreement can be observed.

Next we consider the case of noisy data (10.18) and (10.19) with $p \in \{1, 5, 10\}\%$. The numerically obtained results are illustrated in Figures 10.3–10.5 for $p = 1\%$, 5% and 10%, respectively, and summarised in Table 10.2. From these figures and table it can be seen that as the percentage of noise p decreases from 10% to 5% and then to 1% the numerically obtained solution becomes more stable and accurate.

Table 10.2: Number of iterations, number of function evaluations, value of the objective function (10.17) at final iteration, the $rmse$ values and the computational time, with $p \in \{1, 5, 10\}\%$ noise, for Example 1.

	$p = 1\%$	$p = 5\%$	$p = 10\%$
No. of iterations	8	8	8
No. of function evaluations	657	657	657
Value of objective function (10.17) at final iteration	2.4E-20	3E-20	7.4E-20
$rmse(a)$	4.2E-4	0.0021	0.0043
$rmse(b)$	3.3E-4	0.0017	0.0034
Computational time	61 sec	61 sec	63 sec

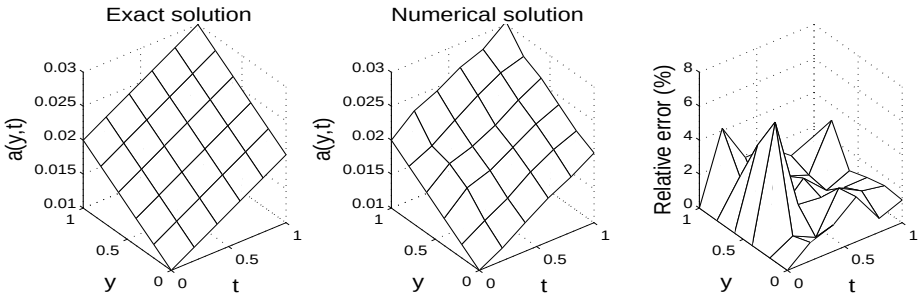

(a)

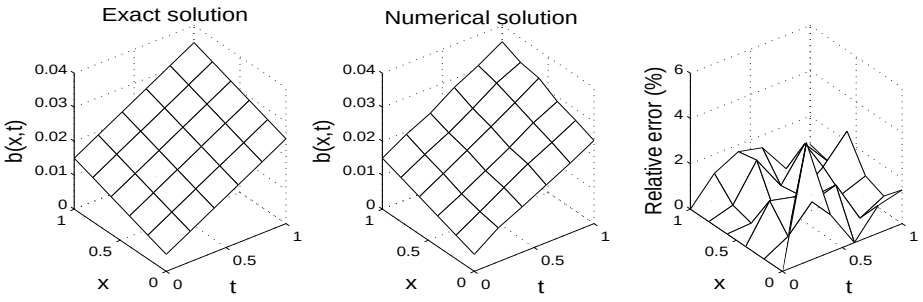

(b)

Figure 10.3: The exact solution (left), numerical solution (middle), error between them (right), for: (a) $a(y,t)$ and (b) $b(x,t)$, with $p = 1\%$ noisy data, for Example 1.

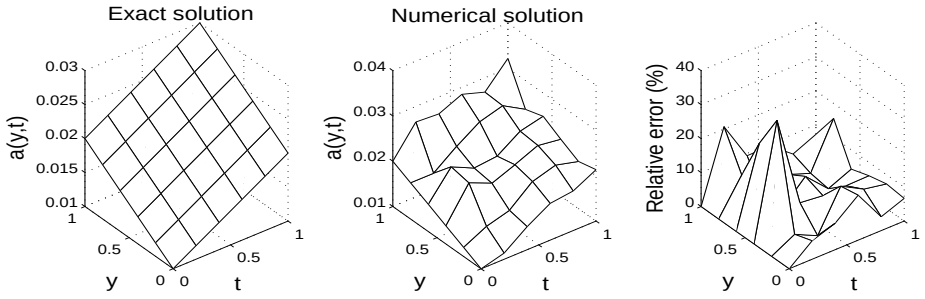

(a)

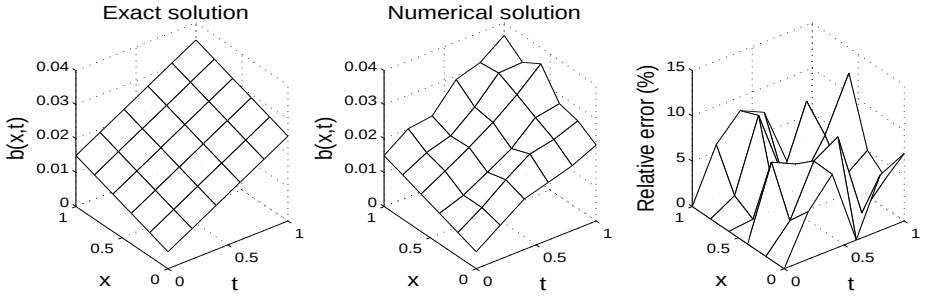

(b)

Figure 10.4: The exact solution (left), numerical solution (middle), error between them (right), for: (a) $a(y,t)$ and (b) $b(x,t)$, with $p = 5\%$ noisy data, for Example 1.

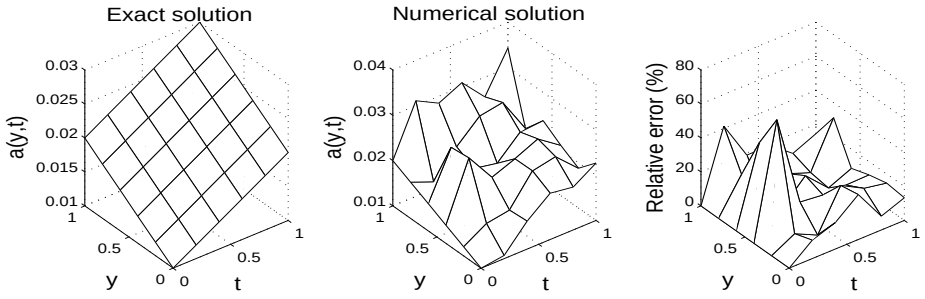

(a)

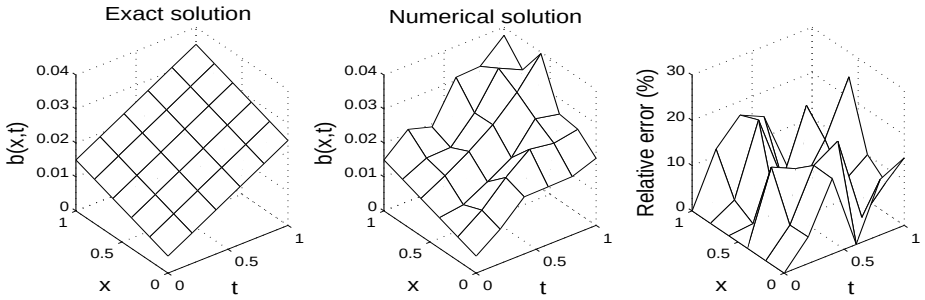

(b)

Figure 10.5: The exact solution (left), numerical solution (middle), error between them (right), for: (a) $a(y,t)$ and (b) $b(x,t)$, with $p = 10\%$ noisy data, for Example 1.

10.6 Conclusions

The inverse problem concerning the identification of the principal direction thermal conductivity components $a(y,t)$ and $b(x,t)$ of an orthotropic material and the temperature $u(x,y,t)$ in the two-dimensional heat equation in a rectangular domain has been investigated. The additional conditions which ensure a unique solvability of solution are given by the heat fluxes μ_5 and μ_6. The direct solver based on an explicit finite difference scheme has been developed. The inverse solver based on a nonlinear least-squares minimization has been solved using the MATLAB toolbox routine *lsqnonlin*. For both exact and noisy data, the numerical results obtained are accurate and stable.

Chapter 11

General conclusions and future work

11.1 Conclusions

The work in this thesis has been devoted to solving various types of inverse coefficient identification problems in the parabolic heat equation. All these inverse problems have practical physical interest in a real situation. For instance, identification of thermal properties of certain material, determination of unknown free boundary of melting or freezing process, and so on.

In inverse coefficient identification problems, one or more coefficients is/are unknown along with the main dependent variable. Therefore, we need more information to retrieve the missing coefficients. This extra information is usually provided as measured over-specified data which contains random noise. If the underlying problem is ill-posed then, this random noise causes huge oscillations and unbounded behavior in the output solution. Consequently, traditional numerical methods are not appropriate unless combined with some sort of regularization.

In this thesis, the inverse problems have been reduced to nonlinear constrained optimization problems by adding penalty regularization terms to stabilize the solution. These smoothing terms which are multiplied by regularization parameters will damp the influence of random measurement errors in the numerical results.

There are several methods proposed to choose a single regularization parameter, e.g. the L-curve method, the discrepancy principle, etc. If multiple regularization parameters are encountered one can try to generalize the L-curve criterion to the L-hypersurface concept, [6], but then the analysis of multiple parameter selection becomes tedious and time consuming. In this thesis, the emphasis was on obtaining accurate and stable numerical solutions to several inverse coefficient identification problems. In a first attempt, the regularization parameter has been

chosen by simple trial and error, i.e. selected based on experience by first choosing a small value and gradually increasing it until any numerical oscillations in the unknown coefficients are removed. But nevertheless more research has to be done in the future regarding the rigorous choice of regularization parameters for ill-posed and nonlinear problems.

In all the inverse problems considered in this thesis, the accuracy and the stability of the numerical results were thoroughly investigated for various mesh sizes and various noise levels added into the input data to mimic the case of measured data. Further, in all problems, we have used a FDM direct solver in the process of the minimization of the residual least-squares functional associated to the gap between the measured and the computed data. The whole iterative process of minimization has been performed using MATLAB optimization toolbox routines, which allow to impose simple bounds on the unknown coefficients and do not need to supply (by the user) the gradient of residual functional.

In Chapter 1, a general introduction to inverse problems has been provided. General description for the direct and inverse Stefan problem are given in Section 1.3 followed by the stability analysis for the inverse problems under investigation based on the Tikhonov's regularization method with appropriate choice of regularization parameters. Moreover, a brief description of two MATLAB optimization toolboxes have been explained along with some commands. A quick overview of numerical methods which can be applied to solve PDEs has been provided and also, a flowchart explaining the stages of our procedure was sketched in Section 1.7.

In Chapter 2, an inverse problem which requires determining the time-dependent diffusivity with initial, periodic boundary conditions and non-local boundary measurement has been investigated. The problem has been reformulated as a nonlinear least-squares optimization problem which has been solved using the MATLAB toolbox routine *lsqnonlin*. Numerical results indicate that accurate, robust and reasonably stable solutions have been obtained. The robustness of the iterative method was tested with respect to the independence on the initial guess, i.e. by performing the iterative process for multiple initial guesses, and the same numerical results have been obtained. This problem seems rather stable and hence, in general, no regularization was found necessary to be employed.

In Chapter 3, a couple of inverse problems which require determining a time-dependent thermal conductivity when the heat capacity is space-dependent but given for the heat equation with overspecified conditions have been investigated. The Inverse Problem I was found to be well-posed, whilst the Inverse Problem II was found to be ill-posed and regularization was needed in order to obtain a stable

solution. Numerical results illustrated for several benchmarks test examples show that an accurate and stable solution has been obtained.

In Chapter 4, three inverse coefficient identification problems for simultaneously determining two time-dependent coefficients in a one-dimensional parabolic heat-type equation from Cauchy boundary data have been considered. The problems have been reformulated as constrained regularization minimization problems. The numerically obtained results are shown to be stable and accurate.

Chapter 5 was concerned with a couple of inverse problems consisting of finding the time-dependent coefficients and the time-dependent heat source term in the parabolic heat equation with integral type overdetermination conditions. Regularization has been imposed when noisy data has been inverted. Numerical results presented and discussed for a couple of test examples show that reasonably accurate and stable numerical solutions have been achieved.

Chapter 6 was concerned to present a numerical approach to identify simultaneously the time and space-dependent coefficients in a parabolic heat-type equation. The overdetermination conditions which ensure a unique solution are given by the heat flux measurement and the total potential heat function specification or, the time-average heat flux. The resulting inverse problems have been reformulated as constrained regularized minimization problems which were solved using the MATLAB optimization toolbox routine *lsqnonlin*, as in previous chapters. The inverse problems have been found rather stable in the time-dependent thermal conductivity coefficient, but less stable in the space-dependent coefficients which multiply the lower-order terms in the governing PDE. Numerical results obtained for a wide range of typical test examples under various noise levels showed that accurate and stable numerical solutions have been achieved.

Chapter 7 was concerned with the inverse identification of a free boundary and the temperature in the heat equation with nonlinear temperature-dependent diffusivity, whilst Chapters 8 and 9 were concerned with one-phase inverse Stefan coefficient identification problems. In these chapters, numerical investigations for the recovery of multiple time-dependent coefficients entering the parabolic heat equation with a free boundary subject to heat flux, specification of energy, Stefan condition, first- and second-order heat moment have been presented. The moving boundary value problem was first transformed, by a simple change of variables, to a problem formulated in a fixed domain. In Chapter 9, the Stefan condition can be replaced by a second-order heat moment specification. It is interesting to remark that, based on the comparison between Examples 3 and 4, the Stefan condition contains more information than the second-order heat moment. Notably, the inclusion of Tikhonov's regularization method, apart from

restoring the stability of the numerical solution, it also reduces the computational time. Numerical results presented and discussed for several test examples show that accurate and stable numerical solutions have been achieved.

Finally, in Chapter 10, the inverse problem concerning the identification of the thermal conductivity of an orthotropic material and the temperature in the two-dimensional heat equation in a rectangular domain has been investigated. The overdetermination conditions which ensure the unique solvability of the solution are given by the specification of a couple of heat fluxes. An explicit FDM has been developed as direct solver, whilst the inverse solver based on a nonlinear least-squares minimization has been efficiently implemented using the MATLAB optimization toolbox routine *lsqnonlin*. For both exact and noisy data, the numerical results have been obtained accurate and stable and hence the regularization was found unnecessary.

11.2 Future work

One can remark that the numerical results presented in this thesis confirm the fact that efficient approaches can be developed for more complicated coefficient identification problems, inverse initial value problems and inverse geometric problems. As far as these features are concerned, one can suggest the following possible future work:

- Extend the numerical FDM implementation to three dimensional problems;
- Investigate multiple-phase inverse coefficient Stefan problems, [111, 114];
- Extend the analysis to identify coefficients that depend both on space and time;
- Investigate criteria to select multiple regularization parameters and employ other minimization methods, e.g. genetic algorithms or globally convergent methods, [5, 40], which do not depend on the initial guess;
- Apply the models in this thesis to real world problems concerned with material characterisation and thermal property identification.

Bibliography

[1] K.R. Aida-zade and A.B. Rahimov. Solution to classes of inverse coefficient problems and problems with nonlocal conditions for parabolic equations. *Differential Equations*, 51(1):83–93, 2015.

[2] A.Ya. Akhundov. An inverse problem for linear parabolic equations. *Doklady Akademii Nauk AzSSR*, 39(5):3–6, 1983.

[3] T.N. Baranger, S. Andrieux, and R. Rischette. Combined energy method and regularization to solve the Cauchy problem for the heat equation. *Inverse Problems in Science and Engineering*, 22(1):199–212, 2014.

[4] J.V. Beck. Nonlinear estimation applied to the nonlinear inverse heat conduction problem. *International Journal of Heat and Mass Transfer*, 13:703–716, 1970.

[5] L. Beilina and M.V. Klibanov. *Approximate Global Convergence and Adaptivity for Coefficient Inverse Problems*. Springer, Berlin, 2012.

[6] M. Belge, M. Kilmer, and E.L. Miller. Efficient determination of multiple regularization parameters in a generalized L-curve framework. *Inverse Problems*, 18(4):1161–1183, 2002.

[7] P. Broadbridge, P. Tritscher, and A. Avagliano. Free boundary problems with nonlinear diffusion. *Mathematical and Computer Modelling*, 18(10):15–34, 1993.

[8] B.M. Budak and A.D. Iskenderov. On a class of boundary value problems with unknown coefficients. *Soviet Mathematics Doklady*, 8:786–789, 1967.

[9] R.H. Byrd, J.C. Gilbert, and J. Nocedal. A trust region method based on interior point techniques for nonlinear programming. *Mathematical Programming*, 89(1):149–185, 2000.

[10] R.H. Byrd, M.E. Hribar, and J. Nocedal. An interior point algorithm for large-scale nonlinear programming. *SIAM Journal on Optimization*, 9(4):877–900, 1999.

[11] J.R. Cannon. *The One-dimensional Heat Equation*. Addison-Wesley, Menlo Park, California, 1984.

[12] J.R. Cannon and P. DuChateau. Determination of unknown physical properties in heat conduction problems. *International Journal of Engineering Science*, 11(7):783–794, 1973.

[13] J.R. Cannon and P. Duchateau. Determining unknown coefficients in a nonlinear heat conduction problem. *SIAM Journal on Applied Mathematics*, 24(3):298–314, 1973.

[14] J.R. Cannon and P. DuChateau. An inverse problem for a nonlinear diffusion equation. *SIAM Journal on Applied Mathematics*, 39(2):272–289, 1980.

[15] J.R. Cannon, P. DuChateau, and K. Steube. Unknown ingredient inverse problems and trace-type functional differential equations. In *Inverse Problems in Partial Differential Equations,(eds. D.L. Colton, R.E. Ewing and W. Rundell)*, pages 187–202. SIAM, Philadelphia, 1990.

[16] J.R. Cannon and J. Hoek. Diffusion subject to the specification of mass. *Journal of Mathematical Analysis and Applications*, 115(2):517–529, 1986.

[17] J.R. Cannon and B.F. Jones Jr. Determination of the diffusivity of an anisotropic medium. *International Journal of Engineering Science*, 1(4):457–460, 1963.

[18] J.R. Cannon and Y. Lin. Determination of a parameter $p(t)$ in some quasi-linear parabolic differential equations. *Inverse Problems*, 4(1):35, 1988.

[19] J.R. Cannon and W. Rundell. Recovering a time dependent coefficient in a parabolic differential equation. *Journal of Mathematical Analysis and Applications*, 160(2):572–582, 1991.

[20] Z. Chen, Y. Lu, and Xu Yang. Multiple-parameter Tikhonov regularization for linear ill-posed operator equations. *Journal of Computational Mathematics*, 26(1):37–55, 2008.

[21] T.F. Coleman and Y. Li. On the convergence of interior-reflective newton methods for nonlinear minimization subject to bounds. *Mathematical Programming*, 67(1-3):189–224, 1994.

[22] T.F. Coleman and Y. Li. An interior trust region approach for nonlinear minimization subject to bounds. *SIAM Journal on Optimization*, 6(2):418–445, 1996.

[23] C. Coles and D.A. Murio. Identification of parameters in the 2-D IHCP. *Computers and Mathematics with Applications*, 40(8):939–956, 2000.

[24] C. Coles and D.A. Murio. Simultaneous space diffusivity and source term reconstruction in 2D IHCP. *Computers and Mathematics with Applications*, 42(12):1549–1564, 2001.

[25] A. Conn, N. Gould, and P. Toint. *Trust Region Methods*. SIAM, Philadelphia, 2000.

[26] G. de Marsily. *Quantitative Hydrogeology*. Academic Press, New York, 1986.

[27] Z. Deng, J. Yu, and L. Yang. Identifying the coefficient of first-order in parabolic equation from final measurement data. *Mathematics and Computers in Simulation*, 77(4):421–435, 2008.

[28] B.H. Dennis, G.S. Dulikravich, and S. Yoshimura. A finite element formulation for the determination of unknown boundary conditions for three-dimensional steady thermoelastic problems. *Journal of Heat Transfer*, 126(1):110–118, 2004.

[29] P. DuChateau and D. Zachmann. *Applied Partial Differential Equations*. Harper & Row, New York, 1989.

[30] T. Elfving, T. Nikazad, and P.C. Hansen. Semi-convergence and relaxation parameters for a class of SIRT algorithms. *Electronic Transactions on Numerical Analysis*, 37:321–336, 2010.

[31] H.W. Engl and P. Kugler. Nonlinear inverse problems: theoretical aspects and some industrial applications. In *Multidisciplinary Methods for Analysis Optimization and Control of Complex Systems, (eds. V. Capasso and J. Priaux)*, volume 6 of *Mathematics in Industry*, pages 3–47. Springer, Berlin, 2005.

[32] A. Erdem, D. Lesnic, and A. Hasanov. Identification of a spacewise dependent heat source. *Applied Mathematical Modelling*, 37(24):10231–10244, 2013.

[33] Y. Fan and D.G. Li. Identifying the heat source for the heat equation with convection term. *International Journal of Mathematical Analysis*, 3(27):1317–1323, 2009.

[34] A. Fatullayev and S. Cula. An iterative procedure for determining an unknown spacewise-dependent coefficient in a parabolic equation. *Applied Mathematics Letters*, 22(7):1033–1037, 2009.

[35] A.G. Fatullayev. Numerical procedure for the determination of an unknown coefficients in parabolic equations. *Computer Physics Communications*, 144(1):29 – 33, 2002.

[36] A.G. Fatullayev. Numerical procedure for the simultaneous determination of unknown coefficients in a parabolic equation. *Applied Mathematics and Computation*, 164(3):697–705, 2005.

[37] A.G. Fatullayev, N. Gasilov, and I. Yusubov. Simultaneous determination of unknown coefficients in a parabolic equation. *Applicable Analysis*, 87(10-11):1167–1177, 2008.

[38] A. Friedman. *Partial Differential Equations*. Prentice-Hall, Englewood Cliffs, New Jersey, 1969.

[39] R.A. Gingold and J.J. Monaghan. Smoothed particle hydrodynamics: theory and application to non-spherical stars. *Monthly Notices of the Royal Astronomical Society*, 181(3):375–389, 1977.

[40] D.E. Golberg. *Genetic Algorithms in Search, Optimization, and Machine Learning*. Addison Wesley Logman, Inc., 1989.

[41] N.L. Goldman. *Inverse Stefan Problems*. Springer Science & Business Media, 1997.

[42] D. Gottlieb and S.A. Orszag. *Numerical Analysis of Spectral Methods: Theory and Applications*. SIAM, Philadelphia, 1977.

[43] J. Hadamard. *Lectures on Cauchy's Problem in Linear Partial Differential Equations*. Yale University Press, New Haven, 2003.

[44] P.C. Hansen. The L-curve and its use in the numerical treatment of inverse problems. In *Computational Inverse Problems in Electrocardiology, (ed. P. Johnston)*, pages 119–142. WIT Press, Southampton, 2001.

[45] A. Hazanee and D. Lesnic. Determination of a time-dependent heat source from nonlocal boundary conditions. *Engineering Analysis with Boundary Elements*, 37(6):936–956, 2013.

[46] A. Hazanee and D. Lesnic. Reconstruction of an additive space-and time-dependent heat source. *European Journal of Computational Mechanics*, 22(5-6):304–329, 2013.

[47] D. Hinestroza, J. Peralta, and L.E. Olivar. Regularization algorithm within two parameters for the identification of the heat conduction coefficient in the parabolic equation. *Mathematical and Computer Modelling*, 57(7):1990–1998, 2013.

[48] Y.C. Hon and M. Li. A computational method for inverse free boundary determination problem. *International Journal for Numerical Methods in Engineering*, 73(9):1291–1309, 2008.

[49] C.-H. Huang and S.-C. Chin. A two-dimensional inverse problem in imaging the thermal conductivity of a non-homogeneous medium. *International Journal of Heat and Mass Transfer*, 43(22):4061–4071, 2000.

[50] L. Huang, X. Sun, Y. Liu, and Z. Cen. Parameter identification for two-dimensional orthotropic material bodies by the boundary element method. *Engineering Analysis with Boundary Elements*, 28(2):109–121, 2004.

[51] W. Hundsdorfer and J.G. Verwer. *Numerical Solution of Time-dependent Advection-diffusion-reaction Equations*. Springer Series in Computational Mathematics, Berlin, 2003.

[52] M.S. Hussein and D. Lesnic. Simultaneous determination of time-dependent coefficients and heat source. *International Journal for Computational Methods in Engineering Science and Mechanics*, submitted, 2015.

[53] M.S. Hussein and D. Lesnic. Determination of a time-dependent thermal diffusivity and free boundary in heat conduction. *International Communications in Heat and Mass Transfer*, 53:154–163, 2014.

[54] M.S. Hussein and D. Lesnic. Identification of the time-dependent conductivity of an inhomogeneous diffusive material. *Applied Mathematics and Computation*, 269:35–58, 2015.

[55] M.S. Hussein and D. Lesnic. Simultaneous determination of time and space-dependent coefficients in a parabolic equation. *Comunications in Nonlinear Science and Numerical Simulation*, 33:194–217, 2016.

[56] M.S. Hussein, D. Lesnic, and M.I. Ismailov. An inverse problem of finding the time-dependent diffusion coefficient from an integral condition. *Mathematical Methods in the Applied Sciences*, 39(5):963–980, 2016.

[57] M.S. Hussein, D. Lesnic, and M.I. Ivanchov. Free boundary determination in nonlinear diffusion. *East Asian Journal on Applied Mathematics*, 3(04):295–310, 2013.

[58] M.S. Hussein, D. Lesnic, and M.I. Ivanchov. Simultaneous determination of time-dependent coefficients in the heat equation. *Computers and Mathematics with Applications*, 67(5):1065–1091, 2014.

[59] M.S. Hussein, D. Lesnic, and M.I. Ivanchov. Identification of a heterogeneous orthotropic conductivity in a rectangular domain. Accepted by *International Journal of Novel Ideas: Mathematics*, 2015.

[60] M.S. Hussein, D. Lesnic, M.I. Ivanchov, and H.A. Snitko. Multiple time-dependent coefficient identification thermal problems with a free boundary. *Applied Numerical Mathematics*, 99:24–50, 2016.

[61] N.I. Ionkin. Solution of a boundary-value problem in heat conduction with a nonclassical boundary condition. *Differential Equations*, 13:204–211, 1977.

[62] M.I. Ismailov and F. Kanca. The inverse problem of finding the time-dependent diffusion coefficient of the heat equation from integral overdetermination data. *Inverse Problems in Science and Engineering*, 20(4):463–476, 2012.

[63] K. Ito and J.-C. Liu. Recovery of inclusions in 2D and 3D domains for Poisson's equation. *Inverse Problems*, 29(7):075005 (20 pages), 2013.

[64] M.I. Ivanchov. Some inverse problems for the heat equation with nonlocal boundary conditions. *Ukrainian Mathematical Journal*, 45(8):1186–1192, 1994.

[65] M.I. Ivanchov. Inverse problem for finding a major coefficient in a parabolic equation. *Matematychni Studii*, 8(2):212–220, 1997.

[66] M.I. Ivanchov. Détermination simultanée de deux coefficients aux variables diverses dans une équation parabolique. *Matematychni Studii*, 10:173–187, 1998.

[67] M.I. Ivanchov. Inverse problem of simultaneous determination of two coefficients in a parabolic equation. *Ukrainian Mathematical Journal*, 52(3):379–387, 2000.

[68] M.I. Ivanchov. Free boundary problem for nonlinear diffusion equation. *Matematychni Studii*, 19:156–164, 2003.

[69] M.I. Ivanchov. Inverse problem with free boundary for heat equation. *Ukrainian Mathematical Journal*, 55(7):1086–1098, 2003.

[70] M.I. Ivanchov. *Inverse Problems for Equations of Parabolic Type*. VNTL Publications, Lviv, Ukraine, 2003.

[71] M.I. Ivanchov. Inverse problem for semilinear parabolic equation. *Matematychni Studii*, 29(2):181–191, 2008.

[72] M.I. Ivanchov and N.V. Pabyrivs'ka. Simultaneous determination of two coefficients of a parabolic equation in the case of nonlocal and integral conditions. *Ukrainian Mathematical Journal*, 53(5):674–684, 2001.

[73] M.I. Ivanchov and H.A. Snitko. Determination of time-dependent coefficients of a parabolic equation in a free boundary domain, nonlinear boundary problems. *Collection of Scientific Works, Donetsk (in Ukrainian)*, 20:28–44, 2011.

[74] N.I. Ivanchov. Inverse problems for the heat-conduction equation with nonlocal boundary conditions. *Ukrainian Mathematical Journal*, 45(8):1186–1192, 1993.

[75] N.I. Ivanchov. On the inverse problem of simultaneous determination of thermal conductivity and specific heat capacity. *Siberian Mathematical Journal*, 35(3):547–555, 1994.

[76] N.I. Ivanchov and N.V. Pabyrivska. On determination of two time-dependent coefficients in a parabolic equation. *Siberian Mathematical Journal*, 43(2):323–329, 2002.

[77] B.T. Johansson, D. Lesnic, and T. Reeve. A method of fundamental solutions for the one-dimensional inverse Stefan problem. *Applied Mathematical Modelling*, 35(9):4367–4378, 2011.

[78] B.F. Jones. The determination of a coefficient in a parabolic differential equation. Part I. existence and uniqueness. *Journal of Mathematics and Mechanics*, 11:907–918, 1962.

[79] A. Joshi, W. Bangerth, and E. Sevick-Muraca. Adaptive finite element based tomography for fluorescence optical imaging in tissue. *Optics Express*, 12(22):5402–5417, 2004.

[80] V.L. Kamynin. Inverse problem of finding the coefficient of a lower derivative in a parabolic equation on the plane. *Differential Equations*, 48(2):214–223, 2012.

[81] V.L. Kamynin. The inverse problem of determining the lower-order coefficient in parabolic equations with integral observation. *Mathematical Notes*, 94(1-2):205–213, 2013.

[82] V.L. Kamynin. Inverse problem of simultaneously determining the right-hand side and the coefficient of a lower order derivative for a parabolic equation on the plane. *Differential Equations*, 50(6):792–804, 2014.

[83] V.L. Kamynin. Inverse problems of simultaneous determination of the time-dependent right-hand side term and the coefficient in a parabolic equation. *Lecture Notes in Computer Science*, 9045:225–232, 2015.

[84] A. Kirsch. *An Introduction to the Mathematical Theory of Inverse Problems*, volume 120. Springer Science & Business Media, New York, 2011.

[85] M.V. Klibanov. A class of inverse problems for nonlinear parabolic equations. *Siberian Mathematical Journal*, 27(5):698–708, 1986.

[86] I. Knowles and A. Yan. The recovery of an anisotropic conductivity in groundwater modelling. *Applicable Analysis*, 81(6):1347–1365, 2002.

[87] O.A. Ladyzenskaja, V.A. Solonnikov, and N.N. Uralceva. *Linear and Quasilinear Equations of Parabolic Type*, volume 23. American Mathematical Society, 1968.

[88] M. Lees. A linear three-level difference scheme for quasilinear parabolic equations. *Mathematics of Computation*, 20(96):516–522, 1966.

[89] D. Lesnic, L. Elliott, and D.B. Ingham. The solution of an inverse heat conduction problem subject to the specification of energies. *International Journal of Heat and Mass Transfer*, 41(1):25–32, 1998.

[90] D. Lesnic, S.A. Yousefi, and M. Ivanchov. Determination of a time-dependent diffusivity from nonlocal conditions. *Journal of Applied Mathematics and Computing*, 41(1-2):301–320, 2013.

[91] R.J. LeVeque. *Finite Volume Methods for Hyperbolic Problems*, volume 31. Cambridge University Press, 2002.

[92] R.J. LeVeque. *Finite Difference Methods for Ordinary and Partial Differential Equations: Steady-State and Time-Dependent Problems*, volume 98. SIAM, 2007.

[93] J. Li and Y.-T. Chen. *Computational Partial Differential Equations Using MATLAB*. CRC Press, 2008.

[94] I.G. Malyshev. Inverse problems for the heat-conduction equation in a domain with a moving boundary. *Ukrainian Mathematical Journal*, 27(5):568–572, 1975.

[95] Mathwoks. Documentation optimization toolbox, www.mathworks.com, September 2012.

[96] V.A. Morozov. On the solution of functional equations by the method of regularization. *Soviet Mathematics Doklady*, 7(1):414–417, 1966.

[97] K.W. Morton and D.F. Mayers. *Numerical Solution of Partial Differential Equations: An Introduction*. Cambridge University Press, 2005.

[98] L.A. Muravei and A.V. Filinovskii. On a problem with nonlocal boundary condition for a parabolic equation. *Math. USSR Sbornik*, 74(1):219–249, 1993.

[99] L.A. Muravei and V.M. Petrov. Some problems of control of diffusion technological processes. In: *Current Problems of Modelling and Control of Systems with Distributed Parameters*, Kiev, 42-43, (in Russian), 1987.

[100] N.V. Muzylev. Uniqueness theorems for some converse problems of heat conduction. *USSR Computational Mathematics and Mathematical Physics*, 20(2):120–134, 1980.

[101] N.V. Muzylev. On the uniqueness of the simultaneous determination of thermal conductivity and volume heat capacity. *USSR Computational Mathematics and Mathematical Physics*, 23(1):69–73, 1983.

[102] K. Parand and J.R. Rad. Kansa method for the solution of a parabolic equation with an unknown spacewise-dependent coefficient subject to an extra measurement. *Computer Physics Communications*, 184(3):582–595, 2012.

[103] M.S. Pilant and W. Rundell. Undetermined coefficient problems for quasi-linear parabolic equations. In *Inverse Problems in Partial Differential Equations,(eds. D.L. Colton, R.E. Ewing and W. Rundell)*, pages 165–185. SIAM, Philadelphia, 1990.

[104] A.I. Prilepko, D.G. Orlovsky, and I.A. Vasin. *Methods for Solving Inverse Problems in Mathematical Physics*. M. Dekker, New York., 2000.

[105] J.N. Reddy. *An Introduction to the Finite Element Method*. McGraw-Hill, New York, 1993.

[106] A. Rhoden, N. Patong, Y. Liu, J. Su, and H. Liu. A globally convergent numerical method for coefficient inverse problems with time-dependent data. In *Applied Inverse Problems, (ed. L. Beilina)*, volume 48 of *Springer Proceedings in Mathematics & Statistics*, pages 105–128. Springer, New York, 2013.

[107] A. Shidfar and G.R. Karamali. Numerical solution of inverse heat conduction problem with nonstationary measurements. *Applied Mathematics and Computation*, 168(1):540–548, 2005.

[108] Z. Shiping and C. Minggen. A new algorithm for determining the leading coefficient in the parabolic equation. *World Academy of Science, Engineering and Technology*, 31:508–512, 2009.

[109] M. Slodička. Determination of a solely time-dependent source in a semilinear parabolic problem by means of boundary measurements. *Journal of Computational and Applied Mathematics*, 289:433–440, 2015.

[110] G.D. Smith. *Numerical Solution of Partial Differential Equations: Finite Difference Methods*. Oxford Applied Mathematics and Computing Science Series, Third edition, 1986.

[111] G.A. Snitko. On a coefficient inverse problem for a parabolic equation in a domain with free boundary. *Journal of Mathematical Sciences*, 200(3):374–388, 2014.

[112] H.A. Snitko. Coefficient inverse problem for a parabolic equation in a domain with free boundary. *Journal of Mathematical Sciences*, 167(1):30–46, 2010.

[113] H.A. Snitko. Inverse problem for determination of time-dependent coefficients of a parabolic equation in a free-boundary domain. *Journal of Mathematical Sciences*, 181(3):350–365, 2012.

[114] H.A. Snitko. Determination of the lowest coefficient for a one-dimensional parabolic equation in a domain with free boundary. *Ukrainian Mathematical Journal*, 65(11):1698–1719, 2014.

[115] P. Tervola. A method to determine the thermal conductivity from measured temperature profiles. *International Journal of Heat and Mass Transfer*, 32(8):1425–1430, 1989.

[116] N. Tian, J. Sun, W. Xu, and C.-H. Lai. An improved quantum-behaved particle swarm optimization with perturbation operator and its application in estimating groundwater contaminant source. *Inverse Problems in Science and Engineering*, 19(2):181–202, 2011.

[117] A.N. Tikhonov. On the stability of inverse problems. *Doklady Akademii Nauk SSSR*, 39:195–198, 1943.

[118] D. Trucu, D.B. Ingham, and D. Lesnic. Space-dependent perfusion coefficient identification in the transient bio-heat equation. *Journal of Engineering Mathematics*, 67(4):307–315, 2010.

[119] K. Van Bockstal and M. Slodicka. Determination of an unknown diffusion coefficient in a semilinear parabolic problem. *Journal of Computational and Applied Mathematics*, 246:104–112, 2013.

[120] H.K. Versteeg and W. Malalasekera. *An Introduction to Computational Fluid Dynamics: The Finite Volume Method*. Pearson Education, 2007.

[121] R.A. Waltz, J. L. Morales, J. Nocedal, and D. Orban. An interior algorithm for nonlinear optimization that combines line search and trust region steps. *Mathematical Programming*, 107(3):391–408, 2006.

[122] P. Wang and K. Zheng. Determination of an unknown coefficient in a nonlinear heat equation. *Journal of Mathematical Analysis and Applications*, 271(2):525–533, 2002.

[123] Y. Wang, C. Yang, and A. Yagola. *Optimization and Regularization for Computational Inverse Problems and Applications*. Springer-Verlag, Berlin, 2011.

[124] Z. Yi and D.A. Murio. Identification of source terms in 2-D IHCP. *Computers and Mathematics with Applications*, 47(10):1517–1533, 2004.

[125] S.A. Yousefi, D. Lesnic, and Z. Barikbin. Satisfier function in Ritz-Galerkin method for the identification of a time-dependent diffusivity. *Journal of Inverse and Ill-Posed Problems*, 20:701–722, 2012.